



Future Constellations for Near Real Time Gravity Processing

Anna F. Purkhauer

Vollständiger Abdruck der von der Fakultät für Luftfahrt, Raumfahrt und Geodäsie der Technischen Universität München zur Erlangung des akademischen Grades eines

Doktor-Ingenieurs (Dr.-Ing.)

genehmigten Dissertation.

Vorsitzender:

Prof. Dr.rer.nat. Ulrich Walter

Prüfende der Dissertation:

1. Prof. Dr.techn. Mag.rer.nat. Roland Pail
2. Prof. Dr.-Ing. Dr. h.c. mult. Reiner Rummel
3. Prof. Dr.-Ing. Annette Eicker

Die Dissertation wurde am 09.04.2020 bei der Technischen Universität München eingereicht und durch die Fakultät für Luftfahrt, Raumfahrt und Geodäsie am 06.05.2020 angenommen.

Das, wobei unsere Berechnungen versagen, nennen wir Zufall.

Albert Einstein

Abstract

The Earth is continuously changing by tectonic forces, erosion and the redistribution of water. Since the first dedicated satellite gravity missions, mass transportation and redistribution of mass can be observed. The GRACE satellite mission and its successor GRACE-FO monitor the time-variable gravity fields on a global scales down to a few hundred kilometres. GRACE observations have sufficient resolution and accuracy to study variations in the complete water cycle, including surface water bodies, soil moisture and groundwater reservoirs. However, not all science requirements can be fulfilled with the current set up. That is why different options for possible future satellite gravity constellations (furthermore called NGGMs) are discussed to improve the monitoring set-up.

This study focuses on possible NGGMs based on the GRACE concept and their positive impact on potential applications in the field of hydrology. The potential performance in terms of gravity field accuracy is evaluated via closed-loop simulations taking into account input signals and error models of instruments. First, as a basis of decision-making regarding NGGMs, the key performance parameters of near-polar single pairs and Bender-type double pair constellations are assessed. Limiting factors of the different constellations are identified and the contribution of all error sources to the error budget is analysed. It is demonstrated that the option with the best price/performance ratio is a double pair mission with an interferometer instrument flying in a higher orbit. This enables the observation of the complete spectrum of Earth's geophysical processes. A double pair mission also allows implementing a near-real time processing scheme including daily solutions without any a priori information. A third pair allows for an extended daily solution. The study also showed that for any additional pair an inclined orbit should be favoured.

Climate change is one of the biggest challenges of our time. One of the effects observable are intensified extreme weather events. As the monitoring of the mass change via NGGMs has an increased spatial and temporal resolution as well as increased accuracy, the potential to use the resulting gravity fields from a near-real time processing for applications is of interest. A tested flood detection processing algorithm showed, that depending on the signal magnitude as well as spatial extent, a detection solely based on gravity fields is possible.

Zusammenfassung

Tektonische Prozesse, Erosion und der Umverteilung von Wasser verändern die Erde ständig. Seit die ersten Schwerefeld-Satelliten die Erde umkreisen, können diese Massenveränderungen hochgenau beobachtet werden. Die Schwerefeldmissionen GRACE und ihr Nachfolger GRACE-FO messen die zeitlichen Veränderungen des Schwerefeldes mit einer Auflösung von bis zu einigen hundert Kilometern. Die Beobachtungen haben eine ausreichende Genauigkeit und Auflösung um die großen Variationen des Wasserzyklus zu erkennen. Allerdings können mit der aktuellen Mission nicht alle wissenschaftlichen Aufgaben erfüllt werden. Daher werden verschiedene Optionen von sogenannten NGGMs (zukünftigen Schwerefeldmissionen) analysiert, um das Messsystem zu verbessern.

Die vorliegende Dissertation hat ihren Fokus auf der Analyse von NGGMs basierend auf dem GRACE Konzept und die damit ermöglichten Anwendungen im Bereich der Hydrologie. Um eine Aussage über die Messgenauigkeit der resultierenden Schwerefelder zu treffen, wurde eine sogenannte "closed-loop-Simulation durchgeführt, die die unterschiedlichen Signale und Fehler der Instrumente berücksichtigt. In einem ersten Schritt sind die wichtigsten Parameter sowie limitierende Faktoren der verschiedenen von einer polaren Einzelpaar Mission sowie einer Doppelpaar Konstellation in Bender-Formation bestimmt und bewertet worden, um eine Entscheidungsgrundlage für zukünftige Missionen zu erstellen. Die beste Option in Bezug auf das Preis-/Leistungsverhältnis ist eine Doppelpaarmission mit einem Interferometer Instrument in einer höheren Umlaufbahn. Diese Konfiguration erlaubt die Beobachtung des gesamten geophysikalischen Spektrums, sowie die Implementierung einer "near-real time" Prozessierung mit täglichen Lösungen ohne zusätzliche Informationen einführen zu müssen. Ein drittes Paar ermöglicht die Erweiterung der täglichen Lösung. Die Untersuchungen zeigen auch, dass es ist empfehlenswert jedes zusätzliche Paar in einem inklinierten Orbit zu fliegen.

Der Klimawandel ist eine der größten Herausforderungen unserer Zeit ist. Einer der beobachtbaren Effekte sind intensivierende Extremwetterereignisse. Die Überwachung der Massenänderung mit erhöhter räumlicher und zeitlicher Auflösung sowie verbesserter Messgenauigkeit schafft die Möglichkeit in fast Echtzeit prozessierte Schwerefelder für Anwendungen zu verwenden. Ein Algorithmus zur Erkennung von Überschwemmungen hat aufgezeigt, dass abhängig von der Signalstärke und räumlicher Ausdehnung, die Detektion ausschließ aus Schwerefeldern möglich ist.

Contents

List of Figures	ix
List of Tables	x
Acronyms and Abbreviations	xi
1. Earth's gravity field from satellites	3
1.1. Measuring gravity	4
1.1.1. On or near Earth	5
1.1.2. From satellites	5
1.2. Dedicated gravity satellite missions	8
1.2.1. CHAMP	8
1.2.2. GRACE/GRACE-FO	9
1.2.3. GOCE	9
1.3. Next generation gravity missions	10
1.3.1. Mission configurations	12
1.3.2. Science and mission requirements	14
1.3.3. From science to services	15
2. Research objectives	19
2.1. Motivation and scope	19
2.2. Research questions	20
2.2.1. GRACE-like vs. NGGM constellation	21
2.2.2. Multi-pair constellations	21
2.2.3. NRT processing	22
2.2.4. NRT data applicability	22
2.3. Publications	23
3. Gravity field processing	25
3.1. Gravity field estimation	25
3.1.1. Forces acting on the satellite	26
3.1.2. Functional model	28
3.2. Least-squares adjustment	30
3.2.1. Data weighting	32

Contents

3.2.2. Parameter elimination	32
3.2.3. Sequential LSA	33
3.2.4. Wiese approach	33
3.3. Simulation	34
3.3.1. Set-up	35
4. Results	41
4.1. GRACE-like vs. NGGM constellation	41
4.2. Multi-pair constellations	42
4.3. NRT processing	43
4.4. NRT data applicability	43
5. Discussion	45
5.1. Understanding the Earth	46
5.1.1. Hydrological cycle	47
5.1.2. Climate change	49
5.2. Observing water	52
5.2.1. Contributions of GRACE/GRACE-FO	53
5.2.2. Current Drawbacks	55
5.2.3. Possibilities with a NGGM	56
5.3. Operational satellite systems	58
5.3.1. Performance requirements	59
5.3.2. Future gravity data	60
5.4. Geodesy, gravity and societal needs	60
6. Conclusions and Outlook	63
6.1. Conclusions	63
6.2. Outlook	64
Bibliography	67
A. Publications	81
A.1. P-I: Consistent quantification of the impact of key mission design parameters on the performance of next-generation gravity missions	81
A.2. P-II: Triple-pair constellation configurations for temporal gravity field retrieval	105
A.3. P-III: Next generation gravity missions: near-real time gravity field retrieval strategy	129
A.4. P-IV: Applicability of NGGM near-real time simulations in flood detection	151

List of Figures

1.1.	Two representations of Earth with the radial component exaggerated: (a) Topography, geometric height, relative to the mean sea-level and (b) Geoid, a surface of equal gravity potential, representing a mean sea-level relative to a best fitting ellipsoid	4
1.2.	The principles of SGG (a) and LL-SST (b). Image Credit: Rummel (2002)	7
1.3.	Dedicated gravity satellite missions: (a) GRACE, observing the changing distance between the satellites. Image Credit: NASA/JPL; (b) GOCE, measuring Earth’s static gravity field and ocean at the highest accuracy. Image Credit: Airbus/ESA	10
1.4.	Single pair SFF constellations for NGGMs: (a) In-line formation flight; (b) Pendulum formation flight; (c) Wheel-type formation flight.	13
1.5.	Double pair SFF constellations for NGGMs: (a) In-line pair with pendulum satellite; (b) Bender-type double pair; (c) MOBILE concept.	14
1.6.	Scientific (yellow) and societal (blue) applications. Image Credit: Pail et al. (2015)	18
3.1.	Gravity field simulation flowchart	38
5.1.	Schematic illustration of the hydrological cycle on the Earth. The water storage in total volume (km^3) is indicated in the boxes. Image Credit: Oki et al. (2004)	48
5.2.	Influence of humans on the water cycle. Image Credit: Oki (2006)	49
5.3.	Observed monthly temperatures (black) and estimated human-caused warming (red) relative to 1850-1900. Image Credit: IPCC	50

List of Tables

1.1. Summary of generic missions by Dickey et al. (1997) expanded by realisation.	8
A.1. Contribution to P-I	82
A.2. Contribution to P-II	106
A.3. Contribution to P-III	130
A.4. Contribution to P-IV	151

Acronyms and Abbreviations

ACC	accelerometer
ADDCON	Additional Constellation and Scientific Analysis Studies of the Next Generation Gravity Mission
AO	atmosphere and ocean
AOHIS	atmosphere, ocean, hydrology, ice and solid Earth
ARMA	autoregressive-moving average
CHAMP	Challenging Minisatellite Payload
CM	center of mass
DLR	Deutsches Zentrum für Luft- und Raumfahrt
DORIS	Doppler Orbitography and Radiopositioning Integrated by Satellite
d/o	degree and order
EC	European Commission
EFAS	European Flood Awareness System
EO	Earth observing
EOP	Earth Orientation Parameters
EGSIEM	European Gravity Service for Improved Emergency Management
ESA	European Space Agency
ESM	Earth System Model
EU	European Union
EUMETSAT	European Organisation for the Exploitation of Meteorological Satellites
EWH	equivalent water height
GFZ	Geoforschungszentrum Potsdam
GHG	greenhouse gas

Acronyms and Abbreviations

GIA	glacial-isostatic adjustment
GIDMaPS	Global Integrated Drought Monitoring and Prediction System
GLDAS	Global Land Data Assimilation System
GLOFAS	Global Flood Awareness System
GLONASS	Globalnaja nawigazionnaja sputnikowaja sistema
GNSS	Global Navigation Satellite System
GOCE	Gravity field and steady-state ocean circulation explorer
GPS	Global Positioning System
GRACE	Gravity Recovery and Climate Experiment
GRACE-FO	Gravity Recovery and Climate Experiment Follow-On
HIS	hydrology, ice and solid Earth
HL	high-low
HL-SST	high-low satellite-to-satellite-tracking
IAPG	Institute of Astronomical and Physical Geodesy
ICGEM	International Centre for Global Earth Models
IERS	International Earth Rotation and Reference Systems Service
InSAR	Interferometric synthetic aperture radar
IPCC	Intergovernmental Panel on Climate Change
IUGG	International Union of Geodesy and Geophysics
KBR	K-Band ranging
LEO	low Earth orbit
LL	low-low
LL-SST	low-low satellite-to-satellite-tracking
LRI	laser-ranging interferometry
LSA	least squares estimation
MEO	medium Earth orbit
MOBILE	mass variation observing system by high-low inter-satellite links
MWI	microwave instrument

NASA	National Aeronautics and Space Administration
NEQ	normal equation
NGGM	next generation gravity mission
NRT	near-real time
MEO	medium Earth orbit
OT	ocean tide
PECE	Predict-Evaluate-Correct-Evaluate
RFPI	Reager's Flood Potential Index
SAR	Synthetic Aperture Radar
SC4MGV	Satellite Constellations for Monitoring the Variations in Earth Gravity Field
SFF	satellite formation flight
SG	superconductive gravimeter
SGG	Spaceborne Gravity Gradiometry
SGGE	Extended Spaceborne Gravity Gradiometry
SH	spherical harmonics
SSI	satellite-to-satellite interferometry
SLR	satellite laser ranging
SST	satellite-to-satellite tracking
TUM	Technical University of Munich
TWS	terrestrial water storage
TWSA	terrestrial water storage anomaly
US	United States of America
VLBI	Very Long Baseline Interferometry
ZKI	Center for Satellite Based Crisis Information

The following dissertation was written to achieve the goal of a PhD. It is of cumulative form. The synoptic overview and discussion are specifically written with the educated layman in mind as a starting point into the fascinating topic of satellite gravimetry.

The published scientific papers are in the annex for deeper insights.

Chapter 1.

Earth's gravity field from satellites

Gravity is the force that attracts a body towards another. It is determined by the mass of an object. The more mass an object has, the stronger is its gravitational pull towards its centre. On Earth's surface it is about 9.8 m s^{-2} . The exact acceleration g varies depending on latitude by about 0.5%, from approximately 9.78 m s^{-2} at the equator to 9.83 m s^{-2} at the poles, due to the Earth flattening and rotation. The distribution of matter within Earth determines the gravity at a certain location on Earth.

Earth's geophysical system and therefore gravity field are not static. Processes like the global water cycle, ice melting, sea-level rise, ocean circulation, and tectonics are responsible for mass redistributions in the Earth system. They thus are translating into temporal changes of the gravity field of the Earth. The redistribution of the masses of solid Earth, ice shields, oceans and even atmosphere cause local and regional variations in the order of 10^{-5} and smaller.

The Earth itself is part of our solar system. Sun, Earth, and Moon are held together by gravity. The Moon is orbiting the Earth approximately once per month, while the Earth orbits the Sun once per year leading to interactions caused by the gravitational pull of the Moon and Sun on the Earth's body.

Examples of different gravity signal change magnitudes listed by Neumeyer (2010) are

- Gravity difference due to Earth's oblateness (equator-pole): $5 \times 10^{-2}\text{ m s}^{-2}$
- Difference due to elevation (high mountain-deep sea): up to $5 \times 10^{-2}\text{ m s}^{-2}$
- Tidal effects due to Moon and Sun expressed in acceleration: $3 \times 10^{-6}\text{ m s}^{-2}$
- Terrestrial mass displacements: in the order of 10^{-7} m s^{-2}

Measuring gravity and the gravity potential is essential to geodesy, the science of measuring and understanding the Earth's fundamental properties: its geometric shape, orientation in space and gravitational field as well as their variations (see Figure 1.1). It is advantageous to monitor time-variable gravity fields globally and continuously as it

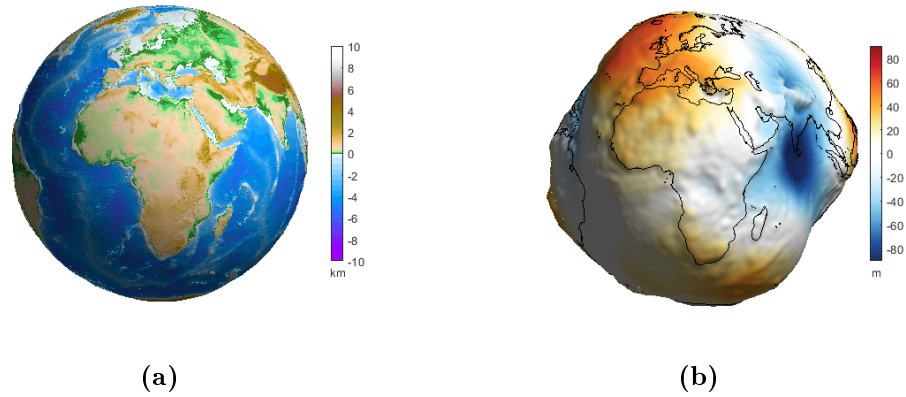


Figure 1.1.: Two representations of Earth with the radial component exaggerated: (a) Topography, geometric height, relative to the mean sea-level and (b) Geoid, a surface of equal gravity potential, representing a mean sea-level relative to a best fitting ellipsoid

provides a unique observation to study and monitor mass redistributions in the Earth system.

1.1. Measuring gravity

Newton's second law of motion states that the force \mathbf{F} applied to a body is proportional to its acceleration \mathbf{a} :

$$\mathbf{F} = m_i \cdot \mathbf{a}. \quad (1.1)$$

The mass m_i is also called inertial mass. This means, the distance of the fall of the object is proportional to the time required for its fall.

When the acceleration is due to gravitational attraction, the acceleration \mathbf{a} is replaced by gravitational acceleration \mathbf{g} derived from Newton's law of universal gravitation:

$$\mathbf{F} = m_g \cdot \mathbf{g}, \quad (1.2)$$

where m_g is the gravitational mass.

While the definitions of mass in Equation 1.1 and 1.2 are different, Einstein’s equivalence principle requires that inertial mass and gravitational mass are equal. The MICROSCOPE satellite mission has found an agreement of $m_g = m_i$ within the a precision of 10^{-15} (Touboul et al., 2017). Accordingly, the gravitational acceleration is the acceleration of the free fall of an object in vacuum.

1.1.1. On or near Earth

We can measure gravity in two primary ways. An absolute gravimeter measures the magnitude of the entire gravity field. In comparison, a relative gravimeter observes the difference of gravity between two locations.

Historically, gravity on Earth was measured using a pendulum and a clock. A more precise method is to time the free fall of an object. Current absolute accelerometers drop an object inside a vacuum chamber and monitor the free-fall trajectory very accurately using a laser interferometer. Repeated observations taking up to 50 hours are necessary to achieve an accuracy of about 10^{-8} m s^{-2} . Terrestrial gravimetry is therefore very costly, labour intensive, and inherently, resulting in a low temporal-spatial resolution. (Niebauer et al., 1995)

The most sensitive relative gravimeter with the lowest drift rate is the superconductive gravimeter (SG). It is used to measure gravity effects with low signal amplitude and temporal resolutions from minutes to years. Neumeyer (2010) estimated the performance at approximately $10^{-11} \text{ m s}^{-2}$.

Terrestrial gravity measurements observe changes of the local gravity field very accurately. However, it is not possible to link or combine ground-based gravity measurements precisely globally. Global solutions are only possible with regionally varying accuracy, due to inconsistent observations, the height problem and large unobserved areas, such as the oceans.

Larger areas are observable if we conduct gravity observations on ships or aeroplanes. It measures the sum of the gravity as well as the inertial acceleration of platforms motions. Air- and shipborne gravimetry determines gravity variations between positions along the trajectory of their moving platform. Due to the impact of the relatively large noise, the biggest challenge of the technique is, to extract tiny accelerations of gravity field changes.

1.1.2. From satellites

Since the first satellite Sputnik measurements from and to space opened new possibilities, as satellites fall around the Earth predominantly determined by Earth’s gravity

Chapter 1. Earth's gravity field from satellites

field. From its weak radio signals, it was possible to determine Earth's oblateness more accurately, than by terrestrial triangulation observations from over 150 years (Merson and King-Hele, 1958, Buchar, 1958). 1959 the first zonal spherical harmonics (SH) coefficients were determined (O'Keefe et al., 1959), Kozai (1961) and Izsak (1963) published the first set of tesseral SH. During the same time, more and more satellites were launched and the observation techniques improved to microwave tracking and satellite laser ranging (SLR), which measures the round trip time of a laser pulse between ground station and satellite.

In the late eighties Global Navigation Satellite System (GNSS), a general term for the American system Global Positioning System (GPS), the Russian system GLONASS, and nowadays the European system Galileo and the Chinese system Beidou, was introduced. These satellite constellations are in an orbit altitude of 20.000 km to 25.000 km, also called medium Earth orbit (MEO). This altitude allows for a global coverage with approximately 30 satellites and also a dampened influence of the gravity field onto the orbit of the satellites.

Altimeter satellite missions like Topex/Poseidon (Bertiger et al., 1994, Schutz, 1997) are flown with an altitude of approximately 1000 km. These satellites in near-Earth orbits can use GNSS for positioning. Due to the low orbit, the perturbations due to the Earth's gravity field in orbit are more significant, and it became possible to monitor the low-frequency gravity field from high precision orbits on a global scale for the first time (Balmino et al., 1976, Lerch et al., 1979). With the launch of dedicated gravity satellite mission, a new era of observing high-resolution gravity fields began.

Satellite-based observations

All satellite-based gravity missions are based on the principle of a differentiator in order to counteract signal attenuation with altitude. This differentiation can be implemented with different sensors and baselines. The actual performance of a system is a combination of its configuration and the accuracy of the main observable.

The Spaceborne Gravity Gradiometry (SGG) concept uses the fact that the center of mass (CM) of a satellite is weightless. However, when the accelerometer is a short distance away from the CM, differential gravity forces occur. If on each axis, a pair of accelerometers is placed, acceleration differences can be measured. This observable is a direct measurement of the gravity field of the Earth and the angular momentum of the satellite. The baseline of a SGG is approx. 50 cm.

When the satellite-to-satellite tracking (SST), meaning a range or range-rate observation between two satellites, is the primary measurement system three possible missions were conceptualized: When measuring orbital perturbations by exploiting the high-low (HL) Microwave Tracking (also known as GNSS), the main observable is the perturbed orbit

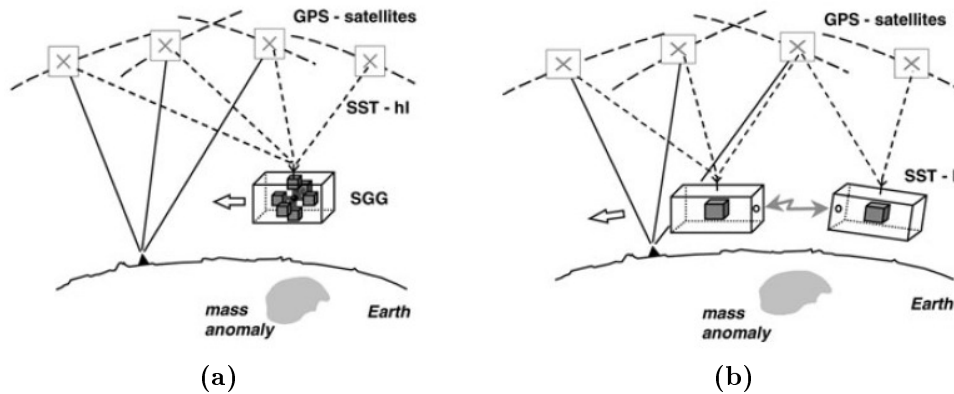


Figure 1.2.: The principles of SGG (a) and LL-SST (b). Image Credit: Rummel (2002)

in centimetre accuracy, giving the weakest performance of the different SST mission concepts. The baseline of the observable can be extended even further towards geostationary satellites as, e.g. Hauk et al. (2017) has analysed. The SST concept can also be implemented between a low Earth orbit (LEO) and a dedicated MEO in an orbit of approximately 10.000 km height (Hauk and Pail, 2019). A low-low satellite-to-satellite-tracking (LL-SST) concept has a shorter baseline of 100 km to 250 km between two satellites in the same orbital plane. The observation geometry is limited, as the observation is always along-track. The performance is improved as the main observable between the satellites has a shorter baseline and is observed with at least micrometre accuracy (c.f. Figure 1.2).

Generic mission concepts

In Dickey et al. (1997) the Committee on Earth Gravity from Space evaluated the potential of generic concepts for dedicated gravimetry missions based on the SGG and SST observations. Within the gradiometry missions, two mission concepts are described as options. SGG missions have only short lifetimes, due to their low orbits. Extended Spaceborne Gravity Gradiometry (SGGE) has a potentially extended lifetime of up to 5 years due to a miniaturized gradiometer. The simplest version of a SST mission is continuously exploiting the GNSS observable aided with the measurement of the non-gravitational forces by an accelerometer (ACC) in the CM of the satellite. As the determination of the gravity field from the orbit only is not very precise, the SST component can be improved, when a pair of satellites is used. The generic missions, according to the report, expanded by the current information of realisation, can be found in Table 1.1.

Apart from the SGGE mission concept all generic missions have been realised by various

Table 1.1.: Summary of generic missions by Dickey et al. (1997) expanded by realisation.

Mission type	Primary Measurement	Ancilliary Equipment	Altitude (km)	Duration (years)	Readiness (1997)	Realisation (2019)
GNSS	HL-SST	ACC	400	5	Current	CHAMP (2000-2010)
SST	LL-SST (Microwave)	ACC	400	5	Mature	GRACE (2002-2017)
SGG	Gradiometer	GNSS	300	0.75	Mature	GOCE (2009-2013)
SSI	LL-SST (Laser)	ACC	400	5	Future?	GRACE-FO (2018-?)
SGGE	Gradiometer	GNSS	400	5	Future?	-

space agencies. The Gravity Recovery and Climate Experiment Follow-On (GRACE-FO) includes the satellite-to-satellite interferometry (SSI) mission concept of a SST laser link as a technology demonstrator.

1.2. Dedicated gravity satellite missions

Since the launch of dedicated gravimetry missions such as Challenging Minisatellite Payload (CHAMP), Gravity field and steady-state ocean circulation explorer (GOCE), Gravity Recovery and Climate Experiment (GRACE) and GRACE-FO the Earth’s gravity field and its temporal variations are monitored, with a short gap from 2017 to 2018, continuously since 2000.

1.2.1. CHAMP

CHAMP (Reigber et al., 1999) was the first LEO satellite mission dedicated to observing the gravitational field of the Earth. It was initiated by Geoforschungszentrum Potsdam (GFZ) and operated by Deutsches Zentrum für Luft- und Raumfahrt (DLR). The satellite was launched in 2000, had a nominal lifetime of 5 years, but operated for ten years. The main objective was to collect simultaneously highly precise gravity and magnetic field measurements and to use the mission for atmospheric and ionospheric research. The missions primary observation system was a high-low satellite-to-satellite-tracking GNSS receiver combined with an accelerometer to measure the non-conservative forces acting on the satellite. While CHAMP was initially planned for determining the low- to medium-frequency wavelengths of the static gravity field up to $n_{max} = 100$, it was also possible to estimate low-frequency time-variable signals up to $d/o = 10$.

1.2.2. GRACE/GRACE-FO

GRACE, see Figure 1.3a, a satellite mission led by National Aeronautics and Space Administration (NASA) with contributions of DLR and GFZ was launched in 2002 (Tapley et al., 2004). The mission surpassed the nominal lifetime of five years by ten years and was decommissioned in 2017 after a battery failure in one of the satellites. GRACE consisted of two identical spacecraft flying approximately 220 km apart in a near-polar orbit at an initial altitude of 500 km and decaying altitude during the mission. Its main objective was to accurately map temporal variations in Earth's gravity field caused by geophysical as well as climate-driven processes. The main measuring unit was the microwave ranging system between the two satellites, combined with GNSS and accelerometer sensors. These observations allow for the recovery of the static gravity field to a spatial resolution of a approximately 150 km kilometres, and a time-variable gravity field with sub-monthly time resolution.

The observed dataset during its mission lifetime enabled the user community to observe various geophysical processes and enabled applications in a wide spectrum of related fields of research. The gravity variations studied by GRACE include hydrological processes (Rodell et al., 2009, Tiwari et al., 2009, Wouters et al., 2011, Lambert et al., 2013), ice mass loss (Luthcke et al., 2013, Velicogna et al., 2014), sea-level rise (Willis et al., 2010, von Schuckmann et al., 2016, Nerem et al., 2018), atmospheric circulation (Hanna et al., 2013, Forootan et al., 2014), changes of the solid Earth-like earthquakes (Han et al., 2010, Tanaka and Heki, 2014), and their interaction.

The successor mission GRACE-FO, launched in 2018, carries on to continuously monitor Earth's time-variable gravity field. The design is based on the GRACE satellites. The sensors are slightly modified compared to GRACE, and a laser-ranging interferometry (LRI) sensor as a technology experiment is added with a minimum operating time of at least one year for improved monitoring.

Due to an anomaly in the microwave instrument (MWI) on one of the GRACE-FO satellites, a switch to the backup unit became necessary. Also, one of the accelerometers started shortly after the launch to perform not according to the specifications. Therefore, a transplant data product from the other satellite has to be used, similar to the last phase of GRACE, leading to a slightly lower performance (Flechtner et al., 2017).

1.2.3. GOCE

In March 2009 the European Space Agency (ESA) Earth Explorer mission GOCE, visualized in Figure 1.3b, was launched (Rummel et al., 2011). After almost triple the nominal mission lifetime, the satellite re-entered the Earth's atmosphere in 2013. The satellite flew in a LEO orbit of 270 km to 224 km during its last mission cycle, to increase



Figure 1.3.: Dedicated gravity satellite missions: (a) GRACE, observing the changing distance between the satellites. Image Credit: NASA/JPL; (b) GOCE, measuring Earth's static gravity field and ocean at the highest accuracy. Image Credit: Airbus/ESA

its sensitivity towards the Earth's gravity field. GOCE's main mission was to determine the global static gravity field in geoid heights with an accuracy of 1 cm to 2 cm at a spatial resolution of 100 km half-wavelength, corresponding to d/o 200 in terms of SH. The mission's main sensor was a three-axis gradiometer measuring acceleration differences along a baseline of 0.5 m. Additionally, an active drag compensation and an angular control to maintain its low orbit were on board.

GOCE is complementary to GRACE. The GRACE mission aims at wavelengths down to 400 km (Visser, 1999) allowing to monitor gravity variations caused by, e.g. ice mass melting and rising sea-level, making the mission invaluable for climate monitoring. However, due to the observation geometry, the distance between the satellites and their altitude, the spatial resolution is limited. GOCE in comparison aims at measuring the static gravity field with the maximum possible spatial resolution down to 70 km to 80 km, which is why a low orbit was chosen for the mission, ultimately limiting the mission lifetime (Bouman et al., 2013).

1.3. Next generation gravity missions

The successful monitoring of the Earth's gravity field by dedicated gravity satellite missions summarized in section 1.2, inevitably raises the question of how to monitor the Earth in the future. Particularly, in the case of GRACE/GRACE-FO, the importance of a continuous time series for a climatological relevant time series is evident. Mass redistribution especially monitored via a global observing system, is a unique observation. NASA's positioning paper "2017-2027 Decadal Survey for Earth Science and

1.3. Next generation gravity missions

Applications from Space"¹ marks mass change as as one of five unique measurements, and assigned high priority.

A future mission should, however, continue not only the observations but also improve the spatio-temporal resolution and at best solve the shortcomings of the successor missions. As increasing the spatial and temporal resolutions are contradictory goals, a compromise has to be found. Especially, as the financial aspect has to be considered as well, a compromise between science and service for society has to be reached.

As there are different aspects and goals for future next generation gravity missions (NGGMs), the following list details the reason as well as a priority for the different goals.

- **Continuity** of the time-variable gravity field monitoring is at the moment the highest priority to enable predictions of the climate. Also, climatological statements should only be made with time series of 30 and more years, because longer periods reduce the chance of distortions due to specific trends. As the gap between GRACE and GRACE-FO has shown, it is only at a low level possible to bridge the gap with other satellite missions and observations (Weigelt et al., 2017). Therefore the decision to prepare for the next satellite mission has to be taken soon, as GRACE-FO has according to prediction a shorter lifetime compared to GRACE. A gravity mission may be a unique observable of the system Earth. However, as long as the observing system does not become a service for the public, the decision about its continuation will always be based on the current priorities in space politics.
- As GRACE-FO is an almost identical successor mission based on GRACE the next step regarding an improved **spatial and temporal resolution** is, after securing the next mission, the next most important goal. Various studies have looked at different constellation designs (Elsaka et al., 2013), see section 1.3.1 for more information. As the best option, a Bender-double pair constellation consisting of a near-polar pair and an inclined pair was identified. This constellation does not only improve the **observation geometry** with the inclusion of the inclined pair, but due to the second pair, a higher spatio-temporal resolution is possible.
- Of similar importance is the **improvement of background models**. Especially, the use of ocean tide models leads to the introduction of an additional error source. Also, models, to separate the signal content from atmosphere, ocean, hydrology, ice and solid Earth (AOHIS) into the individual signals are necessary. The goal to improve the models can be achieved in parallel to the analysis of gravity field data.

¹2017-2027 Decadal Survey for Earth Science and Applications from Space, <http://nas-sites.org/americasclimatechoices/2017-2027-decadal-survey-for-earth-science-and-applications-from-space/>. Retrieved 5.12.2019.

1.3.1. Mission configurations

CHAMP was the first successful dedicated gravity mission but was heavily restricted due to the observation system. GRACE was the first dual-satellite mission in a leader-follower configuration performing satellite formation flight (SFF) to achieve its relative measurement. Two factors are limiting the mission performance. The atmosphere and ocean (AO) and ocean tide (OT) signals are undersampled, leading to aliasing errors and the need to use de-aliasing products. Also, its inherent anisotropic observation geometry is problematic.

While there are different observation concepts, as introduced in Section 1.1.2 and 1.2, the following analysis is based on concepts derived from the GRACE mission. There are three possibilities to increase the performance of a NGGM compared to GRACE: To improve the sensitivity of the observable beyond the limiting along-track direction, to add another satellite/satellite pair and correspondingly more observations or to increase the performance of the instrumentation, especially of the accelerometers.

Inline, Wheel-type, Pendulum pairs

Various studies by Sneeuw et al. (2008), Wiese et al. (2008), Elsaka et al. (2012), Iran Pour et al. (2013) have analysed the performance of various single-pair missions.

GRACE flies in the **in-line** formation (see Figure 1.4a), meaning that the two satellites fly on the same orbit. The gravity field is measured in the along-track direction only.

In the **Pendulum-type** formation flight the two satellites fly on slightly different intersecting orbits, with different inclination or ascending nodes (see Figure 1.4b). The gravity field signal is sampled alternatively in the along-track and cross-track direction. A minimum distance is observed at the poles and a maximum distance at the equator.

The **Wheel-type** formation consists of a satellite pair performing a 2:1 relative elliptical motion (i.e. the semi-major axis has twice the size of the semi-minor one, see Figure 1.4c) about their centre of mass, providing along-track and radial gravity information. If the formation is flown in an inclined orbit, all components of the gravity fields are observed.

Both Wheel- and Pendulum-type formation are demanding regarding the necessary inter-satellite link. The orbits have to be corrected with manoeuvres continuously to sustain the formation over a long period, leading to higher consumption of fuel and accordingly less mission lifetime.

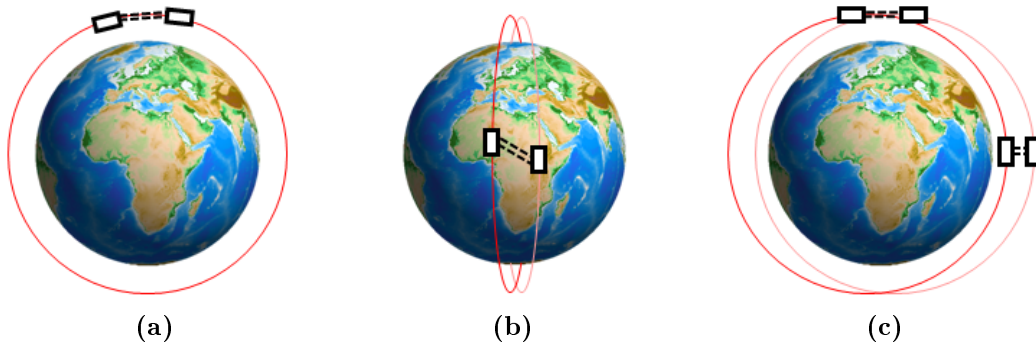


Figure 1.4.: Single pair SFF constellations for NGGMs: (a) In-line formation flight; (b) Pendulum formation flight; (c) Wheel-type formation flight.

Double-pair, Multi-satellite

To obtain a useful spatio-temporal resolution, a Pendulum-type pair can be supplemented by another satellite (see Figure 1.5a). The configuration establishes a second baseline from one of the baseline in-line pairs towards the Pendulum satellite. The sensors observe the along-track component via the in-line pair and the across-track component with the addition.

Bender et al. (2008), Wiese et al. (2011a,b) investigated the possibility of flying two pairs adding an inclined flying satellite pair to a near-polar satellite pair, called Bender design (see Figure 1.5b). This formation allows for faster and more homogeneous sampling of the gravity field, providing higher spatial resolution and reduced temporal aliasing.

The mass variation observing system by high-low inter-satellite links (MOBILE) concept by Pail and Team (2018) proposed in comparison a different observation concept of a high-low tracking (see Figure 1.5c) with μm precision between one LEO and two MEO's as well as new instrumentation (Hauk and Pail, 2019).

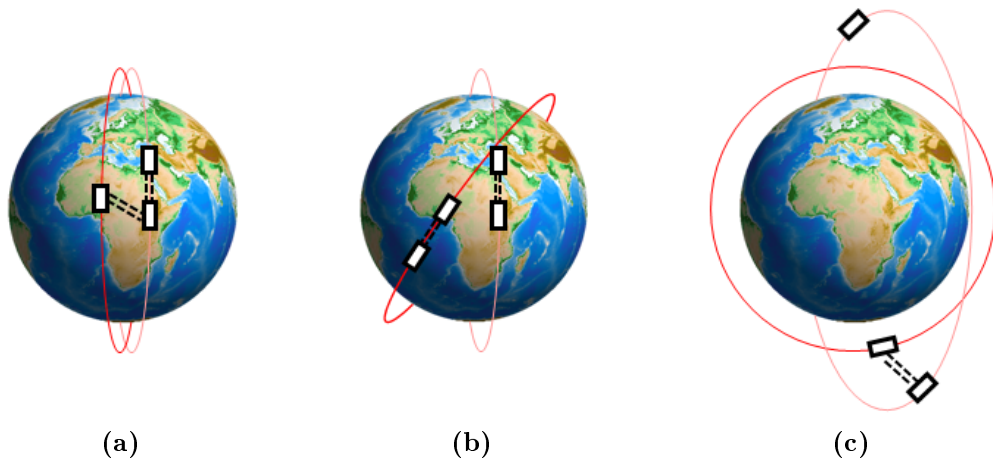


Figure 1.5.: Double pair SFF constellations for NGGMs: (a) In-line pair with pendulum satellite; (b) Bender-type double pair; (c) MOBILE concept.

As Elsaka et al. (2013) states, from a technological point of view missions with no or only minor relative motion between the satellites are easier to realize. For such a mission, only a loose SFF is necessary, and the formation is already tested. However, the choice of a double-pair mission also means an increased cost. Formations with relative motion between the satellites add the need to have a formation control.

1.3.2. Science and mission requirements

Satellite missions have general mission objectives. Global coverage is targeted, meaning a near-polar orbit of at least one satellite (pair). A minimum mission duration of 5 years is preferred to justify the high costs of a satellite mission. Lastly, the aim is an orbit ground track, that allows for a high spatio-temporal resolution. The required accuracy and spatio-temporal resolution are based on the specific needs of science and society.

The aim of a NGGM is to improve our understanding of the time-variable geophysical processes and their role in the system Earth. Each process and signal needs a specific spatial and temporal resolution as well as a required accuracy to be observable.

In the AOHIS component hydrology, various signals of different spatial and temporal resolution as well as magnitude are accumulated. The necessary time scales usually depend on the usage of the data: short temporal resolutions from hourly to daily for prediction and applications in an early warning system to monthly and yearly, for monitoring of geophysical signals and climatological studies.

1.3. Next generation gravity missions

- **Groundwater storage** changes are a slow process with peaks in the summer periods, where groundwater extraction for farming reaches the highest levels. For that reason monthly to yearly temporal resolutions with a spatial scale up to 1000 km is sufficient.
- **Surface water bodies** are in most cases quite small, meaning a spatial resolution of a few kilometres with a high temporal resolution is necessary to enable the prediction of floods. Although their spatial expansion is rather small, the magnitude of the signal change is up to 10 m in equivalent water height (EWH). EWH is the interpretation of the mass change as a thin layer of water change near the Earth's surface.
- **Soil moisture** is an important variable in the climate system and relevant to predict droughts and floods accurately. The expected signal change is up to 40 cm in EWH with a spatial resolution of up to a few 100 km, on time scales from hourly to monthly.
- The temporal resolution of **snow fall and melt** depends on the application. However, in any case, a spatial scale from a few tens up to a few 100 km is a necessity. This observation is of special interest for weather forecasts and early warning systems.
- **Precipitation and evapotranspiration** is a local quantity with only a magnitude of a few centimetres on a spatial scale of less than 100 km.

All these signals are necessary to close the water cycle and understand the processes of water exchange between the sub-systems. This information is needed to manage the water resources and enable valuable information for (extreme) weather forecasts.

The overall science requirements for future missions are a combination of all processes of the system Earth. To increase the reliability of climate prediction, the monitoring of the evolution of ice sheets and glaciers is important. Oceans are monitored to predict sea-level change. To develop an algorithm to detect pre-seismic earthquake signals of the solid Earth are of interest. For geodetic applications like the aim to unify the height systems, improved performance is necessary. These science needs and mission goals have been collected by various studies e.g. ESA (2010, 2011), Panet et al. (2013), Gruber et al. (2014), Pail et al. (2015).

1.3.3. From science to services

Derived from the science and user needs Pail et al. (2015) have extracted standard requirements for a mission requirement. From a scientific standpoint, an increase in the spatio-temporal resolution is essential. If a service for society is targeted, continuous

Chapter 1. Earth's gravity field from satellites

observations and a consistent performance is a requirement, only possible with stable technology and an improved constellation.

GRACE data has been analysed with regard to a range of geophysical processes (see Section 1.2.2). The satellite mission allowed for the first time to observe developments consistently on a large and even global scale. Rodell and Famiglietti (1999) proved the detectability of variations of the continental water storage from time variable gravity fields. The water storage change over landmasses captured by GRACE is a useful indicator of climate variability and the human impact on the environment. Lettenmaier and Famiglietti (2006) write that the data from GRACE benefits the study of the hydrological cycle as the data helps to close Earth's water balance.

As both droughts and floods are costly natural disaster with significant impact, several forecasting and early-warning systems are in place or in development based on different data sources.

European Flood Awareness System (EFAS) is a fully operational observation-based flood monitoring system. Its predictions are based on topographical, meteorological, and hydrological data. The simulated date is assimilated with near-real time (NRT) observation data such as river discharge and water level data and prepared visually on a map (Pappenberger et al., 2011).

The European Union (EU) project FloodMan is a pre-operational NRT flood monitoring system based on space-borne Synthetic Aperture Radar (SAR) and optical data combined with in-situ measurements, hydrological and hydraulic model data (Malnes et al., 2005).

The European Gravity Service for Improved Emergency Management (EGSIEM) project funded by the EU Horizon2020 program, evaluated and established a NRT monitoring based on gravimetric observations. The aim was to provide gravity field solution with a temporal resolution of one day. Another objective was to reduce the latency for gathering the necessary data products. Due to the sparse coverage of GRACE additional geophysical model information is introduced via a Kalman filter least squares estimation (LSA). Also a gravity-based wetness indicator with a 2-day latency (Kvas et al., 2017) that supports the satellite-based flood information service Global Flood Awareness System (GLOFAS) as well as the framework of DLR's Center for Satellite Based Crisis Information (ZKI) was introduced.

The project Global Integrated Drought Monitoring and Prediction System (GIDMaPS) provides drought information combined from multiple drought indices. The information is based satellite- and model-based precipitation data as well as soil moisture data sets (Hao et al., 2014).

Reager and Famiglietti (2009) proposed the Reager's Flood Potential Index (RFPI) to enable a flood monitoring. The index is based on the terrestrial water storage

1.3. Next generation gravity missions

anomaly (TWSA) product derived from GRACE. An evaluation by Molodtsova et al. (2015) found a good agreement between the RFPI flood risks and the observed floods on different spatial scales.

Loon et al. (2017) tested two approaches for estimating groundwater drought in Europe in NRT. The first approach exploited the relationship between meteorological conditions and historic groundwater level observations. The second approach utilizes groundwater anomalies derived from GRACE terrestrial water storage (TWS) and (near-) surface storage simulations by the Global Land Data Assimilation System (GLDAS) models. The GRACE-based detection was found unsuitable for usage in NRT groundwater drought monitoring. The alternative approach is more suitable to quantify groundwater drought in a NRT processing.

NASA provides a weekly groundwater and soil moisture drought indicator² based on gravimetric satellite monthly data sets from GRACE. The drought indicator assimilates GRACE satellite data into a land-surface model and creates a gridded data product (Houborg et al., 2012, Beaudoin et al., 2017).

The presented research and initiatives are an example of the diverse possibilities of the use of gravity satellite missions. In Figure 1.6 major scientific (yellow) and societal (blue) applications are visualized. For the future continuation and success of "gravity", it is of importance to raise awareness in the general public regarding geodesy and gravity field missions, as it is a not well-known field with great potential.

²Drought indicator, <https://grace.jpl.nasa.gov/applications/drought-monitoring/>. Retrieved 5.11.2019.

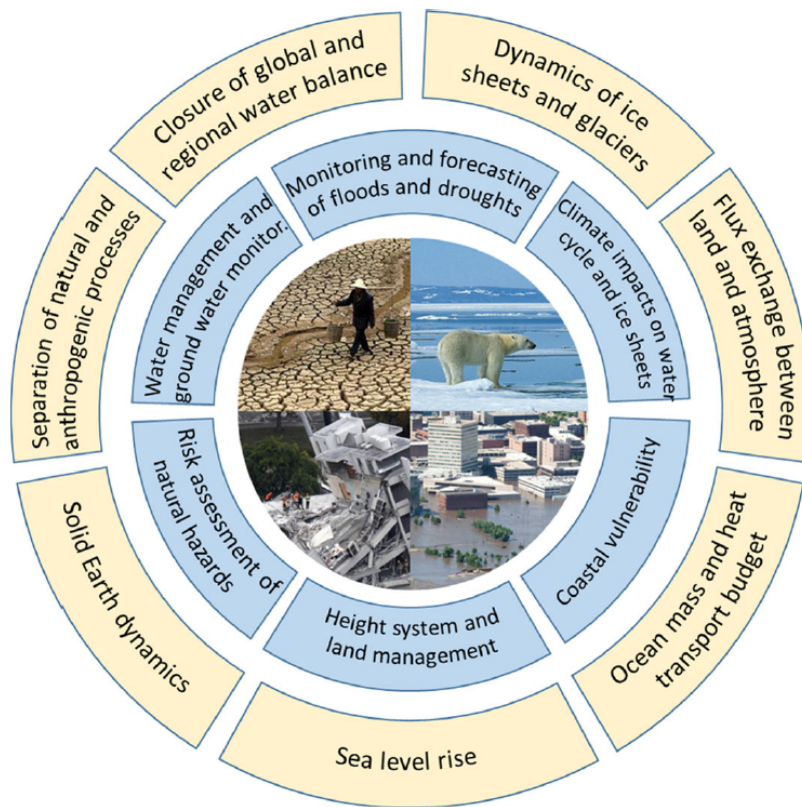


Figure 1.6.: Scientific (yellow) and societal (blue) applications. Image Credit: Pail et al. (2015)

Chapter 2.

Research objectives

The dissertation is of cumulative type since parts of the research and of the results have been published in articles in peer-reviewed scientific journals. This thesis contains the synthesis and synoptic discussion as well as the related publications. The papers are reprinted in the appendix together with a declaration of the contribution of the authors.

2.1. Motivation and scope

Possible NGGMs expected to be launched in the midterm future (2020+) by various space agencies have to meet the following demands: long-term observations to achieve a sustained satellite gravity observation system, an increase of spatial resolution to observe small-scale mass transport phenomena, and an increase of the temporal resolution towards 1 or only a few days (Pail et al., 2015). Numerical simulations of satellite configurations and possible constellations help to design such future missions, which are still fictional at this point.

Additionally, after years of successful exploitation of dedicated gravity missions, the incentive to develop services and applications based on global gravimetric observations of the time-variable gravity field is steadily growing. The aim is to shift the justification of NGGMs away from a solely scientific community driven satellite mission to an operational observing system. Such a system would enable the provision of valuable services for managing Earth's resources like water and the implementation of early-warning system regarding natural disasters like droughts and floods.

NGGM studies consider orbit formations, instrument performance and sensor accuracies as parameters for optimisations. The goal is to mitigate the effect of error sources like sensors, orbit, and coupling errors as well as temporal aliasing, processing and modelling errors. Numerous studies have been investigating the benefits of introducing a second pair of satellites (Wiese et al. (2011c); Wiese et al. (2011a); Loomis et al. (2011)) and

optimizing their formation configuration (Elsaka et al., 2013). Adopting these new concepts for future missions results in a reduction of temporal aliasing errors and improves the error characteristics towards a more isotropic system. Wiese et al. (2011c) introduced a new approach to improve the overall gravity field solution by co-estimating low spatial resolution gravity fields at short time intervals together with a higher resolution gravity field sampled at a longer time interval. Elsaka et al. (2012) studied the potential improvement of SFF gravity field solutions in terms of spherical harmonics truncation of up to degree/order 100, while Murböck and Pail (2014) investigated the design of optimal satellite orbits for temporal gravity retrieval regarding temporal aliasing. Daras and Pail (2017) and Hauk and Pail (2018) presented and analysed a method to co-parametrize ocean tide parameters of the eight main tidal constituents over periods of several years.

ESA commissioned studies of possible future satellite constellations, namely Satellite Constellations for Monitoring the Variations in Earth Gravity Field (SC4MGV) and the subsequent study Additional Constellation and Scientific Analysis Studies of the Next Generation Gravity Mission (ADDCON). The overall objective of these studies is to assess the performance of various constellations of two and more pairs of satellites for the retrieval of time-variable gravity fields. The aim is to overcome the drawbacks in current single-pair gravimetric satellite missions such as GRACE or GRACE-FO.

Based on the available research as a starting point and since the future of dedicated gravity missions is uncertain, the scope of the work is the following:

The dissertation shall answer the question of the performance of possible multi-pair NGGMs based on the GRACE concept and their application as a NRT service provider exemplarily in the field of hydrology.

From this scope the following objectives are derived:

- Improve the basis of decision-making regarding a possible NGGM.
- Quantify the added value of a multi-pair constellation compared to a single pair.
- Propose a NRT processing scheme and demonstrate possible applications for such.

2.2. Research questions

The research goal is split into four parts. Each research question raised is discussed and answered in length within the papers, outlined in section 2.3, and a summary of the main results is provided in Chapter 4. The theoretical background and simulation, which is the basis of the whole thesis, is discussed in Chapter 3, the synoptic discussion can be found in Chapter 5, and the conclusion in Chapter 6.

2.2.1. GRACE-like vs. NGGM constellation

At the moment the GRACE-FO mission is in orbit. Since January 2019 it is operating in science mode. Regarding any future satellite missions, no fixed plans are set yet, leaving a high level of freedom to suggest and if possible, implement a best-case scenario of multiple satellite pairs in orbit. There is a discussion if a GRACE-like scenario should be implemented again or an updated NGGM constellation with two pairs should be considered to enable improvements concerning observation geometry, processing strategies and achievable gravity field performance.

The following questions should help to answer whether a single- or double-pair should be favoured.

1. What are the biggest error sources in gravity field retrieval? Which parameters should be considered and why? What error sources do not play a crucial role in the retrieval?
2. If different input signals are used, is the anticipated improvement/deterioration of the retrieval visible? Which areas of technology, modelling and computation should be considered because of possible improvements?
3. How much does a customised post-processing scheme help? Can the same scheme as for a single-pair concept be used? Which comparison is fair towards each scenario?
4. And finally: What is the recommendation regarding the next gravity satellite mission? Is a GRACE-like or a NGGM constellation preferable? Is the answer to this question depending on factors like retrieval period, error sources or similar?

In addition to improved scientific research, a progression towards services and application is expected. One of the main advantages of a satellite monitoring system is the global and NRT monitoring of the Earth's gravity field.

2.2.2. Multi-pair constellations

As different space agencies look into flying a geodetic gravity mission, a performance analysis of multi-pair scenarios is of interest, to quantify the added value of multiple pairs.

1. What is the optimal constellation when three or more satellites are used? Is there freedom of choice within a range of possible orbits/constellations? Which constellation provides the best temporal and spatial resolution?

2. If the coordination between various operating space agencies proves difficult, what kind of constellation can be expected? What degradation in spatial/temporal resolution would result from it?
3. If a satellite fails or does not provide observations according to the specifications, how does this impact the overall achievable temporal and spatial resolution?
4. How does the maximum daily temporal resolution depend on the number of satellite pairs and various sensor noises?

2.2.3. NRT processing

First NRT schemes have already been implemented based on GRACE/GRACE-FO data. As a NGGM consisting of two satellite pairs would rectify some of the drawbacks of a single-pair mission, a possible NRT processing could increase in performance as well.

1. How could a NRT processing routine be set-up? How can it be realised and implemented? Can the disadvantages of the developed schemes be compensated or removed?
2. What data products are necessary to facilitate NRT processing and how fast are they available? What is the best possible latency that is achievable?
3. What is the lowest time sampling possible for a stable NRT processing?
4. Does a high or low daily parametrization have an impact regarding the overall solution? What conclusion should be drawn from the results?

The NRT scheme had to be implemented in the available software to enable the processing of gravity data in a NRT fashion.

2.2.4. NRT data applicability

As services and applications are of high importance for the future launch of dedicated gravity missions, an analysis regarding future applications of the gravity field data is necessary to assess the potential and possibilities:

1. Which analyses have already been done with gravity data? Are there any NRT services available in the field of AOHIS? Is gravity data already included?
2. How well is NRT gravity field data applicable regarding services and monitoring, such as the detection and possibly even prediction of extreme weather phenomena, droughts, and floods?

3. Is the expected resolution of a multi-pair scenario adequate for the necessary analysis? What are the advantages or possible shortcomings of gravity fields for the envisioned applications? Is the use of a second (complimentary) data source necessary to enable certain applications?

2.3. Publications

Publication I

Consistent quantification of key mission design parameters of next-generation gravity missions

By Anna F. Purkhauser, Christian Siemes, Roland Pail. Published in "Geophysical Journal International".

The publication is dedicated to answering the first research question of the performance of single and double pairs for different altitudes, sensor noises, and input signals. The advantage of a double-pair is the possibility to estimate the whole AOHIS signal. If the AO signal and ocean tide errors are excluded from the simulation, the potential of a double-pair with improved sensors is demonstrated. Even with a tailored post-processing scheme, the single-pair cannot achieve the performance of the double-pair. See A.1.

Publication II

Triple-pair constellation configurations for temporal gravity field retrieval

By Anna F. Purkhauser, Roland Pail. Published in "Remote Sensing", special issue "Geodesy for Gravity and Height Systems".

The publication deals with multi-pair solutions and compares them to a reference double-pair scenario. In the simulations inclined and/or near-polar satellite pairs with GRACE-like or improved (improved ACC, LRI) sensor noise are added and their added value analysed. The potential of a higher parametrized daily solution, one of the main advantages of a multi-pair constellation, is tested and shows a possibility of a maximal degree and order (d/o) of 25 based on the concept. The estimated data products are evaluated using catchments, such as the Amazon or Danube. See A.2.

Publication III

Next generation gravity missions: near-real time gravity field retrieval strategy

By Anna F. Purkhauser, Roland Pail. Published in "Geophysical Journal International".

In this publication, a new approach for a NRT processing scheme is explained. It is a combination of a co-parametrization of low-resolution short-term and higher-resolution longer-term gravity field solutions (Wiese approach) and a sliding window method. In contrast to the already established NRT schemes based on single pairs, the scheme uses no additional data such as information from geophysical models. A simulation shows that a shortening down to 3 days for the overall solution is possible and still delivers stable solutions. See A.3.

Publication IV

Applicability of NGGM near-real time simulations in flood detection

By Anna F. Purkhauser, Julia A. Koch, Roland Pail. Published in "Journal of Geodetic Science".

The applicability of NGGM is an important factor for a new constellation. For the possible detection of floods, a processing scheme is recommended to transform the spatial EWH to a time series that allows for an easy interpretation. The scheme was tested on six months of simulated gravity field data, based on a double-pair scenario. Floods included in the signal component, are later tested using the estimated gravity field. Depending on the signal magnitude, spatial spread and location, the detectability varies. See A.4.

Chapter 3.

Gravity field processing

This chapter addresses the theoretical background of the gravity field estimation, the formulation of the functional model and the main basics of the LSA. The key factors of the simulation and the description of the simulation environment for the gravity field recovery finalize the chapter.

3.1. Gravity field estimation

Newton's law of universal gravity states, that every body attracts every other body by the gravitational force F acting between the two bodies:

$$\mathbf{F} = -G \frac{m_1 m_2}{r^3} \mathbf{r}, \quad (3.1)$$

where m_1 and m_2 are the masses of the two bodies, \mathbf{r} is the relative position vector expressed as $\mathbf{r} = \mathbf{r}_1 - \mathbf{r}_2$, and the Newtonian gravitational constant $G = 6.6743 \text{ m}^3 \text{ kg}^{-1} \text{ s}^{-2}$.

Based on Newton's law of motion, see Equation 1.1, and the law of universal gravity, Kepler's equation of motion in a two-body system can be derived:

$$\mathbf{g} = \frac{\mathbf{F}}{m_1} = -G \frac{m_2}{r^3} \mathbf{r}, \quad (3.2)$$

where \mathbf{r} is a vector pointing from the Earth centre to the satellite.

In the case of a satellite orbiting around the Earth, approximated as a homogeneous sphere with the mass $m_1 = M_E$, the equation can be written as:

$$\mathbf{g} = -G \frac{M_E}{r^3} \mathbf{r}, \quad (3.3)$$

Chapter 3. Gravity field processing

where \mathbf{r} is a vector pointing from the Earth centre to the satellite.

When replacing the simplification of a spherical Earth in Equation 3.3 with constant density by a realistic Earth's body with inhomogeneous density distribution

$$\mathbf{g} = \nabla V, \quad (3.4)$$

V can be expressed by a spherical harmonic series expansion

$$V(r, \varphi, \lambda) = \frac{GM}{a_E} \sum_{n=0}^{n_{max}} \left(\frac{a_e}{r}\right)^{n+1} \sum_{m=0}^n [\bar{C}_{nm} \cos m\lambda + \bar{S}_{nm} \sin m\lambda] \bar{P}_{nm}(\sin \varphi), \quad (3.5)$$

where a_E is the semi-major axis of the Earth, r is the geocentric distance of the satellite and φ , λ are its latitude and longitude. \bar{C}_{nm} and \bar{S}_{nm} are the fully normalized coefficients of a spherical harmonic series expansion of degree n and order m and \bar{P}_{nm} are the fully normalized Legendre polynomials (Hofmann-Wellenhof and Moritz, 2006).

3.1.1. Forces acting on the satellite

The actual path varies from the theoretical two-body path due to perturbations caused by the inhomogeneous density distribution (see Equation 3.5) and resulting variations of the Earth's gravity field, other bodies of mass (Moon, Sun) and additional forces not considered in Keplerian motion.

In case of a perturbed motion, Equation 3.3 takes the form of an inhomogeneous differential equation of second order:

$$\ddot{\mathbf{r}} = \mathbf{g} \quad (3.6)$$

$$\ddot{\mathbf{r}} + \frac{GM_E}{r^3} \mathbf{r} = d\ddot{\mathbf{r}}, \quad (3.7)$$

The perturbing accelerations (acc.) can be expressed as

$$d\ddot{\mathbf{r}} = \underbrace{\ddot{\mathbf{r}}_{et} + \ddot{\mathbf{r}}_{ot} + \ddot{\mathbf{r}}_{nb}}_{\text{conservative acc.}} + \underbrace{\ddot{\mathbf{r}}_{pt} + \ddot{\mathbf{r}}_{drag} + \ddot{\mathbf{r}}_{srp} + \ddot{\mathbf{r}}_{erp} + \ddot{\mathbf{r}}_{gr}}_{\text{non-conservative acc.}} + \ddot{\mathbf{r}}_{other}, \quad (3.8)$$

where $\ddot{\mathbf{r}}_{et}$ is perturbing acceleration due to Earth tides, $\ddot{\mathbf{r}}_{ot}$ due to ocean tides, $\ddot{\mathbf{r}}_{pt}$ due to pole tides, $\ddot{\mathbf{r}}_{nb}$ is the third body attraction, $\ddot{\mathbf{r}}_{drag}$ is the atmospheric drag, $\ddot{\mathbf{r}}_{srp}$

is acceleration due to solar radiation pressure, $\ddot{\mathbf{r}}_{erp}$ is due to Earth radiation pressure (Albedo), $\ddot{\mathbf{r}}_{gr}$ is the effect of general relativity, and $\ddot{\mathbf{r}}_{other}$ represents not modelled or unknown forces.

Direct tides (3rd body)

The satellite itself is affected by the gravitational pull of other celestial bodies relative to that on the Earth's CM. The resulting force acting on the satellite is called direct tidal force $\ddot{\mathbf{r}}_{nb}$. The magnitude of the perturbing acceleration is proportional to the mass of the third body, and inverse proportional to its cube distance. In the case of an Earth-orbiting satellite, like the LEO satellites, Moon and Sun have the most significant impact. Depending on the required precision of the application, the other planets in the solar system can be omitted or not.

Earth and ocean tides

Tides are periodic variations caused by the gravitational forces of the Sun and Moon on the Earth and are categorized into solid Earth and ocean tides. Consequently, these deformations of the Earth affect the motion of the satellite and can be expressed in spherical harmonics.

Solid Earth tides ($\ddot{\mathbf{r}}_{et}$) are the response of the lunisolar pull onto the Earth, leading to time-variable changes of the elastic solid body of the Earth. Time-variable changes resulting from the gravitational pull of the Moon and Sun occurring in the ocean causing cyclic variations in the local sea level are called ocean tides ($\ddot{\mathbf{r}}_{ot}$).

General relativistic effects

According to the general theory of relativity, the Newtonian theory of gravity is only an approximation. For high precision applications correcting terms for the general relativistic effects ($\ddot{\mathbf{r}}_{gr}$) have to be applied.

Non-gravitational forces

Atmospheric drag ($\ddot{\mathbf{r}}_{drag}$) is the resistance, acting on the surface of the satellite caused by Earth's atmosphere and is the largest non-gravitational perturbation for LEO satellites. It results in a decay of the satellite's orbit. The impact of the atmosphere is dependent on solar activity, which influences the atmospheric density. In periods with high solar activity, the satellite decays faster, than during solar minima.

Solar radiation pressure ($\ddot{\mathbf{r}}_{srp}$) results from photons impacting the satellite surface. Its impact depends mainly on the reflective properties and the area-to-mass ratio of the satellite. Additionally, the satellite orbit will be perturbed by the back radiation of the Earth, as Earth reflects on average about 30 % of the solar radiation. It is called Albedo or Earth radiation pressure ($\ddot{\mathbf{r}}_{erp}$).

The changing centrifugal potential due to polar motion causes pole tides ($\ddot{\mathbf{r}}_{pt}$) mainly affecting the geopotential coefficients C_{21} and S_{21} .

3.1.2. Functional model

To enable the estimation of the Earth's gravity field, the SST observations have to be brought into connection with the chosen unknowns. There are several approaches, e.g. the acceleration approach (Reubelt et al., 2003), the energy balance approach (Löcher and Ilk, 2005) and the integral equation approach by Schneider (1969), later adapted by Mayer-Gürr (2006) as the so-called short-arc approach, which is used within this work.

The short-arc approach divides the orbit in short arcs and formulates the satellite's orbit as boundary value problem, creating a relationship between the orbit positions and the parameters of the force models, which have to be integrated twice. The gravity field coefficients have to be parametrized together with the boundary arc positions. Through this formulation, the observed orbit positions can be used directly, avoiding numerical errors through differentiation.

According to Mayer-Gürr (2006) the equation of motion can be expressed in terms of the position of a satellite within an arc

$$\mathbf{r}(\tau) = \mathbf{r}_A(1 - \tau) + \mathbf{r}_B\tau - \underbrace{T_{AB}^2 \int_0^1 K(\tau, \tau') \mathbf{f}(\mathbf{r}(\tau')) d\tau'}_{=\mathbf{h}} \quad (3.9)$$

with the kernel function

$$K(\tau, \tau') = \begin{cases} \tau'(1 - \tau) & \text{for } \tau \leq \tau' \\ \tau(1 - \tau') & \text{for } \tau' > \tau \end{cases}, \quad (3.10)$$

\mathbf{r}_A and \mathbf{r}_B are the start and end position vector of the short arc, $T = t_B - t_A$ denotes the arc length, $\tau = (t - t_A)/T$ is the normalized time, and \mathbf{f} is the sum of the accelerations, see Equation 3.7 and 3.8, acting on the satellite. Equation 3.9 is used for a high-low satellite-to-satellite-tracking (HL-SST) observable, for LL-SST a difference is needed to replicate e.g. the K-Band ranging (KBR) observable, which is a range-rate.

3.1. Gravity field estimation

The formula can be reformulated to be in terms of position differences between two satellites

$$\mathbf{r}^{12}(\tau) = \mathbf{r}_A^{12}(1 - \tau) + \mathbf{r}_B^{12}\tau - T^2 \int_0^1 K(\tau, \tau') \mathbf{f}^{12}(\mathbf{r}(\tau')) d\tau', \quad (3.11)$$

where the indices 1 and 2 represent the two satellites, \mathbf{f}^{12} denotes the difference between the accelerations acting on the different satellites, and $\mathbf{r}_{A/B}^{12}$ is the position difference vector of the two satellites for each boundary point A and B .

As the range rate between the satellites is observed, the relation can be reformulated to velocity by differentiating Equation 3.11 to

$$\dot{\mathbf{r}}^{12}(\tau) = \frac{1}{T}(\mathbf{r}_B^{12} - \mathbf{r}_A^{12}) - T \int_0^1 \frac{\partial K(\tau, \tau')}{\partial \tau} \mathbf{f}^{12}(\mathbf{r}(\tau')) d\tau' \quad (3.12)$$

Projecting the vector onto the line of sight between the two satellites gives the inter-satellite range

$$\rho(\tau) = \|\mathbf{r}^2(\tau) - \mathbf{r}^1(\tau)\| = \mathbf{e}^{12}(\tau) \cdot \mathbf{r}^{12}(\tau) \quad (3.13)$$

where \mathbf{e}^{12} denotes the unit vector in line of sight

$$\mathbf{e}^{12}(\tau) = \frac{\mathbf{r}^{12}(\tau)}{\|\mathbf{r}^{12}(\tau)\|}. \quad (3.14)$$

The same principle is used to formulate the inter-satellite range-rate

$$\dot{\rho}(\tau) = \mathbf{e}^{12}(\tau) \cdot \dot{\mathbf{r}}^{12}(\tau). \quad (3.15)$$

In the case of the short arc approach, the functional model for the boundary values of each arc can be written as

$$\mathbf{l} = \mathbf{B}\mathbf{b} + \mathbf{h}, \quad (3.16)$$

where \mathbf{l} is the observations vector, \mathbf{B} is the matrix with the normalised time values, \mathbf{b} denotes the vector with the arc boundary values and \mathbf{h} is the vector of the integral function of Equation 3.9 or 3.12.

The unknown parameters of the functional model consist of the gravity field coefficients \bar{S}_{nm} and \bar{C}_{nm} in vector \mathbf{x} and the arc boundary values in vector \mathbf{b} .

The relationship in the functional model between the observations and the parameters

$$\mathbf{h} = \mathbf{h}_0 + \mathbf{A}\mathbf{x} \quad (3.17)$$

is achieved through linearization with respect to the unknown parameters \mathbf{x}

$$(\mathbf{A}_{ij}) = \frac{\partial \mathbf{h}(\tau_i)}{\partial x_j}. \quad (3.18)$$

which gives

$$\mathbf{l} - \mathbf{h}_0 = \mathbf{B}\mathbf{b} + \mathbf{A}\mathbf{x}, \quad (3.19)$$

where \mathbf{h}_0 is the reference value for \mathbf{h} . This equation is the linear model to be solved in a LSA, for details see Mayer-Gürr (2006).

3.2. Least-squares adjustment

A LSA is a model to solve an overdetermined system of equations - the full theory on LSA can be looked up in Niemeier (2008) and Jäger et al. (2005). It can also be interpreted as a method for fitting a linear model to observations collected under randomly varying conditions.

The linearised LSA model

$$\mathbf{l} = \mathbf{A}\mathbf{x} + \mathbf{e} \quad (3.20)$$

consists of the design matrix \mathbf{A} connecting the observations \mathbf{l} , e.g. ranges or range-rates between a satellite pair, via a functional model to the unknown parameters \mathbf{x} , e.g. gravity field coefficients. Vector \mathbf{e} is representing the residuals.

The best fit in the least-squares sense is when the sum of the squared residuals (\mathbf{e}) is minimized:

$$\mathbf{e}^T \mathbf{P} \mathbf{e} \rightarrow \text{Minimum}. \quad (3.21)$$

To solve for the unknown parameters $\hat{\mathbf{x}}$ the normal equation (NEQ) system

$$\mathbf{N}\hat{\mathbf{x}} = \mathbf{n}, \quad (3.22)$$

3.2. Least-squares adjustment

consisting of the NEQ matrix expanded by the weight matrix $\mathbf{P} = \sum(e)^{-1}$

$$\mathbf{N} = \mathbf{A}^T \mathbf{P} \mathbf{A}, \quad (3.23)$$

and the right-hand side of the NEQ system

$$\mathbf{n} = \mathbf{A}^T \mathbf{P} \mathbf{l} \quad (3.24)$$

have to be formulated and set-up.

As the functional model is usually a non-linear function, a linearization via expansion into a Taylor series is necessary. Neglecting the higher terms

$$f(\mathbf{x}) = f(\mathbf{x}_0) + \left. \frac{\partial f}{\partial \mathbf{x}} \right|_0 (\mathbf{x} - \mathbf{x}_0) + \dots, \quad (3.25)$$

where $f(\mathbf{x}_0) = \mathbf{l}_0$ is the a priori value of the observation.

The reduced observations, also called "observed-minus-computed", is the difference of the observable and a computed reference value at the Taylor point:

$$\Delta \mathbf{l} = \mathbf{l} - \mathbf{l}_0 = f(\mathbf{x}) - f(\mathbf{x}_0). \quad (3.26)$$

To estimate the corrections the following equation

$$\Delta \hat{\mathbf{x}} = (\mathbf{A}^T \mathbf{P} \mathbf{A})^{-1} \mathbf{A}^T \mathbf{P} \Delta \mathbf{l} \quad (3.27)$$

is used and its result is added to the a priori parameters

$$\hat{\mathbf{x}} = \mathbf{x}_0 + \Delta \hat{\mathbf{x}}. \quad (3.28)$$

3.2.1. Data weighting

When combining two observation types, their different accuracies have to be taken into account. HL-SST have *cm* accuracy and LL-SST observables e.g. *μm* accuracy. There are two options to address this issue. The first is to determine a weighting matrix \mathbf{P} based on the pre-fit residuals. The other weighted combination is by multiplying the LSA elements with their respective variance factor:

$$\mathbf{N} = \frac{1}{\sigma_a^2} \mathbf{N}_a + \frac{1}{\sigma_b^2} \mathbf{N}_b, \quad (3.29)$$

$$\mathbf{n} = \frac{1}{\sigma_a^2} \mathbf{n}_a + \frac{1}{\sigma_b^2} \mathbf{n}_b, \quad (3.30)$$

where the indexes a and b represent the two different observation types.

3.2.2. Parameter elimination

As some parameters, called local parameters, are fundamental to formulating a problem but are not necessary as a result, a pre-elimination is of interest. This step reduces the dimension of the NEQ system significantly and improves in some cases the computational performance when solving for the wanted parameters, called global parameters.

Based on Equation 3.20, parameter vector \mathbf{x} is separated:

$$\Delta \mathbf{l} + \mathbf{e} = \mathbf{A}_1 \mathbf{x}_1 + \mathbf{A}_2 \mathbf{x}_2. \quad (3.31)$$

To eliminate the part $\mathbf{A}_2 \mathbf{x}_2$, the system can be divided up

$$\begin{bmatrix} \mathbf{N}_{11} & \mathbf{N}_{12} \\ \mathbf{N}_{21} & \mathbf{N}_{22} \end{bmatrix} \cdot \begin{bmatrix} \mathbf{x}_1 \\ \mathbf{x}_2 \end{bmatrix} = \begin{bmatrix} \mathbf{n}_1 \\ \mathbf{n}_2 \end{bmatrix} \quad (3.32)$$

and solved for sub-parameter vector \mathbf{x}_1 of interest

$$\mathbf{x}_1 = \mathbf{N}_{11}^{-1} (\mathbf{n}_1 - \mathbf{N}_{12} \mathbf{n}_2). \quad (3.33)$$

The NEQ system can be re-arranged to

$$\mathbf{N}_{22}^* \mathbf{x}_2 = \mathbf{n}_2^* \quad (3.34)$$

with the pre-eliminated NEQ matrix

$$\mathbf{N}_{22}^* = \mathbf{N}_{22} - \mathbf{N}_{21}\mathbf{N}_{11}^{-1}\mathbf{N}_{21} \quad (3.35)$$

and the pre-eliminated right-hand side of the NEQ system

$$\mathbf{n}_2^* = \mathbf{n}_2 - \mathbf{N}_{21}\mathbf{N}_{11}^{-1}\mathbf{n}_1. \quad (3.36)$$

While the pre-eliminated parameters are not solved, they are taken into account in the reduced NEQ system. The processing does not change the result of the estimation of the estimated set of parameters. If of interest, the pre-eliminated parameters can be retrieved at a later point by back-substitution.

3.2.3. Sequential LSA

To reduce the dimension of the NEQ system, a sequential LSA can be used. Within this method, the reduced observation vectors $\Delta\mathbf{l}$ and design matrices are generated per period and accumulated, provided that the observations among different epochs are uncorrelated.

$$\mathbf{N} = \sum_i \mathbf{A}_i^T \mathbf{P}_i \mathbf{A}_i \quad (3.37)$$

$$\mathbf{n} = \sum_i \mathbf{A}_i^T \mathbf{P}_i \mathbf{l}_i \quad (3.38)$$

The short arc approach automatically includes the sequential LSA. This step is essential for all gravity field processing strategies, due to the size of observations: A gravity field with a resolution of d/o 120 means 14400 unknown gravity field coefficients, a sampling of 5 s means over half a million observations per month.

3.2.4. Wiese approach

The Wiese approach, first proposed by Wiese et al. (2011c), is a gravity field processing technique to reduce temporal aliasing effects in the gravity field solution. The approach co-parametrizes low-resolution gravity field solutions at short time intervals together with higher resolution gravity field solutions, for a longer time interval. The technique reduces the aliasing effect by extracting the long-wavelength geophysical signals into the daily solutions. While the primary goal of the Wiese approach is to reduce temporal

aliasing effects, as a by-product uncorrelated short-period gravity field solutions are estimated.

To estimate the daily gravity fields, their coefficient parameters are included in the set of local parameters according to 3.2.2. For the solution, the computed daily solutions are averaged in a weighted mean. Their maximum degree of expansion depends on the number of satellites in the solution.

3.3. Simulation

As described in the previous sections, the estimation of gravity field models is a complex topic: The functional model is not linear, and needs many steps to allow for the optimization. The vast number of observations and parameters is affecting the computational performance of the estimation. Accordingly, the NEQ matrices are big and need a lot of storage space.

Due to these facts, the infinite solution space for the best option for a NGGM, has to be narrowed to a few select cases. The goal of the gravity field processing is to derive a potentially best model expressed in spherical harmonic coefficients. Therefore, factors impacting the gravity field performance have to be analysed, and a decision regarding their properties has to be taken.

Orbit design

Orbits can be adjusted in terms of orbit altitude, inter-satellite distance, inclination, and repeat mode. These parameters influence, both directly and indirectly, the performance of the gravity field retrieval.

The orbit altitude is the most crucial parameter impacting the performance of the estimation, due to the decreasing sensitivity with higher altitude expressed by the attenuation factor

$$\left[\frac{R_E}{r} \right]^{n+1}. \quad (3.39)$$

GRACE, a non-drag free mission, has a nominal initial orbit altitude of 500 km, which declines due to atmospheric drag and solar activity. Depending, on whether a drag compensation system is included in the satellites, a GRACE-like orbit or a lower orbit around 350 km can be chosen (Murböck et al., 2013).

The choice regarding the inter-satellite distance is a trade-off between instrument performance and relative accuracy (Wiese et al., 2008). The global spatial coverage depends on the inclination of the orbital plane. The GRACE near-polar orbit was chosen explicitly to have a small polar gap. An inclined pair would, therefore, be an optimal addition to a polar pair. The choice of the ground track, the path on Earth directly below the satellite, and the repeat orbit, meaning repeating the ground track, should be investigated. Stricter orbit maintenance means more orbit manoeuvres and accordingly fuel consumption.

Sensors

The LRI currently flying on-board of the GRACE-FO with a nm-level accuracy as a technology demonstrator is expected to be the main instrument of a possible NGGM concept.

The second instrument significantly influencing the accuracy of the gravity field estimation is the ACC. Its poor noise behaviour especially the low-frequency decreases the performance of the lower degree and order gravity field coefficients. Studies regarding hybrid or cold-atom ACC show a possibility for improved performance in the future (Abrykosov et al., 2019).

Multi-pairs

All single-pair concepts have restrictions regarding the improvement of the spatio-temporal resolution. An increase in spatial sampling leads automatically to a decrease in temporal sampling.

Multi-pair concepts, described in Section 1.3.1, enable a higher spatio-temporal resolution and, depending on the specific configuration, even improvements regarding the sensitivity towards non-along-track components. The Wheel- and Pendulum-types are demanding regarding their implementation and need a high control of their orbits relative to each other. The concept of two satellite pairs, like, e.g. the Bender-type double pair concept, is more realistic from an engineering point of view (Bender et al., 2008).

3.3.1. Set-up

For the simulation, a closed-loop simulator available at the Institute of Astronomical and Physical Geodesy (IAPG) at Technical University of Munich (TUM) is used. The software was set up by Yi (2012) for the processing of GOCE and GRACE and altered

Chapter 3. Gravity field processing

to be used as a simulation software by Daras (2016). For the performed simulations, the code was updated to fit the purpose of the research questions asked within this thesis.

A flowchart of the simulation software is shown in Figure 3.1. The software is implemented in three independent processing steps, namely the orbit integration (Part I), the set-up of the NEQ's system (Part II), and lastly the accumulation, pre-elimination and estimation step (Part III). These steps are separated for two reasons: For processing reasons, since the set-up of the matrices can be parallelized resulting in better performance, and secondly, since based on the results of each step various scenarios can be processed, resulting in shorter computation times.

The simulation aims to gain an understanding of what a particular constellation or sensor configuration would mean for the performance of the gravity field determination. Products based on real observations such as a GNSS orbit, inter-satellite range or the non-gravitational forces observed by the accelerometers are not available for NGGMs. The observations have to be created with probable real-life effects and noise to enable a realistic simulation. These simulated observations are then the basis for the computation of the reduced observation vector according to Section 3.2.

The observations of the accelerometer and star-camera are not simulated explicitly. They are taken into account implicitly by adding their sensor noise to the exploited observations. As residual drag, not observed by the accelerometer, and the star camera noise are only insignificant components within the error budget, their impact can be usually omitted.

Part I: Orbit Simulation

The first step, orbit integration, is marked in blue in Figure 3.1. It is the most time-intensive part of the software package. As input, the following data sets and input variables have to be set:

- **Input information:** Keplerian orbit elements or state vector, integration step size, maximum d/o of the input gravity fields
- **Input signals:** Static gravity field, time-variable gravity field, "true" force model, GNSS noise time series

Based on the state vector, the numerical integration of the equation of motion is done with a multistep method by Shampine and Gordon (1975), which applies a modified divided difference form of the Adams Predict-Evaluate-Correct-Evaluate (PECE) formula. A detailed description can be found in Yi (2012).

Part II: Set-up of NEQ system

As a second step, marked in yellow in Figure 3.1, the NEQ system is set up. The functional model, as explained in Section 3.1.2 and Mayer-Gürr (2006), is used as basis. The system is set up arcwise, based on a period defined by the user. An arc time of 6 *h* has proven to be optimally suited to the estimation.

- **Input information:** Arc length, time period of processing, maximum d/o of the estimation
- **Input signals:** Orbit with/without noise, "reference" ocean tide model, accelerometer noise, SST noise, optional: Star camera noise

When estimating gravity fields from GRACE-like satellite pair missions, two observables are used:

- The LL-SST observable has a very high accuracy of μm or better, is however only a line-of-sight scalar observation in along-track direction.
- The HL-SST observable has a low accuracy of some *cm*. It is an absolute observation with 3D character.

The observation types are complementary and are both needed to create a stable system, that enables the desired performance.

The matrices and vectors of each observation type are combined and then accumulated day-wise per pair. As the individual days are independent of each other, the NEQ's can be processed in parallel. The final daily NEQ system per satellite pair is stored for the last step.

Part III: Solution of NEQ system

As the last step, marked in red in Figure 3.1, the stored NEQ parts are accumulated according to the user's input:

- **Input information:** Maximum d/o of the estimation, the period of processing, retrieval period, number of satellite pairs, optional: maximum d/o of Wiese approach processing
- **Input signals:** Stored NEQ system

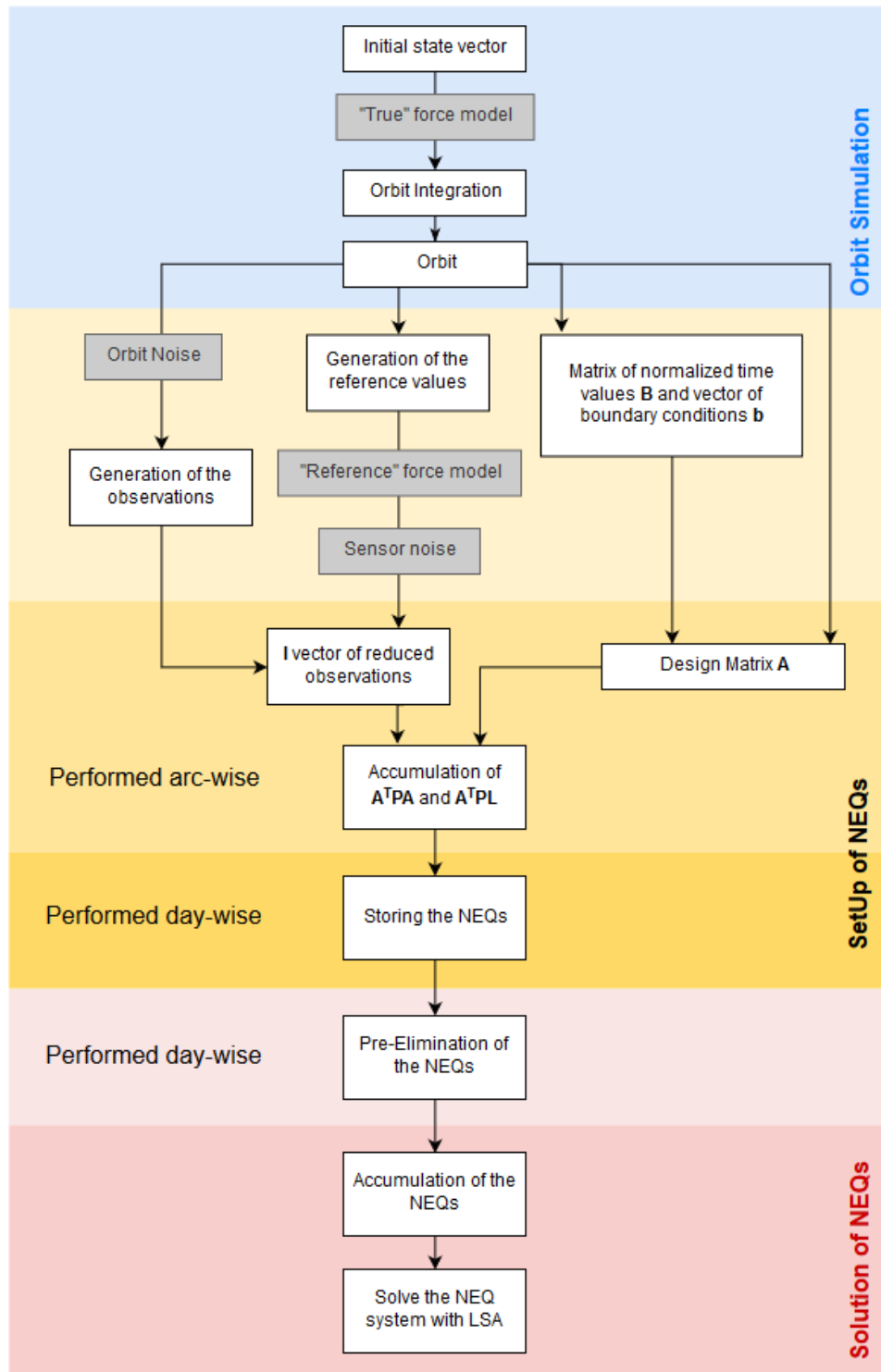


Figure 3.1.: Gravity field simulation flowchart

As a first step, the local parameters are pre-eliminated. In the case of standard processing, only the boundary value parameters are eliminated, see Section 3.2.2. If the Wiese processing is chosen, the daily low-degree SH coefficients up to the designated maximum daily degree are also eliminated. Next, the NEQ system is accumulated depending on the retrieval period and solved. In the Wiese processing, the daily gravity fields are estimated as the last step.

Chapter 4.

Results

The following chapter provides answers to the question posed in Chapter 2. They are a summary of the results presented in the papers. For detailed information such as simulation set-up, please refer to the original manuscripts in the Annex.

4.1. GRACE-like vs. NGGM constellation

The first research objective 2.2.1 whether a GRACE-like single or Bender-type double pair is the best option for moving forward was answered in Purkhauser et al. (2020) (also called P-I), see A.1. From a science performance point of view, the double-pair is always the preferred option. However, as the basis for decision making a cost-benefit analysis has to be included and this may change the answer.

Q1: The key parameters impacting the performance of a gravity mission are the number of satellite pairs, orbit altitude and sensor noise. These factors are combined in all possible combinations to enable a thorough investigation. Star camera noise was excluded from the analysis, as its impact is not significant. As intersatellite distance 100 km was set.

Q2: As input signal, the full AOHIS and the hydrology, ice and solid Earth (HIS) with and without AO de-aliasing errors and OT models are used. In the case of a double-pair scenario, ocean tide models play a significant role as they introduce further errors and degrade the possible accuracy of the performance. We recommend therefore further research and development of such models.

Q3: The single-pair scenario is post-processed with different de-stripping methods and filters, as such post-processing is standard with the current missions. The same post-processing scheme applied to the double-pair resulted in a deteriorated solution compared to the unfiltered solution. As single pair missions can not retrieve the full AOHIS, the comparison was mainly made on HIS signal level.

Q4: We simulated all scenarios for two months, with a retrieval period of 7 days. The best single pair scenario is in a low orbit and with a laser interferometry sensor. The restrictions of a single pair, however, cannot be overcome. All double pair scenarios can retrieve the full AOHIS signal, independent of selected sensors and altitude. The best option regarding performance is the double-pair, as the full AOHIS can be retrieved, with the interferometry sensor (already test on GRACE-FO) and a low orbit. When taking cost and feasibility into account, a higher orbit is favoured as the higher altitude allows for a less stringent SFF.

4.2. Multi-pair constellations

As various space agencies look into flying a gravity satellite mission, the question of the impact of a third pair arises, see Chapter 2.2.2. Paper P-II (Purkhauser and Pail, 2020), see A.2, answers the question based on a low flying Bender-type double pair with a laser interferometry sensor. The respective third pair has the same orbit height and either a KBR or LRI sensor.

Q1: As various studies by different teams showed, there is big freedom in choosing a constellation. A Bender-type double-pair was used as a base scenario to reduce the number of possibilities. The third pair was either in a near-polar or inclined orbit. As expected, the third pair does improve the performance. However, this improvement is not as significant as the difference between a single and double pair. The best add-on is the inclined pair with an improved set of sensors.

Q2: The question of how a sub-optimal constellation would impact the overall performance is not answered directly. As an aim, cooperation between space agencies to provide the best possible constellation is envisioned. An impression of sub-optimal performance can be obtained when looking at the various monthly GRACE gravity fields, with suboptimal ground tracks.

Q3: If a satellite in a multi-pair constellation fails, a single- or double-pair constellation preserves. As the third pair is preferably positioned in an inclined orbit, as a worst-case scenario, two inclined pairs with a polar gap are left.

Q4: The daily solution of a Wiese processing can be increased up to d/o 25 due to the additional observations. The daily spatial resolution is of importance for NRT processing schemes.

4.3. NRT processing

As the service character of NGGM missions should be emphasised, research objective 2.2.3 was to develop a NRT method to retrieve signals with short latency. The goal is to deliver products with a short temporal resolution for the prediction of, e.g. floods. The resulting approach can be found in Purkhauser and Pail (2019), also called P-III, see A.3

Q1: The proposed NRT approach is a combination of the Wiese approach (Wiese et al., 2011c), co-estimating low-resolution daily gravity fields with high-resolution longer-term gravity fields, and a sliding window averaging (see 2.2.3 and A.3). Compared to other approaches, the advantage is, that no geophysical a priori models are necessary as input to constrain the solution.

Q2: To process NRT solutions rapid processing of Earth Orientation Parameters (EOP), GNSS and the gravity data themselves is necessary. If a signal separation is necessary, AO de-aliasing products are also needed. Currently, the data is available between one to three days.

Q3: The NRT processing was tested with a three day retrieval period and achieved stable results. The period was not further shortened.

Q4: Tests show that the crossing point between signal and error curve for the daily solutions is around d/o 15. The best performance overall was achieved when estimating the daily solutions with d/o 15. To improve the daily solution, it is also possible to attach the overall solution starting at d/o 16 onto the daily solution increasing the spatial resolution with reasonable accuracy.

To quantify the capabilities of the proposed NRT approach, a numerical closed-loop simulation of a Bender-type constellation with an optimal orbit design and a LRI sensor was performed according to Chapter 3. The base retrieval period was set to 7 days, as the used orbits have a near-repeat ground track of 7 days.

4.4. NRT data applicability

The potential of gravity data regarding services and applications is of interest. The questions of chapter 2.2.4 are therefore the basis of a processing scheme for the detection of floods in publication P-IV (Purkhauser et al. (2019), see A.4) and a test of multi-pairs in paper P-II (see A.2).

Q1: The currently available data sets and services based on GRACE can be found in chapter 1.3.3.

Chapter 4. Results

Q2: To test the simulated gravity field solutions for the envisioned applications in time-critical fields, a test scheme based on a double-pair NRT data set was set up. To ensure, that floods are visible in the data, we checked the hydrology component of the ESA Earth System Model (ESM) first. Different definitions of areas like catchments and general circle forms are tested and used as the basis for an average EWH value. We retrieved the AOHIS and HIS signal and checked for the identification of flood events.

Q3: As especially the AO component superimposes part of the hydrology signal, the floods are only visually clearly detectable in about 20% of the cases. An additional 40% were visible but not clearly distinguishable as flood due to other peaks in the data. The analysis has to be refined, but also additional complementary data is still necessary to give reliable results.

Lastly, the performance of triple-pairs in comparison to double-pairs was tested in catchments and ice drainage basins in Greenland. The additional polar pair improves the performance compared to a Bender-type double pair by 11%, while an inclined pair improves the result on average by 21%.

Chapter 5.

Discussion

Geodesy produces data products that are essential for various scientific analyses in Earth science.

Kosuke Heki described in his International Union of Geodesy and Geophysics (IUGG) 2019 union lecture¹ quite clearly the connections between various fields of Earth science and geodesy:

Millimeter accuracy of GNSS positioning enabled precise mapping of tectonic plate/block boundaries and rapid determination of fault parameters after earthquakes. It also brought discovery of silent fault slips undetectable with seismometers. Precise determination of the Earth's equipotential surface (geoid) with satellite gravimetry enabled oceanographers to isolate dynamic topography and map ocean currents. Satellite altimetry revealed global mean sea-level rise and short-term disturbances caused by water exchange with land, which can also be investigated by satellite gravimetry. Atmospheric water vapour information from GNSS data analyses improved routine numerical weather forecasts. Dual-frequency GNSS receiver became an important tool to study space weather. Satellite gravimetry also let us constrain mass loss of inaccessible mountain glaciers.

Within the last 20 years, a significant improvement in techniques and accuracies was achieved. According to Seeber (2008), the following new fields in geodesy have evolved:

- The dedicated gravity field satellite mission CHAMP, GRACE and GOCE for the determination of the Earth's gravity field were successfully flown. Currently, GRACE-FO monitors the temporal gravity field. Various space agencies took already the first steps to fly a NGGM to continue monitoring.
- Apart from the US American system GPS, the Russian Globalnaja nawigazionnaja sputnikowaja sistema (GLONASS), the European civilian system Galileo and the Chinese Beidou are fully operable in space. GNSS observations are routinely used

¹IUGG Montreal 2019, <http://iugg2019montreal.com/union-lectures.html>. Retrieved 23.10.2019.

for surveying and time transfers, monitoring of Earth's rotation, plate tectonics and polar motion as well as for orbit determination and SST tracking.

- The space techniques Very Long Baseline Interferometry (VLBI), SLR, Doppler Orbitography and Radiopositioning Integrated by Satellite (DORIS) and GNSS alone or in combination determine key geodetic parameters related to reference frames, Earth's rotation, and gravity field.
- Altimeter missions map the surface of the ocean topography. Interferometric synthetic aperture radar (InSAR) generates digital elevation models.
- The establishment of services based on geodetic satellites for monitoring and disaster prevention is on its way.

The strength of geodesy is to deliver all these observations with complete objectivity. The only bias is due to, e.g. sensors and influences of the mediums, through which the observation signal passes. Therefore, each observation and derived data needs information about its accuracy, e.g. its variance.

The following chapter gives information about the hydrological cycle, one of the main observables of gravity missions, and the impact of climate change on Earth's geophysical system. The achievement in observing the Earth by EO satellites and especially gravity satellite missions are outlined. Next, the advantages and drawbacks of gravity missions are reviewed. The possibilities of potential systems and services based on NGGMs are discussed. Lastly, the importance of improved public relations is emphasized to make geodesy more apparent to a broader audience in the face of challenges like climate change.

5.1. Understanding the Earth

The main goal of a satellite gravity mission is observing the sum of all Earth's mass distribution and its changes. The underlying geophysical processes, which are responsible for the changes in the Earth's gravity field, have periods from hours to decades and even longer time scales. Their spatial extent can range from a few hundred meters to thousands of kilometres. In the observable, the different geophysical signals are superimposed. Signal separation is necessary to understand the geophysical and climatological processes. Especially the hydrology component is not only interesting for science but of major importance for humankind in general. *Hydro* is derived from the Greek word for water. Hydrology is the study of water, which is one of our most important natural resources for both ecosystems and human uses on Earth.

Water is the basis of life on Earth and had and still has a lasting effect on its physical shape. Compared to other planets, water is on Earth available in all three phases:

Water vapour, liquid, and solid ice. Over two-thirds of the Earth's surface is covered by water reflecting in blue, giving the Earth also the name blue planet. However, water accounts for only 0.02% of its mass. The supply is limited by nature and distributed unequally across Earth. The total amount of water on Earth amounts to approximately $1.3 \times 10^{18} \text{ m}^3$ (Oki et al., 2004). Nearly 97% of the water is contained in the oceans. The remainder of the water, the Earth's freshwater reserves, can be found in ice, snow, groundwater and soil moisture, with only 0.3% accessible for human use (Schneider et al., 2011).

5.1.1. Hydrological cycle

The hydrological cycle is the continuous circulation of water within the Earth's system. The cycle starts with water evaporating from landmasses and water bodies, eventually returning to the Earth as rain and snow. It describes a constant exchange of water between oceans, atmosphere, land surface, biosphere, soils, groundwater systems, and the solid Earth.

Oki et al. (2004) describes the various states and fluxes of water, illustrated by Figure 5.1 schematically, as follows: Water is temporarily stored in different subsystems like rivers, oceans, soil and atmosphere. "Precipitation" has high spatio-temporal variability and describes the water transfer from atmosphere to Earth's surface. "Evaporation" is the process of turning liquid from the surface into vapour due to an increase in temperature. "Transpiration" is the process of evaporation through the surface or skin of a plant. Compared to evaporation from the soil surface, the water can stem from deeper layers of the soil. "Runoff" is the discharge of water into the oceans. The atmosphere distributes mainly water vapour and around the globe. All fluxes are essential to close the global water cycle.

The hydrological cycle is closely related to the atmospheric cycle, oceanic circulation and heat exchange, making water and its cycle essential in the Earth system (Oki, 2006). The cycle is also responsible for the exchange of heat and moisture between land and sea: When water condensates, heat is released, implicitly warming the environment. In comparison, the evaporation of water cools the environment. The water cycle is crucial to fill up Earth's freshwater resources and moderate extremes in the climate.

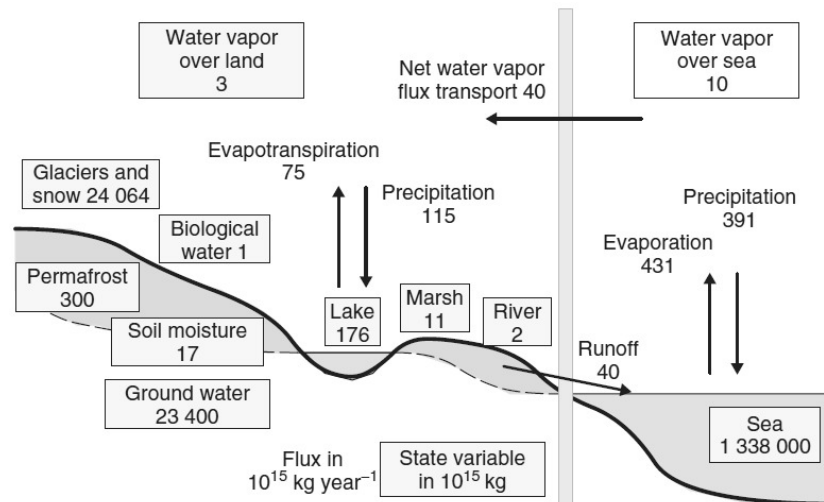


Figure 5.1.: Schematic illustration of the hydrological cycle on the Earth. The water storage in total volume (km^3) is indicated in the boxes. Image Credit: Oki et al. (2004)

According to Woods (2006) "variability [in the hydrological cycle] occurs naturally, and also because of human activity (e.g. land cultivation, urbanization, and forest management)". This variability in time and space exists for every hydrological variable. Precipitation patterns change in volume, intensity and frequency and either benefit or deteriorate the environment. Trenberth (2008) states that

Steady, moderate rains soak into the soil and benefit plants, while the same rainfall amounts in a short period of time may cause local flooding and runoff, leaving the soils much drier at the end of the day.

The hydrological cycle, however, has changed through the centuries without any influence by humankind: Thick ice covered vast areas of now fertile land with moderate climate during previous ice ages (Woods, 2006).

Hydrological extremes, i.e. floods and droughts, are states with too much or too little water. They can also be distinguished by their temporal and spatial resolution. Floods are usually caused by extensive precipitation or snow-melt, can develop rather rapidly and affect a smaller region. Droughts, in comparison, occur in larger areas due to a prolonged period of no or very little rainfall and in some cases high temperatures. (Trenberth, 2008) In a stable climate system, these extremes are counterbalanced over a longer period (Roads et al., 2006).

Human activities affect the hydrological cycle by a variety of measures. Humans adjusted nature for their needs by, e.g. building dams in rivers and streams for electricity production, by extracting water as drinking water and for the irrigation of farmland, by

deforestation of large areas of land for farming and by ground sealing and river regulations. With rising population and accordingly, more consumption, the impact on the hydrological cycle has increased. Figure 5.2 illustrates a simplification of "the impacts of a growing population and economic activities associated with consumptive life style on hydrological cycles". Both population growth and economic growth in industrialized as well as developing countries increase the amount of water used for agriculture, industry and personal lifestyle. As more land is used for food production or is used for industrial buildings, its hydrological properties change and a substantial amount of greenhouse gases (GHGs) are produced, leading ultimately to climate change. (Oki, 2006)

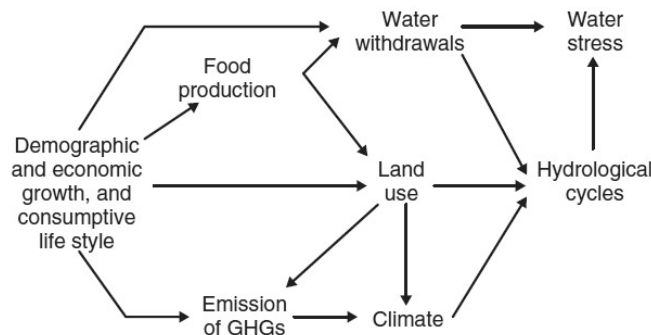


Figure 5.2.: Influence of humans on the water cycle. Image Credit: Oki (2006)

5.1.2. Climate change

The climate change induced by a growing concentration of carbon dioxide and other trace gases in the atmosphere resulting from globally increasing population and economic growth increases the atmospheric *greenhouse* effect. The *greenhouse* effect is a natural process on Earth trapping solar radiation in the atmosphere, which is necessary to sustain life on Earth. However, as more and more anthropogenic GHGs enter the Earth system, the radiation patterns change, causing an increase in the temperature and accordingly changes in other climate variables. The global warming also implies changing precipitation patterns, changes in the hydrological cycles and intensifying weather extremes.

The Intergovernmental Panel on Climate Change (IPCC) special report on *Global Warming of 1.5 °C* (SR15)² (hereinafter referred to as IPCC report), see also Allen et al. (2018), reports that the global temperature has already risen on average by approximately 1 °C. However, the increase is not equal around the globe. Over land regions temperature rises higher than the global annual average is observed (Seneviratne et al., 2016). The Arctic is affected by warming two to three times higher than the average. The main cause

²ICPP Report, <https://www.ipcc.ch/sr15/>. Retrieved 11.11.2019.

Chapter 5. Discussion

of the more intense warming in the Arctic region is the so-called ice-albedo feedback (Budyko, 1969, Masson-Delmotte et al., 2013). When the warming melts ice and uncovers the ground, more sunlight is absorbed, leading to increased heating. In comparison, the temperature over the ocean is less affected, because water is slower to absorb and release heat (Sejas et al., 2014). As the warming is concentrated on land masses, 20% to 40% of the global population have already experienced a warming of more than 1.5°C in at least one season (Allen et al., 2018). The short summary for policy makers of the IPCC report says that "estimated anthropogenic global warming matches the level of observed warming to within $\pm 20\%$ ". Currently, 0.2°C is added to the average temperature every decade due to both "past and ongoing emissions" (see Figure 5.3). The report also states that global warming "is likely to reach 1.5°C [above pre-industrial levels] between 2030 and 2050", if the temperature increase due to human-caused effects stays at the same level.

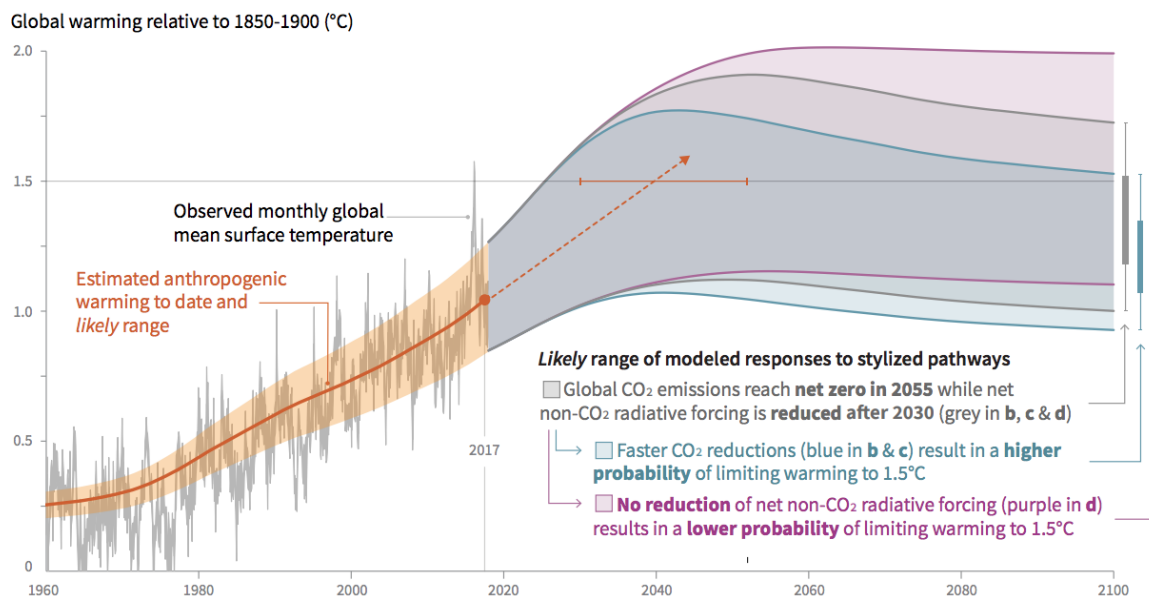


Figure 5.3.: Observed monthly temperatures (black) and estimated human-caused warming (red) relative to 1850-1900. Image Credit: IPCC

The IPCC report also clearly states that the

temperature rise to date has already resulted in profound alterations to human and natural systems, bringing increases in some types of extreme weather, droughts, floods, sea-level rise and biodiversity loss, and causing unprecedented risks to vulnerable persons and populations.

Weather extremes

When the air temperature rises, the water vapour capacity of the atmosphere increases exponentially. As the evaporation depends on the difference of surface and the surrounding air, higher temperature means increased evaporation. Climate change then alters precipitation patterns regarding duration, intensity, and frequency.

Han and Roads (2004) write that studies so far have indicated that precipitation patterns are getting more extreme. Increasing temperatures dry out the Earth's surface and increase the potential of droughts (Dai et al., 2004). Droughts increase the risk of wildfires and crop failure. In this situation, rain can potentially intensify the situation, as dry soil is unable to hold the water. In Trenberth et al. (2003) the intensification of the character of precipitation is analysed. The study concludes that global warming increases the risk of heavy rain and snow events, which must be compensated by the reduction in duration and frequency. Meaning intenser than regular rainstorms and potentially floods in some areas.

Roads et al. (2006) state that apart from intensifying precipitation patterns, the overall hydrological characteristic of an area can change. A lack of snow in the cold season, e.g. due to too warm weather, reduces the available water due to snow-melt in spring. Less water throughout the year goes hand in hand with less evaporation, one of the cooling mechanisms of the system Earth. Not to be overlooked are the impact of the vegetation and sealed soil. Apart from the changes in the spatial distribution of weather patterns, the temporal variability intensified and stem from different weather effects as e.g. the "periods of intense convection are usually followed by even longer times of clear weather" (Roads et al., 2006).

According to the IPCC report, a warming of 1.5°C makes weather extremes common events around the world. Hoegh-Guldberg et al. (2018) expect extreme precipitation to become more frequent in the high latitude areas, while around the equator hot extremes are projected. The drought frequency and magnitude, as well as heatwaves, are dependent on the absolute temperature rise.

Sea-level rise

The sea-level is and was never static. Over the last 500.000 years, the sea-level oscillated by more than 100 m. The sea-level changes were always associated with temperature changes and changes in the radiation patterns on Earth (Church et al., 2010). Ocean water expands as it warms up, which means an increase in volume. Due to global warming, the melting of polar caps and glaciers increases, meaning higher losses due to evaporation, snow-melt, and run-off (Church et al., 2013). This water is added to the ocean, and as a consequence, the sea-level is rising, threatening coastal cities and shallow

islands. If all freshwater stored in ice and glaciers would melt the sea-level would rise about 80 m (Baumgartner and Reichel, 1975).

The difference of a 1.5 °C vs 2 °C warming regarding the global sea-level according to the IPCC report headline statements³ means that on average till 2100 "only" a rise of around 0.1 m has to be expected. However, the sea-level rise will continue long afterwards. The thermal expansion will continue even after the greenhouse gas concentrations have stabilized. Also, there is a risk that the temperature increase will destabilize the situation in Greenland and Antarctic ice, causing a potential multi-meter sea-level increase. (Hoegh-Guldberg et al., 2018)

Various processes are responsible for the height changes of the ocean surface, leading to sea-level change at regional scales. Historically, much of the variability in the sea-level is due to phenomena like the El Niño and the Pacific Decadal Oscillation over time scales of years to several decades. The effects associated with climate change from anthropogenic sources are expected to accumulate over time and dominate the sea-level change. It is commonly assumed that melting ice distributes globally around the oceans. Due to the Earth's gravity field, changes in ocean currents, winds and topography the melting results in regional variations in sea-level change. Around melting ice sheets, e.g. the sea-level falls due to less gravitational attraction between ice and ocean water, combined with the so-called glacial-isostatic adjustment (GIA), due to the ice melts. The global average change is, however, a useful singular number that represents a reasonable estimate of sea-level change. However, depending on the coastal location, a significant deviation from the global average value can be observed. (Church et al., 2013)

5.2. Observing water

As especially freshwater is such an important and limited commodity, monitoring of water is of importance. Data is necessary to calibrate global water models, to predict future weather as well as to determine the availability of water and to classify the exact water use. Even in the absence of human-induced climate change the hydrological behaviour varies yearly and per decade. To differentiate natural and anthropogenic global warming, the understanding of the baseline climatology is therefore of importance.

For cost and technological reasons *in situ* measurements of the hydrological cycle are often not feasible. Large inhabitable areas such as oceans, polar regions, and deserts, as well as rain forests, lead to a lack of spatially homogeneously distributed measurements. Aside from this lack of data, available observations like precipitation and snow accumulation are frequently difficult to interpret. With the help of satellites, a more complete

³ICPP Report, headline statements, <https://www.ipcc.ch/sr15/resources/headline-statements/>. Retrieved 16.12.2019.

global and continuous data set can be observed. As an example, the global mapping of cloud properties, precipitation, water vapour, and sea ice as well as snow-cover, ocean topography and heat content are now done routinely via remote sensing. (Robertson, 2006)

With the growing length of satellite-based data sets, it is becoming possible to analyse the climate system as a whole. Furthermore, as the hydrological cycle is at the centre of many issues, its observation is important, to answer questions about the water cycle, weather, hydrology, and the physical climate change:

- What is the magnitude of the hydrological cycle and how is it changing with time?
- How are extreme hydrological events related to climate variability?
- What potential exists for predicting the hydrological cycle, especially the near-term future? What do we need to realize it?

Gravity satellites missions offer a unique observable for an improved and global monitoring of groundwater, its depletion, and recharge. On the same general level, the cryosphere and atmosphere can be monitored globally and continuously, which is the significant advantage of a satellite-based observation system.

5.2.1. Contributions of GRACE/GRACE-FO

While the geophysical system of Earth was never static, due to the human-made climate change more and more unexpected changes happen, which makes the need to monitor the world globally more pressing. The GRACE mission consisting of a satellite pair and aiming at observing the time-variable gravity field was a pioneering mission. For the first time, it was possible to measure and quantify mass trends and fluctuations. This unique parameter can tell a lot about our planet and its changes. The most significant achievements and contributions of GRACE are collected in Tapley et al. (2019).

Observing ice mass loss

The poles store some of the most significant ice mass reservoirs and its current melting already account for more than half of the sea-level rise (Vaughan et al., 2013). It is therefore of particular interest to not only understand the phenomena but also quantify the ice mass loss because they affect global sea-levels. One of the longest datasets is available from altimeter missions like ICESat, observing elevation change and providing ice mass observations through measurements of the ice-sheet volume change (Kwok et al., 2019). The most significant uncertainty lies in the conversion of volume to mass change, as an assumption regarding the underlying density needs to be taken into account (Gunter

Chapter 5. Discussion

et al., 2009). As the observations are indirect and their accuracy also depends on the surface structure, they only enable the estimation of a multi-annual trend.

Another option is to estimate the ice mass loss with climate models, which quantify the difference between gained ice mass through snowfall and loss by sublimation, ice melt, and discharge. The accuracy of the models depends on the available input data, such as discharge measurement. (Lenaerts et al., 2019)

GRACE enabled direct observation of the ice mass change for the first time. The mission provides a sub-annual trend over its observation time series, with at least a monthly solution, depending on the desired spatial resolution. However, as the full AOHIS is observed, the impact of, e.g. the solid Earth component, meaning the GIA, has to be considered. Considering the GIA is especially crucial for the Antarctica, where the GIA, a slow rebound of the Earth's mantle after the past ice-sheet retreats, is known only with reduced accuracy (Caron et al., 2018). Not only the poles but also other glacier regions have been monitored with GRACE, especially when their spatial extent is significant or their change or signal amplitude is strong enough.

A comparison of the different observations and methods for the estimation of the ice-sheet mass balance can be found in Shepherd et al. (2012). The paper finds a good agreement between the different satellite methods and a regional climate model. Also, a better certainty when combining the satellite datasets is observed.

Observing the sea-level rise

A direct result of climate change is the rise of the sea-level. As already mentioned, the dominant mechanisms responsible are ice mass melt in the polar and glacier regions as well as a thermal expansion due to the higher ocean temperatures. Historically, local measurements at tide gauges were made, and also gave the first indication of sea-level rise in the twentieth century (Lambeck et al., 2002). With altimeter missions like TOPEX/Poseidon and Jason, it is since the nineties possible to observe the mean sea-level height. These measurements indicate an accelerated rise of approximately 3 mm a year during the last 25 years (Nerem et al., 2018).

Argo⁴ is a global mission consisting of thousands of free-floating profiling floats that measure temperature, salinity, and heat content of the upper 2000 m of the world oceans. With this information the steric variations due to thermal expansion of seawater, one of the two major components of the sea level rise, can be computed (Riser et al., 2016).

Complementary, GRACE observes the ocean mass change on a global scale. While ice mass loss means a reduction of mass in the gravity over ice sheets, a gravity gain over the ocean can be observed. As sea-level rise is a threat to humans living in coastal regions,

⁴Argo Project, <http://www.argo.ucsd.edu/>. Retrieved 12.11.2019.

the relative sea-level rise at any given coastline is essential information. Gravity and also altimeter missions observe the sea-level change in a fixed reference frame and have to be related to the local frames.

Several studies like Willis et al. (2008), Leuliette and Miller (2009), Cazenave et al. (2009) have compared the different datasets to better understand the sea-level rise and its various components, confirming a sea-level rise of 1.5 ± 0.6 mm per year from 2005 to 2010.

Observing the terrestrial water storage

TWS is defined as a vertically integrated measure of water availability of all forms above and below the Earth's surface: Surface water, soil moisture, groundwater and snow, and ice (Famiglietti, 2004). The variable provides an indicator of water availability and uses.

There is no comprehensive global monitoring system to observe surface water (river discharge, seasonal floodplain inundation, wetlands, inland water bodies). Stream gauges have long been used to measure the river discharge. However, if a significant flow occurs outside of the nominal riverbank, an important quantity may be unobserved (Famiglietti, 2004). Remote sensing can observe globally river discharges as well as surface water storage. It measures the elevation of large water bodies and rivers, which then can be related to storage volumes. Accurate information on soil moisture content is also essential as it is a critical environmental variable, available through various passive radiometer missions (Petropoulos et al., 2015). Terrestrial groundwater measurements are very costly, have limited spatial coverage and are rarely available, as a monitoring well is necessary.

GRACE, in comparison, observed the whole spectrum of water on and below the surface and provided insights into where global groundwater resources may be shrinking or growing. The mission indicated areas of dry soil, which may contribute to droughts and monitored changes in the solid Earth. Studies conducted by e.g. Famiglietti et al. (2011), Sun et al. (2010), Yeh et al. (2006), Long et al. (2013, 2014), Rodell et al. (2009) have confirmed the capability of GRACE to observe TWS changes on continental and regional scales.

5.2.2. Current Drawbacks

Every observation method has advantages and drawbacks. While some of them can or will be solved over time, others are directly linked to the technology or system.

To fully understand climate variability, a time series of 30+ years is necessary. Otherwise, weather phenomena, natural and human-made climate change are hard to distinguish. Satellite-based dataset records are currently often not long enough. In the case of gravimetric missions, a data set of almost 20 years of continuous observations is available. Based on the preliminary plans to fly a NGGM by NASA, ESA and possibly other nations, this issue may be unfounded soon.

Gravity observations, same as remote sensing, are an inverse observation strategy. Both systems observe various superimposed signals as a whole, which means, that the observation itself does not give a solution for a particular variable itself. A priori variables are needed to separate the different signal contents. With better measurements, these models can be improved. A first simple separation is possible, by splitting up a signal over water and continents, meaning no ocean signal can be observed over the continents and vice versa. However, direct observation of, e.g. the atmosphere alone can never be done.

The achievements already indicate, that with satellite observations a continuous global coverage is possible. However, this coverage has the disadvantage that the spatio-temporal resolution is limited. The orbit altitude sets one of the limits: Higher non-dedicated satellites, used as test mass, only allow for a low resolution (e.g. Earth flattening), while a dedicated mission, such as presented in Section 1.2, allows for a lower orbit and a tailored sensor system. Increasing temporal and spatial resolution are also conflicting demands. Especially a high temporal resolution, such as a daily gravity field, means a limited spatial resolution of approximately $1000km$.

Traditional terrestrial gravimetry on the ground, in comparison, can measure the gravity with high temporal resolution. However, the observed data is often inhomogeneous, and considerable variations in the terrain limit the possible applications. Furthermore, traditional terrestrial gravimeters cannot be used at sea. These observations are mostly relevant for scientific observations, e.g. long time studies of a specific location, or in the exploration for oil reservoirs.

Satellite-based gravity field data can be aided by air- and shipborne gravimetry measurements. Since it is possible to position every sensor via GNSS, they can operate routinely and provide additional high-resolution information, that enables the development of regional gravity fields. However, both terrestrial and air- and shipborne observations do not allow to monitor the temporal gravity field as these observations are only carried out upon request.

5.2.3. Possibilities with a NGGM

The GRACE-like sensor system, where the satellites themselves are a test mass in orbit around the Earth is an established option for observing the time-variable gravity field.

Therefore, most studies suggest NGGM options based on such a system.

Currently, ESA and NASA are preparing an inter-agency cooperation on NGGMs. While it is obvious that a mission with two satellite pairs gives more accurate time-variable gravity field models than a mission with a single satellite pair, it is important to quantify the improvement. The quantification enables the agencies and funding bodies to make an informed trade-off between the costs and the value of the mission for science and services.

Various study groups performed individual simulations to analyse different aspects of possible NGGMs from a scientific and technical point of view. However, these studies are not directly comparable due to different assumptions regarding mission design and instrumentation. The goal of paper P-I (see A.1) is to systematically analyse and quantify the key mission parameters (number of satellite pairs, orbit altitude and, sensors) and the impact of various error sources (AO models, OT models and post-processing) in a consistent simulation environment. The most important take-away messages are:

- A single pair mission with laser interferometry in a low orbit with a drag compensation system is the only possible single pair option to increase the performance compared to the GRACE/GRACE-FO. Dionisio et al. (2018) showed that a tailored propulsion system would allow flying for 11 years at an altitude of about 340 km.
- When flying a double-pair, the LRI currently tested on GRACE-FO can be better exploited, limited in this scenario by ocean tide and AO models. As a low orbit is not the driving factor for the mission performance, the higher priority can be given to flying two satellite pairs.
- AO modelling for signal separation is in any case important. However, in the case of a double-pair, ocean tide models prevent an even better performance and have to be improved significantly.

Publication P-II (see A.2) answers the question if a multi-pair constellation would improve the performance significantly, especially within the context that, e.g. China is planning to fly gravity field missions. We looked at the possibility of adding a third near-polar or inclined pair to the constellation. The performance increase of such a pair is significantly smaller than the second pair as a third pair improves the performance only according to the \sqrt{n} -rule, but strengthens the continuity in the case of failures.

It could be shown that a multi-pair constellation, improved sensors, technology and models, significant improvement is possible. Is this spatial as well as temporal resolution high enough? The honest answer is: No, not for every single application and service. However, the gain in performance with the second pair is significant, as the suggested double-pair constellation solves one of the major drawbacks of a single-pair mission: The resolvability of the full AOHIS signal. The third pair in comparison is valuable,

especially if continuous service is the goal. However, the most critical next step is a double-pair constellation.

5.3. Operational satellite systems

An operational service-based satellite system has to meet a certain performance standard. The best known operational (geodetic) satellite constellation are the positioning, navigation and timing systems GPS, GLONASS and Galileo. As these services have become essential for society, a failure would have far-reaching consequences. Via specification documents the target performance like the positioning accuracy, information about the reliability of the data also called data integrity, and availability and continuity of the service within the specified accuracy, are defined for the Galileo system⁵.

The Copernicus program⁶ consisting of the Sentinels satellite constellations is coordinated by the EU and ESA. Each satellite is equipped with several sensors, so that Copernicus can offer services in the fields of atmosphere, marine, land, climate, emergency and security. The missions are always based on two satellites in orbit to fulfil performance requirements like e.g. coverage and revisit times and protect against failure.

Another example is the fleet of satellites operated by European Organisation for the Exploitation of Meteorological Satellites (EUMETSAT)⁷. The Earth observing (EO) satellites observe data for weather, climate and environmental monitoring. As the satellites are vital to ensure information about especially potentially dangerous weather, the policy is to have always two operable satellites in orbit.

For an operational service based on a NGGM two contrary data sets are of interest: A long-term monitoring, with temporal resolutions up to a month, to catch (semi-)annual trends, and NRT data sets for predictions and forecasts. Figure 1.6 collects the main scientific as well as societal applications. Especially the monitoring and forecasting of floods and droughts, which is a focus of this thesis, water management and monitoring, as well as the risk assessment of natural hazards, are applications where the NRT aspect is essential.

⁵European GNSS (Galileo) Open Service Signal In Space Interface Control Document, <https://www.gsc-europa.eu/>. Retrieved 30.11.2019.

⁶Copernicus program, <https://www.copernicus.eu/>. Retrieved 9.12.2019.

⁷EUMETSAT, <https://www.eumetsat.int>. Retrieved 9.12.2019.

5.3.1. Performance requirements

To operate a time-variable gravity field mission successfully, at least one satellite pair with functioning sensor systems is necessary. The mission lifetime of GRACE has already shown various performance impacting cases. During some months the orbit configuration of short repeat cycles does not allow to solve for higher degrees. One accelerometer was powered off due to limited battery capacity and replaced by a so-called transplant in the last months. In the end, the satellite mission was decommissioned because of failing systems. Klinger et al. (2016) visualised all processable monthly gravity fields based on the GRACE data. The representation shows, the apparent impact of performance and availability of the data on the result. Since an operational service, which has to guarantee continuous observations, as well as consistent quality, is envisioned, two satellite pairs are essential. Also, a constant altitude and constant uniform ground track coverage per period are desirable.

The requirement for a NRT service, apart from a continuous performance and availability, are the desired spatio-temporal resolution and the required latencies. An ideal scenario would allow a daily temporal resolution paired with a spatial resolution of less than 100 km. The spatio-temporal sampling, however, underlies the Heisenberg rule (Weigelt et al., 2013): The better the temporal sampling, the worse the spatial sampling and vice versa. Regarding the analysed NGGM constellations both ambivalent goals can be reached significantly better than in the case of a single pair. Initial service capabilities may be based on a single pair. The operational performance can then be established on a double-pair as it enables the estimation of the full AOHIS.

The latency of the processed solutions is dependent on the timely availability of data products necessary to compute gravity field solutions. Gravimetric satellite observations need up-to-date EOP. The International Earth Rotation and Reference Systems Service (IERS)⁸ provides rapid daily EOP data within 1-3 days, and additionally predictions for the following days. For the orbit computation rapid GNSS orbits and clocks are available at the University of Bern within 17 hours. During the GRACE mission, the L1B quick look data was offered with a latency of approximately one day. AO de-aliasing products are, if even necessary, provided within a time frame of one day. If a reduction of the latency is requested, the data acquisition of the listed data sets will have to be provided more quickly.

As extensive processing is necessary to deliver the end product for the user, several steps ensure the exclusion of outliers and the estimation of possible biases. This pre-processing ascertains data integrity. Accuracy information of the delivered data products is essential to use the gravity fields correctly.

⁸IERS EOP, <https://www.iers.org/>. Retrieved 2.12.2019.

5.3.2. Future gravity data

In Section 1.3.3 science initiatives and services based on the single-pair missions GRACE and GRACE-FO are presented. A growing number of different gravity field models are listed on the official homepage of the International Centre for Global Earth Models (ICGEM)⁹. There are so many different gravity field models with small differences available that it is not easy to differentiate and evaluate the individual models, their accuracies and limitations. Improved processing and models still allow for small improvements in the performance of gravity fields. The aim, however, is to make the data available and useful for society: Which services and applications can use the data of a (future) gravity field mission?

Strategies based on Kalman filtering and single-pair data sets were tested to facilitate the need for NRT data sets (Kurtenbach et al., 2009). In paper P-III (see A.3) a NRT processing scheme based on a co-parametrization of low-resolution daily and longer-term gravity field solutions (Wiese et al., 2011c), combined with a sliding window averaging, was set up for a potential double pair constellation. Compared to the Kalman filter approach, the proposed NRT concept is independent of any prior information about the gravity field and its changes, meaning that a regularization is unnecessary. The enhanced spatial-temporal resolution facilitates the possibility to self-dealias high-frequency atmospheric and oceanic signals. Additionally, short time-scale gravity field solutions are provided. Tests showed that the retrieval period can be shortened to three days, while the stable processing of the solutions is guaranteed.

A test of these short-term gravity field data sets regarding the potential to detect floods was performed in publication P-IV (see A.4). The results are to a certain point promising, but again show, that the gravity field as an individual observation on a short term basis and therefore with limited spatial resolution would gain from the combination with other observations. Within publication P-II (see A.2) the added benefit of a third pair regarding applications is investigated. The most significant potential of a multi-pair constellation is the possibility to estimate daily gravity fields up to d/o 25+ independent of any a-priori information.

5.4. Geodesy, gravity and societal needs

Climate change is the challenge of the 21st century. In the United States of America 66% believe that global warming is caused by human activity, which is an all-time high. However, according to the same Gallup¹⁰ poll only 45% think that global warming

⁹ICGEM homepage, <http://icgem.gfz-potsdam.de>. Retrieved 14.11.2019.

¹⁰Gallup poll on global warming, <https://news.gallup.com>. Retrieved 22.10.2019.

5.4. Geodesy, gravity and societal needs

will pose a severe threat in their lifetime. The Special Eurobarometer 490¹¹ on climate change concluded that within the EU overall 93 % think of the climate change as a severe problem. The question of which issue is considered the single most serious problem facing the world as a whole was answered by almost a quarter with climate change.

Climate change, both natural and anthropogenic, has various impacts on different geophysical systems of our planet. Some can be felt already. Others are not instantaneously associated with climate change. Sea-level rise, a direct result of climate change, leads to the direct impact of land loss and indirect consequences such as agricultural production loss, migration, and damages in coastal areas. Similar impact chains can be formed starting at other climate-related changes: Temperature rise and a decrease in precipitation lead to drought, impacting soil moisture. Additionally, the soil degrades due to, e.g. erosion or soil salinity. Unusable farmland reduces productivity, destroys livelihoods and leads in the end again to migration. Rapidly changing precipitation patterns lead even in moderate climatic zones to problems with sinking groundwater levels, less snow coverage in the winter and unpredictable weather conditions.

The second Climate Monitoring Report¹² of the German government states an average temperature increase of 1.5 °C between 1881 and 2018. 0.3 °C of the whole warming happened in the last five years. Global warming is no longer a problem of the future, but can already be experienced in Germany. The surface temperature of the North Sea has increased, resulting in greater fluctuations in the weather pattern, heavy rainfalls and flooding. The warm temperatures of the last decade also lead to a reduction of the ground water level, threatening the ecosystem as well as economy.

In the decade of "fake-news" scientists as sources of information, compared to, e.g. politicians or industry leaders, are trusted by nearly three-quarters of people worldwide¹³. The scientific consensus on anthropogenic global warming was more than 97 % in 2013 (Cook et al., 2013). Their credibility is however still sometimes disputed (Skuce et al., 2016). Only a minority of US Americans (39 %) report strong trust in information from climate scientists (Funk, 2007). On the other hand, a study by Fischer et al. (2019) suggests that Germans have a good understanding of the science behind climate change, but are sometimes a bit too confident about their actual knowledge base. A study by Gehlbach et al. (2019) found that emphasizing the general trust in science helps to increase the belief in climate change facts as well.

Our knowledge of the climate system is based on collected data on climate variables. In the mid-1800s, mainly data for weather forecasts were collected. These datasets are mostly lost in various analogue archives and have to be rescued, e.g. by the Operation

¹¹Special Eurobarometer 490, <https://ec.europa.eu>. Retrieved 22.10.2019.

¹²Climate Monitoring Report of the German government, <https://www.umweltbundesamt.de/>. Retrieved 2.12.2019.

¹³Wellcome Global Monitor, <https://www.sciencemag.org/>. Retrieved 14.11.2019.

Chapter 5. Discussion

Weather Rescue¹⁴. Nowadays, an abundance of climate data from model simulations, Earth-orbiting satellites (like the gravity missions GRACE and GRACE-FO) and in situ observations are collected daily. Each of these sources has its own advantages, limitations, and uses, that have to be considered. Satellite-based datasets have the crucial strength of global coverage, but frequently lack continuity as missions last on average five years. In situ observations, in comparison, are direct observations, with a usually sparse global coverage (Faghmous and Kumar, 2014).

The main significant challenges for everyone involved in a scientific field related to climate change is to ensure that the ever-expanding volume of data is easily and freely available. Additionally, it has to be made sure that these data sets are formatted in such a form that a broad community from a diverse field of sciences can use them. Notably, the description of model usability and limitations, e.g. spatial and temporal sampling uncertainties, instrument changes and quality control, are of importance to ensure, that the results based on the dataset are correct. The availability is especially important as a growing number of scientists from related fields, professionals in resource management and politicians are seeking information to reach well-informed decisions for the future. The goal has to be to make the data understandable and available, so everybody has access and can use climate data in one or another way in his or her daily life. (Overpeck et al., 2011)

Geodesy serves as a component of the global effort to observe the system Earth and produce permanently updated data sets. As the discussion showed, it adds a substantial contribution, which needs to be communicated to the public. It is time that geodesy gains public recognition as part of normal life, so that the continuation of the satellite missions, as well as sustainable research, is secured. Moreover, geodesy may be one of the answers to monitor our ever-changing world and deliver the objective data basis needed to fight climate change.

¹⁴Operation Weather Rescue, <https://www.zooniverse.org/projects/edh/weather-rescue/>. Retrieved 19.11.2019.

Chapter 6.

Conclusions and Outlook

6.1. Conclusions

Since the launch of the first satellite Sputnik-1 gravity can be observed from space. A new era started with the dedicated satellite missions CHAMP, GRACE and GOCE (see Section 1.2), resulting in a substantial improvement of our knowledge of the Earth's gravity field. Currently, GRACE-FO is in orbit, raising the question of which future mission will continue the successful time series of temporal gravity fields and improve its performance.

The primary research objective (see Chapter 2) of this thesis was to investigate the potential of a second and third satellite pair in a future LL-SST mission regarding its overall performance, a possible NRT processing scheme and tested a flood detection application. The full-scale simulation software (see Chapter 3) based on the short-arc approach enabled the analysis.

Publication I, see A.1, looks at possible single and double pair scenarios and the key parameters influencing their performance. The consistent quantification allows evaluating each factor impacting the performance. The results enabled the establishment of a priority list identifying a double pair mission with a LRI sensor as a priority. A double-pair mission allows not only to retrieve the full AOHIS, but also gives a significant improvement in the performance.

For the case of a double pair solution consisting of a near-polar and an inclined pair, publication III, see A.3, analyses the potential of a NRT processing without a priori information. The proposal of the Wiese approach combined with a sliding window averaging improves not only the overall solution, but also estimates long-wavelength daily gravity fields. The investigation also showed that a reduction of the retrieval period to only three days still allows processing stable solutions.

The double-pair data set was then investigated in Publication IV, see A.4, regarding its potential in flood detection. Only flood events visible in the simulated time-variable

Chapter 6. Conclusions and Outlook

gravity field were used. A new processing chain for the detection was tested successfully, but also showed, that only 20% of floods were detectable without any additional data.

Lastly, a third satellite pair was added and investigated in publication II, see A.2. The additional pair was in one case set up as a near-polar pair, and in a second case as an inclined pair. While an improvement, compared to a double pair solution, could be observed due to increased redundancy of observations, the impact of the second pair on the solution was more significant. The biggest advantage of a multi-pair solution is the possibility to estimate daily gravity fields with higher spatial resolution.

Based on the analysed scenarios, I highly recommend lobbying on the one hand at different space agencies regarding a NGGM mission. But as the long-term service character is also essential, a collaboration with another service-influenced business model might also be of interest: Micro-constellations focused on, e.g. the distribution of high-speed internet. First investigations into micro-satellite constellations and strings of micro-satellites have already been done with promising results (Yunck et al., 2016, Deccia et al., 2017, 2018, Pfaffenzeller et al., 2019). These satellite constellations cannot reach the performance of a dedicated gravity mission but have the advantage of a continuous monitoring functionality.

In the discussion, the importance of observing the time-variable component of the Earth itself is emphasised. The observation system of GRACE allowed for the first time to observe the complete hydrological system, see Section 5.1. While a satellite-based gravity monitoring system has its inherent limitations, such as the conflicting parameters of spatial and temporal resolution, continuous, consistent and global observation is a real advantage. The gap between GRACE and GRACE-FO is one of the disadvantages of a satellite-based system, as a satellite has to be replaced from time to time. As observing mass change has been defined as one of NASA's highest priorities in Earth observation, the intent to continue the time series exists.

6.2. Outlook

In less than two decades since the initial gravimetric mission, gravity field missions have made themselves indispensable. Through their unique view of our world, they have enhanced our knowledge considerably. Part of the thesis was to establish a basis for decisions regarding possible NGGM for European stakeholders. An initial step towards a possible European NGGM contribution was made via the *ESA's Council at Ministerial Level, Space19+* to continue the efforts in the field of EO¹. In the first phase of a potential NGGM mission the efforts of industry are supported by geodetic research on data level with simulations of achievable performances.

¹ESA news, http://www.esa.int/About_Us/Corporate_news/. Retrieved 16.12.2019.

In line with a broader scope of NGGM, the focus of geodesy has to be placed on the potential of data based on a multi-pair (2+) constellation. This means the improvement of processing strategies, necessary background models as well as research into possible applications. The simulated data sets generated within this thesis allow for a starting point for research in the extensive field of applications. Gravity missions deliver global time-variable gravity fields - possibly in NRT with a latency of a day. The combination with other data sources of different spatio-temporal resolution is a worthwhile investigation as each measurement has its advantages and drawbacks. In a possible synergistic approach, individual limitations can be reduced or even eliminated.

In addition, I am also interested in studying possible commercial options as space experiences a wave of commercialization potentially opening the option to co-opt one of the many planned mega constellations. The communication constellation Starlink by SpaceX has permission for the launch of 12.000 satellites, with a pending application for up to 30.000 satellites in three orbit altitudes from 340 km to 1325 km. SpaceX already launched 122 satellites (as of Nov. 2019)². The company Planet operates a fleet of micro satellites for Earth imagery in a 500 km Sun-synchronous orbit³. Both of these constellations are not designed for a gravity mission. However, these satellites (with small adaptations) could be potentially used for the monitoring of the temporal gravity field as both fly in LEO orbits.

²SpaceX launch, <https://www.spacex.com/news/2019/11/11/starlink-mission>. Retrieved 18.12.2019.

³Planet, <https://www.planet.com/>. Retrieved 18.12.2019.

Bibliography

- Abrykosov, P., Pail, R., Gruber, T., Zahzam, N., Bresson, A., Hardy, E., Christophe, B., Bidel, Y., Carraz, O., and Siemes, C. (2019). Impact of a novel hybrid accelerometer on satellite gravimetry performance. *Advances in Space Research*, 63(10):3235 – 3248. DOI: 10.1016/j.asr.2019.01.034.
- Allen, M., Dube, O., Solecki, W., Aragón-Durand, F., Cramer, W., Humphreys, S., Kainuma, M., Kala, J., Mahowald, N., Mulugetta, Y., Perez, R., Wairiu, M., , and Zickfeld, K. (2018). *Framing and Context*, chapter Global Warming of 1.5°C. An IPCC Special Report on the impacts of global warming of 1.5°C above pre-industrial levels and related global greenhouse gas emission pathways, in the context of strengthening the global response to the threat of climate change, sustainable development, and efforts to eradicate poverty. URL: <https://www.ipcc.ch/sr15/>.
- Balmino, G., Reigber, C., and Moynot, B. (1976). A geopotential model determined from recent satellite observing campaigns (GRIM1). *manuscripta geodaetica*, 1(1):41–69.
- Baumgartner, A. and Reichel, E. (1975). *The World Water Balance*. Elsevier, New York.
- Beaudoing, H., Rodell, M., Getirana, A., and Li, B. (2017). Groundwater and soil moisture conditions from GRACE data assimilation 14 7-days 0.125 x 0.125 degree v2.0. Goddard Earth Sciences Data and Information Services Center (GES DISC).
- Bender, P. L., Wiese, D. N., and Nerem, R. S. (2008). A possible dual-GRACE mission with 90 degree and 63 degree inclination orbits. Paper presented at third international symposium on formation flying, ESA, Noordwijk, Netherlands.
- Bertiger, W. I., Bar-Sever, Y. E., Christensen, E. J., Davis, E. S., Guinn, J. R., Haines, B. J., Ibanez-Meier, R. W., Jee, J. R., Lichten, S. M., Melbourne, W. G., Muellerschoen, R. J., Munson, T. N., Vigue, Y., Wu, S. C., Yunck, T. P., Schutz, B. E., Abusali, P. A. M., Rim, H. J., Watkins, M. M., and Willis, P. (1994). GPS precise tracking of TOPEX/POSEIDON: Results and implications. *Journal of Geophysical Research*, 99(C12):24449. DOI: 10.1029/94jc01171.
- Bouman, J., Floberghagen, R., and Rummel, R. (2013). More than 50 years of progress in satellite gravimetry. *Eos, Transactions American Geophysical Union*, 94(31):269–270. DOI: 10.1002/2013eo310001.

Bibliography

- Buchar, E. (1958). Motion of the nodal line of the second Russian earth satellite (1957 β) and flattening of the earth. *Nature*, 182(4629):198–199. DOI: 10.1038/182198b0.
- Budyko, M. I. (1969). The effect of solar radiation variations on the climate of the earth. *Tellus*, 21(5):611–619. DOI: 10.3402/tellusa.v21i5.10109.
- Caron, L., Ivins, E. R., Larour, E., Adhikari, S., Nilsson, J., and Blewitt, G. (2018). GIA model statistics for GRACE hydrology, cryosphere, and ocean science. *Geophysical Research Letters*, 45(5):2203–2212. DOI: 10.1002/2017gl076644.
- Cazenave, A., Dominh, K., Guinehut, S., Berthier, E., Llovel, W., Ramillien, G., Ablain, M., and Larnicol, G. (2009). Sea level budget over 2003–2008: A reevaluation from GRACE space gravimetry, satellite altimetry and argo. *Global and Planetary Change*, 65(1-2):83–88. DOI: 10.1016/j.gloplacha.2008.10.004.
- Church, J., Clark, P., Cazenave, A., Gregory, J., Jevrejeva, S., Levermann, A., Merrifield, M., Milne, G., Nerem, R., Nunn, P., Payne, A., Pfeffer, W., Stammer, D., and Unnikrishnan, A. (2013). *Sea Level Change*, chapter Climate Change 2013: The Physical Science Basis. Contribution of Working Group I to the Fifth Assessment Report of the Intergovernmental Panel on Climate Change. Cambridge University Press, Cambridge, United Kingdom and New York, NY, USA. URL: <https://www.ipcc.ch/report/ar5/wg1/>.
- Church, J. A., Aarup, T., Woodworth, P. L., Wilson, W. S., Nicholls, R. J., Rayner, R., Lambeck, K., Mitchum, G. T., Steffen, K., Cazenave, A., Blewitt, G., Mitrovica, J. X., and Lowe, J. A. (2010). *Sea-Level Rise and Variability: Synthesis and Outlook for the Future*, chapter 13, pages 402–419. John Wiley and Sons, Ltd. DOI: 10.1002/9781444323276.ch13.
- Cook, J., Nuccitelli, D., Green, S. A., Richardson, M., Winkler, B., Painting, R., Way, R., Jacobs, P., and Skuce, A. (2013). Quantifying the consensus on anthropogenic global warming in the scientific literature. *Environmental Research Letters*, 8(2):024024. DOI: 10.1088/1748-9326/8/2/024024.
- Dai, A., Trenberth, K. E., and Qian, T. (2004). A global dataset of palmer drought severity index for 1870–2002: Relationship with soil moisture and effects of surface warming. *Journal of Hydrometeorology*, 5(6):1117–1130. DOI: 10.1175/jhm-386.1.
- Daras, I. (2016). *Gravity field processing towards future LL-SST satellite missions*. PhD thesis, Technische Universität München. URL: <http://www.dgk.badw.de/fileadmin/docs/c-770.pdf>.
- Daras, I. and Pail, R. (2017). Treatment of temporal aliasing effects in the context of next generation satellite gravimetry missions. *Journal of Geophysical Research: Solid Earth*, 122(9):7343–7362. DOI: 10.1002/2017JB014250.

- Deccia, C., Nerem, R., and Wiese, D. (2018). Designing a GRACE-type satellite constellation for hydrologic science. American Geophysical Union (AGU). Fall Meeting 2018.
- Deccia, C., Nerem, R., and Yunck, T. (2017). A smallsat constellation mission architecture for a GRACE-type mission design. American Geophysical Union (AGU). Fall Meeting 2017.
- Dickey, J., Bentley, C., Bilham, R., Carton, J., Eanes, R., Herring, T., Kaula, W., Lagerloef, G., Rojstaczer, S., Smith, W., van der Dool, H., Wahr, J., and Zuber, M. (1997). Satellite gravity and the geosphere. committee on Earth Gravity from Space, National Academy Press, Washington D.C.
- Dionisio, S., Anselmi, A., Bonino, L., Cesare, S., Massotti, L., and Silvestrin, P. (2018). The “next generation gravity mission”: challenges and consolidation of the system concepts and technological innovations. In *15th International Conference on Space Operations*. American Institute of Aeronautics and Astronautics. DOI: 10.2514/6.2018-2495.
- Elsaka, B., Kusche, J., and Ilk, K.-H. (2012). Recovery of the earth’s gravity field from formation-flying satellites: Temporal aliasing issues. *Advances in Space Research*, 50(11):1534–1552. DOI: 10.1016/j.asr.2012.07.016.
- Elsaka, B., Raimondo, J.-C., Brieden, P., Reubelt, T., Kusche, J., Flechtner, F., Pour, S. I., Sneeuw, N., and Müller, J. (2013). Comparing seven candidate mission configurations for temporal gravity field retrieval through full-scale numerical simulation. *Journal of Geodesy*, 88(1):31–43. DOI: 10.1007/s00190-013-0665-9.
- ESA (2010). Assessment of a next generation gravity mission to monitor the variations of earth’s gravity field. Technical report, ESA Contract No. 22643/09/NL/AF.
- ESA (2011). Assessment of a next generation gravity mission to monitor the variations of earth’s gravity field. Technical report, ESTEC Contract No. 22672/09/NL/AF.
- Faghmous, J. H. and Kumar, V. (2014). Spatio-temporal data mining for climate data: Advances, challenges, and opportunities. In *Studies in Big Data*, pages 83–116. Springer Berlin Heidelberg. DOI: 10.1007/978-3-642-40837-3_3.
- Famiglietti, J. S. (2004). Remote sensing of terrestrial water storage, soil moisture and surface waters. In *Geophysical Monograph Series*, pages 197–207. American Geophysical Union. DOI: 10.1029/150gm16.
- Famiglietti, J. S., Lo, M., Ho, S. L., Bethune, J., Anderson, K. J., Syed, T. H., Swenson, S. C., de Linage, C. R., and Rodell, M. (2011). Satellites measure recent rates of groundwater depletion in california’s central valley. *Geophysical Research Letters*, 38(3). DOI: 10.1029/2010gl046442.

Bibliography

- Fischer, H., Amelung, D., and Said, N. (2019). The accuracy of German citizens' confidence in their climate change knowledge. *Nature Climate Change*, 9(10):776–780. DOI: 10.1038/s41558-019-0563-0.
- Flechtner, F., Webb, F., and Watkins, M. (2017). Current status of the GRACE follow-on mission. EGU2017-4566, Vienna, Austria.
- Forootan, E., Didova, O., Schumacher, M., Kusche, J., and Elsaka, B. (2014). Comparisons of atmospheric mass variations derived from ECMWF reanalysis and operational fields, over 2003–2011. *Journal of Geodesy*, 88(5):503–514. DOI: 10.1007/s00190-014-0696-x.
- Funk, C. (2007). Mixed messages about public trust in science. *Issues in Science and Technology*, 33(1).
- Gehlbach, H., Robinson, C. D., and Vriesema, C. C. (2019). Leveraging cognitive consistency to nudge conservative climate change beliefs. *Journal of Environmental Psychology*, 61:134–137. DOI: 10.1016/j.jenvp.2018.12.004.
- Gruber, T., Murböck, M., and Team, N.-D. (2014). e2.motion - earth system mass transport mission (square) - concept for a next generation gravity field mission. Technical Report 318, C.H. Beck.
- Gunter, B., Urban, T., Riva, R., Helsen, M., Harpold, R., Poole, S., Nagel, P., Schutz, B., and Tapley, B. (2009). A comparison of coincident GRACE and ICESat data over antarctica. *Journal of Geodesy*, 83(11):1051–1060. DOI: 10.1007/s00190-009-0323-4.
- Han, J. and Roads, J. O. (2004). U.S. climate sensitivity simulated with the NCEP regional spectral model. *Climatic Change*, 62(1-3):115–154. DOI: 10.1023/b:clim.0000013675.66917.15.
- Han, S.-C., Sauber, J., and Luthcke, S. (2010). Regional gravity decrease after the 2010 maule (chile) earthquake indicates large-scale mass redistribution. *Geophysical Research Letters*, 37(23). DOI: 10.1029/2010gl045449.
- Hanna, E., Fettweis, X., Mernild, S. H., Cappelen, J., Ribergaard, M. H., Shuman, C. A., Steffen, K., Wood, L., and Mote, T. L. (2013). Atmospheric and oceanic climate forcing of the exceptional Greenland ice sheet surface melt in summer 2012. *International Journal of Climatology*, 34(4):1022–1037. DOI: 10.1002/joc.3743.
- Hao, Z., AghaKouchak, A., Nakhjiri, N., and Farahmand, A. (2014). Global integrated drought monitoring and prediction system. *Scientific Data*, 1(1). DOI: 10.1038/sdata.2014.1.
- Hauk, M. and Pail, R. (2018). Treatment of ocean tide aliasing in the context of a next generation gravity field mission. *Geophysical Journal International*, 214(1):345–365. DOI: 10.1093/gji/ggy145.

- Hauk, M. and Pail, R. (2019). Gravity field recovery using high-precision, high-low inter-satellite links. *Remote Sensing*, 11(5):537. DOI: 10.3390/rs11050537.
- Hauk, M., Schlicht, A., Pail, R., and Murböck, M. (2017). Gravity field recovery in the framework of a geodesy and time reference in space (GETRIS). *Advances in Space Research*, 59(8):2032–2047. DOI: 10.1016/j.asr.2017.01.028.
- Hoegh-Guldberg, O., Jacob, D., Taylor, M., Bindi, M., Brown, S., Camilloni, I., Diedhiou, A., Djalante, R., Ebi, K., Engelbrecht, F., Guiot, J., Hijioka, Y., Mehrotra, S., Payne, A., Seneviratne, S., Thomas, A., Warren, R., , and Zhou, G. (2018). *Impacts of 1.5°C Global Warming on Natural and Human Systems*, chapter Global Warming of 1.5°C. An IPCC Special Report on the impacts of global warming of 1.5°C above pre-industrial levels and related global greenhouse gas emission pathways, in the context of strengthening the global response to the threat of climate change, sustainable development, and efforts to eradicate poverty.
- Hofmann-Wellenhof, B. and Moritz, H. (2006). *Physical Geodesy*. Springer Vienna. DOI: 10.1007/978-3-211-33545-1.
- Houborg, R., Rodell, M., Li, B., Reichle, R., and Zaitchik, B. F. (2012). Drought indicators based on model-assimilated gravity recovery and climate experiment (GRACE) terrestrial water storage observations. *Water Resources Research*, 48(7). DOI: 10.1029/2011wr011291.
- Iran Pour, S., Reubelt, T., and Sneeuw, N. (2013). Quality assessment of sub-nyquist recovery from future gravity satellite missions. *Advances in Space Research*, 52(5):916–929. DOI: 10.1016/j.asr.2013.05.026.
- Izsak, I. G. (1963). A note on perturbation theory. *The Astronomical Journal*, 68:559. DOI: 10.1086/109180.
- Jäger, R. R., Müller, T., and Saler, H. (2005). *Klassische und robuste Ausgleichungsverfahren - ein Leitfaden für Ausbildung und Praxis von Geodäten und Geoinformatikern*. Wichmann, Heidelberg, 1. edition.
- Klinger, B., Mayer-Gürr, T., Behzadpour, S., Ellmer, M., Kvas, A., and Zehentner, N. (2016). The new ITSG-Grace2016 release. DOI: 10.13140/RG.2.1.1856.7280.
- Kozai, Y. (1961). The gravitational field of the earth derived from motions of three satellites. *The Astronomical Journal*, 66:8. DOI: 10.1086/108349.
- Kurtenbach, E., Mayer-Gürr, T., and Eicker, A. (2009). Deriving daily snapshots of the earth’s gravity field from GRACE L1B data using Kalman filtering. *Geophysical Research Letters*, 36(17). DOI: 10.1029/2009gl039564.

Bibliography

- Kvas, A., Christian, G., Gouweleeuw, B., Chen, Q., Poropat, L., Flechtner, F., Mayer-Gürr, T., and Güntner, A. (2017). First results of the EGSiEM near real-time service. EGU2017-15174, Vienna, Austria.
- Kwok, R., Kacimi, S., Markus, T., Kurtz, N. T., Studinger, M., Sonntag, J. G., Manizade, S. S., Boisvert, L. N., and Harbeck, J. P. (2019). ICESat-2 surface height and sea ice freeboard assessed with ATM lidar acquisitions from operation IceBridge. *Geophysical Research Letters*, 46(20):11228–11236. DOI: 10.1029/2019gl084976.
- Lambeck, K., Esat, T., and Potter, E.-K. (2002). Links between climate and sea level for the past three million years. *Nature*, 419:199–206. DOI: 10.1038/nature01089.
- Lambert, A., Huang, J., van der Kamp, G., Henton, J., Mazzotti, S., James, T. S., Courtier, N., and Barr, A. G. (2013). Measuring water accumulation rates using GRACE data in areas experiencing glacial isostatic adjustment: The nelson river basin. *Geophysical Research Letters*, 40(23):6118–6122. DOI: 10.1002/2013gl057973.
- Lenaerts, J. T. M., Medley, B., Broeke, M. R., and Wouters, B. (2019). Observing and modeling ice sheet surface mass balance. *Reviews of Geophysics*, 57(2):376–420. DOI: 10.1029/2018rg000622.
- Lerch, F. J., Klosko, S. M., Laubscher, R. E., and Wagner, C. A. (1979). Gravity model improvement using Geos 3 (GEM 9 and 10). *Journal of Geophysical Research*, 84(B8):3897. DOI: 10.1029/jb084ib08p03897.
- Lettenmaier, D. P. and Famiglietti, J. S. (2006). Water from on high. *Nature*, 444(7119):562–563. DOI: 10.1038/444562a.
- Leuliette, E. W. and Miller, L. (2009). Closing the sea level rise budget with altimetry, argo, and GRACE. *Geophysical Research Letters*, 36(4). DOI: 10.1029/2008gl036010.
- Löcher, A. and Ilk, K. H. (2005). Energy balance relations for validation of gravity field models and orbit determinations applied to the CHAMP mission. In Reigber, C., Lühr, H., Schwintzer, P., and Wickert, J., editors, *Earth Observation with CHAMP*, pages 53–58. Springer-Verlag. DOI: 10.1007/3-540-26800-6_8.
- Long, D., Scanlon, B. R., Longuevergne, L., Sun, A. Y., Fernando, D. N., and Save, H. (2013). GRACE satellite monitoring of large depletion in water storage in response to the 2011 drought in Texas. *Geophysical Research Letters*, 40(13):3395–3401. DOI: 10.1002/grl.50655.
- Long, D., Shen, Y., Sun, A., Hong, Y., Longuevergne, L., Yang, Y., Li, B., and Chen, L. (2014). Drought and flood monitoring for a large karst plateau in southwest china using extended GRACE data. *Remote Sensing of Environment*, 155:145–160. DOI: 10.1016/j.rse.2014.08.006.

- Loomis, B. D., Nerem, R. S., and Luthcke, S. B. (2011). Simulation study of a follow-on gravity mission to GRACE. *Journal of Geodesy*, 86(5):319–335. DOI: 10.1007/s00190-011-0521-8.
- Loon, A. F. V., Kumar, R., and Mishra, V. (2017). Testing the use of standardised indices and GRACE satellite data to estimate the european 2015 groundwater drought in near-real time. *Hydrology and Earth System Sciences*, 21(4):1947–1971. DOI: 10.5194/hess-21-1947-2017.
- Luthcke, S. B., Sabaka, T., Loomis, B., Arendt, A., McCarthy, J., and Camp, J. (2013). Antarctica, Greenland and Gulf of Alaska land-ice evolution from an iterated GRACE global mascon solution. *Journal of Glaciology*, 59(216):613–631. DOI: 10.3189/2013jog12j147.
- Malnes, E., Solbø, S., Lauknes, I., Evertsen, G., Tøllefsen, T., Solheim, I., and Indegard, M. (2005). FLOODMAN - global near-real time flood monitoring for hydrological users. ACTIF workshop, At Tromsø, Norway.
- Masson-Delmotte, V., Schulz, M., Abe-Ouchi, A., Beer, J., Ganopolski, J., González Rouco, J. F., Jansen, E., Lambeck, K., Luterbacher, J., Naish, T., Osborn, T., Otto-Bliesner, B., Quinn, T., Ramesh, R., Rojas, M., Shao, X., and Timmermann, A. (2013). *Information from paleoclimate archives*, pages 383–464. Cambridge University Press, Cambridge, UK. DOI: 10.1017/CBO9781107415324.013.
- Mayer-Gürr, T. (2006). *Gravitationsfeldbestimmung aus der Analyse kurzer Bahnbögen am Beispiel der Satellitenmissionen CHAMP und GRACE*. PhD thesis, Universität Bonn. URL: <http://hss.ulb.uni-bonn.de/2006/0904/0904.pdf>.
- Merson, R. H. and King-Hele, D. G. (1958). Use of artificial satellites to explore the earth’s gravitational field: Results from Sputnik 2. *Nature*, 182(4636):640–641. DOI: 10.1038/182640a0.
- Molodtsova, T., Molodtsov, S., Kirilenko, A., Zhang, X., and VanLooy, J. (2015). Evaluating flood potential with GRACE in the United States. *Natural Hazards and Earth System Sciences Discussions*, 3(11):6977–6996. DOI: 10.5194/nhessd-3-6977-2015.
- Murböck, M. and Pail, R. (2014). Reducing non-tidal aliasing effects by future gravity satellite formations. In Rizos, C. and Willis, P., editors, *Earth on the Edge: Science for a Sustainable Planet, IAG Symposia*, volume 139, pages 407–412. Springer. DOI: 10.1007/978-3-642-37222-3_54.
- Murböck, M., Pail, R., Daras, I., and Gruber, T. (2013). Optimal orbits for temporal gravity recovery regarding temporal aliasing. *Journal of Geodesy*, 88(2):113–126. DOI: 10.1007/s00190-013-0671-y.

Bibliography

- Nerem, R. S., Beckley, B. D., Fasullo, J. T., Hamlington, B. D., Masters, D., and Mitchum, G. T. (2018). Climate-change-driven accelerated sea-level rise detected in the altimeter era. *Proceedings of the National Academy of Sciences*, 115(9):2022–2025. DOI: 10.1073/pnas.1717312115.
- Neumeyer, J. (2010). Superconducting gravimetry. In Xu, G., editor, *Sciences of Geodesy - I*, pages 339–413. Springer Berlin Heidelberg. DOI: 10.1007/978-3-642-11741-1_10.
- Niebauer, T. M., Sasagawa, G. S., Faller, J. E., Hilt, R., and Klopping, F. (1995). A new generation of absolute gravimeters. *Metrologia*, 32(3):159–180. DOI: 10.1088/0026-1394/32/3/004.
- Niemeier, W. (2008). *Ausgleichsrechnung - statistische Auswertemethoden*. Walter de Gruyter, Berlin, 2. edition.
- O’Keefe, J. A., Eckels, A., and Squires, R. K. (1959). The gravitational field of the earth. *The Astronomical Journal*, 64:245. DOI: 10.1086/107928.
- Oki, T. (2006). The hydrologic cycles and global circulation. In *Encyclopedia of Hydrological Sciences*. DOI: 10.1002/0470848944.hsa001.
- Oki, T., Entekhabi, D., and Harrold, T. I. (2004). The global water cycle. In *Geophysical Monograph Series*, pages 225–237. American Geophysical Union. DOI: 10.1029/150gm18.
- Overpeck, J. T., Meehl, G. A., Bony, S., and Easterling, D. R. (2011). Climate data challenges in the 21st century. *Science*, 331(6018):700–702. DOI: 10.1126/science.1197869.
- Pail, R., Bingham, R., Braitenberg, C., Dobslaw, H., Eicker, A., Güntner, A., Horwath, M., Ivins, E., Longuevergne, L., Panet, I., and Wouters, B. (2015). Science and user needs for observing global mass transport to understand global change and to benefit society. *Surveys in Geophysics*, 36(6):743–772. DOI: 10.1007/s10712-015-9348-9.
- Pail, R. and Team, E. G. S. (2018). Mass variation observing system by high-low inter-satellite links (MOBILE) - a mission proposal in response to ESA’s earth explorer 10 call. In *International Symposium Gravity, Geoid and Height Systems 2*, Copenhagen.
- Panet, I., Flury, J., Biancale, R., Gruber, T., Johannessen, J., van den Broeke, M., van Dam, T., Gegout, P., Hughes, C., Ramillien, G., Sasgen, I., Seoane, L., and Thomas, M. (2013). Earth system mass transport mission (e.motion): A concept for future earth gravity field measurements from space. *Surveys in Geophysics*, 34(2):141–163. DOI: 10.1007/s10712-012-9209-8.
- Pappenberger, F., Thielen, J., and Medico, M. D. (2011). The impact of weather forecast improvements on large scale hydrology: analysing a decade of forecasts of the european flood alert system. *Hydrological Processes*, 25(7):1091–1113. DOI: 10.1002/hyp.7772.

- Petropoulos, G. P., Ireland, G., and Barrett, B. (2015). Surface soil moisture retrievals from remote sensing: Current status, products and future trends. *Physics and Chemistry of the Earth, Parts A/B/C*, 83-84:36–56. DOI: 10.1016/j.pce.2015.02.009.
- Pfaffenzeller, N., Pail, R., and Yunck, T. (2019). Gravity field retrieval with constellations and formations of small satellites in the context of next generation gravity field missions (NGGMs). In *2019 GRACE and GRACE-FO Science Team Meeting*, Pasadena.
- Purkhauser, A. F., Koch, J. A., and Pail, R. (2019). Applicability of NGGM near-real time simulations in flood detection. *Journal of Geodetic Science*, 9(1):111–126. DOI: 10.1515/jogs-2019-0011.
- Purkhauser, A. F. and Pail, R. (2019). Next generation gravity missions: near-real time gravity field retrieval strategy. *Geophysical Journal International*, 217(2):1314–1333. DOI: 10.1093/gji/ggz084.
- Purkhauser, A. F. and Pail, R. (2020). Triple-pair constellation configurations for temporal gravity field retrieval. *Remote Sensing*, 12(5):831. DOI: 10.3390/rs12050831.
- Purkhauser, A. F., Siemes, C., and Pail, R. (2020). Consistent quantification of the impact of key mission design parameters on the performance of next-generation gravity missions. *Geophysical Journal International*, 221(2):1190–1210. DOI: 10.1093/gji/ggaa070.
- Reager, J. T. and Famiglietti, J. S. (2009). Global terrestrial water storage capacity and flood potential using GRACE. *Geophysical Research Letters*, 36(23). DOI: 10.1029/2009gl040826.
- Reigber, C., Schwintzer, P., and Lühr, H. (1999). The CHAMP geopotential mission. *Bollettino di Geofisica Teorica ed Applicata*, 40:285–289.
- Reubelt, T., Austen, G., and Grafarend, E. (2003). Space gravity spectroscopy - determination of the earth's gravitational field by means of newton interpolated LEO ephemeris case studies on dynamic (CHAMP rapid science orbit) and kinematic orbits. *Advances in Geosciences*, 1:127–135. DOI: 10.5194/adgeo-1-127-2003.
- Riser, S. C., Freeland, H. J., Roemmich, D., Wijffels, S., Troisi, A., Belbéoch, M., Gilbert, D., Xu, J., Pouliquen, S., Thresher, A., Traon, P.-Y. L., Maze, G., Klein, B., Ravichandran, M., Grant, F., Poulain, P.-M., Suga, T., Lim, B., Sterl, A., Sutton, P., Mork, K.-A., Vélez-Belchí, P. J., Ansorge, I., King, B., Turton, J., Baringer, M., and Jayne, S. R. (2016). Fifteen years of ocean observations with the global argo array. *Nature Climate Change*, 6(2):145–153. DOI: 10.1038/nclimate2872.
- Roads, J., Oglesby, R., Hoffman, F., and Robertson, F. (2006). Acceleration of the global hydrologic cycle. In *Encyclopedia of Hydrological Sciences*. DOI: 10.1002/0470848944.hsa204.

Bibliography

- Robertson, F. R. (2006). Observations of the global water cycle - satellites. In *Encyclopedia of Hydrological Sciences*. DOI: 10.1002/0470848944.hsa182.
- Rodell, M. and Famiglietti, J. S. (1999). Detectability of variations in continental water storage from satellite observations of the time dependent gravity field. *Water Resources Research*, 35(9):2705–2723. DOI: 10.1029/1999wr900141.
- Rodell, M., Velicogna, I., and Famiglietti, J. S. (2009). Satellite-based estimates of groundwater depletion in India. *Nature*, 460(7258):999–1002. DOI: 10.1038/nature08238.
- Rummel, R. (2002). Gravity gradiometry: From Loránd Eötvös to modern space age. *Acta Geodaetica et Geophysica Hungarica*, 37(4):435–444. DOI: 10.1556/ageod.37.2002.4.7.
- Rummel, R., Yi, W., and Stummer, C. (2011). GOCE gravitational gradiometry. *Journal of Geodesy*, 85(11):777–790. DOI: 10.1007/s00190-011-0500-0.
- Schneider, M. (1969). Outline of a general orbit determination method. In Champion, K. S. W., Smith, P. A., and Smith-Rose, R. L., editors, *Space Research IX, Proceedings of Open Meetings of Working Groups (OMWG) on Physical Sciences of the 11th Plenary Meeting of the Committee on Space Research (COSPAR), Tokyo*, pages 37–40. North-Holland Publishing Company.
- Schneider, S. H., Root, T. L., and Mastrandrea, M. D., editors (2011). *Encyclopedia of Climate and Weather*. Oxford University Press. DOI: 10.1093/acref/9780199765324.001.0001.
- Schutz, B. E. (1997). New observational techniques and precise orbit determination of artificial satellites. *Celestial mechanis and dynamical Astronomy*, 66(1):79–85. DOI: 10.1007/bf00048826.
- Seeber, G. (2008). *Satellite Geodesy - Foundations, Methods, and Applications*. Walter de Gruyter, Berlin, 1. edition.
- Sejas, S. A., Albert, O. S., Cai, M., and Deng, Y. (2014). Feedback attribution of the land-sea warming contrast in a global warming simulation of the NCAR CCSM4. *Environmental Research Letters*, 9(12):124005. DOI: 10.1088/1748-9326/9/12/124005.
- Seneviratne, S. I., Donat, M. G., Pitman, A. J., Knutti, R., and Wilby, R. L. (2016). Allowable CO₂ emissions based on regional and impact-related climate targets. *Nature*, 529(7587):477–483. DOI: 10.1038/nature16542.
- Shampine, L. F. and Gordon, M. K. (1975). *Computer solution of ordinary differential equations - the initial value problem*. W.H. Freeman, San Francisco.

- Shepherd, A., Ivins, E. R., A, G., Barletta, V. R., Bentley, M. J., Bettadpur, S., Briggs, K. H., Bromwich, D. H., Forsberg, R., Galin, N., Horwath, M., Jacobs, S., Joughin, I., King, M. A., Lenaerts, J. T. M., Li, J., Ligtenberg, S. R. M., Luckman, A., Luthcke, S. B., McMillan, M., Meister, R., Milne, G., Mouginot, J., Muir, A., Nicolas, J. P., Paden, J., Payne, A. J., Pritchard, H., Rignot, E., Rott, H., Sørensen, L. S., Scambos, T. A., Scheuchl, B., Schrama, E. J. O., Smith, B., Sundal, A. V., van Angelen, J. H., van de Berg, W. J., van den Broeke, M. R., Vaughan, D. G., Velicogna, I., Wahr, J., Whitehouse, P. L., Wingham, D. J., Yi, D., Young, D., and Zwally, H. J. (2012). A reconciled estimate of ice-sheet mass balance. *Science*, 338(6111):1183–1189. DOI: 10.1126/science.1228102.
- Skuce, A. G., Cook, J., Richardson, M., Winkler, B., Rice, K., Green, S. A., Jacobs, P., and Nuccitelli, D. (2016). Does it matter if the consensus on anthropogenic global warming is 97% or 99.99%? *Bulletin of Science, Technology and Society*, 36(3):150–156. DOI: 10.1177/0270467617702781.
- Sneeuw, N., Sharifi, M., and Keller, W. (2008). Gravity recovery from formation flight missions. In Freymueller, J. T., editor, *International Association of Geodesy Symposia*, volume 132, pages 29–34. Springer Berlin Heidelberg. DOI: 10.1007/978-3-540-74584-6_5.
- Sun, A. Y., Green, R., Rodell, M., and Swenson, S. (2010). Inferring aquifer storage parameters using satellite and in situ measurements: Estimation under uncertainty. *Geophysical Research Letters*, 37(10). DOI: 10.1029/2010gl043231.
- Tanaka, Y. and Heki, K. (2014). Long- and short-term postseismic gravity changes of megathrust earthquakes from satellite gravimetry. *Geophysical Research Letters*, 41(15):5451–5456. DOI: 10.1002/2014gl060559.
- Tapley, B. D., Bettadpur, S., Watkins, M., and Reigber, C. (2004). The gravity recovery and climate experiment: Mission overview and early results. *Geophysical Research Letters*, 31(9). DOI: 10.1029/2004gl019920.
- Tapley, B. D., Watkins, M. M., Flechtner, F., Reigber, C., Bettadpur, S., Rodell, M., Sasgen, I., Famiglietti, J. S., Landerer, F. W., Chambers, D. P., Reager, J. T., Gardner, A. S., Save, H., Ivins, E. R., Swenson, S. C., Boening, C., Dahle, C., Wiese, D. N., Dobslaw, H., Tamisiea, M. E., and Velicogna, I. (2019). Contributions of GRACE to understanding climate change. *Nature Climate Change*, 9(5):358–369. DOI: 10.1038/s41558-019-0456-2.
- Tiwari, V. M., Wahr, J., and Swenson, S. (2009). Dwindling groundwater resources in northern India, from satellite gravity observations. *Geophysical Research Letters*, 36(18). DOI: 10.1029/2009gl039401.

Bibliography

- Touboul, P., Metris, G., Rodrigues, M., Andre, Y., Baghi, Q., Berge, J., Boulanger, D., Bremer, S., Carle, P., Chhun, R., Christophe, B., Cipolla, V., Damour, T., Danto, P., Dittus, H., Fayet, P., Foulon, B., Gageant, C., Guidotti, P.-Y., Hagedorn, D., Hardy, E., Huynh, P.-A., Inchauspe, H., Kayser, P., Lala, S., Lämmerzahl, C., Lebat, V., Leseur, P., Liorzou, F., List, M., Löffler, F., Panet, I., Pouilloux, B., Prieur, P., Rebray, A., Reynaud, S., Rievers, B., Robert, A., Selig, H., Serron, L., Sumner, T., Tanguy, N., and Visser, P. (2017). MICROSCOPE mission: First results of a space test of the equivalence principle. *Physical Review Letters*, 119(23). DOI: 10.1103/physrevlett.119.231101.
- Trenberth, K. E. (2008). The impact of climate change and variability on heavy precipitation, floods, and droughts. In *Encyclopedia of Hydrological Sciences*. DOI: 10.1002/0470848944.hsa211.
- Trenberth, K. E., Dai, A., Rasmussen, R. M., and Parsons, D. B. (2003). The changing character of precipitation. *Bulletin of the American Meteorological Society*, 84(9):1205–1218. DOI: 10.1175/bams-84-9-1205.
- Vaughan, D., Comiso, J., Allison, I., Carrasco, J., Kaser, G., R. Kwok, P. M., Murray, T., Paul, F., Ren, J., Rignot, E., Solomina, O., Steffen, K., and Zhang, T. (2013). Observations: Cryosphere. In *Climate Change 2013 - The Physical Science Basis*, pages 317–382. Cambridge University Press. DOI: 10.1017/cbo9781107415324.012.
- Velicogna, I., Sutterley, T. C., and van den Broeke, M. R. (2014). Regional acceleration in ice mass loss from Greenland and Antarctica using GRACE time-variable gravity data. *Geophysical Research Letters*, 41(22):8130–8137. DOI: 10.1002/2014gl061052.
- Visser, P. (1999). Gravity field determination with GOCE and GRACE. *Advances in Space Research*, 23(4):771–776. DOI: 10.1016/s0273-1177(99)00154-4.
- von Schuckmann, K., Palmer, M. D., Trenberth, K. E., Cazenave, A., Chambers, D., Champollion, N., Hansen, J., Josey, S. A., Loeb, N., Mathieu, P.-P., Meyssignac, B., and Wild, M. (2016). An imperative to monitor earth’s energy imbalance. *Nature Climate Change*, 6(2):138–144. DOI: 10.1038/nclimate2876.
- Weigelt, M., Jäggi, A., Meyer, U., Arnold, D., Grahl, A., Sonica, K., Dahle, C., and Flechtner, F. (2017). HL-SST and SLR bridging the gap between GRACE and GRACE-follow on.
- Weigelt, M., van Dam, T., Jäggi, A., Prange, L., Tourian, M. J., Keller, W., and Sneeuw, N. (2013). Time-variable gravity signal in Greenland revealed by high-low satellite-to-satellite tracking. *Journal of Geophysical Research: Solid Earth*, 118(7):3848–3859. DOI: 10.1002/jgrb.50283.

- Wiese, D. N., Folkner, W. M., and Nerem, R. S. (2008). Alternative mission architectures for a gravity recovery satellite mission. *Journal of Geodesy*, 83(6):569–581. DOI: 10.1007/s00190-008-0274-1.
- Wiese, D. N., Nerem, R. S., and Han, S.-C. (2011a). Expected improvements in determining continental hydrology, ice mass variations, ocean bottom pressure signals, and earthquakes using two pairs of dedicated satellites for temporal gravity recovery. *Journal of Geophysical Research: Solid Earth*, 116(B11). DOI: 10.1029/2011jb008375.
- Wiese, D. N., Nerem, R. S., and Lemoine, F. G. (2011b). Design considerations for a dedicated gravity recovery satellite mission consisting of two pairs of satellites. *Journal of Geodesy*, 86(2):81–98. DOI: 10.1007/s00190-011-0493-8.
- Wiese, D. N., Visser, P., and Nerem, R. S. (2011c). Estimating low resolution gravity fields at short time intervals to reduce temporal aliasing errors. *Advances in Space Research*, 48(6):1094–1107. DOI: 10.1016/j.asr.2011.05.027.
- Willis, J., Chambers, D., Kuo, C.-Y., and Shum, C. (2010). Global sea level rise: Recent progress and challenges for the decade to come. *Oceanography*, 23(4):26–37. DOI: 10.5670/oceanog.2010.03.
- Willis, J. K., Chambers, D. P., and Nerem, R. S. (2008). Assessing the globally averaged sea level budget on seasonal to interannual timescales. *Journal of Geophysical Research*, 113(C6). DOI: 10.1029/2007jc004517.
- Woods, R. (2006). Hydrologic concepts of variability and scale. In *Encyclopedia of Hydrological Sciences*. DOI: 10.1002/0470848944.hsa002.
- Wouters, B., Riva, R. E. M., Lavallée, D. A., and Bamber, J. L. (2011). Seasonal variations in sea level induced by continental water mass: First results from GRACE. *Geophysical Research Letters*, 38(3). DOI: 10.1029/2010gl046128.
- Yeh, P. J.-F., Swenson, S. C., Famiglietti, J. S., and Rodell, M. (2006). Remote sensing of groundwater storage changes in illinois using the gravity recovery and climate experiment (GRACE). *Water Resources Research*, 42(12). DOI: 10.1029/2006wr005374.
- Yi, W. (2012). *The Earth’s gravity field from GOCE*. Dissertation, Technische Universität München. URL: <https://mediatum.ub.tum.de/doc/1135526/1135526.pdf>.
- Yunck, T. P., Jr., C. C. L., Saltman, A., Williams, A., and Villa, M. (2016). CICERO: Nanosat arrays for continuous Earth remote observation. In Pagano, T. S., editor, *CubeSats and NanoSats for Remote Sensing*, volume 9978, pages 41 – 48. International Society for Optics and Photonics, SPIE. DOI: 10.1117/12.2238879.

Appendix A.

Publications

A.1. P-I: Consistent quantification of the impact of key mission design parameters on the performance of next-generation gravity missions

Reference: Purkhauser, A. F., Siemes, C., and Pail, R. (2020). Consistent quantification of the impact of key mission design parameters on the performance of next-generation gravity missions. *Geophysical Journal International*, 221(2):1190–1210. DOI: 10.1093/gji/ggaa070

Copyright: This work originally has been published in *Geophysical Journal International*: <https://doi.org/10.1093/gji/ggaa070>. The Copyright has been transferred to Oxford University Press.

Abstract

The GRACE and GRACE-FO missions have been observing time variations of the Earth's gravity field for more than 15 years. For a possible successor mission, the need to continue mass change observations have to be balanced with the ambition for monitoring capabilities with enhanced spatial and temporal resolution that will enable improved scientific results and will serve operational services and applications. Various study groups performed individual simulations to analyse different aspects of possible NGGMs from a scientific and technical point of view. As these studies are not directly comparable due to different assumptions regarding mission design and instrumentation, the goal of this paper is to systematically analyse and quantify the key mission parameters (number of satellite pairs, orbit altitude, sensors) and the impact of various error sources (AO, OT models, post-processing) in a consistent simulation environment. Our study demonstrates that a single-pair mission with laser interferometry in a low orbit with a drag compensation system would be the only possibility within the single-pair options to increase the performance compared to the GRACE/GRACE-FO. Tailored

Appendix A. Publications

post-processing is not able to achieve the same performance as a double-pair mission without post-processing. Also, such a mission concept does not solve the problems of temporal aliasing due to observation geometry. In contrast, double-pair concepts have the potential to retrieve the full AOHIS signal and in some cases even double the performance to the comparable single-pair scenario. When combining a double-pair with laser interferometry and an improved accelerometer, the sensor noise is, apart from the ocean tide modeling errors, one of the limiting factors. Therefore, the next big step for observing the gravity field globally with a satellite mission can only be taken by launching a double pair mission. With this quantification of possible of key architecture features of a future satellite gravity mission the study aims to improve the available information to allow for an informed decision making and give an indication of priority for the different mission concepts.

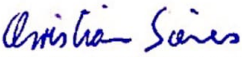

Declaration of own contribution



Table A.1.: Contribution to P-I

Involved in	Estimated contribution
Ideas and conceptual design	90%
Computation and results	100%
Analysis and interpretation	90%
Manuscript, figures and tables	90%
Total	92,5%

Confirmation by Co-Authors

I hereby confirm the correctness of the declaration of the contribution of Anna F. Purkhauser for the publication P-IV in Table A.1:


.....
Christian Siemes Date
(TU Delft (formerly ESA), The Netherlands)



.....
Roland Pail Date
(IAPG, LRG, TUM)


Consistent quantification of the impact of key mission design parameters on the performance of next-generation gravity missions

Anna F. Purkhauser,¹ Christian Siemes² and Roland Pail¹

¹Chair of Astronomical and Physical Geodesy, Arcisstraße 21, 80333 Munich, Germany. E-mail: anna.purkhauser@tum.de

²ESA – European Space Agency, Noordwijk, The Netherlands

Accepted 2020 January 31. Received 2020 January 15; in original form 2019 August 2

SUMMARY

The GRACE and GRACE-FO missions have been observing time variations of the Earth's gravity field for more than 15 yr. For a possible successor mission, the need to continue mass change observations have to be balanced with the ambition for monitoring capabilities with an enhanced spatial and temporal resolution that will enable improved scientific results and will serve operational services and applications. Various study groups performed individual simulations to analyse different aspects of possible NNGMs from a scientific and technical point of view. As these studies are not directly comparable due to different assumptions regarding mission design and instrumentation, the goal of this paper is to systematically analyse and quantify the key mission parameters (number of satellite pairs, orbit altitude, sensors) and the impact of various error sources (AO, OT models, post-processing) in a consistent simulation environment. Our study demonstrates that a single-pair mission with laser interferometry in a low orbit with a drag compensation system would be the only possibility within the single-pair options to increase the performance compared to the GRACE/GRACE-FO. Tailored post-processing is not able to achieve the same performance as a double-pair mission without post-processing. Also, such a mission concept does not solve the problems of temporal aliasing due to observation geometry. In contrast, double-pair concepts have the potential to retrieve the full AOHIS signal and in some cases even double the performance to the comparable single-pair scenario. When combining a double-pair with laser interferometry and an improved accelerometer, the sensor noise is, apart from the ocean tide modelling errors, one of the limiting factors. Therefore, the next big step for observing the gravity field globally with a satellite mission can only be taken by launching a double pair mission. With this quantification of key architecture features of a future satellite gravity mission, the study aims to improve the available information to allow for an informed decision making and give an indication of priority for the different mission concepts.

Key words: Satellite geodesy; Satellite gravity; Time variable gravity.

1 INTRODUCTION

Earth's gravity field is continuously changing due to geophysical processes causing mass changes in the global water cycle (Rodell *et al.* 2018), atmosphere (Forootan *et al.* 2014), plate tectonics (Panet *et al.* 2014), earthquakes (Han *et al.* 2013) and glacial isostatic adjustment (GIA; Ivins *et al.* 2011) as well as cryosphere (Luthcke *et al.* 2013; Velicogna *et al.* 2014). Monitoring of the variations in the gravity field is therefore fundamental for many applications in Earth sciences. Dedicated gravity field missions like the *CHallenging Minisatellite Payload* (CHAMP, 2000–2010; Reigber *et al.* 1999), the *Gravity Recovery and Climate Experiment* (GRACE, 2002–2017; Tapley *et al.* 2004) as well as its current successor *GRACE Follow-On* (GRACE-FO, 2018–?; Flechtner *et al.*

2017) and *Gravity recovery and steady-state Ocean Circulation Explorer* (GOCE, 2009–2013; Rummel *et al.* 2011) have strongly improved the accuracy, spatial as well as the temporal resolution of the Earth's global gravity field.

After more than 15 yr of successfully collecting (temporal) gravity data, the GRACE mission was decommissioned due to a battery failure in the end of 2017. The successor mission GRACE-FO was launched in May of 2018 to continue monitoring the temporal gravity field of the Earth and is designed to operate at least 5 yr (Kornfeld *et al.* 2019). It is designed as a copy of GRACE with the addition of laser ranging interferometer (LRI) as a technology demonstrator and aims at the continuation of the observations.

The user requirements collected by Pail *et al.* (2015) underline the need for long-term, sustained gravity observations with increased

spatial and temporal resolution to observe small-scale, short-time mass transport phenomena. Therefore, a series of studies of a next generation gravity mission (NGGM) concepts have been performed to find an optimal mission concept in terms of improved temporal and spatial resolution. Sharifi *et al.* (2007), Sneeuw *et al.* (2008), Wiese *et al.* (2008), Elsaka *et al.* (2012) and Iran Pour *et al.* (2013) investigated the performance of single-pair missions. The main disadvantage of single-pair concepts is their anisotropic error behaviour due to the intersatellite ranging only in flight direction, leading to the typical striping patterns in temporal gravity solutions due to an insufficient amount of observations to estimate AO (atmosphere and ocean). In Gruber *et al.* (2014) a single-pair mission in pendulum formation was investigated and proposed as a candidate mission in response to the ESA (European Space Agency) Earth Explorer (EE) 8 call. The pendulum formation allows also the observation of the cross-track component, thus improving the error characteristics of this mission concept. Bender *et al.* (2008), Wiese *et al.* (2011a, 2012) and Daras & Pail (2017) analysed the possibility of flying, in addition to an in-line pair in polar orbit, a second satellite pair in an inclined orbit (Bender constellation), thus further improving the isotropy of the error behaviour due to the two different orbit planes. A study by Elsaka (2014) concluded that the gain in accuracy of the Bender double-pair constellation is higher compared with the single-pair pendulum formation, and is therefore preferred. In Hauk *et al.* (2017) a mission concept based on high-precision intersatellite tracking among satellites in Medium Earth Orbits (MEOs) and Low Earth Orbiters (LEOs) was investigated, leading to the mission proposal MOBILE (*mass variation observing system by high–low intersatellite links*) in response to ESA's EE10 call (Hauk & Pail 2019; Pail *et al.* 2019).

Currently, ESA and NASA are preparing an interagency cooperation on NGGMs. While it is obvious that a mission with two satellite pairs gives more accurate time-variable gravity field models than a mission with a single satellite pair, it is important to quantify the improvement. This will enable agencies and funding bodies to make an informed trade-off between the costs and the value of the mission for science and services. Another important element that has a significant impact on the mission architecture and costs is the option to implement a drag compensation or even a drag-free system, which would allow to fly for 11 yr at an altitude of about 340 km (Dionisio *et al.* 2018). This offers several advantages over a mission architecture without drag compensation system like, for example the GRACE and GRACE-FO missions:

1. The altitude is much lower during most of the mission lifetime compared to the altitude profile of the GRACE mission presented by Guo *et al.* (2018), used in gravity field models by, for example Dahle *et al.* (2019). This means that the gravity signal in the ranging measurements will be larger, which is obviously beneficial for the accuracy of time-variable gravity field models.

2. A lesson learned from the GOCE mission is that a drag-free system allows to maintain the altitude and hence the ground track pattern very accurately (Floberghagen *et al.* 2011). Together with a constant performance of the instruments (Siemes *et al.* 2019), this will lead to time-variable gravity field models of consistently high quality throughout the mission lifetime, which is an important aspect for services. In particular, undesirable short repeat cycles as experienced by the GRACE mission (*cf.* Gooding *et al.* 2007) are completely avoided.

3. Accelerometers require a 'quiet' onboard environment for reaching the best measurement accuracy (Floberghagen *et al.* 2011). A drag-free system will help to achieve this.

On the downside, a drag-free system increases the power demand and the complexity of the satellite system significantly (Dionisio *et al.* 2018). Also, the lowest coefficients need to be accurately determined for applications such as climate monitoring, where GOCE was less sensitive. Finally, the choice of the accelerometers and ranging system is a key element of the mission architecture. We compare GRACE-like accelerometers and microwave interferometers with the more accurate GOCE-like accelerometers and GRACE-FO-like laser-interferometer in order to quantify possible improvements due to advanced instrumentation. The effect of the intersatellite distance was investigated by Sneeuw (2000), who found that a distance of 100 km is optimal. Larger distances studied by Reubelt *et al.* (2014) did not show any improvements on gravity field coefficient level. The 100 km distance might not be optimal for all potential target signals, but turns out to be a good compromise. We therefore assume a distance of 100 km in all simulations, noting that deviations of up to 100 per cent have no significant impact on the mission architecture. This is evident from the GRACE-FO mission, which features microwave and laser interferometry over a distance of about 200 km.

Based on these options for the mission architecture, the retrieval of the time-variable gravity field signals and their separation into contributions from the atmosphere (A), ocean (O), land hydrology (H), land ice mass (I) and solid Earth (S) are of interest. In the following we will use different combinations of the letters A, O, H, I and S to refer to the gravity signals due to mass change in the atmosphere, ocean, land hydrology, land ice mass and solid Earth, respectively. We use the Earth system model developed by Dobsław *et al.* (2015) for including realistic AOHIS signals and Dobsław *et al.* (2016) for realistically perturbed AO signals. We deploy the latter in the commonly used approach of 'AO dealiasing', where the AO signal is reduced from the ranging observations prior to the gravity field model retrieval, which implies that the retrieved gravity field model represents mass change in HIS. Since the accuracy of models for AO dealiasing is regarded as one of the limiting factors for the accuracy of the time-variable gravity field models (Flechtner *et al.*, 2016), we will also use the approach developed by Wiese *et al.* (2011b), who suggested estimating a gravity field model representing the full AOHIS signal. In order to account for short-term mass change in AO, daily low-degree gravity field models are co-estimated. Further, we investigate the impact of ocean tide model errors and the retrieval length of the gravity field estimation. Lastly, the question if a smart post-processing of a single-pair mission, which plays an important role when using GRACE/GRACE-FO data, is compatible with a double-pair concept is of interest.

Various studies with different simulation approaches have looked at specific aspects of the above mentioned options. One of the most well-known facts is that the performance of a satellite regarding the gravity field resolution is depending on the orbit altitude, already pointed out in Dickey *et al.* (1997) as trade-off between mission life time and maximizing sensitivity. Murböck & Pail (2014) looked at optimal orbits regarding temporal aliasing and homogeneous ground-track coverage. Wiese *et al.* (2012) optimized the inclination of a second pair. In the ESA-funded SC4MGV study (*Assessment of Satellite Constellations for Monitoring the Variations in Earth Gravity Field*, Iran Pour *et al.* 2015) a blind optimization of Bender double-pair missions was carried out. One of the main findings was that there is a certain degree of freedom in the orbit design of Bender-type mission concepts. In the ESA-study ADDCON (*Additional Constellation & Scientific Analysis of the Next Generation Gravity Mission Concept*; Purkhauer *et al.* 2018) specific ground track patterns and their impact on the performance were analysed.

Flechtner *et al.* (2016) studied the probable improvements for GRACE-FO when using the LRI instead of the microwave instrument (MWI) on recoverable monthly gravity fields. The study found that on a global scale an improvement in the order of 23 per cent could be expected. Abrykosov *et al.* (2019) assessed the value of the hybrid accelerometer for gravity field retrieval for GRACE-type and Bender-type missions. While a hybrid accelerometer is widely unaffected by scale factor instabilities, when assuming currently technologically feasible error levels the impact on gravity field level is rather small.

As single-pair missions cannot resolve the high-frequent AO components, the modelling of the atmospheric and oceanic mass variations as well as the use of dealiasing product is of importance. Daras & Pail (2017) have shown that a NGGM could, opposed to a GRACE-like single-pair mission, retrieve the full AOHIS signal, which would be free of AO dealiasing model errors.

Errors in the ocean tide models are considered as one of the major sources of error in the estimation of temporal gravity fields from GRACE data (Knudsen & Anderson 2002, Seo *et al.* 2008). Flechtner *et al.* (2015) stated that for GRACE-FO one of the biggest error sources to date are, apart from the accelerometer and the AO errors, ocean tide model errors. Visser (2010); Visser *et al.* (2010); Wiese *et al.* (2011b) and Daras & Pail (2017) have also pointed out that ocean tide model errors are potentially the limiting source for NGGMs

The gravity field of the Earth is frequently parametrized using global spherical harmonics (SH) functions. This study also uses SH. One of the advantages is that the SH degrees can be directly linked to a spatial wavelength. However, this parametrization comes with the disadvantage of full matrices and numerical instability due to non-orthogonality of the global base function in the discrete case. Approaches based on the orthogonal spherical Slepian functions (after Slepian 1983) with an improved numerical stability and the potential to deal with irregular data distribution such as polar gaps have been developed and analysed by Albertella *et al.* (1999), Pail *et al.* (2001), Simons & Dahle (2006) and tested by, for example Harig & Simons (2012). The ‘mascon’ or ‘mass concentration’ approach, first introduced by Muller & Sjorgen (1968), in comparison uses regional basis functions and usually also additional regional constraints. Recent approaches in the field of global gravity field modelling use e.g. radial basis functions (Eicker *et al.* 2013) or point-mass modelling techniques (Baur & Sneeuw 2011).

The gravity field solutions retrieved from GRACE/GRACE-FO data are typically treated with destriping and filtering techniques, which are applied in a post-processing step (e.g. Swenson & Wahr 2006; Kusche 2007; Werth *et al.* 2009; Horvath *et al.* 2018). While the community most often relies on the Gaussian filter, Devaraju (2015) studied the suitability of different low-pass filters and came to the conclusion that no single filter performs best, when looking at different performance metrics. Flechtner *et al.* (2015) found that any increase in the performance by an LRI was decreased significantly when using anisotropic filtering.

This overview of various studies shows that many important factors for the design of NGGMs have been investigated in one kind or another. However, the simulation environments, assumptions and inputs vary from study to study, so that the results are not directly comparable. Therefore, this study evaluates the above mentioned options in a systematic way taking into account the most up-to-date prediction of the instruments’ performance in the frame of a full-fledged numerical simulation environment. This will allow not only a qualitative, but a quantitative assessment of the achievable

gravity field model accuracy with respect to key mission architecture options. With this quantification of possible features of future GRACE-like mission or a NGGM the study aims to improve the available information to allow for an informed decision making and give an indication of priority for the different mission concepts.

The paper is organized as follows. Section 2 reviews gravity satellite mission design, specifically the topics of orbit altitude and ground track as well as sensor noise. The methodology of the full-scale closed-loop simulation, based on the software available at the Institute of Astronomical and Physical Geodesy (IAPG) of the Technical University Munich (TUM), is described in Section 3. The parametrization and the post-processing are also included in this section. Section 4 contains the obtained gravity results, a comparison regarding the analysed factors and finally the conclusions regarding the possible accuracies reached by various options of simulated constellations in Section 5.

2 GRAVITY SATELLITE MISSION DESIGN

Since the Bender constellation is based on the technology and scientifically mature GRACE concept, it has evolved as one of the most promising options for the realization of an NGGM (Elsaka *et al.* 2014). All other factors, apart from the intersatellite distance and exact inclination, which are both less relevant for the mission design and can be adjusted at a later point, are addressed within this study on the gravity satellite mission design.

Fig. 1 shows a schematic view of the analysed single-pair mission in a near-polar orbit (left), which allows observing ice mass change. In comparison, the analysed Bender double-pair constellation, comprising of a near-polar pair and an inclined pair with an inclination of 70° is visualized in the right figure. The inclined pair (in dashed orange) leaves a polar gap of $\pm 20^\circ$ at the poles.

2.1 Impact of a second satellite pair

One of the major error sources results from the observation geometry of single-pairs leading to an anisotropic characteristic of a near-polar orbit causing the GRACE-typical striping effects (Flechtner *et al.* 2006) as well as from temporal aliasing errors. The latter ones are caused by high-frequency tidal and non-tidal mass variations that cannot be captured by the satellite mission due to its limited temporal and spatial resolution. This undersampling in space and time of fast mass change is predominated by AO masses. Usually, these short-term mass variations are reduced *a priori* based on external geophysical models, so-called AO de-aliasing models (e.g. Dobslaw *et al.* 2016). While AO signals contain a wide range of frequencies, very distinct excitation frequencies are introduced by OT, which are computed from ocean tide models (Knudsen & Andersen 2002, Seo *et al.* 2008). However, all these geophysical models are not free of errors, and therefore add another error source to the processing, which aliases into the gravity field solution (Han *et al.* 2005; King *et al.* 2011; Daras & Pail 2017). In fact, OT and AO model errors are among the dominant error sources of temporal gravity field retrieval.

In contrast, Bender-type missions double the observation amount and have a more isotropic error due to the added east–west components because of the additional inclined pair. This enables better mitigation of aliasing effects. By the combination of two satellite pairs in differently inclined orbit planes, the isotropy of the resulting

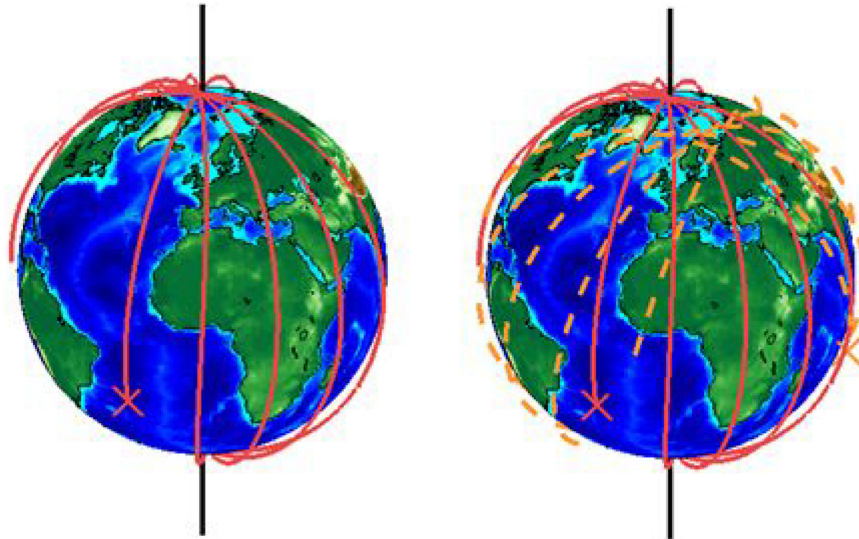


Figure 1. Polar single-pair (left-hand panel) versus Bender double-pair (right-hand panel) constellation in 3-D visualization after five revolutions, with the position of the satellite marked with an 'X'. The near-polar orbit is visualized in red, the inclined orbit in dashed orange.

error structure is improved significantly. On the other hand, such a double-pair formation allows for the direct estimation of OT parameters (Hauk & Pail 2018). Hand in hand with the design of NGGM concepts, also the corresponding processing strategies can be further developed. As an example, by using the Wiese approach (Wiese *et al.* 2011b; Daras & Pail 2017), which is the co-parametrization of low-resolution short period (e.g. daily) and longer-term gravity field solutions (3–11 or even more days) to directly recover non-tidal high-frequency signals especially from atmosphere and ocean, they do not alias into the solution anymore. Alternatively, Kalman smoother approach introduced by Kurtenbach *et al.* 2009, which requires that signal variances are known, can be used. The approach uses a recursive Kalman filtering scheme to estimate daily gravity field solutions for, for example GRACE data and takes into account statistical information on process dynamics and noise from geophysical models to gain in temporal resolution. Further details can be found in Jaeggi *et al.* (2019), Kvas *et al.* (2019) and Gruber & Gouweleeuw (2019).

2.2 Orbit altitude

Dedicated gravity missions require a low altitude in order to increase sensitivity towards the gravity field. However, a low altitude is usually also related to a shorter mission lifetime due to the increase in the atmospheric drag with decreasing altitude, causing the satellite orbit to decay faster. Since a long mission lifetime is desired either a higher orbit around 500 km initial altitude like GRACE/GRACE-FO has to be chosen. Or fuel to operate a drag compensation system counteracting non-gravitational forces acting on the satellite is required to achieve a similar lifetime at approximately 350 km of orbit altitude (Dionisio *et al.* 2018).

The near-polar orbits used within this study are based on a GRACE-type orbit. The inclined orbit is tailored towards the near-polar orbit, meaning an optimal spacing of their ground-tracks as well as the same drift rate. To enable the assessment of the impact of the orbit altitude two sets of double-pairs in a low altitude of approximately 350 km and the second set in a higher altitude of

approximately 500 km are defined. To achieve the same characteristics of the inclined pair towards the near-polar pair, the difference in height is not exactly the same (see Table 1).

2.2.1 Groundtrack

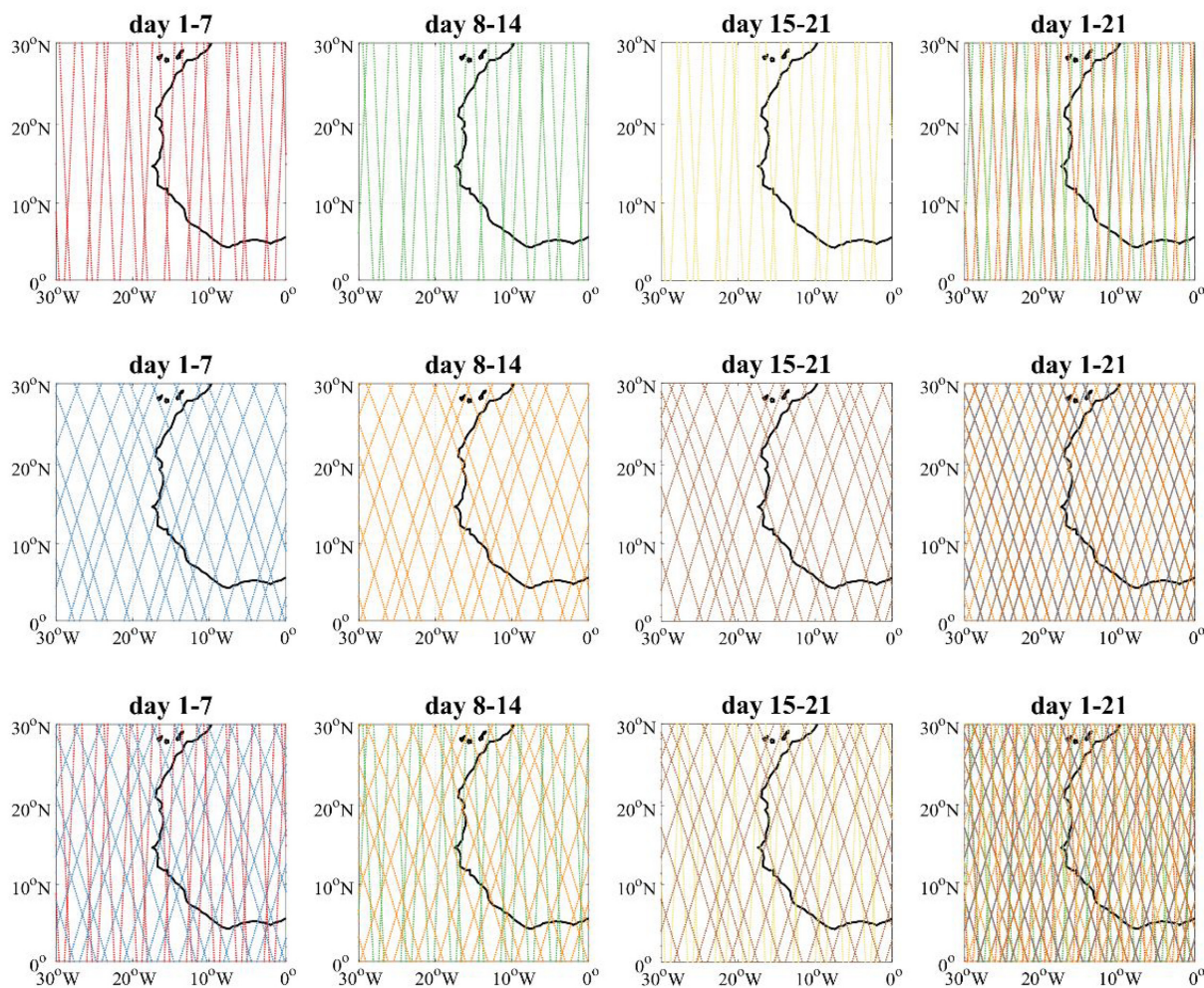
Another objective of dedicated gravity missions is to ensure a dense ground track coverage to maximize spatial resolution within the retrieval period and to keep the retrieval period overall short so that the time resolution of the gravity field solution can be maximized as well. Compared to other orbit designs, the chosen orbits take into account a common drift of the ground track pattern for both pairs, since an exact repeat orbit is not desirable due to fact that the associated ground track spacing would not allow for a high-degree gravity field recovery even if longer periods of data are used according to the Nyquist-Colombo sampling rule for space-borne gravimetry (Klokočník *et al.* 2008; Visser *et al.* 2011; Weigelt *et al.* 2012).

From various tested orbits within the ADDCON project, a 7-d near-repeat orbit, with a common ground track pattern, which shifts by 1.3° after 7 d (see Table 1) was chosen. This way, it is guaranteed that a 7-d gravity field solution can be calculated to the best possible resolution available, due to the homogeneously spread ground track. Additionally, a good monthly gravity field retrieval performance is ensured due to the repeat after approximately 21 d. The orbit was integrated over 1 yr, to guarantee a stable behaviour. Based on the used background forces no orbit maneuvers are necessary during this time period to maintain the main orbit parameters as well as the intersatellite distance.

Fig. 2 shows the ground tracks of the analysed orbits. In the first row, the polar orbit is visualized, in the second row the inclined orbit, while in the third row both orbits are displayed together. In the first column the first 7 d, which is also the defined retrieval period is shown, followed by the next two retrieval periods as well as the combined ground tracks in the last row. The homogeneous ground track is visible in the combined plot in the bottom right, allowing a high spatial resolution.

Table 1. Orbits and their altitude, inclination, the satellite distance and drift rate.

Satellite pair	Altitude [km]	Inclination [°]	Satellite distance [km]	Drift rate/nodal days [deg. d ⁻¹]
Near-polar	340	89	100	1.3/7
Inclined	355	70	100	1.3/7
Near-polar	505	89	100	1.3/7
Inclined	475	70	100	1.3/7

**Figure 2.** Ground track (350 km altitude constellation) over an area of Africa above the equator for the polar, inclined and both pairs for the first, second and third retrieval period as well as a combination of the retrieval periods to showcase the drift rate of the orbit design.

2.3 Sensor noise

From the instrument and payload point of view, the accelerometer and the ranging instrument have the largest impact on the achievable gravity field performance, while the star camera and orbit errors are only minor contributors to the total error budget. The GRACE mission has demonstrated successfully the use of an intersatellite ranging using a K-band ranging (KBR) system with a ranging accuracy on the micrometer level for measuring the distance variations due to the differential accelerations on the two satellites in orbit. In the successor mission GRACE-FO, a LRI with a performance at the nanometer level was included as a technology demonstrator to operate in parallel with the microwave ranging system (Sheard *et al.* 2012). But, not only instrument accuracy but also the ability to either co-estimate or model AO are performance drivers (Flechtner *et al.* 2006; Hauk & Pail 2018).

So far all realized gravity field missions have used electrostatic accelerometers (EA) for measuring the non-gravitational accelerations acting on the spacecraft. This type of accelerometer has a non-constant bias and is sensitive towards temperature, limiting the performance of the long-wavelength gravity field signal retrieval (Flechtner *et al.* 2016; Touboul *et al.* 2016). Studies on accelerometers based on cold atom interferometry (CAI) have shown promising results on ground (Gustavson *et al.* 1997; Peters *et al.* 2001; McGuirk *et al.* 2002). While CAI accelerometers are less sensitive towards temperature and, their performance is not yet as good as EA's. A first assessment of hybrid instruments combining the EA and CAI concepts, to calibrate the EA, has demonstrated that equal or better retrieval performance can be achieved (Christophe *et al.* 2015, 2018; Abrykosov *et al.* 2019). However, they are not yet considered to be technologically mature enough as payload in a NGGM.

For the LL-SST observable the following two error sources were considered: the ranging instrument noise and the accelerometer (ACC) noise. The noise of the error sources are all frequency dependent and are approximated by analytical equations. The noise time-series are scaled by the spectrum of normal distributed random time-series with the individual spectral models.

The two noise scenarios defined for the LL-SST observable are: A GRACE-like noise representing a noise level of ACC and SST resembling the error characteristics of the instruments implemented on the GRACE mission, and an NGGM noise scenario with improved ACC and LRI noise characteristics.

2.3.1 GRACE-like noise

The principal measurement unit of the intersatellite distance, the KBR system, is characterized by an analytical noise model described by the amplitude spectral density (ASD) and expressed in terms of range rates:

$$d_{\text{range rates}} = 2 \cdot \alpha \cdot 2\pi f \sqrt{\left(\frac{10^{-2}\text{Hz}}{f}\right)^2 + 1} \frac{\text{m}}{\text{s}\sqrt{\text{Hz}}} \quad (1)$$

with α being 10^{-6} (Iran Pour *et al.* 2015). The performance of the KBR instrument is visualized in Fig. 3(left-hand panel) in green.

The on-board accelerometer senses the linear non-gravitational accelerations and the angular accelerations acting on the satellites with air drag being the main contributor. The noise performance was modelled after Touboul *et al.* (2016). In Fig. 3 both the ultra-sensitive axis (in red), as well as the less sensitive cross-track axis performance (in blue) are shown.

2.3.2 NGGM noise

In the case of NGGM noise, the principal measurement unit is observed by the laser interferometry instrument. Its noise can be described by eq. (1) and the α being set to 10^{-8} , meaning an improvement of factor 100. The Laser interferometer range performance is visualized in green, in Fig. 3 (right-hand panel).

The improved accelerometer is expressed by:

$$\begin{aligned} d_{\text{acc. } x} &= d_{\text{acc. } z} \\ &= 10^{-11} \sqrt{\left(\frac{10^{-3}\text{Hz}}{f}\right)^4 / \left(\left(\frac{10^{-5}\text{Hz}}{f}\right)^4 + 1\right) + 1 + \left(\frac{f}{10^{-1}\text{Hz}}\right)^4} \\ &\quad \times \frac{\text{m}}{\text{s}^2\sqrt{\text{Hz}}}, \end{aligned} \quad (2)$$

$$d_{\text{acc. } y} = 10 \cdot d_{\text{acc. } z}, \quad (3)$$

with x being the along-track, y across-track and z the quasi-radial component. In Fig. 3 (left-hand panel) the improved NGGM noise is visualized in blue and red (sensitive axes).

The satellite in approximately 350 km orbit altitude is assumed to fly in drag-free mode, with the biggest parts of the non-gravitational forces are compensated by a propulsion system consisting of ion thrusters, while at 500 km a drag compensation is not necessary to maintain the orbits.

3 SIMULATION ENVIRONMENT

The gravity field recovery approach used for the simulation is a modified integral equation or short-arc approach (Schneider 1969; Mayer-Gürr 2006). The computation of the satellites' orbit is divided into equal arcs and formulated as a boundary value problem connecting the node points and the positions on the orbit mathematically. The positions at the node points are set up as unknowns and co-estimated with the gravity field. A modification by Yi (2012) guarantees a smooth transition from one arc to the next by including the condition that the ending and starting node point must be identical.

The simulation was carried out with the full-scale gravity field estimation software for closed-loop simulations (Daras *et al.* 2015; Daras 2016). The software is divided into three major sequential processing steps as visualized in Fig. 4.

In the first step marked in blue in Fig. 4, the dynamic orbits are integrated based on a set of initial state vectors and force models. The numerical integrator follows a multistep method for numerical integration (Shampine & Gordon 1975) with a modified divided difference form of the Adams Predict-Evaluate-Correct-Evaluate (PECE) formulas and local extrapolation (Montenbruck & Gill 2000).

The gravity fields are parametrized as spherical harmonics (SH). The assembling of the NEQ systems is done with SH base functions of the Earth's gravitational potential V , which can be expressed by the series expansion (Hofmann-Wellenhof & Moritz 2005):

$$\begin{aligned} V(r, \theta, \lambda) &= \frac{GM}{a} \sum_{n=0}^{\infty} \left(\frac{a}{r}\right)^{n+1} \sum_{m=0}^n \bar{P}_{nm}(\cos\theta) \\ &\quad \times (\bar{C}_{nm} \cos m\lambda + \bar{S}_{nm} \sin m\lambda), \end{aligned} \quad (4)$$

where GM represents the product of the gravitational constant and the Earth's mass, a the semi-major axis of the Earth, \bar{P}_{nm} the fully normalized Legendre polynomial of degree n and order m , \bar{C}_{nm} and \bar{S}_{nm} the fully normalized SH coefficients, and the location is given by the radius r (geocentric distance of the satellite), geocentric colatitude θ and longitude λ .

The functional model follows the typical formulation used for low-low satellite-to-satellite (LL-SST) missions like GRACE, which comprises of a high-low satellite-to-satellite (HL-SST), namely the GNSS positions of the satellites, and an LL-SST component. In Fig. 4 marked in yellow the computation of the observation vector and the various components of the design matrix \mathbf{A} per arc and observation type is visualized. Also, the left and right sides of the normal equation are computed and accumulated to daily normal equations (NEQ). This part is the most computationally intensive task and can be processed in parallel per day and satellite.

The third step is the accumulation of the NEQ's and the least squares adjustment (LSA) marked in red in Fig. 4. During the accumulation a pre-eliminations of local parameters, such as the boundary conditions \mathbf{b} and daily SH coefficients in the case of the Wiese approach, is carried out, to decrease the size of the NEQ's. The LSA with the combined NEQ's according to the time period of interest is processed.

The simulation is carried based on the defined constellations (see Table 1). As static gravity field the GOCO05s model (Mayer-Gürr *et al.* 2015) up to maximum expansion degree and order (d/o) 120 is included in all generated dynamic orbits. The updated Earth System Model (ESM) of ESA (Dobslaw *et al.* 2015) is introduced in the reference world scenario to simulate the non-tidal time-varying gravity field due to mass change. The ESA ESM model is available as 6-hourly snapshots as combined AOHIS as well as separate components and are used as input to generate dynamic orbits. As

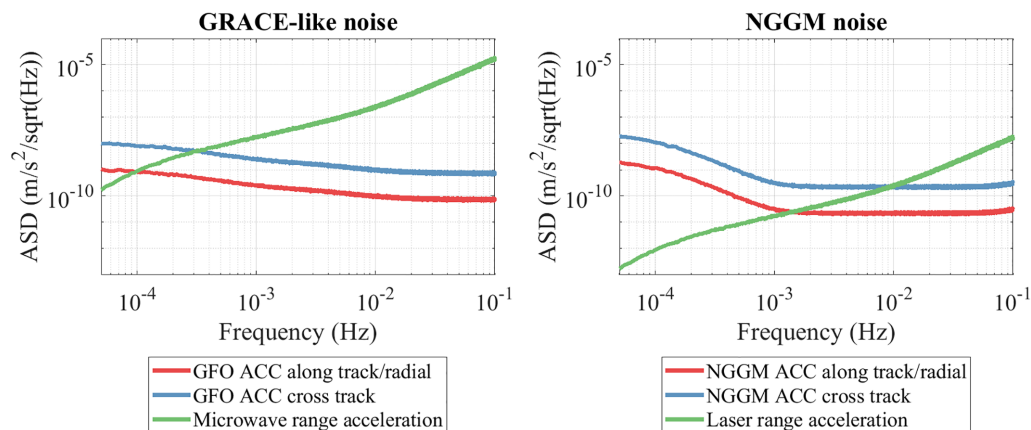


Figure 3. Amplitude spectral density (ASD) of the GRACE-like noise (left-hand panel) and NGGM noise (right-hand panel).

AO error the included error files of the ESM is used. As ‘true’ OT model the GOT4.7 (Goddard Ocean Tide) model by Ray (1999) is used, as ‘reference’ OT model the EOT08a (Empirical Ocean Tide) model by Savcenko & Bosch (2008) is used. The resulting OT errors are represented by the difference of these two models. Additionally, the computed observations are superimposed by sensor noise for the GNSS (1 cm white noise), SST and accelerometer sensors (see Fig. 3).

Assuming stationary sensor noise, the corresponding stochastic model, which is used for weighting of the observations, can be accomplished from a series of digital filter coefficients fitted to the power spectral density of the prefit residuals from a noise-only computation. The HL-SST and LL-SST observations are considered as uncorrelated, so that the weighting matrices can be set up separately.

In addition to the sensor noise, the simulations include sources for aliasing due to undersampling of the full AOHIS signal to be recovered, uncertainties in the non-tidal AO dealiasing models (included in the ESA-ESM), and uncertainties in the OT model (introduced by the differences between the two different ocean tide models).

High-frequency tidal and non-tidal mass variations cannot be captured by the satellite mission due to undersampling. Fast non-tidal mass change is largely caused by AO, whereas HIS has significantly less fast variations (Dobslaw *et al.* 2013). The impact of aliasing in the processing can be mitigated by two different approaches. AO dealiasing products can be used, so that only the HIS signal content and OT model errors remain, while AO model errors are newly introduced. Secondly, via a coparametrization of low-resolution spherical harmonic coefficients for short time periods, also called Wiese approach (Wiese *et al.* 2011b). The Wiese approach can be used for the single-pair, but its advantage takes effect with a more frequent sampling rate of a Bender-pair formation. The main goals of the Wiese approach is to reduce aliasing effects and thus to improve the higher degree SH coefficients. It has to be remarked, that the Wiese approach does not completely prevent high frequency aliasing of the AO signal. In our case all signals with periods below 2 d will cause temporal aliasing. Therefore, a combination of, that is AO dealiasing with an a priori product for high-frequency signals in combination with a Wiese approach might be most beneficial. As a by-product the approach also provides gravity field retrievals with daily resolution.

Table 2 summarizes the different retrieval types analysed within this study. The first column indicates the used signal input. If only

HIS is used, an AO dealiasing is implied. Unless otherwise stated the single-pair is always processed without the Wiese approach. This processing is furthermore called ‘nominal processing’ and means that only the standard LSA is applied. The double pair processing always co-estimates daily gravity field till d/o 15–this is indicated by ‘Wiese’ in the second column. This leads to four cases, the first being the full retrieval, which is the worst case for the single-pair, however a realistic case for the double-pair. Next, only HIS is estimated. AO and OT errors, which were already successfully co-estimated (Mayer-Gürr *et al.* 2012; Hauk & Pail 2018), are excluded one after another to allow the quantification of each error on the retrieved GF estimation. The case of neither AO nor OT errors can be termed theoretical and should quantify what is possible with a perfect OT model.

3.1 POST-PROCESSING

In order to improve the single-pair solutions usually filters are applied to temporal gravity solutions in post-processing to reduce the correlated noise causing the typical striping patterns. They aim at the suppression of noise and removal of the GRACE-typical striping artefacts, but in parallel also dampen the signal and reduces the spatial resolution.

Three filter methods were applied as post-processing onto the polar single-pair solutions:

(1) The widely used isotropic Gaussian filter (Jekeli 1981) is using a weighting function derived from the Gaussian probability density function. Its weight mimics a Gaussian function, where the kernel diverges towards zero the further away from the kernel centre. As filter radius 200, 300, 350 and 500 km were tested.

(2) The anisotropic Swenson and Wahr filter (2006, shortened to Swenson filter from now on) is based on a polynomial fitting and selects and reduces the striping errors present in GRACE. The idea is to only apply smoothing to those coefficients that have larger errors, thus reducing the correlation among highly correlated coefficient groups. The filter settings are according to the published paper: Keeping the first 4 d/o coefficients unchanged, usage of a quadratic polynomial fitting to the coefficients and the use of a moving window with the width depending on the degree [d/o 70 in case of this study, implemented by Feng (2018)].

(3) The idea of the VADER filter (Horvath *et al.* 2018) is based on DDK decorrelation filters previously published by Kusche (2007)

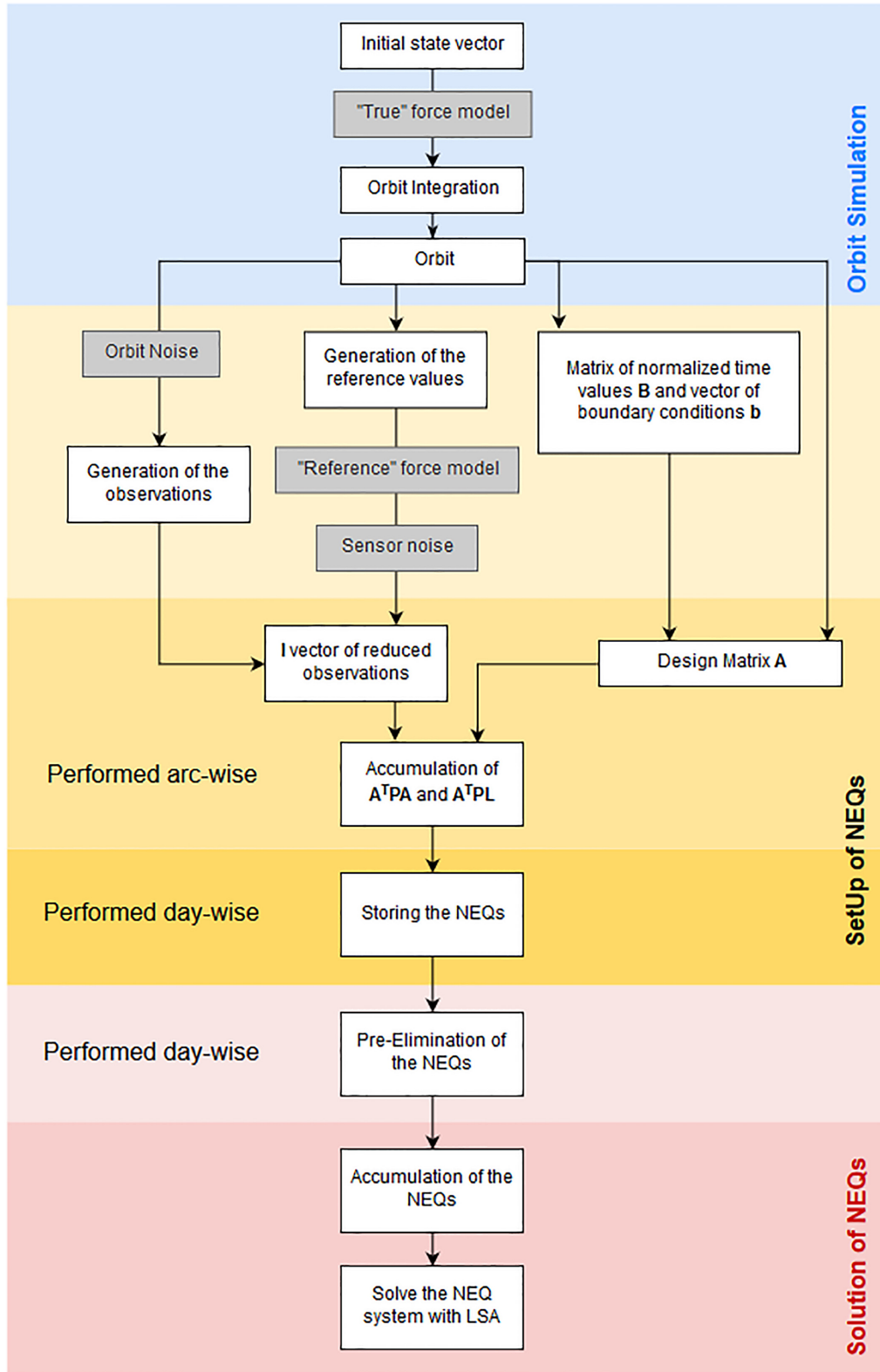


Figure 4. Simulation steps of the closed loop simulation: Orbit simulation, setup of the NEQ's and Solution of NEQs.

and Kusche *et al.* (2009), but with a time-dependent error variance–covariance matrix. The filter kernel is implemented with the following equation

$$\hat{x}_\alpha^{\text{VADER}} = (N + \alpha M)^{-1} N \hat{x} = W_\alpha \hat{x}, \quad (5)$$

where \hat{x} is the estimated gravity field solution in spherical harmonics, $\hat{x}_\alpha^{\text{VADER}}$ the filtered spherical harmonics, N is the normal equation matrix, M representing the signal variance matrix and α is the weighting factor. Weighting factors between 0.1 and 5000 were investigated.

Table 2. Retrieval types with included error types.

Retrieved signal	Dealiasing appr. [single-/double-p.]	AO error	OT error	Single-pair	Double-pair
AOHIS	–/Wiese	–	Incl.	Worst case	Realistic case
HIS	–/Wiese	Incl.	Incl.	Realistic case	Realistic case
HIS	–/Wiese	–	Incl.	Best case	Best case
HIS	–/Wiese	–	–	Theoretical	Theoretical

Table 3. Scenarios of the simulation with numbering. The colour-code indicated in the first eight base scenarios is used consistently throughout the paper.

Orbit altitude	Noise	AOHIS, OT error		HIS, AO error, OT error		HIS, OT error		HIS	
		Polar single-pair	Bender double-pair	Polar single-pair	Bender double-pair	Polar single-pair	Bender double-pair	Polar single-pair	Bender double-pair
500 km	GRACE-like	101	102	103a	104a	103b	104b	103c	104c
	NGGM	201	202	203a	204a	203b	204b	203c	204c
350 km	GRACE-like	301	302	303a	304a	303b	304b	303c	304c
	NGGM	401	402	403a	404a	403b	404b	403c	404c

To keep the comparison between the (polar) single-pair scenario with the expected striping, and (Bender) double-pair scenarios as objective as possible, the results are compared before and after applying a filter.

4 RESULTS

We calculated eight 7-d solutions for January and February 2002 with the numerical closed-loop simulation software described in Section 3. Based on the two chosen constellations (see Fig. 1), altitudes (see Table 1) and two introduced noise characteristics (see Fig. 3) eight baseline scenarios were defined. Four different retrieval types are tested (see Table 2): the full AOHIS versus HIS retrieval and also the impact of AO and OT error. Within each retrieval type group of eight scenarios, the same colors, as defined in Table 3, are used.

All scenarios are computed till d/o 70 and if not otherwise noted for a 7-d retrieval period. For all Bender double-pair scenarios, the Wiese approach till d/o 15 is added into the processing chain. While all solutions were computed for the specified 2-months, the shown degree rms errors always represent the average degree rms of all estimated solutions to simplify the figures.

The comparison is done in the spatial as well as the frequency domain. In the latter case, the performance is expressed by the degree rms signal/errors in terms of equivalent water heights (EWH, Wahr *et al.* 1998; Schrama *et al.* 2007)

$$\sigma_n (EWH) = \frac{a\rho_e}{3\rho_w} \frac{2n+1}{1+k_n} \sqrt{\sum_{m=0}^n (c_{nm}^2 + s_{nm}^2)}, \quad (6)$$

where ρ_w and ρ_e represent the average density of water and Earth, a the semi-major axis of the Earth, k_n the love numbers and c_{nm} and s_{nm} represent the SH coefficients.

4.1 Full AOHIS retrieval incl. OT error, 7-d solutions

Using the full AOHIS signal as input and including OT errors represents the real situation of a gravity satellite mission. The sensors observe the full time-variable gravity signal. As discussed in Table 2 the retrieval of the full AOHIS signal without using an AO dealiasing product is the worst case for the single pair, due to undersampling. However, this case also shows one of the biggest advantages of a double-pair of enabling a signal separation and observing the full AOHIS signal. The details regarding the following eight scenarios are listed in Table 4. Within the double-pair scenario 102, the daily GF solutions are only computed till d/o 10 due to the overall weak performance of the scenario. A daily solution till d/o 15 deteriorated the solution significantly due to overparametrization.

Fig. 5 shows all eight scenarios in terms of degree rms error curves. The single-pair scenarios are visualized in solid lines, while the double-pair scenarios are visualized in dashed lines in the colours defined in Table 3. In the case of the single-pair, all variations of noise and altitude give a similar maximal observable d/o of less than 15 due to not using any dealiasing.

A visible characteristic of the polar single-pair scenarios with the GRACE-like noise is the oscillating pattern (especially scenario 101 and 301). The improved sensors used in the single-pair scenarios 201 and 401 mean a reduced noise level and a smoother degree RMS curve.

Within the double-pair scenarios, the best performing scenarios use both the NGGM noise. The added value of the better sensor noise characteristics is also visible in their cumulative error which is 1.8 cm and better. The only difference between these two scenarios is the orbit altitude of 350 km versus 500 km. Due to the higher orbit scenario 202 crosses the signal curve around 25 to 30, while scenario 402 with a lower orbit can be resolved up to d/o 37. The advantage of the lower altitude comes with the disadvantage of needing a drag compensation system and to maintain the low orbit, while a GRACE-like concept in the higher orbit does not.

4.2 HIS retrieval incl. AO and OT error, 7-d solutions

The next step in the gravity field retrieval is to use AO dealiasing models, to estimate the HIS signal only. In the case of the single-pair scenarios, this step is necessary due to undersampling of the AO signal, while the double-pair scenario can retrieve the full AOHIS signal but cannot separate the signals. In this set of scenarios both AO errors, due to the usage of the AO dealiasing products, and OT errors are considered—the details are listed in Table 5.

The best single-pair solution is again scenario 403a with the low altitude and NGGM noise, which combined gives a large improvement compared to the other three single-pair solutions. Both, the higher altitude as well as the GRACE-like noise impact the solutions independently negatively and prevent any significant improvement. These scenarios also remain similar or only insignificantly improved

Table 4. Detailed scenario description of Sc. X01 (single-pair) and X02 (double-pair) incl. cumulative error (average of all computed solutions).

Sc.	Constellation	Altitude	Dealiasing appr.	Noise level	Cum. Error EWH [cm] d/o 30
101	Single-pair	500 km	None	GRACE-I.	36.99
102	Double-pair	500 km	Wiese, $I_{\max} = 10$	GRACE-I.	5.72
201	Single-pair	500 km	None	NGGM	11.49
202	Double-pair	500 km	Wiese, $I_{\max} = 15$	NGGM	1.79
301	Single-pair	350 km	None	GRACE-I.	21.28
302	Double-pair	350 km	Wiese, $I_{\max} = 15$	GRACE-I.	2.76
401	Single-pair	350 km	None	NGGM	6.75
402	Double-pair	350 km	Wiese, $I_{\max} = 15$	NGGM	1.16

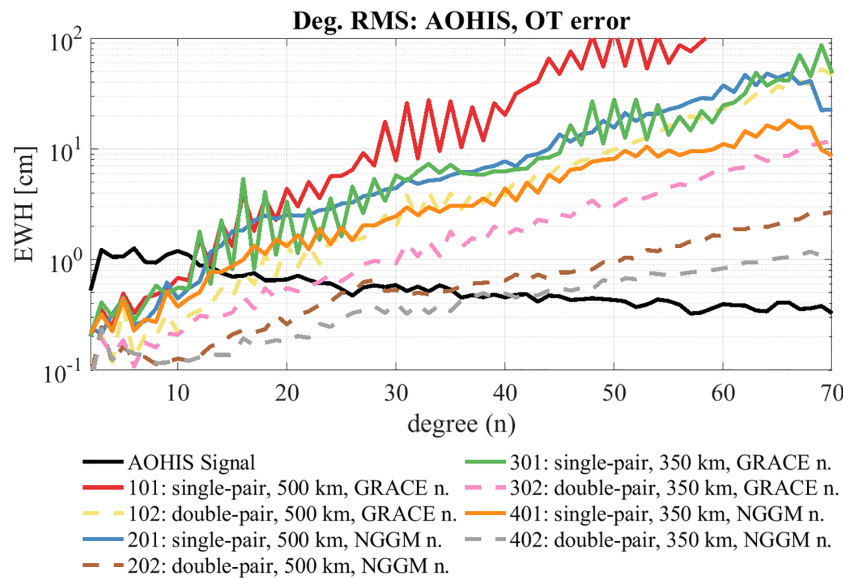


Figure 5. AOHIS (incl. OT error) scenarios according to Table 4 as degree rms in EWH up to d/o 70. The AOHIS signal is visualized in black. Single-pair scenarios are visualized with solid lines, double-pair scenarios are visualized with dashed lines. For more information on the individual scenario see Tables 3 and 4.

Table 5. Detailed scenario description of Sc. X03a (single-pair) and X04a (double-pair) incl. cumulative error (average of all computed solutions).

Sc.	Constellation	Altitude	Dealiasing approach	Noise level	Cum. Error EWH [cm] d/o 30
103a	Single-pair	500 km	None	GRACE-I.	12.44
104a	Double-pair	500 km	Wiese, $I_{\max} = 15$	GRACE-I.	3.86
203a	Single-pair	500 km	None	NGGM	6.48
204a	Double-pair	500 km	Wiese, $I_{\max} = 15$	NGGM	1.47
303a	Single-pair	350 km	None	GRACE-I.	3.40
304a	Double-pair	350 km	Wiese, $I_{\max} = 15$	GRACE-I.	2.50
403a	Single-pair	350 km	None	NGGM	1.49
404a	Double-pair	350 km	Wiese, $I_{\max} = 15$	NGGM	0.77

compared to the full AOHIS retrieval. This points towards the conclusion that neither a low altitude nor an improved sensor set alone can improve the overall retrieved gravity field in the case of single-pair missions.

Within the double-pair processing, the Wiese approach is used. Since the AO is excluded from the input signal, the approach estimates day-to-day variations within the retrieval period from the HIS signal. To separate the signal the use of AO products is the only available possibility at the moment. When using the AO dealiasing on the double-pair scenarios improvements can be mainly observed in the higher degrees.

The best single-pair scenario has its SNR crossing point at 32°. The best double-pair solution has an improvement of more than 24 additional degrees and an improved average cumulative error of

0.77 cm (compared to 1.49 cm EWH of the comparable single-pair) at d/o 30 can be observed.

4.3 HIS retrieval incl. OT error, 7-d solutions

In this group of simulations, we assume a perfect AO dealiasing. This is simulated by including only HIS as a temporal input signal, together with OT errors. The details of the scenarios are listed in Table 6. Compared to the scenarios in with AO errors included, an improvement in the lower degrees is expected. This can be verified in Fig. 9 in Section 4.5.

The scenarios relative to each other are the same as in Fig. 6, however, due to the exclusion of AO errors, an improvement overall

Table 6. Detailed scenario description of Sc. X03b (single-pair) and X04b (double-pair) incl. cumulative error (average of all computed solutions).

Sc.	Constellation	Altitude	Dealiasing approach	Noise level	Cum. Error EWH [cm] d/o 30
103b	Single-pair	500 km	None	GRACE-I.	12.43
104b	Double-pair	500 km	Wiese, $l_{\max} = 15$	GRACE-I.	3.78
203b	Single-pair	500 km	None	NGGM	6.42
204b	Double-pair	500 km	Wiese, $l_{\max} = 15$	NGGM	1.24
303b	Single-pair	350 km	None	GRACE-I.	3.36
304b	Double-pair	350 km	Wiese, $l_{\max} = 15$	GRACE-I.	2.34
403b	Single-pair	350 km	None	NGGM	1.37
404b	Double-pair	350 km	Wiese, $l_{\max} = 15$	NGGM	0.55

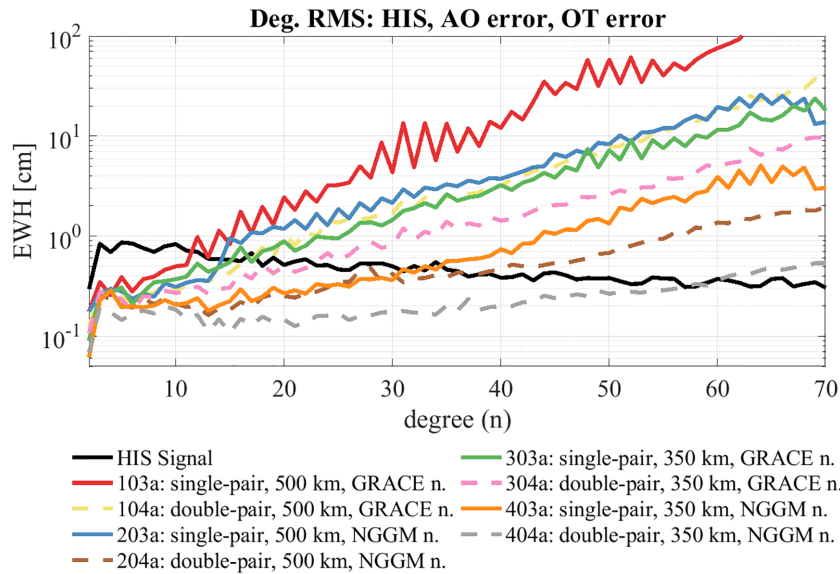


Figure 6. HIS (incl. AO and OT error) scenarios according to Table 5 as degree RMS in EWH up to d/o 70. The HIS signal is visualized in black. Single-pair scenarios are visualized with solid lines, double-pair scenarios are visualized with dashed lines. For more information on the individual scenario see Tables 3 and 5.

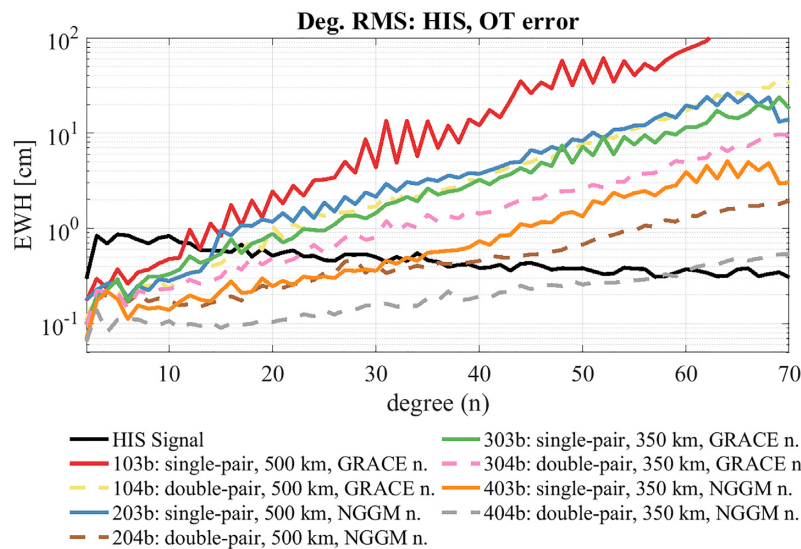


Figure 7. HIS (incl. OT error) scenarios according to Table 6 as degree RMS in EWH up to d/o 70. The AOHIS signal is visualized in dashed black. Single-pair scenarios are visualized with solid lines, double-pair scenarios are visualized with dashed lines. For more information on the individual scenario see Tables 3 and 6.

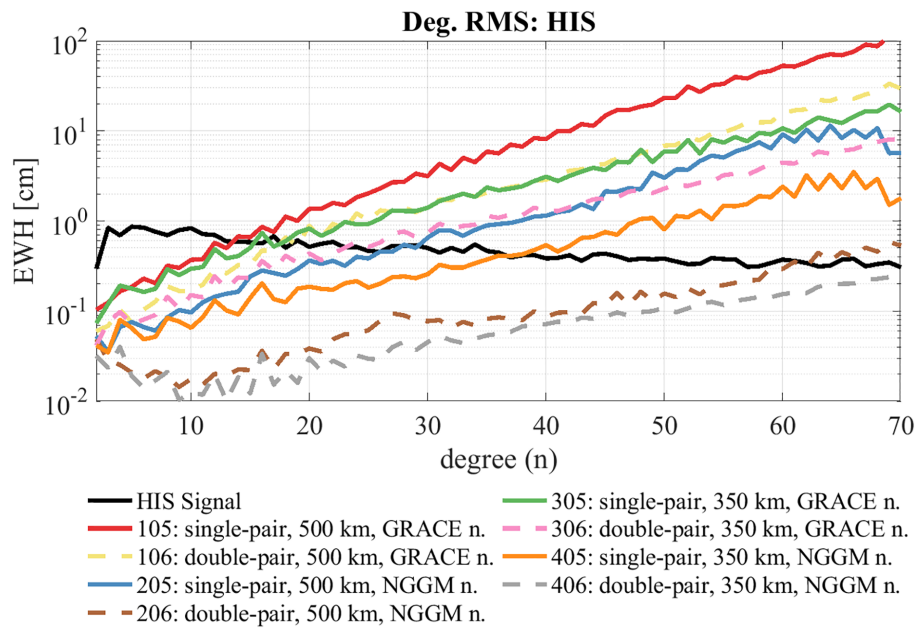


Figure 8. HIS (excl. OT error) scenarios according to Table 7 as degree rms in EWH up to d/o 70. The AOHIS signal is visualized in dashed black. Single-pair scenarios are visualized with solid lines, double-pair scenarios are visualized with dashed lines. For more information on the individual scenario see Tables 3 and 7.

in the lower degrees in all scenarios can be observed. In the double-pair scenario 404b, a bigger reduction especially in the first five degrees and till d/o 25 is visible. The cumulative errors listed in Table 6 are very similar to the values of the scenarios of Table 5, indicating a potential of improvement, however very limited to the low degrees.

4.4 HIS retrieval without OT error, 7-d solutions

As already discussed in Section 2, and implicitly shown in the simulations in Sections 4.1, 4.2 and 4.3, one of the major error sources are in the ocean tide models (Visser 2010; Visser *et al.* 2010; Wiese *et al.* 2011a; Daras & Pail 2017). Various simulations have shown that the errors in ocean tide models are potentially even the limiting source of accuracy for NGGMs (Knudsen & Andersen 2002; Seo *et al.* 2008). The Wiese approach gives good results especially for the double-pair constellation and enables a self-dealiasing of AO signals (Daras & Pail 2017). Additionally, the ocean tides can be co-estimated and then used as a de-aliasing model (Hauk & Pail 2018) to improve the resolvability of the temporal gravity fields. To quantify the possible improvement when using a perfectly modelled OT, the OT errors are excluded from this last set of scenarios.

Fig. 8 shows again the eight base scenarios (details in Table 7). While all scenarios are improved by removing the OT errors, the degree rms error curves of the double-pair scenarios with the NGGM noise show the full potential of the constellation. The error curve first declines, before it moves towards the signal curve at a shallow angle. At this point, it has to be remarked that the performance of the accelerometer noise prevents an even better result, especially in the lower degrees.

The possibilities for a double-pair scenario with an improved sensor noise is very clearly visible, independently of the orbit height. Both constellations again show that the orbit altitude is, all in all,

not the main driver of the gravity field performance in the low to medium degrees. However, the possibilities to reach this (at this point fictional) accuracy level is only possible with a double-pair constellation, due to the improved observation sampling, geometry, and possibility of self-dealiasing.

4.5 Comparison of all scenarios

While in the separate plots in Figs 5–8 the impact of the analysed factors of the constellation, orbit altitude and noise characteristics is visible, the overview graphs in Fig. 9 shows the improvements when removing signal content and the AO and OT error amongst each scenario. The structure of the figure is the same as in Table 3. The AOHIS including the OT error scenarios are plotted in blue, the HIS scenarios with both AO and OT errors are shown in red, and the HIS scenarios with OT error are visualized in green and the HIS scenarios without OT errors are shown in orange. Both AOHIS (in black) and the HIS signal (in dashed black) curves are included in each graph. For the Bender double-pair constellation (right column) processing the Wiese approach with a daily solution of d/o 10 or 15 was used. In the first row an altitude of 500 km and the GRACE-like noise was used, in the second row again 500 km, but with the improved NGGM noise. The scenarios in the third row are based on the lower orbit height of 350 km, and again the GRACE-like noise first, while in the last row the improved NGGM noise is again used.

Regarding the constellation, the addition of a second inclined pair improves the sampling and the observation geometry and allows the mitigating of the temporal aliasing errors via the Wiese approach. The overall performance is in any combination of altitude and noise characteristics better than the polar single-pair.

Apart from the constellation, the biggest impact on the performance of the tested cases has the improved noise characteristics. Specifically the laser sensor noise instead of KBR, which means a

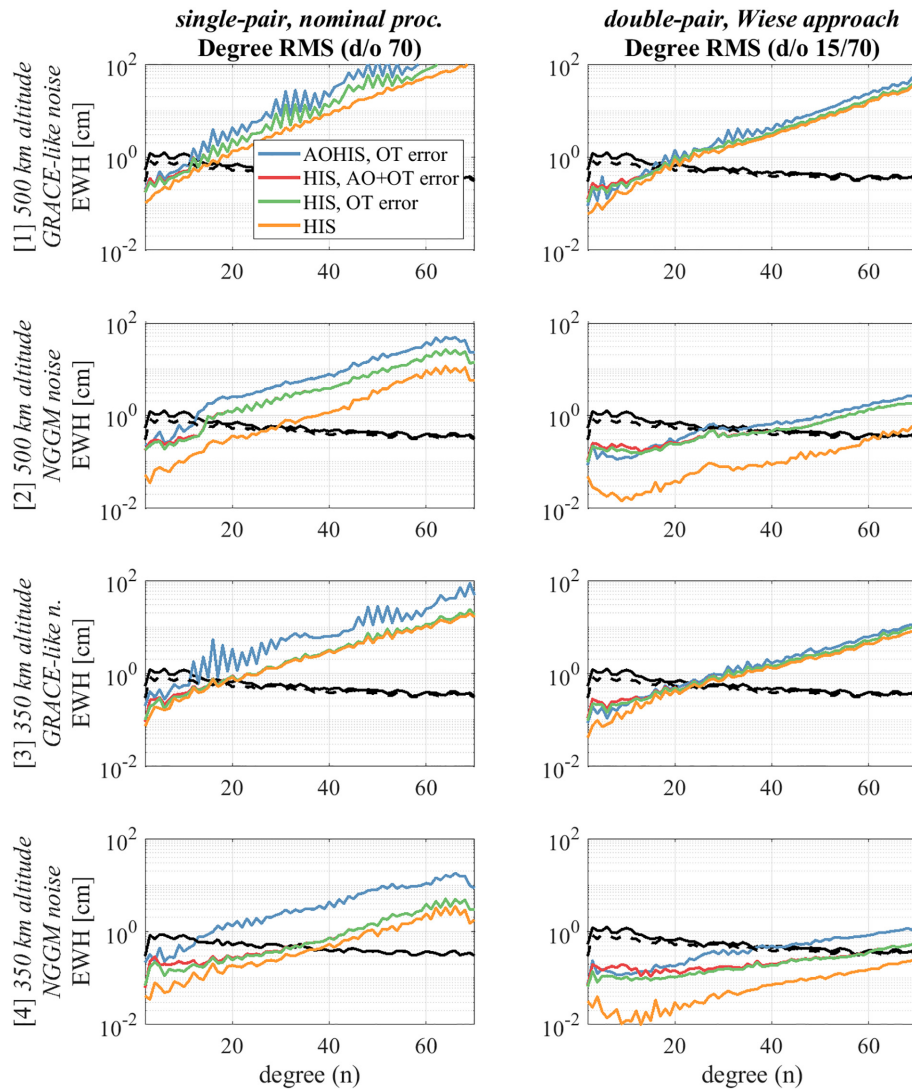


Figure 9. All 24 scenarios according to Tab. 3 as degree rms in EWH up to d/o 70. The AOHIS signal is visualized in black, the HIS signal is visualized in the dashed black line. The blue error curves correspond to the scenarios with the AOHIS signal as input, the HIS scenarios with AO and OT error are displayed in red, HIS scenarios with OT error are displayed in green, while the HIS scenarios without OT errors are visualized in orange.

Table 7. Detailed scenario description of Sc. X03c (single-pair) and X04c (double-pair) incl. cumulative error (average of all comp. solutions).

Sc.	Constellation	Altitude	Dealiasing approach	Noise level	Cum. Error EWH [cm] d/o 30
103c	Single-pair	500 km	None	GRACE-I.	7.31
104c	Double-pair	500 km	Wiese, $l_{\max} = 15$	GRACE-I.	3.31
203c	Single-pair	500 km	None	NGGM	1.77
204c	Double-pair	500 km	Wiese, $l_{\max} = 15$	NGGM	0.25
303c	Single-pair	350 km	None	GRACE-I.	3.39
304c	Double-pair	350 km	Wiese, $l_{\max} = 15$	GRACE-I.	1.79
403c	Single-pair	350 km	None	NGGM	0.81
404c	Double-pair	350 km	Wiese, $l_{\max} = 15$	NGGM	0.14

significantly lower noise level (see Fig. 3 as reference). The improvement is visible when combined with a single-pair or a double-pair with any orbit. The biggest limiting factor in the lower degrees is still the ACC, which is not within the scope of this paper.

As already indicated by the individual scenarios (Figs 5–8), the orbit does not play a crucial role for the double-pair. However, this is a conclusion for the analysed weekly solution. Long-term solutions of a month or longer, which are resolved to higher maximum

degrees, are more sensitive to altitude. If the main target of the mission is the temporal variation of the gravity field with main signal amplitudes in the lower SH degrees, for a double-pair mission it is not absolutely required to go into very low orbit altitudes. This conclusion is important because a mission at 350 km altitude or below would require an electric propulsion system to keep the low orbit altitude during a rather long mission lifetime, which would increase the complexity and the cost of the mission significantly.

When looking at the impact of the constellation, sensor noise and orbit altitude, as well as the used input signal content and errors, a clear distinction between the scenarios is becoming more and more visible. In all four graphs of the single-pair in Fig. 9 improvements are visible when omitting the AO (from blue to red error curve). When omitting the OT error (from green to orange) improvements for all scenarios are visible, however, the biggest improvement can be seen for the double-pair scenario with NGGM noise. In these cases the instrument errors are no longer the limiting factors. The improvement of the background models is therefore very valuable.

4.5.1 Spatial analysis

Fig. 10 shows the errors of the first solution of three of the retrieved test sets, meaning 24 scenarios, as spatial plot resolved till d/o 30. The scenarios are in the same order as listed in Table 3, however without scenario X03b and X04b. For comparison reasons, the same color bar is used for all graphs (± 10 cm). Due to the same colour bar, the improvements in the solutions are especially visible. The AOHIS single-pair solutions are the worst, and also have the worst GRACE-like striping. The best two (double-pair) scenarios are, as Fig. 9 suggests, double pair scenarios 202 and 402. When removing AO and later on also the OT errors, the improvements are, especially when using the NGGM noise, remarkable.

The similar level as the double-pairs can only be reached by the best single-pair scenario, and then only at the HIS level. When looking at the cumulative errors scenario 402 and 403a have at d/o 30 a similar error level. However, it has to be said that the error curve of scenario 403a crosses the signal curve already around d/o 30, while scenario 402 is only starting at around d/o 40 to be 100 per cent error.

4.6 Post-processing

All analyzed scenarios show a clear advantage of the Bender double-pair constellation over a polar single-pair. An aspect that has not been examined at this point is if it is possible to reach the performance of a Bender double-pair constellation after applying post-processing to the single-pair solution. If a similar performance could be achieved, the added value of a second pair would be reduced.

Fig. 11 displays the best double-pair scenario (404a) compared to the single-pair scenario (403a) with and without the three filters presented in chapter 3 applied. The top plot within the figure visualizes all degree rms curves of the scenarios listed in Table 8. The Gaussian filter radius is set to 300 km, which is a good compromise between smoothing the data and losing too much signal overall. The Swenson and Wahr filter is applied starting at d/o 5 and is combined with the Gaussian filter. The VADER filter is adjusted by the weighting factor α , which is set to 50.

The spatial representation of each scenario is at the bottom of Fig. 11. The single-pair plot (middle left) shows the GRACE-typical striping. In comparison, the areas covered additionally with the inclined pair in the double-pair scenario has lower errors. The Gaussian filter removes some striping, but also creates new errors, especially, over the continents as the spatial representation shows. The combination of Swenson filter, starting at d/o 5, and the Gaussian filter with 300 km has good result regarding resolvability (the signal and error curve cross after d/o 40), but spatial errors, especially in the polar regions, appear, which are not present in the unfiltered solution. The VADER filter improves the performance of the single-pair scenario best due to the usage of the parameter

variance-covariance matrix within the filter kernel W , however, the striping appears to be even more dominant.

In the cumulative errors (see Table 8) the effects of the filters are clearly visible. Till d/o 30, where the single-pair itself is resolvable, only the Gaussian filter gives a small improvement. When looking at the cumulative error at d/o 50 the filtering improves the error by a factor 2. However the overall the performance is still a factor 2 worse than the double-pair cumulative error. While the tested filters improve the solution regarding resolvability, the overall performance of the double-constellation is never reached. The collected user requirements by Pail *et al.* (2015), however, clearly state the need for an improved spatial and temporal resolution, which cannot be achieved by a post-processed single-pair.

4.7 Retrieval periods

One of the driving forces when designing the orbit was a drifting orbit so that the ground track pattern allows for a high resolvability. As a test the best two scenarios for both single- and double-pair were analysed for the retrieval periods 14, 21 and 28 d. Table 9 shows the processing details. The single-pair scenarios with longer retrieval periods are processed with the Wiese approach, due to less high frequency noise in the gravity field solutions.

All the tested time periods are a multiple of the original retrieval period of 7 d and should accordingly behave according to the \sqrt{n} -principle. In Fig. 12 the degree rms curves of the scenarios listed in Table 9 are visualized. As expected the biggest improvement is visible when doubling the original time period of 7 d. Further steps toward longer time periods up to an approximately monthly solution of 28 d shows less and less improvement.

When comparing the performance of the single-pair with the double-pair constellation, the biggest difference is the gradient of the error curve. The single-pair degree RMS crosses the signal curve sooner and also at a steeper angle. This leads to an improvement of the single-pair scenarios from approx. d/o 15 to approximately d/o 23 in the AOHIS case and approx. d/o 33 to 40 in the HIS case. In comparison, the double-pair error curves have overall a shallower rise and therefore cross the signal curve at a later point (starting at d/o 35 and 56 for the 7-d retrieval period) and at a narrower angle. The maximum performance d/o for the presented case is therefore approx. d/o 56 and over 70.

Thus, while the 7-d ground track pattern and the derived retrieval period of the same 7-d period are chosen to accommodate possible services and applications in an operational mode, a monthly solution or any other long-term solution is still feasible with the analysed constellation and its ground tracks.

In Fig. 13 the results are visualized as a 2-D matrix with the retrieval periods on one axis against the spatial resolution in km on the other. The degrees are converted with eq. (7) to a spatial resolution in kilometres

$$\lambda = \frac{\pi R}{n}, \quad (7)$$

where R is the Earth radius, n is the spherical harmonics degree and λ the half wavelength in kilometers at the equator.

The elements of the matrix are the averaged cumulative errors computed from the solutions presented in Fig. 12. Each solution is evaluated at various d/o. The rest of the data points are interpolated based on the computed error grid and presented as contours of error levels, with blue being the best and red the worst cumulative errors. The not observable gravity field resolutions are marked with black hatching. This representation allows for an easy and fast overview

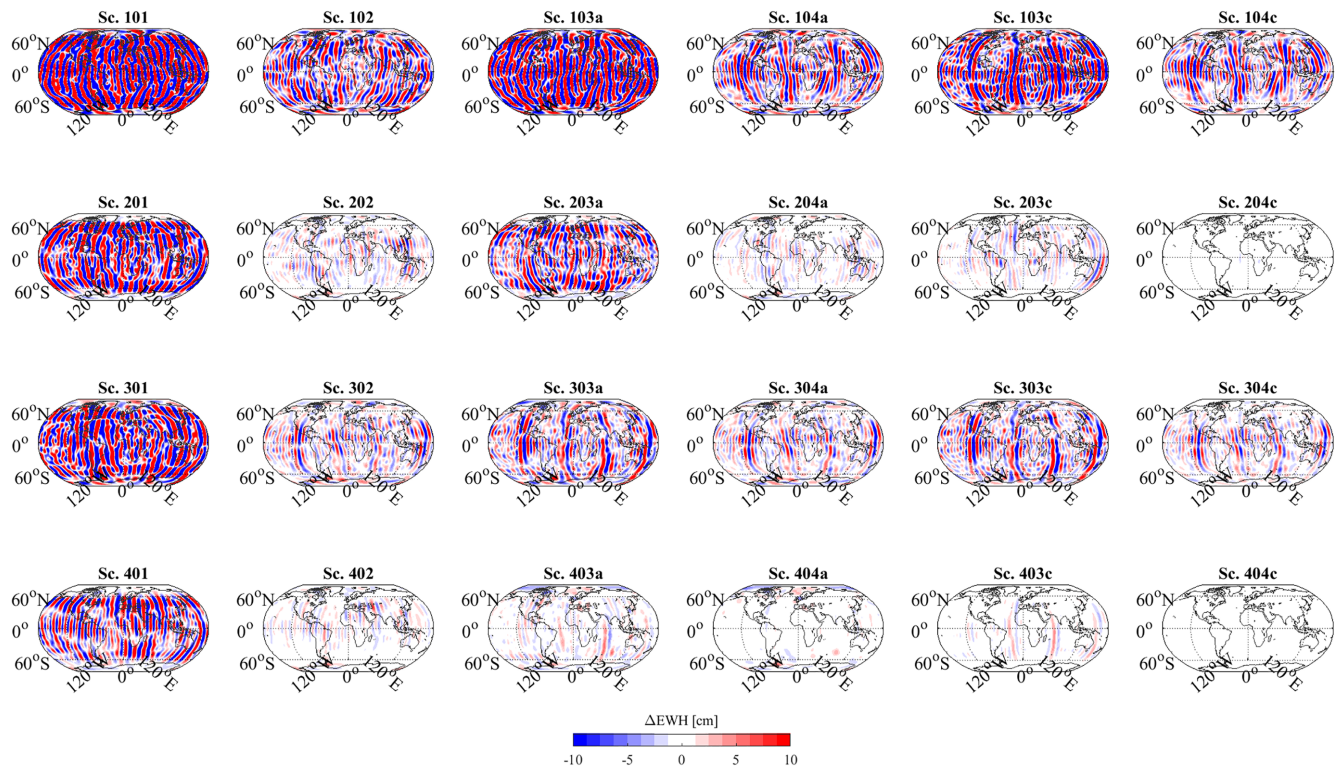


Figure 10. Scenarios X01, X02, X03a, X04a and X03c, X04c according to Table 3 in spatial representation of ΔEWH up to d/o 30.

of the possibility of a single- and double-pair in the full AOHIS as well as HIS retrieval based on retrieval period and spatial resolution.

5 CONCLUSION

The presented results intend to answer the question as to how much various design parameters impact the gravity field retrieval performance of a single-pair as well as double-pair solution, how much a second pair improves the performance of a gravity mission and if an adjusted post-processing scheme for a single-pair mission would improve the single-pair solutions to a level where the added value of the second pair is not significant anymore.

In general, it can be stated, that in all processed scenarios the double-pair constellations perform better than the corresponding single-pair scenarios. When retrieving the full AOHIS signal (scenarios X01 and X02) the number of pairs has the biggest impact on the retrieved temporal gravity field. When only retrieving the HIS signal with AO and OT errors included (scenarios X03a and X04a), the biggest improvement can be observed for the polar single-pair and the double-pair, when using the low orbit and the NGGM noise characteristics. Within the single-pair scenarios the low orbit combined with an NGGM noise is the only possibility overall for improvement of the gravity field retrieval performance. A low orbit, however, means a drag-free satellite with an adjusted sensor system is needed. In the case of the double-pair, this low orbit is not absolutely essential.

The exclusion of AO errors (X03b and X04b) is primarily visible in the lower degrees and reduces the noise for all scenarios equally. When only using the HIS without taking into account OT errors (scenarios X03c and X04c) another big step can be achieved especially for the double-pair constellation combined with the NGGM noise. In these scenarios, the advantage of the improved LL-SST can be used to the fullest extent, as the single-pair is no longer

the limiting factor. In the first degrees though an improvement is not visible, because in these degrees the accelerometer noise is still dominant. Simulations of novel hybrid accelerometer, however, have shown, that in a noise-only simulation a substantial gain can be observed, which is however significantly reduced when including temporal aliasing effects (Abrykosov *et al.* 2019). It has to be remarked, that to approximate these optimum-case results (scenarios X03c and X04c) the ocean tide modelling has to be improved significantly, for example by OT co-estimation, to enable significant improvements.

The orbit altitude in the 7-d GF solutions is not the main driver regarding the achievable performance. This means when choosing the orbit altitude, there is certain freedom for the double-pair and could also be based on budgetary considerations since the orbit altitude determines what sensors are necessary to successfully fly such a satellite mission. An improved noise characteristic with a laser LL-SST tracking is however clearly necessary to enable the full exploitation of the double-pair (see Fig. 14, right-hand panel).

With a tailored post-processing, a higher spatial resolution for the single-pair towards the performance of the double-pair is possible. However, these techniques come with the disadvantages of artefacts due to the filtering process. The Gaussian filter performs best regarding destriping, but also removes a lot of signals and displaces errors into continental areas. The best results are achieved by the VADER filter. The performance of the double-pair, however, cannot be reached and is still a factor 2 worse after the filtering at d/o 50.

In order not to base the conclusions only on a 7-d solution, also different retrieval periods of multiples of the 7 d were tested for the best performing single- and double-pair scenarios. For all cases the \sqrt{n} -rule regarding the longer retrieval periods holds. Both single- and double-pair have an increase of +25 per cent

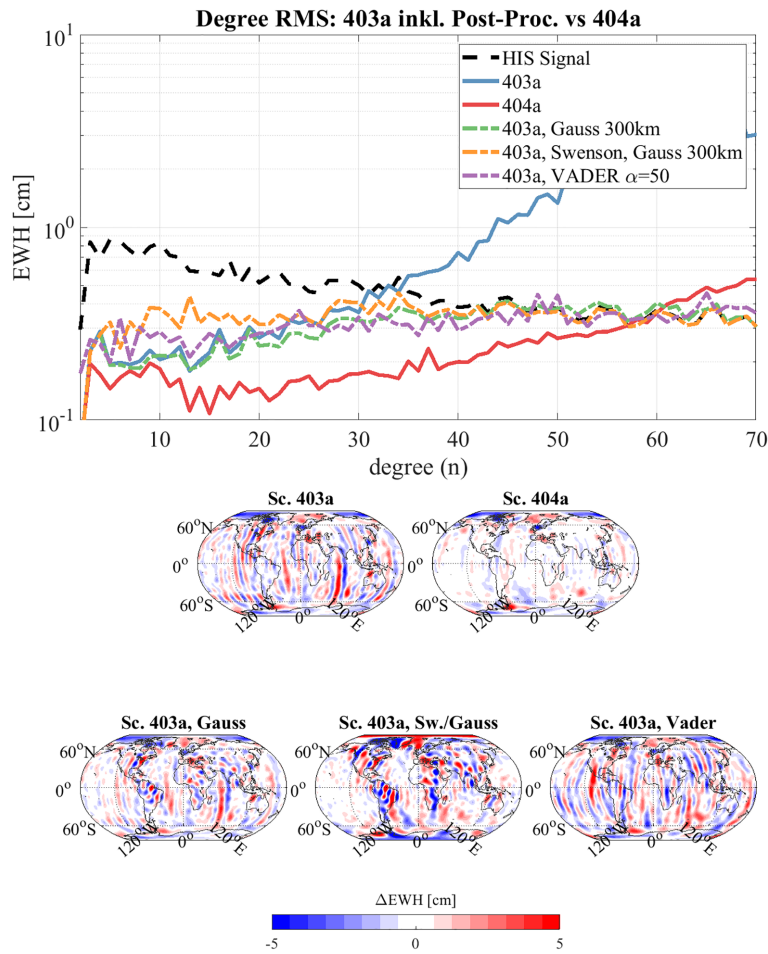


Figure 11. Degree rms and spatial plot of ΔEWH (till $d/o30$) in cm of scenario 403a and 404a (HIS input signal, filtered/unfiltered). First row: Degree rms of the 403/4a scenario. HIS signal in the black dashed line. Sc. 403a single-pair in blue, sc. 404a double-pair scenario in red. The single-pair scenario is additionally filtered with a Gaussian filter of 300 km, Swenson (starting at d/o 15) and a Gaussian filter of 300 km, as well as VADER filtered with factor 50. The corresponding filtered signals are visualized in lighter dashed lines of the same colour. The spatial plots are a difference of the filtered estimated coefficients and the unfiltered reference coefficients of the shown degree rms filter scenarios till d/o 30.

Table 8. Double-pair scenario 404a and single-pair scenario 403a incl. different filter settings. Cumulative error is average from all computed solutions.

Sc.	Filter	Cum. Error EWH [cm] d/o 30	Cum. Error EWH [cm] d/o 50
404a	None	0.77	1.22
403a	None	1.49	4.34
403a	Gauss (300 km)	1.38	2.22
403a	Swenson (d/o 5+) and Gauss (300 km)	1.69	2.48
403a	Vader ($\alpha = 50$)	1.61	2.14

Table 9. Sc. 401 and 403a (polar single-pair) and Sc. 402 and 404a (Bender double-pair) with different retrieval periods. Cumulative error is average from all computed solutions.

Sc.	Dealiasing Appr.	Retr. P. [d]	Cum. Error EWH [cm] d/o 30	Sc.	Dealiasing Appr.	Retr. P. [d]	Cum. Error EWH [cm] d/o 30
401	None	7	6.75	403a	None	7	1.49
(i)	Wiese, $l_{max} = 10$	14	5.21	(i)	Wiese, $l_{max} = 10$	14	1.16
(ii)	Wiese, $l_{max} = 10$	21	2.79	(ii)	Wiese, $l_{max} = 10$	21	0.77
(iii)	Wiese, $l_{max} = 10$	28	2.95	(iii)	Wiese, $l_{max} = 10$	28	0.84
402	Wiese, $l_{max} = 15$	7	1.16	404a	Wiese, $l_{max} = 15$	7	0.77
(i)	Wiese, $l_{max} = 15$	14	0.97	(i)	Wiese, $l_{max} = 15$	14	0.60
(ii)	Wiese, $l_{max} = 15$	21	0.65	(ii)	Wiese, $l_{max} = 15$	21	0.42
(iii)	Wiese, $l_{max} = 15$	28	0.69	(iii)	Wiese, $l_{max} = 15$	28	0.44

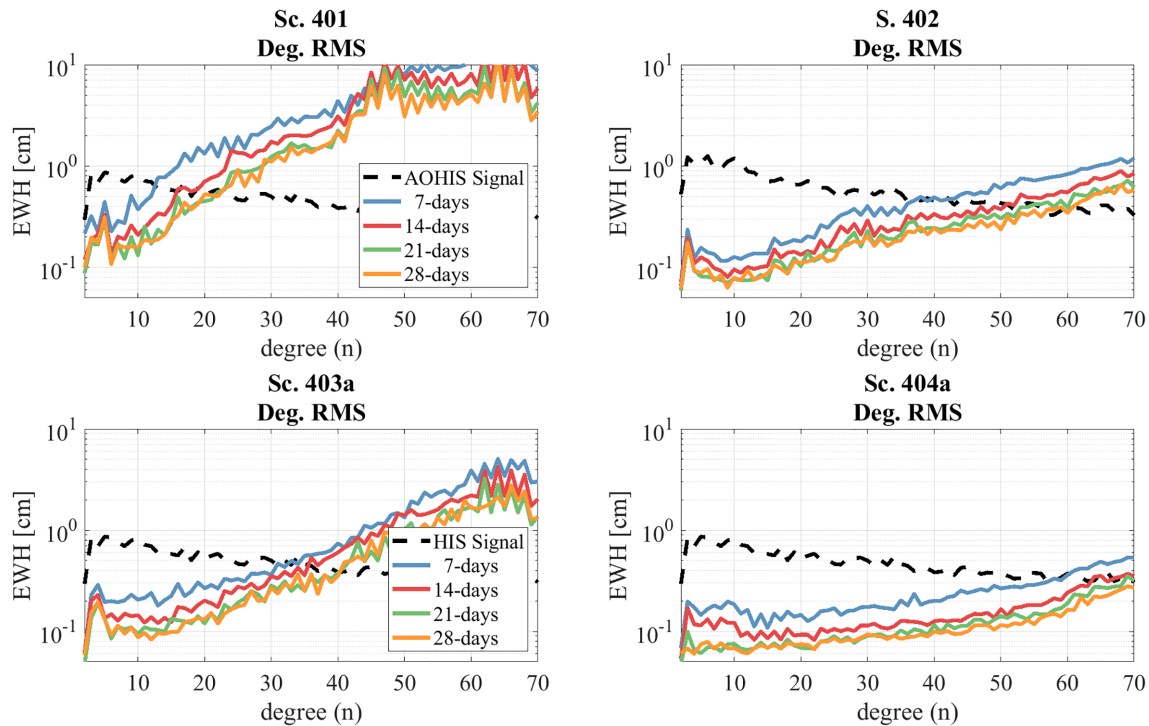


Figure 12. Different retrieval periods on the improvement in resolvability based on scenario 401 (top left-hand panel) and 402 (top right-hand panel) and scenarios 403a (bottom left-hand panel) and 404a (bottom right-hand panel). These scenarios use all NGGM noise and a low orbit.

improvement in resolvability on d/o level (see Fig. 14, left-hand panel).

Based on the results of the study, we conclude that a low flying single-pair with a low orbit and NGGM noise would give an improvement compared to a higher-flying single-pair. In terms of resolvability in d/o, this means a 100 per cent improvement compared to the other single-pair scenarios and a decrease of 6.42 to 1.37 cm in cumulative error till d/o 30 when compared to the higher flying single-pair with NGGM noise. However, this mission would still not solve the problems of temporal aliasing due to observation geometry, the impossibility to retrieve AO and also that post-processing strategies are creating artefacts.

Therefore the next big step for observing the gravity field globally via a satellite mission can only be taken, when a double pair mission is launched. It is also the only possibility to observe the full AOHIS signal. On the level of the full retrieval, the double-pair with a low orbit and NGGM noise has a 166 per cent improvement to the same single-pair scenario and a decrease of the cumulative error till d/o 30 from 6.75 to 1.16 cm EWH. On HIS level the advantage of the double-pair is reduced to 88 per cent improvement of resolvability in d/o. However, if a high orbit altitude is considered, the possible improvement is 100 per cent in terms of d/o. Expressed in cumulative errors this means a reduction from 1.49 to 0.77 cm EWH. Lastly, no or only light post-processing is needed, for example a very light Gaussian filter.

These results do not only confirm the different individual results by the various study groups as listed in the introduction, but also fill the gaps as we looked at every combination of factors. This allows for a comparison, quantification and also comprehension of all the different combinations and the impact of one different specification on the whole performance as the different factors have complex interdependencies.

If the single factors and their impact on the gravity field estimation performance are sorted by priority, a clear picture of the best path forward emerges, see Table 10. As already mentioned in the introduction, it is obvious that a mission with two satellite pairs enables a much more accurate estimation of time-variable gravity field models. This fact was again stressed by the results of the simulation. We also could show, that improvements via a LRI with a double-pair is clearly visible in the gravity fields. Therefore, the first priority is a double-pair with an LRI sensor. As the orbit is not the driving factor for the mission performance in the lower SH degrees, for the first step a higher orbit is recommended in the case of existing cost constraints.

The second big step, for example visualized in Fig. 14 (right-hand panel), can be taken with an improved ocean tide modelling. As this step is on the one hand dependent on the double-pair constellation, and also on an improved processing, for example Hauk & Pail (2018), it is set as priority 2. A more general improvement is the development of a strategy for adequate filter options and AO dealiasing models, which is still the only possibility to separate the signals. This step is especially necessary for single-pair missions, and could be also listed as first priority to improve the current mission's data sets. As the priority list is tailored towards the important steps for the future, it is listed as priority 3 with a focus on signal separation, which is important for applications usually based on only one of the signal parts.

Lastly, with a long-term timeframe, the low-flying constellation, which would also enable an improvement of the static gravity field estimation is set as priority 4. To enable the necessary development of a propulsion and thruster system (Dionisio *et al.* 2018), the item is listed as last priority. However, it is important to emphasize that the development has to proceed in parallel with any NGGM so that the following mission has the potential to fly in a low orbit with a

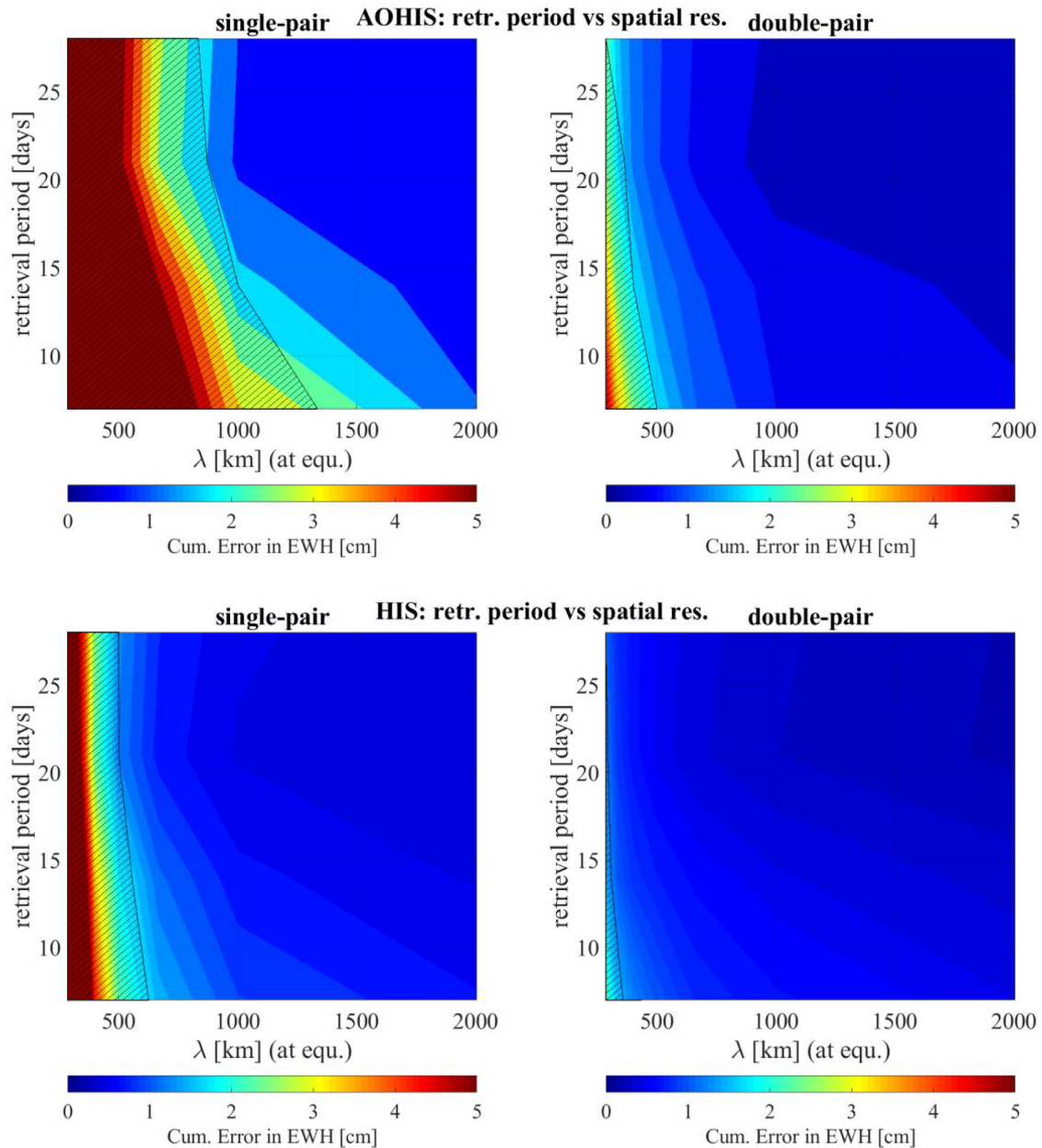


Figure 13. Average cumulative errors of the best AOHIS scenarios (401 and 402, at the top) and best HIS scenario (403a and 404a, at the bottom) with different retrieval periods and up to different degrees transformed to spatial resolution. The cross-hatched signals are not observable, meaning the global SNR is bigger than 1.

drag-free concept. The possible single-pair mission option in a low orbit is not listed due to the limited scientific potential compared to a double-pair mission.

The priorities and their justifications listed in Table 10 give a general recommendation of the best trade-off between the costs and the value of the mission for science and services. The indicated order is such, that the individual factors give the highest impact on the final result: time-variable gravity field estimation and all its application within the wide range of geophysics.

ACKNOWLEDGEMENTS

A big part of the investigations presented in this paper was performed in the framework of the study ‘Assessment of satellite constellations for monitoring the variations in Earth gravity field (AD-DCON)’, ESA-ESTEC, Contract AO/1-7317/12/NL/AF funded by the European Space Agency. We also acknowledge the provision of supercomputing resources by the Leibniz Supercomputing Centre (LRZ; Address: Boltzmannstraße 1, 85748 Garching bei München, Germany).

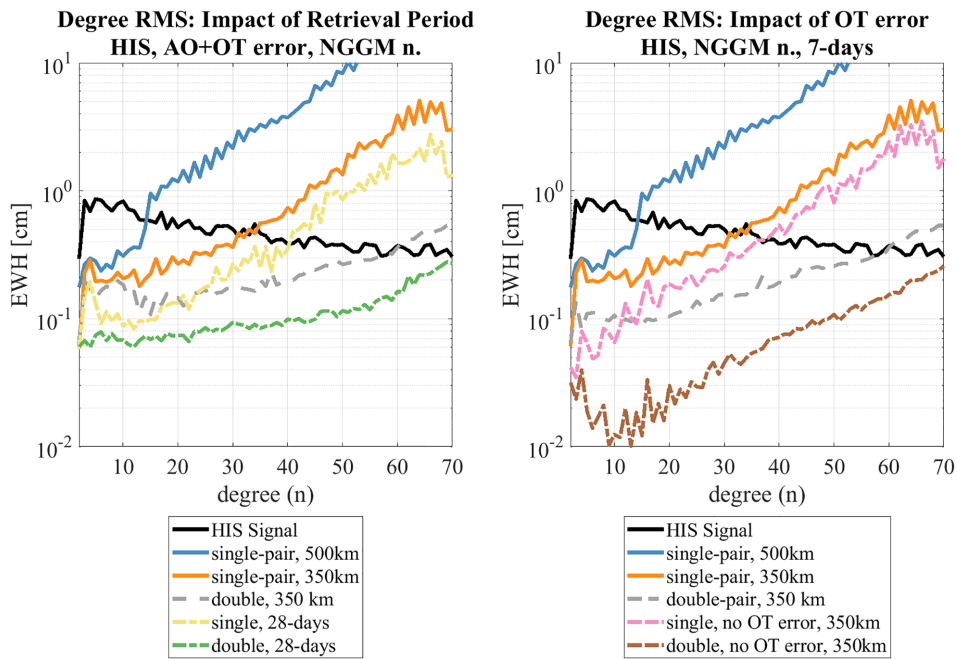


Figure 14. Potential of double-pairs in degree rms (based on HIS as input signal, AO + OT error incl., NGGM noise). Impact of retrieval period (left-hand panel) and OT errors (right-hand panel) on the performance.

Table 10. Priority of different aspects towards the NGGM.

Priority	What?	Why?
1	Bender-type double-pair mission With improved ACC/LRI instrumentation	Technology mature, full AOHIS retrieval possible Performance of GF est. is directly improved
2	Improvement of ocean tide models	Big improvement possible, especially when P-1 is fulfilled
3	Improvement of AO dealiasing model Development of general usable de-stripping/filtering techniques	Signal separation still unsolved For applications based on the gravity field data necessary
4	Lower altitude, when interested in a static field also	Spacecraft propulsion is an open issue, P-1 can be deployed instantaneously as technology is mature

REFERENCES

Abrykosov, P., Pail, R., Gruber, T., Zahzam, N., Bresson, A., Hardy, E. & Siemes, C., 2019. Impact of a novel hybrid accelerometer on satellite gravimetry performance, *Adv. Space Res.*, doi:10.1016/j.asr.2019.01.034.

Albertella, A., Sansò, F. & Sneeuw, N., 1999. Band-limited functions on a bounded spherical domain: the Slepian problem on the sphere, *J. Geod.*, **73**(9), 436–447.

Baur, O. & Sneeuw, N., 2011. Assessing Greenland ice mass loss by means of point-mass modelling: a viable methodology, *J. Geod.*, **85**, 607–615.

Bender, P.L., Wiese, D. & Nerem, R.S., 2008. A possible dual-GRACE mission with 90 degree and 63 degree inclination orbits, in *Proceedings of the 3rd International Symposium on Formation Flying, Missions and Technologies*, ESA/ESTEC, Noordwijk, 23–25 April 2008, 1–6.

Christophe, B., Boulanger, D., Foulon, B., Huynh, P.A., Lebat, V., Liorzou, F. & Perrot, E., 2015. A new generation of ultra-sensitive electrostatic accelerometers for GRACE Follow-on and towards the next generation gravity missions, *Acta Astronaut.*, **117**, 1–7.

Christophe, B. et al. 2018. *Status of Development of the Future Accelerometers for Next Generation Gravity Missions*, International Association of Geodesy Symposia, Springer, 10.1007/1345_2018_42.

Dahle, C. et al. 2019. The GFZ GRACE RL06 monthly gravity field time series: processing details and quality assessment, *Rem. Sens.*, **11**(18), 2116.

Daras, I., Pail, R., Murböck, M. & Yi, W., 2015. Gravity field processing with enhanced numerical precision for LL-SST missions, *J. Geod.*, **89**(2), 99–110.

Daras, I., 2016. *Gravity Field Processing Towards Future LL-SST Satellite Missions; Deutsche Geodätische Kommission der Bayerischen Akademie der Wissenschaften, Reihe C, Dissertationen, Heft 770, Verlag der Bayerischen Akademie der Wissenschaften*, pp. 23–39. ISBN(Print) 978-3-7696-5182-9, ISSN 0065–5325, 2016.

Daras, I. & Pail, R., 2017. Treatment of temporal aliasing effects in the context of next generation satellite gravimetry missions, *J. geophys. Res.*, **22**(9), 7343–7362.

Devaraju, B., 2015. *Understanding filtering on the sphere: Experiences from filtering GRACE data*. PhD thesis, Universität Stuttgart.

Dickey, J.O. et al., 1997. *Satellite Gravity And The Geosphere, Committee on Earth Gravity from Space*, National Academy Press.

Dionisio, S., Anselmi, A., Bonino, L., Cesare, S., Massotti, L. & Silvestrin, P., 2018. The “Next Generation Gravity Mission”: challenges and consolidation of the system concepts and technological innovations, AIAA 2018–2495, Session: MDM - Mission Engineering and Planning. doi:10.2514/6.2018-2495.

Dobslaw, H., Flechtner, F., Bergmann-Wolf, I., Dahle, C., Dill, R., Esselborn, S., Sasgen, I. & Thomas, M., 2013. Simulating high-frequency atmosphere-ocean variability for dealiasing of satellite gravity observations: AOD1b RL05: atmosphere-ocean mass variability: AOD1b, *J. geophys. Res.*, **118**(7), 3704–3711.

Dobslaw, H., Bergmann-Wolf, I., Dill, R., Forootan, E., Klemann, V., Kusche, J. & Sasgen, I., 2015. The updated ESA Earth System Model for future gravity mission simulation studies, *J. Geod.*, **89**, 505–513.

Dobslaw, H., Bergmann-Wolf, I., Forootan, E., Dahle, C., Mayer-Gürr, T., Kusche, J. & Flechtner, F., 2016. Modeling of present-day atmosphere and

- ocean non-tidal de-aliasing errors for future gravity mission simulations, *J. Geod.*, **90**(5), 423–436.
- Eicker, A., Schall, J. & Kusche, J., 2013. Regional gravity modelling from spaceborne data: case studies with GOCE, *Geophys. J. Int.*, **196**(3), 1431–1440.
- Elsaka, B., Kusche, J. & Ilk, K.-H., 2012. Recovery of the Earth's gravity field from formation-flying satellites: temporal aliasing issues, *Adv. Space Res.*, **50**, 1534–1552.
- Elsaka, B., Raimondo, J.-C., Brieden, Ph., Reubelt, T., Kusche, J., Flechtner, F., Iran Pour, S., Sneeuw, N. & Müller, J., 2014. Comparing Seven Candidate Mission Configurations for Temporal Gravity Retrieval through Full-Scale Numerical Simulation, *J. Geod.*, **88**, 31–43.
- Elsaka, B., Raimondo, J., Brieden, P.J. *et al.* 2014. Comparing seven candidate mission configurations for temporal gravity retrieval through full-scale numerical simulation, *J. Geod.*, **88**, 31–43.
- Feng, W., 2018. GRAMAT: a comprehensive Matlab toolbox for estimating global mass variations from GRACE satellite data, *Earth Sci Inform.* doi:10.1007/s12145-018-0368-0.
- Flechtner, F., Schmidt, R. & Meyer, U., 2006. De-aliasing of Short-term Atmospheric and Oceanic Mass Variations for GRACE, *Observation of the Earth System from Space*, doi:10.1007/3-540-29522-4_7.
- Flechtner, F., Neumayer, K.H., Dahle, C., Dobslaw, H., Güntner, A., Raimondo, J.C. & Fagiolini, E., 2016. What can be expected from the GRACE-FO laser ranging interferometer for earth science applications? *Surv. Geophys.*, **37**(2), 453–470.
- Flechtner, F., Webb, F. & Watkins, M., 2017. Current status of the GRACE follow-on mission, *Geophys. Res. Abstr.*, Vol. **19**, EGU2017–4566, EGU General Assembly 2017.
- Floborghagen, R., Fehring, M., Lamarre, D., Muzi, D., Frommknecht, B., Steiger, Ch, Piñeiro, J. & da Costa, A., 2011. Mission design, operation and exploitation of the gravity field and steady-state ocean circulation explorer mission, *J. Geod.*, **85**(11), 749–758.
- Foorotan, E., Didova, O., Schumacher, M., Kusche, J. & Elsaka, B., 2014. Comparisons of atmospheric mass variations derived from ECMWF re-analysis and operational fields over 2003–2011, *J. Geod.*, **88**, 503–514.
- Gooding, R.H., Wagner, C.A., Klokočnik, J., Kostelecky, J. & Gruber, Ch, 2007. CHAMP and GRACE resonances, and the gravity field of the Earth, *Adv. Space Res.*, **39**(10), 1604–1611.
- Gruber, Ch & Gouweleeuw, B., 2019. Short-latency monitoring of continental, ocean- and atmospheric mass variations using GRACE intersatellite accelerations, *Geophys. J. Int.*, **217**(1), 714–728.
- Gruber, Th & Murböck, M. the NGGM-D Team, 2014. e2.motion - Earth System Mass Transport Mission (Square) - Concept for a Next Generation Gravity Field Mission, C.H. Beck.
- Guo, N., Zhou, X., Li, K. & Wu, B., 2018. Research on the impact factors of GRACE precise orbit determination by dynamic method, *J. appl. Geod.*, **12**(3), 249–257.
- Gustavson, T.L., Bouyer, P. & Kasevich, M.A., 1997. Precision rotation measurements with an atom interferometer gyroscope, *Phys. Rev. Lett.*, **78**, 2046–2049.
- Han, S., Shum, C. & Matsumoto, K., 2005. GRACE observations of M2 and S2 ocean tides underneath the Filchner-Ronne and Larsen ice shelves, Antarctica, *Geophys. Res. Lett.*, **32**, L20311.
- Han, S., Riva, R., Sauber, J. & Okal, E., 2013. Source parameter inversion for recent great earthquakes from a decade-long observation of global gravity fields, *J. geophys. Res.*, **118**, 1240–1267.
- Hauk, M., Schlicht, A., Pail, R. & Murböck, M., 2017. Gravity field recovery in the framework of a Geodesy and Time Reference in Space (GETRIS), *Adv. Space Res.* **59**(8), 2032–2047.
- Hauk, M. & Pail, R., 2018. Treatment of ocean tide aliasing in the context of a next generation gravity field mission, *Geophys. J. Int.*, **214**, 345–365.
- Hauk, M. & Pail, R., 2019. Gravity field recovery using high-precision, high-low inter-satellite links, *Rem. Sens.*, **11**(5), 537.
- Harig, C. & Simons, F.J., 2012. Mapping Greenland's mass loss in space and time, *Proc. Natl. Acad. Sci.*, **109**(49), 19934–19937.
- Hofmann-Wellenhof, B. & Moritz, H., 2005. *Physical Geodesy*, 2nd edn, Springer.
- Horvath, A., Murböck, M., Pail, R. & Horvath, M., 2018. Decorrelation of GRACE time variable gravity field solutions using full covariance information, *Geosciences*, **8**(9), ISSN 2076–3263.
- Iran Pour, S., Reubelt, T. & Sneeuw, N., 2013. Quality assessment of sub-nyquist recovery from future gravity satellite missions, *J. Adv. Space Res.*, **52**, 916–929.
- Iran Pour, S. *et al.* 2015. Assessment of satellite constellations for monitoring the variations in earth gravity field – SC4MGV, ESA – ESTEC Contract No. AO/1-7317/12/NL/AF, Final Report.
- Ivins, E., Watkins, M., Yuan, D.N., Dietrich, R., Casassa, G. & Rülke, A., 2011. On land ice loss and glacial isostatic adjustment at the Drake Passage: 2003–2009, *J. geophys. Res.*, **116**, B02403.
- Jäggi, A. *et al.* 2019. European Gravity Service for Improved Emergency Management (EGSIEM)—from concept to implementation, *Geophys. J. Int.*, **218**(3), 1572–1590
- Jekeli, C., 1981. *Alternative Methods to Smooth The Earth's Gravity Field*, Tech. Rep. 327, Department of Geodetic Science and Surveying, Ohio State Univ., Columbus, OH
- King, M., Padman, L., Nicholls, K., Clarke, P.J., Gudmundsson, G.H., Kulesa, B. & Shepherd, A., 2011. Ocean tides in the Wedell Sea: new observations on the Filchner-Ronne and Larsen C ice shelves and model validation, *J. geophys. Res.*, **116**, C06006.
- Knudsen, P. & Andersen, O., 2002. Correcting GRACE gravity fields for ocean tide effects, *Geophys. Res. Lett.*, **29**(8), 1178.
- Kornfeld, R.P., Arnold, B.W., Gross, M.A., Dahya, N.T. & Klipstein, W.M., 2019. GRACE-FO: the gravity recovery and climate experiment follow-on mission, *J. Spacecraft Rockets*, <https://doi.org/10.2514/1.A34326>
- Kusche, J., 2007. Approximate decorrelation and non-isotropic smoothing of time-variable GRACE-type gravity field models, *J. Geod.*, **81**(11), 733–749.
- Kusche, J., Schmidt, R., Petrovic, S. & Rietbroek, R., 2009. Decorrelated GRACE time-variable gravity solutions by GFZ, and their validation using a hydrological model, *J. Geod.*, **83**, 903–913.
- Kurtenbach, E., Mayer-Gürr, T. & Eicker, A., 2009. Deriving daily snapshots of the Earth's gravity field from GRACE L1B data using Kalman filtering, *Geophys. Res. Lett.*, doi:10.1029/2009GL039564.
- Kvas, A., Gruber, C., Gouweleeuw, B., Güntner, A., Mayer-Gürr, T. & Flechtner, F., 2019, The EGSIEM near real-time service based on GRACE Mission data – review and outlook, in *Paper presented at 27th IUGG General Assembly*, Montreal, Canada.
- Klokočnik, J., Wagner, C.A., Kostelecký, J., Bezděk, A., Novák, P. & McAdoo, D., 2008. Variations in the accuracy of gravity recovery due to ground track variability: GRACE, CHAMP, and GOCE, *J. Geod.*, **82**, 917–927.
- Luthcke, S.B., Sabaka, T., Loomis, B., Arendt, A., McCarthy, J. & Camp, J., 2013. Antarctica, Greenland, and Gulf of Alaska land-ice evolution from an iterated GRACE global mascon solution, *J. Glaciol.*, **59**(216), 613–631.
- Mayer-Gürr, T., 2006. *Gravitationsfeldbestimmung aus der Analyse kurzer Bahnbögen am Beispiel der Satellitenmissionen CHAMP und GRACE*, <http://hss.ulb.uni-bonn.de/2006/0904/0904.htm>.
- Mayer-Gürr, T., Savcenko, R., Bosch, W., Daras, I., Flechtner, F. & Dahle, C., 2012. Ocean tides from satellite altimetry and GRACE, *J. Geodyn.*, **59–60**, 28–38.
- Mayer-Gürr, T. *et al.* 2015. The combined satellite gravity field model GOCO05s, *Geophys. Res. Abstracts*, **17**, EGU2015-12364, European Geosciences Union General Assembly 2015 (Vienna, Austria). doi:10.13140/RG.2.1.4688.6807.
- McGuirk, J.M., Foster, G.T., Fixler, J.B., Snadden, M.J. & Kasevich, M.A., 2002. Sensitive absolute gravity gradiometry using atom interferometry, *Phys. Rev. A*, **65**, 033608.
- Montenbruck, O. & Gill, E., 2000. Satellite Orbits, doi:10.1007/978-3-642-58351-3.
- Murböck, M. & Pail, R., 2014. Reducing non-tidal aliasing effects by future gravity satellite formations, In *Earth on the Edge: Science for a Sustainable Planet, IAG Symposia*, **139**, pp. 407–412, eds Rizos, C & Willis, P, Springer. ISBN 978-3-642-37221-6.

- Muller, P.M. & Sjogren, W.L., 1968. Mascons: lunar mass concentrations, *Science: New Series*, **161**(3842), 680–684.
- Pail, R., Plank, G. & Schuh, W.D., 2001. Spatially restricted data distributions on the sphere: the method of orthonormalized functions and applications, *J. Geod.*, **75**(1), 44–56.
- Pail, R. IUGG Expert Panel et al. IUGG Expert Panel, 2015. Science and user needs for observing global mass transport to understand global change and to benefit society, *Surv. Geophys.*, **36**(6), 743–772.
- Pail, R. et al. 2019. Mass variation observing system by high low inter-satellite links (MOBILE) – a new concept for sustained observation of mass transport from space, *J. Geod. Sci.*, doi:10.1515/jogs-2019-0006
- Panet, I., Pajot-Métivier, G., Greff-Lefftz, M., Métivier, L., Diamant, M. & Manda, M., 2014. Mapping the mass distribution of Earth's mantle using satellite-derived gravity gradients, *Nat. Geosci.*, **7**, 131–135.
- Peters, A., Chung, K.Y. & Chu, S., 2001. High-precision gravity measurements using atom interferometry, *Metrologia*, **38**(1), 25.
- Purkhauser, A.F. et al. 2018. Gravity field retrieval of next generation gravity missions regarding geophysical services: results of the ESA-ADDCON project, European Geosciences Union General Assembly 2018. <https://meetingorganizer.copernicus.org/EGU2018/EGU2018-2770.pdf>.
- Ray, R.D., 1999. A global ocean tide model from topex/Poseidon altimetry: Got99.2, *Tech. rep.*, NASA Technical Memorandum 209478.
- Reigber, C., Schwintzer, P. & Lühr, H., 1999. The CHAMP geopotential mission, *Bollettino di Geofisica Teoretica ed Applicata*, 40/3–4, September–December 1999, Proceedings of the Second Joint Meeting of the International Gravity and the International Geoid Commission, Trieste 1998 September 7–12, ISSN 0006–6729, pp. 285–289, eds Marson I. & Sünkel H.
- Reubelt, T. et al. 2014. *Future Gravity Field Satellite Missions*, pp. 165–230. Springer-Verlag.
- Rodell, M., Famiglietti, J.S., Wiese, D.N., Reager, J.T., Beaulieu, H.K., Landerer, F.W. & Lo, M.H., 2018. Emerging trends in global freshwater availability, *Nature*, **557**(7707), 651–659.
- Rummel, R., Yi, W. & Stummer, C., 2011. GOCE gravitational gradiometry, *J. Geod.*, **85**(11), 777–790.
- Savcenko, R. & Bosch, W., 2008. EOT08a – Empirical Ocean Tide Model from Multi-Mission Satellite Altimetry, DGFI Report, München, Germany, 81.
- Schneider, M., 1969. Outline of a general orbit determination method, in *Space Research IX, Proceedings of Open Meetings of Working Groups (OMWG) on Physical Sciences of the 11th Plenary Meeting of the Committee on Space Research (COSPAR)*, Tokyo, eds. Champion, K.S.W. & P.A.
- Schrama, E.J.O., Wouters, B. & Lavallée, D.A., 2007. Signal and noise in gravity recovery and climate experiment (GRACE) observed surface mass variation, *J. geophys. Res.*, **116**(B2), B02407.
- Seo, K.W., Wilson, C.R., Han, S.C. & Waliser, D.E., 2008. Gravity recovery and climate experiment (GRACE) alias error from ocean tides, *J. geophys. Res.*, **113**, B03405.
- Shampine, L.F. & Gordon, M.K., 1975. *Computer Solution of Ordinary Differential Equations: The Initial Value Problem*, W.H. Freeman.
- Sharifi, M., Sneeuw, N. & Keller, W., 2007. Gravity recovery capability of four generic satellite formations, Gravity Field of the Earth. General Command of Mapping.
- Sheard, B.S., Heinzel, G., Danzmann, K., Shaddock, D.A., Klipstein, W.M. & olkner, W.M., 2012. Intersatellite laser ranging instrument for the GRACE follow-on mission, *J. Geod.*, **86**(12), 1083–1095.
- Siemes, C., Rexer, M., Schlicht, A. & Haagmans, R., 2019. GOCE gradiometer data calibration, *J. Geod.*, **93**(9), 1603–1630.
- Simons, F.J. & Dahlen, F.A., 2006. Spherical Slepian functions and the polar gap in geodesy, *Geophys. J. Int.*, **166**(3), 1039–1061.
- Slepian, D., 1983. Some comments on Fourier-analysis, uncertainty and modeling, *SIAM Rev.*, **25**(3), 379–393.
- Sneeuw, N., 2000. A semi-analytical approach to gravity field analysis from satellite observations. *Dissertation*, Technische Universität München, München. <https://mediatum.ub.tum.de/601028>.
- Sneeuw, N., Sharifi, M. & Keller, M., 2008. Gravity recovery from formation flight missions, *VI Hotine-Marussi Symposium on Theoretical and Computational Geodesy*, **132**, 29–34.
- Swenson, S. & Wahr, J., 2006. Post-processing removal of correlated errors in GRACE data, *Geophys. Res. Lett.*, **33**(8), L08402.
- Tapley, B.D., Bettadpur, S., Watkins, M. & Reigber, C., 2004. The gravity recovery and climate experiment mission overview and early results, *Geophys. Res. Lett.*, **31**, L09607.
- Touboul, P., Metris, G., Selig, H., Le Traon, O., Bresson, A., Zahzam, N., Christophe, B. & Rodrigues, M., 2016. Gravitation and geodesy with inertial sensors, from ground to space, *Testing Aerospace Res.*, 12 December 2019. doi:10.12762/2016.AL12-11.
- Velicogna, I., Sutterley, T.C. & van den Broeke, M.R., 2014. Regional acceleration in ice mass loss from Greenland and Antarctica using GRACE time-variable gravity data, *Geophys. Res. Lett.*, **41**(22), 8130–8137.
- Visser, P., 2010. Designing Earth gravity field missions for the future: a case study, in *Gravity, Geoid and Earth Observation, International Association of Geodesy Symposia*, **135**, pp. 131–138, Springer-Verlag.
- Visser, P., Sneeuw, N., Reubelt, T., Losch, M. & van Dam, T., 2010. Spaceborne gravimetric satellite onstellations and ocean tides: aliasing effects, *Geophys. J. Int.*, **181**(2), 789–805.
- Visser, P.M.A.M., Schrama, E.J.O., Sneeuw, N. & Weigelt, M., 2011. Dependency of resolvable gravitational spatial resolution on space-borne observation techniques, in *Geodesy for Planet Earth. International Association of Geodesy Symposia*, Vol **136**, pp. 373–379, eds Kenyon S., Pacino M., Marti U., Springer. doi:10.1007/978-3-642-20338-1_45.
- Wahr, J., Molenaar, M. & Bryan, F., 1998. Time variability of the Earth's gravity field: Hydrological and oceanic effects and their possible detection using GRACE, *J. geophys. Res.*, **201**, B12.
- Weigelt, M., Sneeuw, N., Schrama, E. & Visser, P., 2012. An improved sampling rule for mapping geopotential functions of a planet from a near polar orbit, *J. Geod.*, **87**, 127–142.
- Wiese, D.N., Folkner, W.M. & Nerem, R.S., 2008. Alternative mission architectures for a gravity recovery satellite mission, *J. Geod.*, **83**(6), 569–581.
- Wiese, D., Nerem, R. & Han, S.-C., 2011a. Expected improvements in determining continental hydrology, ice mass variations, ocean bottom pressure signals, and earthquakes using two pairs of dedicated satellites for temporal gravity recovery, *J. geophys. Res.*, **116**, 405.
- Wiese, D.N., Visser, P. & Nerem, R.S., 2011b. Estimating low resolution gravity fields at short time intervals to reduce temporal aliasing errors, *Adv. Space Res.* **48**(6), 1094–1107.
- Wiese, D., Nerem, R. & Lemoine, F., 2012. Design considerations for a dedicated gravity recovery satellite mission consisting of two pairs of satellites, *J. Geod.* **86**:81–98.
- Werth, S., Güntner, A., Schmidt, R. & Kusche, J., 2009. Evaluation of GRACE filter tools from a hydrological perspective, *Geophys. J. Int.*, **179** (3), 1499–1515.
- Yi, W., 2012. The Earth's gravitational field from GOCE, *Dissertation*, CGE Report No. 2, Centre of Geodetic Earth System Research, ISBN (Print) 978-3-934205-34-5. ISSN 2195–7126, 2012. <https://mediatum.ub.tum.de/doc/1135526/1135526.pdf>.

A.2. P-II: Triple-pair constellation configurations for temporal gravity field retrieval

Reference: Purkhauser, A. F. and Pail, R. (2020). Triple-pair constellation configurations for temporal gravity field retrieval. *Remote Sensing*, 12(5):831. DOI: 10.3390/rs12050831

Copyright: This work originally has been published in the special issue Geodesy for Gravity and Height Systems of Remote Sensing: <https://doi.org/10.3390/rs12050831>. This work is licensed under the Creative Commons Attribution 4.0 Public License.

Abstract

The goal of next-generation gravity missions (NGGM) is to improve the monitoring of mass transport in the Earth system by an increased space-time sampling capability as well as higher accuracies of a new generation of instrumentation, but also to continue the monitoring time series obtained by past and current missions such as GRACE and GRACE Follow-On. As the likelihood of three satellite pairs being simultaneously in orbit in the mid-term future increased, we have performed a closed-loop simulation to investigate the impact of a third pair in either polar or inclined orbit as an addition to a Bender-type constellation with NGGM instrumentation. For the additional pair, GRACE-like as well as NGGM instrumentation was tested. The analysis showed that the third pair mainly increases the redundancy of the monitoring system but does not significantly improve de-aliasing capabilities. The best-performing triple-pair scenario comprises a third inclined pair with NGGM sensors. Starting with a Bender-type constellation of a polar and an inclined satellite pair, simulation results indicate an average improvement of 11% in case of adding the third pair in a near-polar orbit, and of 21% for the third pair placed in an inclined orbit. The most important advantage of a multi-pair constellation, however, is the possibility to recover daily gravity fields with higher spatial resolution. In the case of the investigated triple-pair scenarios, a meaningful daily resolution with a maximum spherical harmonic degree of 26 can be achieved, while a higher daily parametrization up to degree 40 results in spatial aliasing and thus would need additional constraints or prior information.

Appendix A. Publications


Declaration of own contribution


Table A.2.: Contribution to P-II

Involved in	Estimated contribution
Ideas and conceptual design	100%
Computation and results	100%
Analysis and interpretation	90%
Manuscript, figures and tables	90%
Total	95%

Confirmation by Co-Authors

I hereby confirm the correctness of the declaration of the contribution of Anna F. Purkhauser for the publication P-II in Table A.2:


.....
Roland Pail
(IAPG, LRG, TUM)


.....
Date

Article

Triple-Pair Constellation Configurations for Temporal Gravity Field Retrieval

Anna F. Purkhauser *  and Roland Pail 

Chair of Astronomical and Physical Geodesy, Technical University of Munich, Arcisstraße 21, 80333 Munich, Germany; roland.pail@tum.de

* Correspondence: anna.purkhauser@tum.de; Tel.: +49-89-289-231-81

Received: 11 February 2020; Accepted: 3 March 2020; Published: 4 March 2020



Abstract: The goal of next-generation gravity missions (NGGM) is to improve the monitoring of mass transport in the Earth system by an increased space-time sampling capability as well as higher accuracies of a new generation of instrumentation, but also to continue the monitoring time series obtained by past and current missions such as GRACE and GRACE Follow-On. As the likelihood of three satellite pairs being simultaneously in orbit in the mid-term future increased, we have performed a closed-loop simulation to investigate the impact of a third pair in either polar or inclined orbit as an addition to a Bender-type constellation with NGGM instrumentation. For the additional pair, GRACE-like as well as NGGM instrumentation was tested. The analysis showed that the third pair mainly increases the redundancy of the monitoring system but does not significantly improve de-aliasing capabilities. The best-performing triple-pair scenario comprises a third inclined pair with NGGM sensors. Starting with a Bender-type constellation of a polar and an inclined satellite pair, simulation results indicate an average improvement of 11% in case of adding the third pair in a near-polar orbit, and of 21% for the third pair placed in an inclined orbit. The most important advantage of a multi-pair constellation, however, is the possibility to recover daily gravity fields with higher spatial resolution. In the case of the investigated triple-pair scenarios, a meaningful daily resolution with a maximum spherical harmonic degree of 26 can be achieved, while a higher daily parametrization up to degree 40 results in spatial aliasing and thus would need additional constraints or prior information.

Keywords: future gravity missions; time variable gravity; near-real time; numerical simulation; spherical harmonics

1. Introduction

Dedicated gravimetric satellite missions like the Challenging Minisatellite Payload (CHAMP; [1]) and the Gravity Recovery and Climate Experiment (GRACE; [2]) and GRACE Follow-On (FO; [3]) missions have been providing, for nearly two decades, essential observations of the changes of the Earth's gravity field on a global scale. This monitoring is fundamental for applications in Earth sciences, such as hydrology [4], atmosphere [5], plate tectonics [6], earthquakes [7], and glacial isostatic adjustment (GIA; [8]) as well as cryosphere [9,10].

The GRACE-FO mission was launched in May of 2018 to continue monitoring the temporal gravity field of the Earth, after the GRACE mission was decommissioned due to a battery failure at the end of 2017. However, the observed data from GRACE/GRACE-FO have limitations regarding spatial and temporal resolution, homogeneity, as well as sensitivity. The user requirements collected by [11] underline the need for long-term, sustained gravity observations with increased spatial and temporal resolution to observe small-scale, short-time mass transport phenomena.

To find optimal mission concepts with improved spatial and temporal resolutions, various studies have been performed: The authors of [12–16] investigated the performance of single-pair missions. The authors of [17–20] analyzed flying a second inclined pair in addition to an in-line pair in polar orbit (furthermore called Bender-type constellation), thus improving the space-time sampling and having available multi-directional observations as compared to a single polar-pair due to the two different orbit planes.

Mission proposals in response to European Space Agency (ESA) Earth Explorer calls 8, 9, and 10 like e.motion with a single pair in a pendulum constellation [21], e.motion2 [22] based on a Bender-type concept, or the innovative high–low tracking formation mission MOBILE [23] also achieve improved error characteristics. While the e.motion and e.motion2 mission proposals are based on the observation system of low-low satellite-to-satellite tracking (LL-SST) as implemented in GRACE and GRACE-FO, the MOBILE concept proposes a different observation strategy of high-precision high–low tracking as well as new instrumentation. All three proposals emphasize the need for continuous and sustained observations of the Earth’s mass transport on a global scale from space.

A study by [24] has concluded that the gain in accuracy of the Bender double-pair constellation is higher compared with the single-pair pendulum formation and is therefore preferred. The ESA-funded SC4MGV study (Assessment of Satellite Constellations for Monitoring the Variations in Earth Gravity Field, [15]) found that there is a certain degree of freedom in the orbit design of Bender-type mission concepts. In the follow-on ESA-study ADDCON (Additional Constellation and Scientific Analysis of the Next Generation Gravity Mission Concept; [25]) an analysis regarding orbit height and instruments showed that a Bender pair with improved instrumentation gave the best results for a seven-day reference solution [26].

In the context of observing short period signals within short latencies, daily solutions in near-real time are needed. However, the potential to use the retrieved gravity fields for applications with high temporal variations, like hydrology and earthquake monitoring, is limited by the requirement to recover gravity field variations as detailed as possible, i.e., with highest spatial resolution. An increase in temporal resolution means less observations per analysis period and therefore a reduced redundancy in the parameter estimation process. For possible NGGM constellations with at least two pairs, the co-estimation of long-wavelength gravity field solutions for short time periods such as one day, further called Wiese approach, was successfully tested in closed-loop simulations [20,27].

As various space agencies are considering flying a GRACE-like or NGGM mission, the potential of triple pairs compared to a Bender-type double pair is of interest. The most significant advantage of an additional pair to a Bender-type constellation, apart from an improved performance, is the possibility to increase and resolve daily Wiese solutions with higher spatial resolution. Additionally, for time-critical monitoring applications (e.g., early-warning and forecasting systems) information in near-real time (NRT) is of essence, meaning an NRT processing scheme [28] is necessary. This paper evaluated three scenarios with two and three pairs and analyses their potential for NRT processing and the highest possible daily resolution for applications such as the monitoring of hydrological extremes such as droughts and floods.

The paper is organized as follows: Section 2 reviews the satellite mission design as well as the space-time sampling of various applications. The methodology of the full-scale closed-loop simulation, based on the software available at the Institute of Astronomical and Physical Geodesy (IAPG) of the Technical University Munich (TUM), is described in Section 3. Section 4 contains the obtained gravity results in the spatial as well as the frequency domain, and finally, the conclusions regarding the possible improvements on gravity field as well as on application level are presented in Section 5.

2. Constellation Design

2.1. Orbit Constellation

Two orbits are the basis to form double- and triple-pair constellations. In Table 1, the general information regarding the used orbits is listed. The letter “p” represents the polar orbit, while the letter “i” stands for the inclined orbit. These letters are also used for the scenario description within the paper later on. Both orbits have a seven-day repeat cycle and a drift rate of $1.3^\circ/\text{cycle}$. The resulting homogeneous ground track coverage allows for stable seven-day gravity field solutions. Additionally, the dense ground track spacing over longer periods due to the drifting orbit design allows for a high-degree gravity field recovery for more extended periods according to the Nyquist–Colombo sampling rule for space-borne gravimetry [29,30].

Table 1. Basic information on the simulated orbits forming the constellations.

Orbit	Altitude	Inclination	Repeat Cycle	Drift Rate
Polar (p)	~340 km	89°	7 days	$1.3^\circ / \text{cycle}$
Inclined (i)	~ 355 km	70°		

Figure 1 shows a 3D and a schematic view of the analyzed in-line satellite pair constellations based on the Bender double-pair. The Bender double-pair constellation is comprised of a near-polar pair and an inclined pair with an inclination of 70° . The polar pair is placed in an orbit plane with an ascending node of 0° , and the inclined pair in an orbit plane with an ascending node of 90° . The polar gap of the inclined pair (orbit ground tracks in red) is clearly visible at the North Pole. This basic Bender constellation, also described in Table 2, is assumed to have an improved set of sensors on board (see Section 3.2).

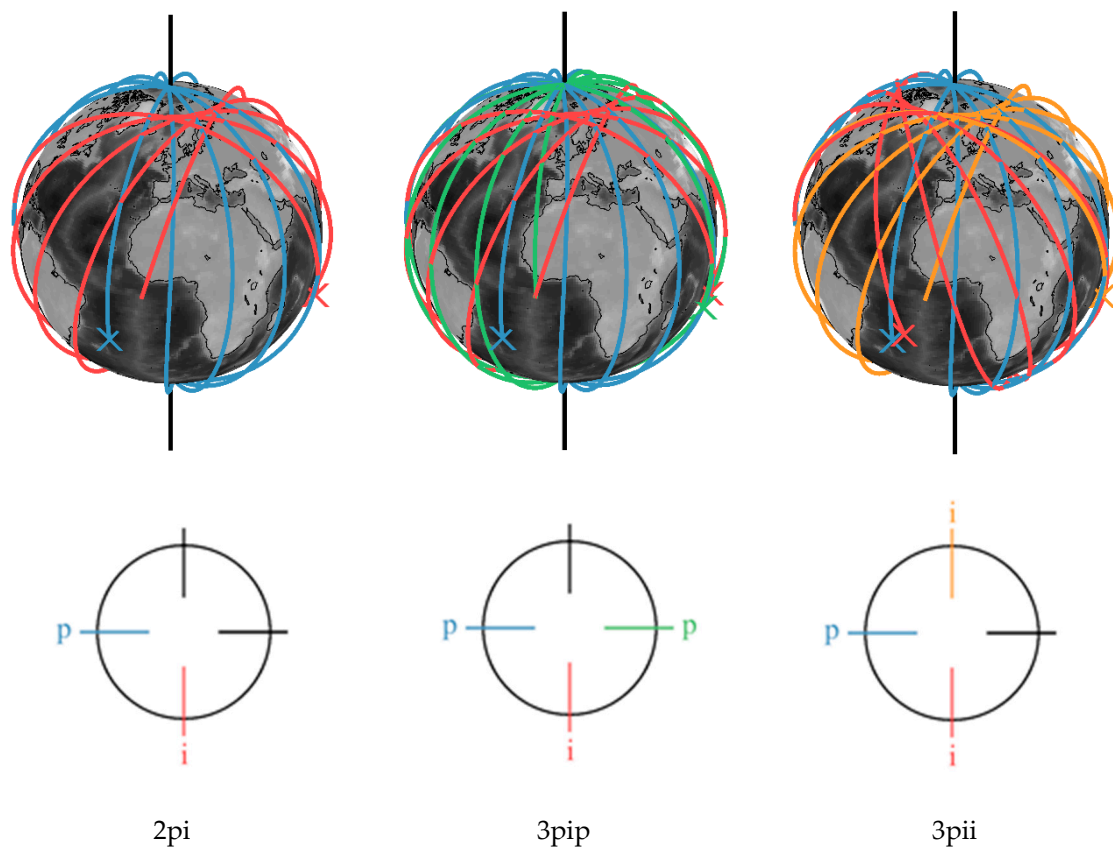


Figure 1. Constellations of in-line satellite pairs. (2pi) Bender double-pair, (3pip) triple-pair with additional polar pair, (3pii) triple-pair with additional inclined pair.

Table 2. Scenario description with the angle of the ascending node (Ω) included. Acronyms for polar (p) and inclined (i) are used.

Scenario	Description	Ω_1	Ω_2	Ω_3
2pi	Double-pair, Bender (NGGM noise)	0°	90°	
3pip	Triple-pair, Bender + polar	0°	90°	180°
a	3rd pair GRACE-like noise			
b	3rd pair NGGM noise			
3pii	Triple-pair, Bender + inclined	0°	90°	270°
a	3rd pair GRACE-like noise			
b	3rd pair NGGM noise			

The third pair is then placed in an orbit plane that is perpendicular to the orbit plane of the already existing polar or inclined pair. In case of triple-pair scenario 3pip, this means a second polar pair with an ascending node of 180°, and in case of triple-pair scenario 3pii, it means a second inclined pair with an ascending node of 270° (cf. Table 2) and the same inclination as the first inclined pair. The added satellite pairs are equipped with sensors featuring either a GRACE-like (a) or NGGM (b) noise (see Section 3.2). Through this distribution, an optimal spatial and temporal resolution is enabled, which is especially relevant for the aspired daily solution with the highest possible spatial resolution.

2.2. Space-Time Sampling

Science requirements for applications in solid Earth, hydrology, ocean, ice, atmosphere, and corresponding science fields were collected by [31] and visualized in 2D bubble plots; see Figure 2. The extent of the bubbles visualizes an estimation of the necessary temporal and spatial

resolution to enable their observation and, subsequently, the monitoring by gravity satellite mission constellation. The bubbles together with the expected temporal and spatial resolution of the satellite mission gives a good first indication if a mission is able to observe specific features. In Figure 2, the possible performance of double (blue) and multi-pair (light green) constellations is visualized. The lines are a combination of the published original diagram in [31] and the ground tracks as well as results of the presented scenarios. However, it has to be stated that a general statement like the shown bubble plot is only a rough indication. Additionally, the observability also depends on the signal amplitude, which is not considered in Figure 2.

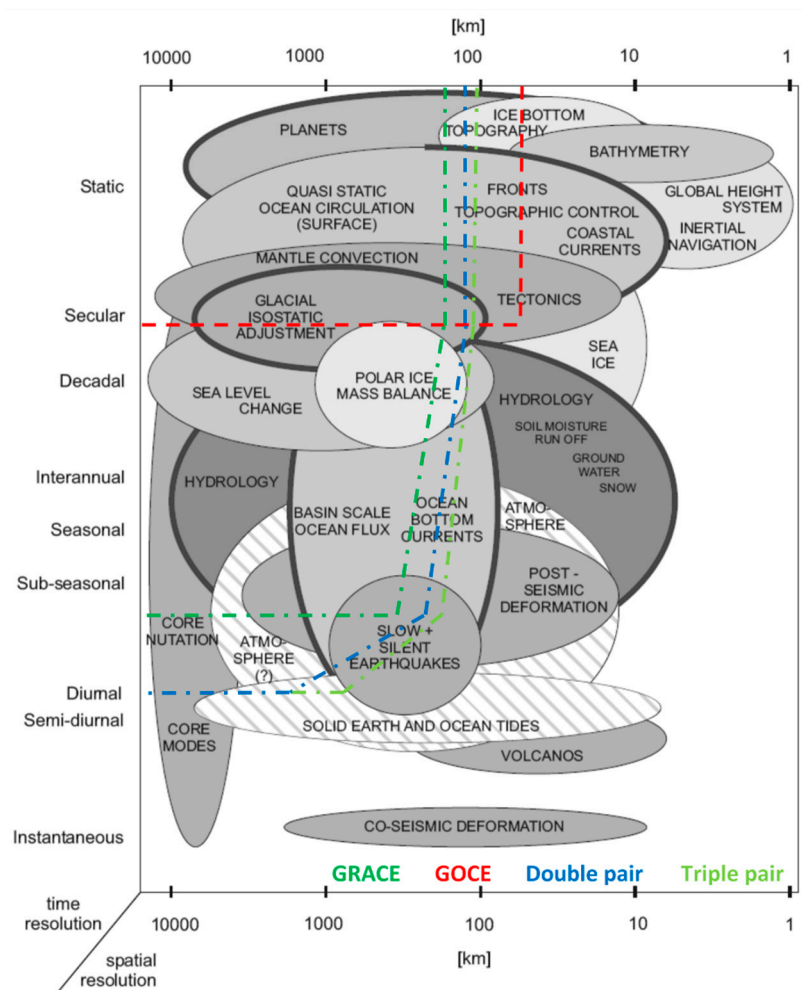


Figure 2. Temporal and spatial scales of time-varying gravity field as well as the spatial and temporal limits of Gravity Recovery and Climate Experiment (GRACE), Gravity field and steady-state ocean circulation explorer (GOCE), and possible next-generation gravity missions (NGGM) constellations. Based on [31].

After the successful exploitation of CHAMP, GRACE, and GOCE (Gravity field and steady-state ocean circulation explorer) and the additional knowledge based on their observations, various studies on necessary accuracies of future gravity fields were published. The authors of [11] collected updated science and user needs by a panel of scientists representing the main fields of application of possible NGGM concepts to form consolidated requirements for a compromise of all applications with the possibility to optimize for a specific field of application.

One of the major problems of a GRACE-like single-pair mission is temporal aliasing of high-frequency mass transport signals that are mainly due to processes in the atmosphere and the oceans, which cannot be captured due to the limited temporal resolution of the mission. This requires a-priori

atmosphere and ocean (AO) de-aliasing based on external models. These temporal aliasing effects are significantly reduced by multi-pairs, e.g., [20] investigated the capabilities of Bender double-pair constellations to observe the full AOHIS (atmosphere, ocean, hydrology, ice, and solid Earth) signal instead of a-priori modelling of AO and the estimation of the hydrology, ice, and solid Earth (HIS) components only. Lastly, the anisotropic error behavior that is typical for GRACE-like solutions is a well-known phenomenon and typically treated with different filter approaches [32–34]. Multi-pair constellations inherently have additional observations and especially the addition of observations in an inclined orbit, as in the Bender-type constellation, add signal content and improve the anisotropic error behavior, and therefore decrease the GRACE striping significantly.

3. Closed-Loop Simulation

3.1. Numerical Simulator

The full-scale gravity field estimation software [35,36] available at the IAPG was used to execute the closed-loop simulations. The numerical orbit integration follows a multistep method for the numerical integration according to [37] with a modified divided difference form of the Adams Predict-Evaluate-Correct-Evaluate (PECE) formulas and local extrapolation [38].

In the generation of the dynamic models, the static gravity field GOCO05s model [39] up to maximum expansion degree and order (d/o) 120 is included. To simulate the non-tidal time-varying gravity field due to mass change, the updated Earth System Model (ESM) of ESA [40], furthermore called reference AOHIS, is used as reference world. The differences of the ocean tide (OT) model GOT4.7 (Goddard Ocean Tide) model [41] and the EOT11a (Empirical Ocean Tide) model [42] are used to replicate the ocean tide model errors.

The functional model follows the typical formulation used for LL-SST missions like GRACE (cf. Table 3). The “true” dynamic orbits as well as the “true” GNSS HL-SST and LL-SST observations are additionally superimposed by the noise models described in Section 3.2 depending on the scenario. The impact of orbit errors on the gravity field processing is taken into account by propagating 1 cm white noise of the integrated orbit positions of each satellite.

Table 3. Force and noise models of the “true” and “reference” world used in the full-scale simulations.

Model	“True” World	Reference World
Static gravity field (GF) model	GOCO05s	GOCO05s
Time varying GF model	AOHIS	-
Ocean tide model	EOT11a	GOT4.7
Noise model	SST, acc. noise	-

The assembling of the NEQ systems is done with spherical harmonics (SH) base functions of the Earth’s gravitational potential V and is expressed by the series expansion [43]:

$$V(r, \theta, \lambda) = \frac{GM}{a} \sum_{n=0}^{\infty} \left(\frac{a}{r}\right)^{n+1} \sum_{m=0}^n \bar{P}_{nm}(\cos\theta) (\bar{C}_{nm} \cos m\lambda + \bar{S}_{nm} \sin m\lambda), \quad (1)$$

where GM represents the product of the gravitational constant and the Earth’s mass, a the semi-major axis of the Earth, \bar{P}_{nm} is the fully normalized Legendre polynomial of degree n and order m , \bar{C}_{nm} and \bar{S}_{nm} are the fully normalized SH coefficients, and the location is given by the radius r (geocentric distance of the satellite), geocentric co-latitude θ , and longitude λ .

The stochastic model is approximated for each satellite pair individually by using a combination of digital Butterworth ARMA filters [44,45] that best represent the amplitude spectral density (ASD) of the pre-fit residuals of a noise-only computation. Assuming uncorrelated high–low and low–low SST observations, weighting matrices are set up for all observation components separately.

The gravity field parameters are estimated by solving full normal equations of a least-squares system based on a standard Gauss–Markov model using weighted least squares with stochastic models following the simulated instrument noise levels. From the resulting gravity field coefficients, the average of the true mass transport model from the same period is removed to enable the analyses of quality and performance of the gravity retrieval.

3.2. Noise

While the basic Bender-type constellation is assumed to have a set of improved sensors, the additional satellite pairs are simulated with a GRACE-like or a NGGM noise setting. The GRACE-like noise represents a noise level of accelerometer (ACC) and satellite-to-satellite tracking (SST) resembling the error characteristics of the instruments implemented on the GRACE mission, and an NGGM noise scenario with improved ACC and laser ranging interferometer (LRI) noise characteristics. The HL-SST observable always has the same white noise of 1 cm propagated along the orbit. The satellites are assumed to fly in drag-compensation mode in approximately 350 km orbit altitude so that the most significant parts of the non-gravitational forces are compensated by a propulsion system consisting of ion thrusters.

3.2.1. GRACE-Like Noise

An analytical noise model characterizes the main measurement unit, the K-Band Ranging system (KBR) to observe the inter-satellite distances. The ASD describes the noise model analytically and is expressed in terms of range rates (rr) [17],

$$d_{rr} = 2 \cdot 10^{-6} \cdot 2\pi f \sqrt{\left(\frac{10^{-2}\text{Hz}}{f}\right)^2 + 1} \frac{m}{s \sqrt{\text{Hz}}}, \quad (2)$$

where f is defined as frequency. The on-board accelerometer senses the linear non-gravitational accelerations and the angular accelerations acting on the satellites with air drag being the main contributor. The ACC is modeled after [46].

3.2.2. NGGM Noise

In the case of NGGM noise, the principal measurement is observed by the laser interferometry instrument, meaning an improvement of factor 100

$$d_{rr} = 2 \cdot 10^{-8} \cdot 2\pi f \sqrt{\left(\frac{10^{-2}\text{Hz}}{f}\right)^2 + 1} \frac{m}{s \sqrt{\text{Hz}}}. \quad (3)$$

Additionally, an improved accelerometer is implemented

$$d_{acc. x} = d_{acc. z} = 10^{-11} \sqrt{\frac{\left(\frac{10^{-3}\text{Hz}}{f}\right)^4}{\left(\frac{10^{-5}\text{Hz}}{f}\right)^4 + 1} + 1 + \left(\frac{f}{10^{-1}\text{Hz}}\right)^4} \frac{m}{s^2 \sqrt{\text{Hz}}}, d_{acc. y} = 10 \cdot d_{acc. z} \quad (4)$$

with x being the along-track, y is across-track, and z is the quasi-radial component. The error assumption was provided by the consultancy support of Thales Alenia Space Italia (TAS-I).

4. Results

We calculated eight seven-day solutions for January and February 2002 with the numerical closed-loop simulation software described in Chapter 3 for the double (estimated until d/o 70) and triple (estimated until d/o 90) pairs defined in Table 2. All scenarios were processed with the Wiese

approach, which co-parametrizes low-resolution daily gravity field solutions and longer-term gravity field solution. For the evaluation of long-term applications, the time series was extended to one year for selected scenarios and processed with the NRT approach. In order to summarize the results and to simplify the corresponding figures, the shown degree root mean square (RMS) errors always represent the average degree RMS of all estimated seven-day solutions.

We compared the results in the spatial as well as the frequency domain. The gravity field was transformed to equivalent water heights (EWH). In terms of degree RMS signal/errors, this means

$$\sigma_n(EWH) = \frac{a\rho_e}{3\rho_w} \frac{2n+1}{1+k_n} \sqrt{\sum_{m=0}^n (c_{nm}^2 + s_{nm}^2)}, \quad (5)$$

where ρ_w and ρ_e represent the average density of water and Earth, a the semi-major axis of the Earth, k_n is the Love numbers, and c_{nm} and s_{nm} represent the SH coefficients or coefficient differences to the true solution [47,48].

4.1. Double vs. Triple Pairs

In this section, we compare the achievable performance of double pair and triple-pair scenarios. Figure 3 shows degree RMS curves for the double pair (estimated up to d/o 70) and the triple-pair (estimated up to d/o 90) scenarios as defined in Table 2 in terms of an average of the seven-day solutions of the two-monthly observation period. Daily spherical harmonic coefficients (Wiese parameters) up to d/o 15 were co-estimated, as recommended by [28]. The double pair scenarios 2pi in blue is shown as a reference. The triple-pair scenarios 3pip with the third pair being in a polar orbit (red and green) exhibited small improvements, especially in the lower degrees. Additionally, the crossover between signal and errors degree RMS curves was approximately 5 degrees higher than for the reference double pair scenario. The best performance is visible for scenario 3pii,b with the third pair in an inclined orbit and also laser instrumentation for the SST (lilac curve). With this constellation, the performance in terms of spatial resolution can be improved by 10 degrees compared to the double pair.

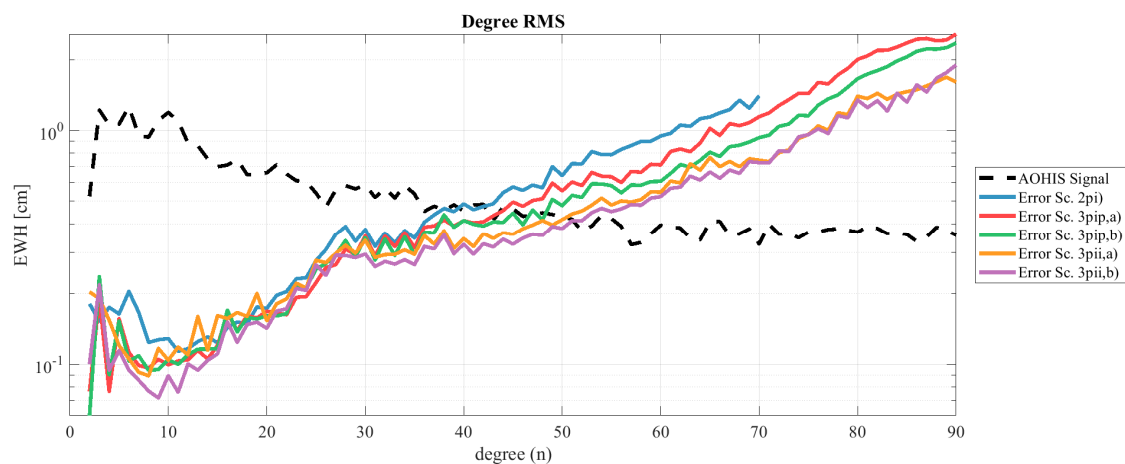


Figure 3. Degree root mean square (RMS) of double pair (estimated until d/o 70) vs. triple pair (estimated until d/o 90) scenarios of the whole solution. Daily Wiese solution estimated until d/o 15.

Figure 4a shows coefficient differences of the second solution (08/01/2002 to 14/01/2002) with respect to the reference AOHIS signal for the true reference of scenario 2pi (computed up to d/o 70), 3pip, and 3pii (computed up to d/o 90) for noise scenario b (NGGM noise). Obviously, the main gain in performance of the triple-pairs scenario 3pii including two inclined pairs occurred in the sectorial and near-sectorial coefficients, expressing the improved de-stripping capabilities of this constellation. Figure 4b shows the spatial representation of these differences of the recovered and the true solution in

terms of EWH difference grids up to d/o 50 due to the crossover of the signal and error curve in Figure 3. The improved performance of scenario 3pii can be seen especially in the spatial representation in Figure 4b. Compared to the other scenarios, the striping effect was reduced, but still visible. In Table 4, the cumulative errors in centimeters EWH of selected upper maximum d/o 10 to 50 are provided. While a third polar pair showed only small improvements of about 5% to 10% compared to the Bender double pair scenario 2pi, a second inclined pair resulted in significantly improvements of about 20% to 40%. The expected improvement of the square-root-n rule led to an expected improvement of 22%, reached by the second inclined pair.

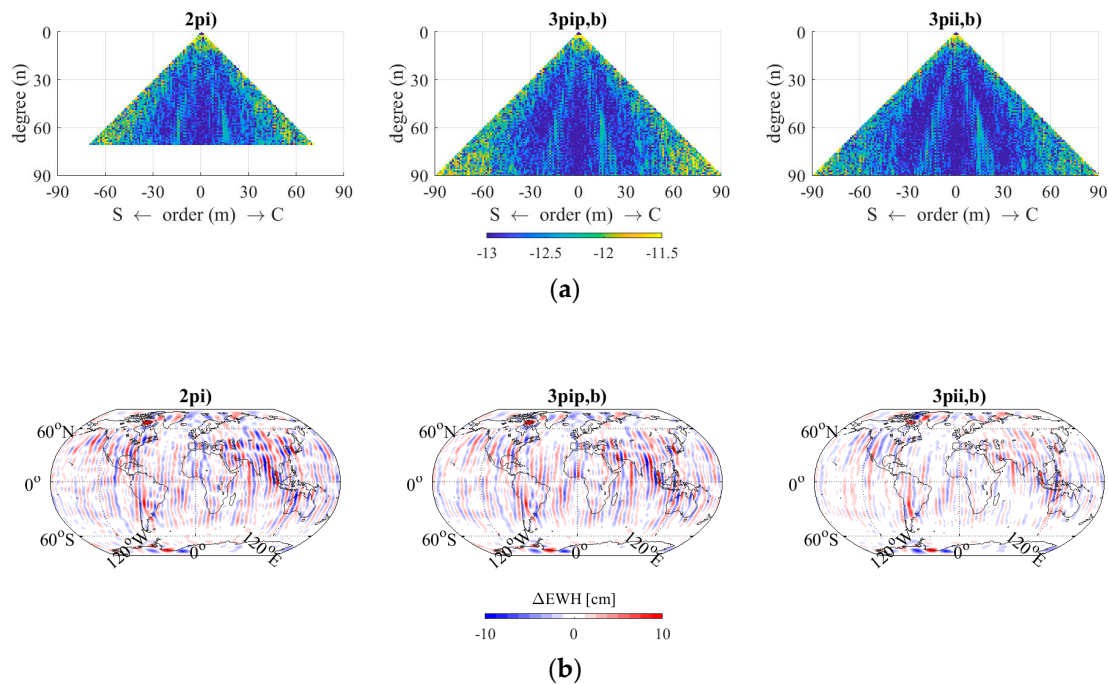


Figure 4. Double- vs. triple-pair scenarios (solution from 08/01/2002 to 14/01/2002). (a) Coefficient differences of scenario 2pi (computed up to d/o 70), 3pip, and 3pii (computed up to d/o 90) with all sensors set to the NNGM noise. (b) Spatial representation in terms of equivalent water heights (EWH) differences to the true solution up to d/o 50.

Table 4. Cumulative error in cm EWH of scenarios at different maximum d/o from 10 to d/o 50 (latest crossing point of signal and error curve).

Scenario // Cumulative Error at	d/o 10	20	30	40	50 in [cm] EWH
2pi	0.60	0.75	1.15	1.73	2.58
3pip,a	0.55	0.71	1.17	1.78	2.48
3pip,b	0.55	0.71	1.18	1.79	2.48
3pii,a	0.47	0.65	1.06	1.50	1.96
3pii,b	0.38	0.53	0.91	1.32	1.74

Spatial representations of the improvements of the triple pairs compared to the double pair solution are shown in Figure 5, which depicts the difference of the estimated to the reference solution of the best solution. For this, we analyzed an EWH difference grid up to d/o 50 for a seven-day solution and computed the difference of the estimated and reference field for every point of the grid. Blue means the double pair scenario 2pi had the smaller difference value, thus was closer to the reference and visualized in the figure, while red means the respective triple-pair scenario 3pip,b or 3pii,b had the smaller difference value and was closer to the truth and visualized. When comparing scenario 3pip,b with the double pair (Figure 5a), a clear improvement of the triple-pair scenario was not apparent.

While in Canada, the triple pair had a lower difference value, the double pair performed better over Antarctica. Overall, the triple pair had lower difference values in the Northern hemisphere, while in the Southern part, an ambiguous picture was visible.

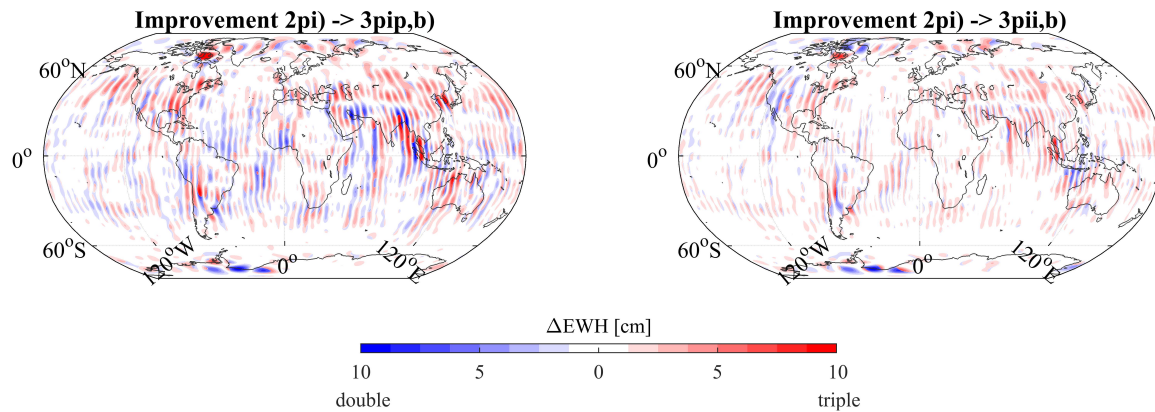


Figure 5. Difference of estimated vs. reference solution (up to d/o 50) of triple-pair scenarios 3pip,b and 3pii,b compared to double pair scenario 2pi in EWH [cm] of the seven-day solution from 08/01/2002 until 14/01/2002. Red means the triple-pair scenarios are closer to the truth, blue means the double pair scenario is closer to the truth. (a) Comparison of double pair scenario 2pi to triple-pair scenario 3pip,b. (b) Comparison of double pair scenario 2pi to triple-pair scenario 3pii,b.

Scenario 3pii,b compared to the double pair (Figure 5b) showed a significant improvement for the triple-pair scenario. The double pair was only better than the triple-pair scenario in a few limited areas. Also, the overall magnitude of the difference decreased. The anisotropic error behavior of a classic GRACE-like near-polar pair was further reduced by the second inclined pair. Such a constellation came, however, with the drawback of only one near-polar pair, which was the basis of every temporal gravity field mission so far. The near-polar pair is important as the ground track has the best global coverage. If the polar pair failed, the polar areas would not be observed at all by the remaining constellation. Within the processing, a regularization would have to be applied if global base functions such as SH are used for parameterization.

Although both triple-pair scenarios had the same amount of observations, the third inclined pair's along-track observations added more information, further reducing the variability between -60° and 60° latitude. The variability decreased in scenario 3pii,b, and not only in the area covered by the inclined pairs, but also in the polar region covered by only one near-polar pair. The result shows that the introduction of the third pair in an inclined orbit in scenario 3pii,b adds relevant signal and stabilizes the solution overall.

In Figure 6, the standard deviation of the difference between the simulated and the reference solutions over the whole computation period (one year), furthermore called RMS variability, of both triple-pair scenarios is visualized. For each grid point, the RMS variability value over the time period is shown. The higher the RMS variability, the darker red the grid point is colored. A detail of the Pacific Ocean is selected as this is an area of little to no temporal gravity signal. The result again shows a decreased striping pattern in scenario 3pii,b in Figure 6b compared to scenario 3pip,b in Figure 6a. The reduced striping pattern is therefore a result of the improved instrument noise and the better observation geometry. The RMS variability is reduced significantly from 2.24 cm EWH to 1.7 cm EWH globally for scenario 3pii,b, supporting the previous statement.

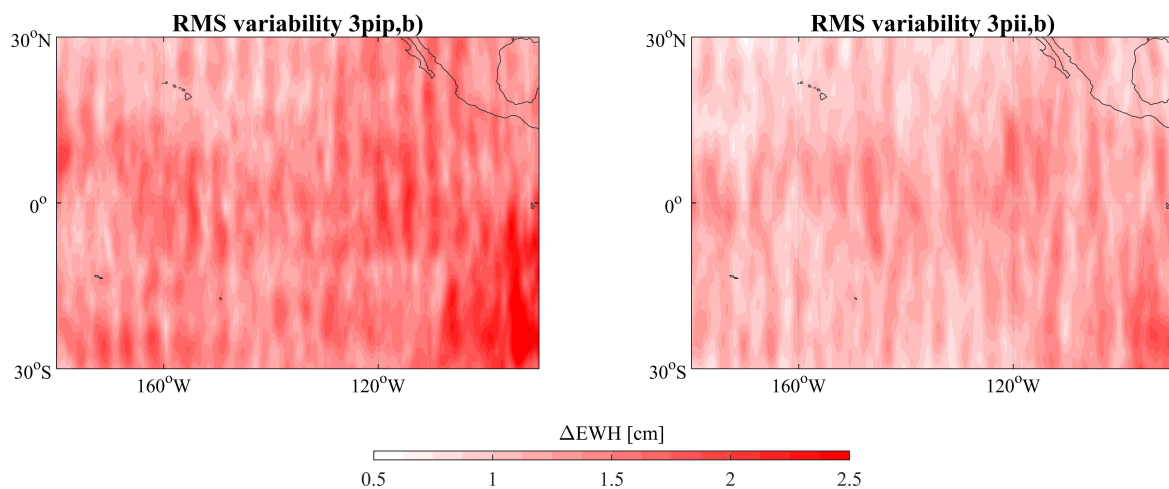


Figure 6. RMS variability over one year of triple-pair scenarios. Standard deviation computed from reference minus estimated solution until d/o 50. (a) RMS variability detail of triple-pair scenario 3pip,b. (b) RMS variability detail of triple-pair scenario 3pii,b.

To visualize the impact of the daily parametrization on the double pair scenario, Figure 7a shows degree RMS curves of double pair scenario 2pi (estimated up to d/o 70) and triple-pair scenario 3pii,b (estimated up to d/o 90) in terms of an average of the seven-day solutions of the two-monthly observation period with either a co-estimated daily gravity field up to d/o 15 or 20. The daily gravity field solution based on the triple-pair scenario 3pii,b shows a significant improvement in the first 10 degrees (Figure 7b). If a higher degree is chosen, the limits of the double pair scenario become visible in the seven-day solution. For any higher daily solution, a triple-pair scenario is necessary to avoid spatial under-sampling.

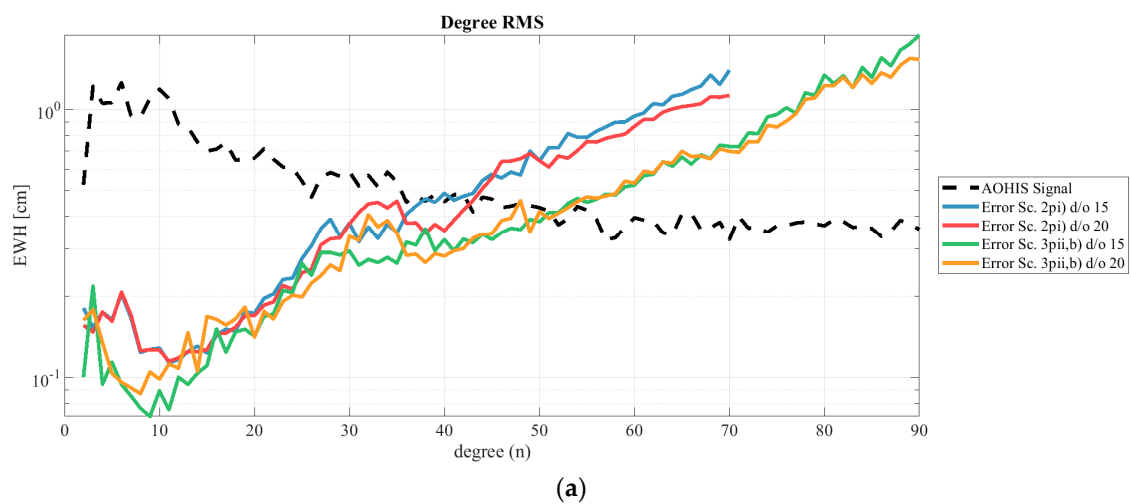


Figure 7. Cont.

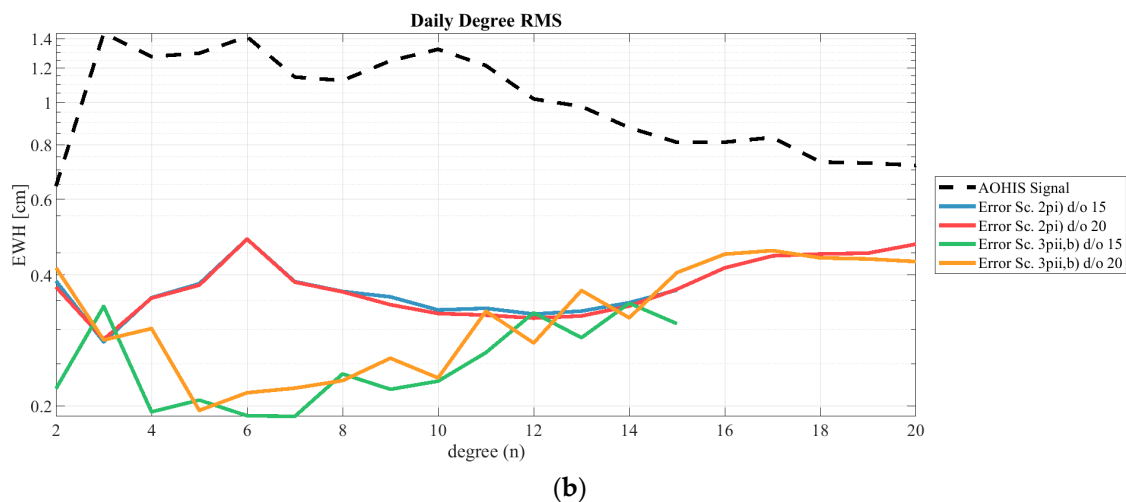


Figure 7. Degree RMS of scenario 2pi and 3pii,b. (a) Seven-day solution degree RMS with daily parametrization up to d/o 15 and 20. (b) Degree RMS of daily solutions with parametrization up to d/o 15 and 20.

4.2. Higher-Degree Daily Resolution

As indicated, the most significant advantage of an additional pair is the expected improved performance of the daily solution. We chose the best-performing triple-pair scenario 3pii,b as the test scenario. The maximum daily degree and order varied between d/o 10 and d/o 40 with a step size of 5. Figure 8a shows the degree RMS of the overall solution, and Figure 8b shows the daily solution. In the overall solution, the nominal processing (without co-estimating daily gravity field parameters) is also included in red. When assessing the results of the daily solutions, the lowest daily d/o as well as the highest d/o are not recommended. When computing daily solution up to d/o 10, the result in Figure 8b shows clearly that the solution was under-parametrized and performed worst in the lower degrees. The daily solution up to d/o 20 performed best in the overall solution and should be preferred if the quality of the long-term solution has the highest priority. With a crossing point of the signal and error curve at approximately d/o 26, we recommend a daily parametrization up to d/o 25 or 30. The cumulative errors in Table 5 (without omission error) and Table 6 (including omission errors) confirm that the best solutions with the highest d/o are solutions 25 to 35, as they have the lowest error values at the investigated degrees (values marked with “1”). In Table 5, we used the AOHIS signal up to the respective SH degree of the solution as a reference, while the full AOHIS signal up to d/o 40 was used for the results shown in Table 6. Therefore, the first case provides only the commissioning error of the solutions, while the latter case includes also unresolved signals (omission error). The cumulative error of the daily solution estimated up to d/o 40 has the worst performance starting at d/o 25 (values marked with “2”). Considering the processing time, which increases with higher daily parametrization, and the performance of the daily solutions, the maximum daily d/o resolution should be chosen using the crossing point of the signal and error curves as a guideline.

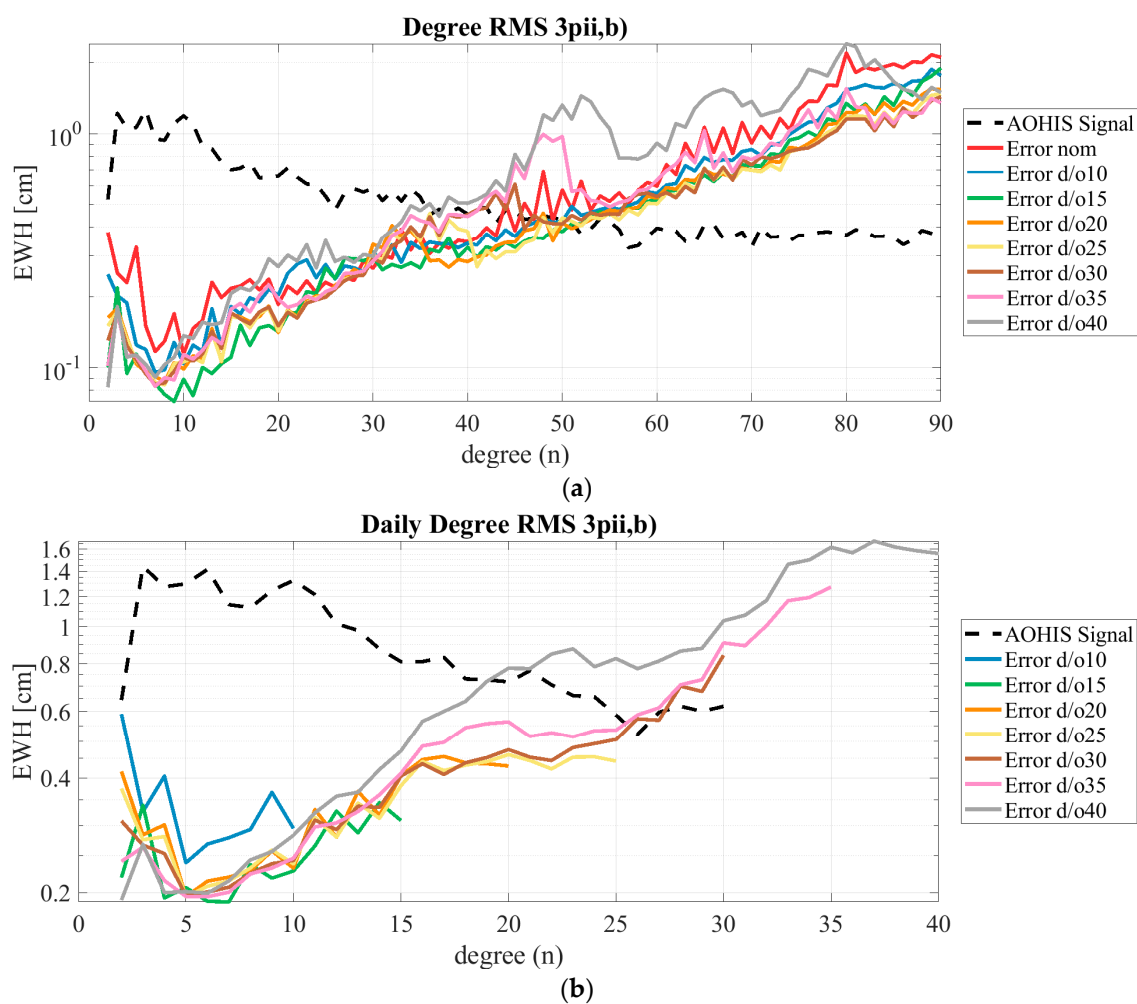


Figure 8. Degree RMS of scenario 3pii,b with different daily d/o. The nominal processing of the scenario is included as comparison. (a) Degree RMS average of the overall solutions, (b) Daily degree RMS average of the daily solutions. Compare to Table 5.

Table 5. Daily cumulative error of different daily solutions from scenario 3pii,b excluding omission error in cm EWH. Compare to Table 6. The best values are marked with “1”. The values marked with “2” implicate an over-parametrization, impacting the result negatively.

Daily d/o \\ Cumulative Error at	d/o 10	15	20	25	30	35	40 in [cm] EWH
10	1.33	-	-	-	-	-	-
15	0.97	0.97	-	-	-	-	-
20	0.91	0.91	1.55	-	-	-	-
25	0.84	0.84	1.44 ¹	1.82 ¹	-	-	-
30	0.74	0.74	1.40 ¹	1.83 ¹	2.27 ¹	-	-
35	0.71	0.71	1.37 ¹	1.84 ¹	2.23 ¹	3.03	-
40	0.70	0.70	1.49	2.53 ²	3.00 ²	3.88 ²	5.97

Table 6. Daily Cumulative error of different daily solutions from scenario 3pii,b including omission error (reference solution up to d/o 40) in cm EWH. Compare to Table 5. The best values are marked with “1”. The values marked with “2” implicate an over-parametrization, impacting the result negatively.

Daily d/o \\ Cumulative Error at	d/o 10	15	20	25	30	35	40 in [cm] EWH
10	4.44	-	-	-	-	-	-
15	4.33	3.66	-	-	-	-	-
20	4.32	3.59	3.25	-	-	-	-
25	4.30	3.56	3.21 ¹	2.91 ¹	-	-	-
30	4.29	3.54	3.19 ¹	2.93 ¹	2.93 ¹	-	-
35	4.28	3.53	3.19 ¹	2.94 ¹	2.94 ¹	2.94	-
40	4.28	3.56	3.29	3.45 ²	3.45 ²	3.45 ²	3.45

To visualize the spatial difference of daily solutions from scenario 3pii,b with different maximum d/o, Figure 9 shows the daily temporal gravity field, as well the difference of daily solutions with different maximum d/o to the reference, for the whole Earth as well as exemplarily for a detail in the Northern Hemisphere over Europe and Africa. The reference gravity field is always used up to d/o 40 in order to include also the non-resolved signals. The increasing signal as well as the emerging error characteristics can be easily tracked among the different resolutions. The figure visualizes the importance of higher spatial resolution, as the details of the temporal gravity field are revealed. The last two rows with d/o 35 and 40 show an increased error, corresponding to the daily degree RMS in Figure 8b. The maximum daily d/o resolution of 40 demonstrates quite clearly the problems that emerge when the daily solution is over-parametrized. Additional constraints would be necessary to handle the arising spatial aliasing in the solution. Additionally, the solution pushes the numerical stability of the overall system to its limit and would potentially need additional constraints or a regularization scheme.

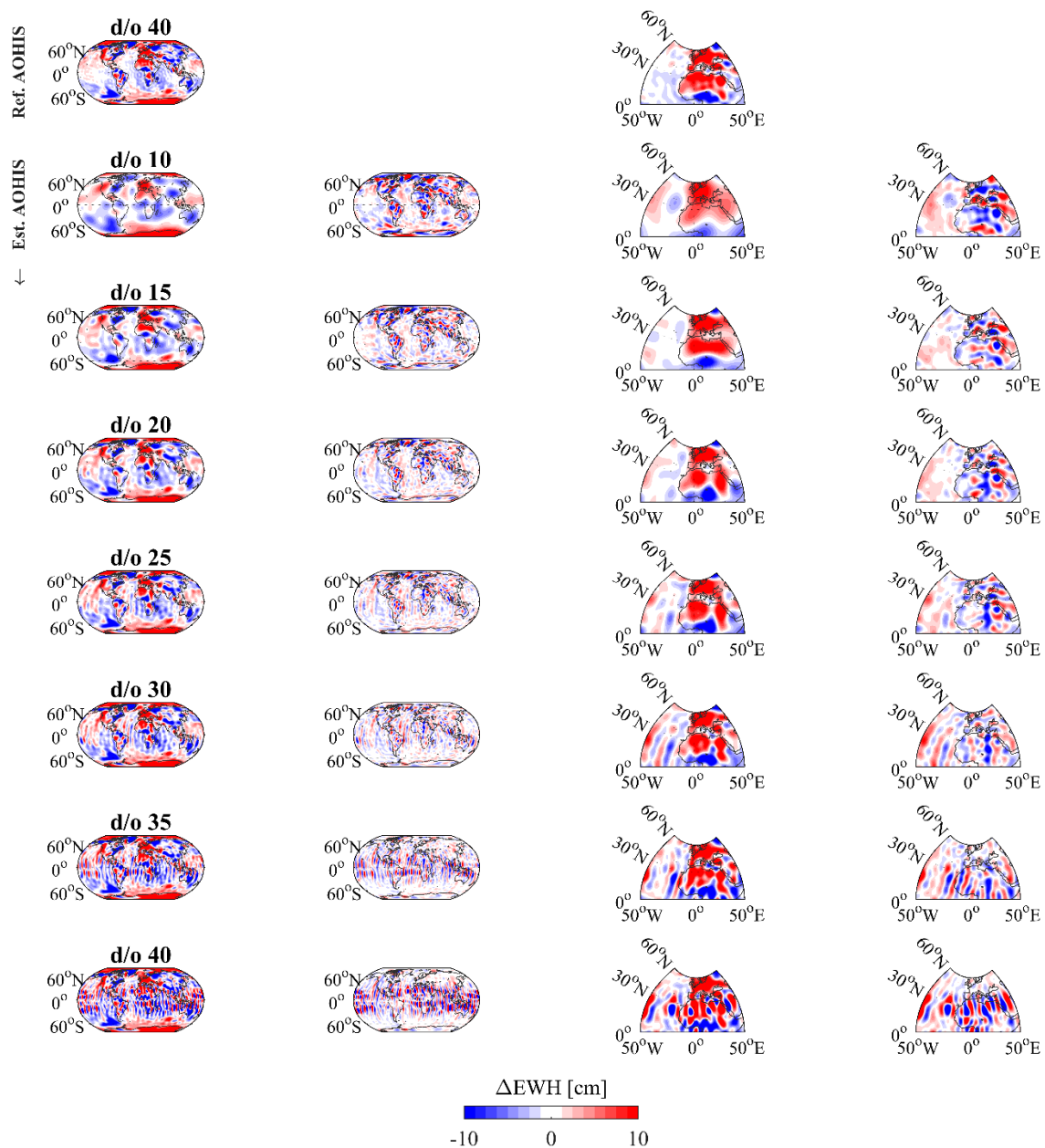


Figure 9. Spatial representation of the daily solutions for 11/01/2002 with different daily maximum degree based on scenario 3pii,p per row. Columns 1 and 3 show the estimated gravity field. Columns 2 and 4 show the difference to the reference atmosphere, ocean, hydrology, ice, and solid Earth (AOHIS) (d/o 40), such including the omission error. Columns 3 and 4 show a snapshot of the Northern hemisphere.

Figure 10 visualizes in the spatial domain the error of the gravity field combined with the ground track pattern for the daily solution up to d/o 30 and 40. As the ground track is designed to cover the Earth within a seven-day period optimally, the daily ground track coverage is not ideal. In Figure 10a,b, a daily solution parametrized up to d/o 30 is visualized and shows only a subtle striping pattern. In comparison, the parametrization up to d/o 40 in Figure 10c,d, shows the spatial aliasing, also very prominently visible in the detail picture of the Northern hemisphere in Figure 9. The error is especially dominant in areas that are not covered by ground tracks. Overall, the example shows that an optimal choice of the daily maximum degree is of great importance to the resulting daily gravity field.

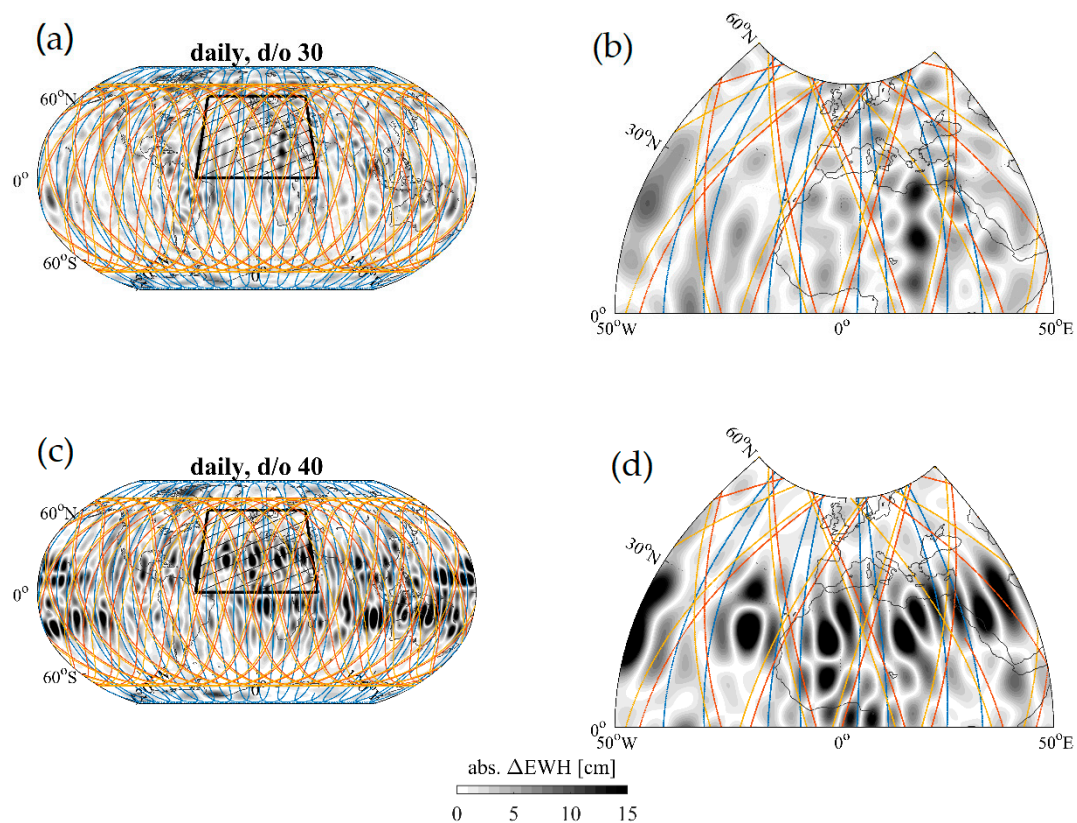


Figure 10. Spatial representation of daily solution (11/01/2002) and ground tracks. Global representation in first column, detail in column 2. (a,b) Solution up to d/o 30 (c,d); Solution up to d/o 40. Omission error included.

4.3. Applications

For the assessment of the results regarding potential applications, we computed time series for a whole year based on scenario 2pi (computed up to d/o 70), 3pip,b, and 3pii,b (computed up to d/o 90) with daily solutions up to d/o 15, and retrieval periods of seven days. All values of the time series are retrieved from the respective coefficient estimates in the selected areas up to d/o 50. We selected and evaluated 12 areas listed in Table 7 with signals in hydrology and ice. The catchment and basins borders are used as boundaries. To cover various scenarios, five large catchments, five small catchments, and two ice drainage basins were selected. Figure 11 shows a time series in EWH for the Amazon region (a), the Danube catchment (b), a small part of California (c), and of the southwest (SW) of Greenland (d) over a whole year. As a reference, the AOHIS from the ESA ESM processed the same way is visualized in the dashed blue line. In the Amazon time series, the mass increase due to the rain period is detectable. The small catchment of the San Joaquin River in Southern California covers part of the drought area, as 2002 was one of the driest seasons since records are taken. As the catchment is rather small, an increased error is visible.

Table 7 summarizes the standard deviation of the differences of the solutions to their reference of the selected catchments and basins and of the three scenarios. Also, the gain of the triple-pair scenarios compared to the double pair scenario is determined. The gain is the standard deviation difference with the standard deviation of the double pair, multiplied by 100. It shows that the second polar pair gave a smaller benefit in average 10.7%, while the second inclined pair improved on average by 21%. One of the examples of Greenland shows that the gain is even visible in areas, where the inclined pair does not add observations. When only evaluating the big catchment, both triple-pair scenarios perform similar with more than 20% improvement. When investigating the small catchments, however, the performance of the triple-pair scenario 3pip,b declines to a small improvement only of 5%, while

scenario 3pii,b has the same improvement as for the big catchments (cf. Table 7). In the ice drainage basins, triple pair 3pip,b performs even worse than the double pair.

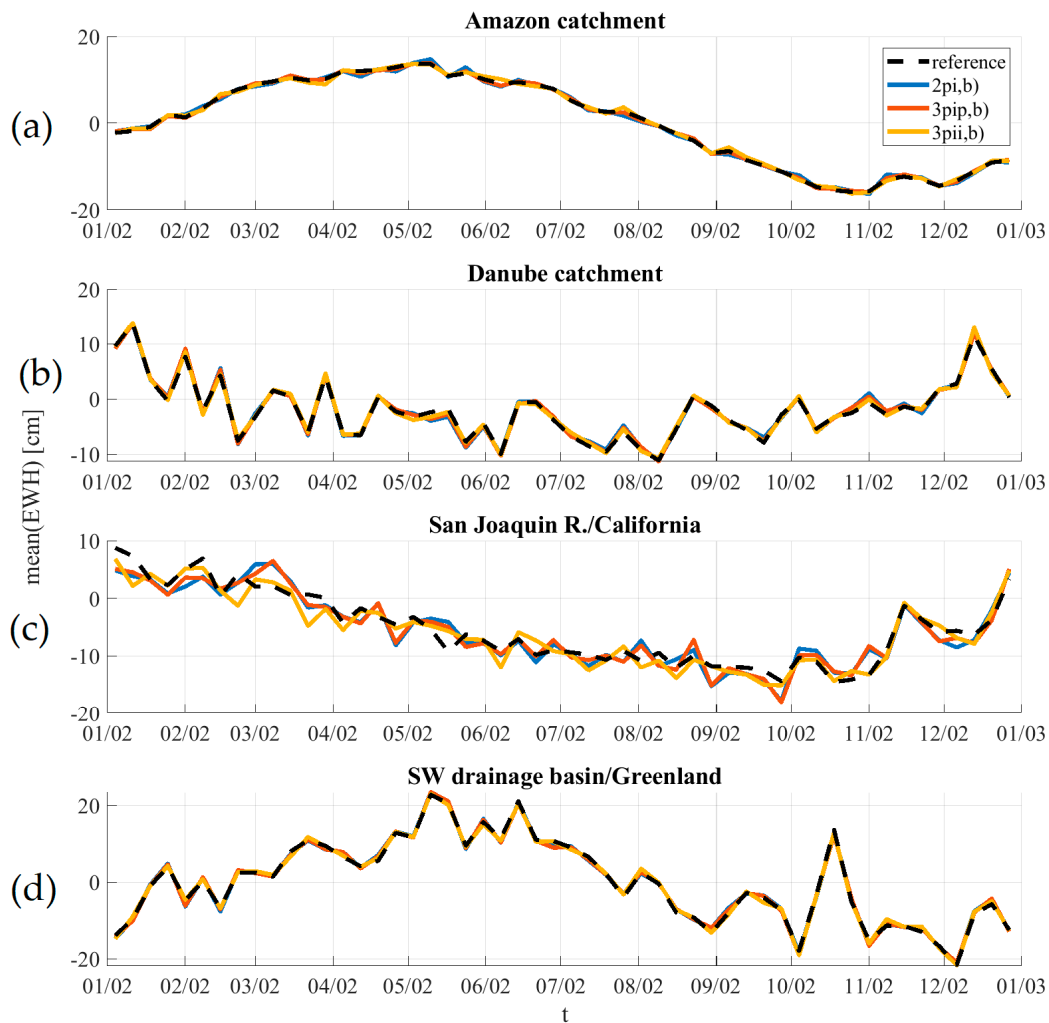


Figure 11. Time series for four selected catchments in EWH (cm) (a) Amazon basin, (b) Danube basin, (c) San Joaquin River/California, (d) South-East drainage basin/Greenland extracted from seven-day solutions up to d/o 50 based on scenario 2pi, 3pip,b, and 3pii,b. Compare to Table 7. Daily Wiese solution co-parametrized up to d/o 15.

Table 7. Standard deviation of Scenario 2pi, 3pip,b, and 3pii,b up d/o 50 (with daily d/o 15) and the gain of the triple-pair scenarios compared to the double pair scenario. Computed over one year of the indicated catchments in cm EWH. Clustered: Big catchments, small catchments, ice drainage basins according to the Rignot basins, IMBIE project (<http://imbie.org/imbie-2016/drainage-basins/>). Additionally, in the last two columns are the standard deviation of daily solutions based on Scenario 3pii,b, once co-estimated up to d/o 15 and once co-estimated up to d/o 25.

Catchment \ \ Scenario	2pi Std. [cm]	3pip,b Std. [cm]	Gain [%]	3pii,b Std. [cm]	Gain [%]	d/o 15 Std. [cm]	d/o 25 Std. [cm]
Mississippi	0.57	0.53	7.3	0.41	28.3	0.90	0.91
Amazon	0.56	0.29	48.3	0.43	23.1	0.71	0.65
Danube	0.65	0.54	16.9	0.46	29.9	0.89	1.04
Yangtze R.	0.66	0.49	25.9	0.59	9.7	0.73	0.71
Ganges	0.66	0.55	17.5	0.54	18.5	0.98	1.04
San Joaquin R.	2.24	2.08	7.2	1.81	18.9	1.13	1.79
Fitzroy R.	3.43	3.35	2.3	2.45	28.5	1.27	3.14
Elbe	2.49	2.29	7.8	1.70	31.6	1.03	1.38
Dead sea	2.22	2.13	4.4	1.90	14.8	1.17	1.77
Upper Mississippi	1.79	1.73	3.4	1.26	29.7	1.39	1.77
SW Greenl.	0.79	0.77	2.3	0.63	20.3	1.05	0.91
NE Greenl.	0.97	1.11	-14.8	0.97	-0.4	0.82	1.30
Average	1.42	1.32	10.7	1.10	21.1	1.01	1.39

Based on scenario 3pii,b, a scenario with daily solution co-estimated up to d/o 25 was also computed, to analyze the possibility of a higher daily solution. Figure 12 therefore visualizes the daily solutions up to d/o 15 and 25 from scenario 3pii,b for the Danube catchment and the ice drainage basin in SW Greenland over two months. The corresponding standard deviations can be found in Table 7. In both examples, a difference between the d/o 15 and 25 curve is visible and can be explained by the omission error. Figure 13 compares the seven-day solution to the d/o 25 daily solution. In the Greenland example (b), both curves have the same base characteristics. However, in the daily curve, the omission error is visible, as the curve is missing signal amplitude. The Danube time series (a) in comparison visualizes the fact that the daily solution has the same signal strength and adds additional time-variable information. Both examples in Figure 13 show that both daily and weekly solutions have advantages, depending on the characteristic of the underlying geophysical signals. Based on the individual applications demand, the spatial and temporal resolutions have to be balanced.

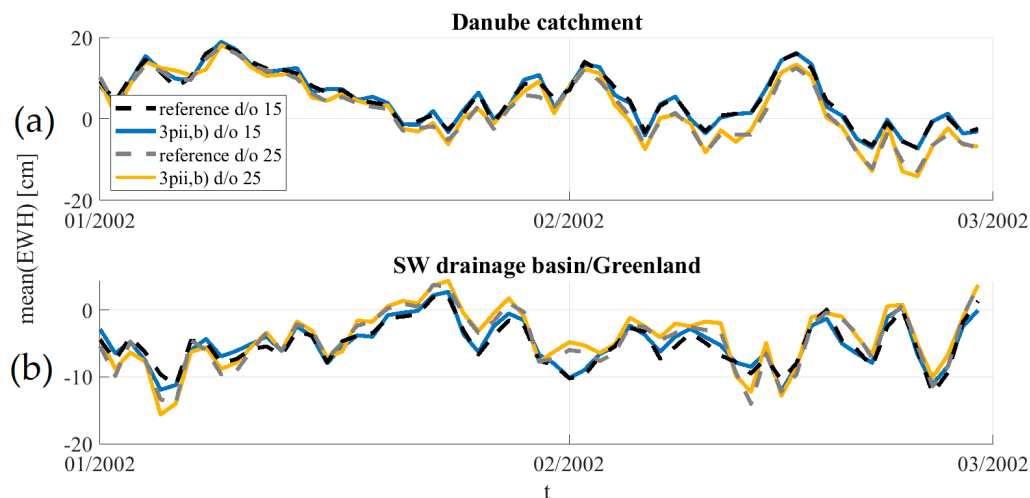


Figure 12. Time series in EWH (cm) for Danube catchment (a) and SW drainage basin in Greenland (b) of Scenario 3pii,b extracted from daily solutions with d/o 15 and 25. Two-month period extracted from the one year processed.

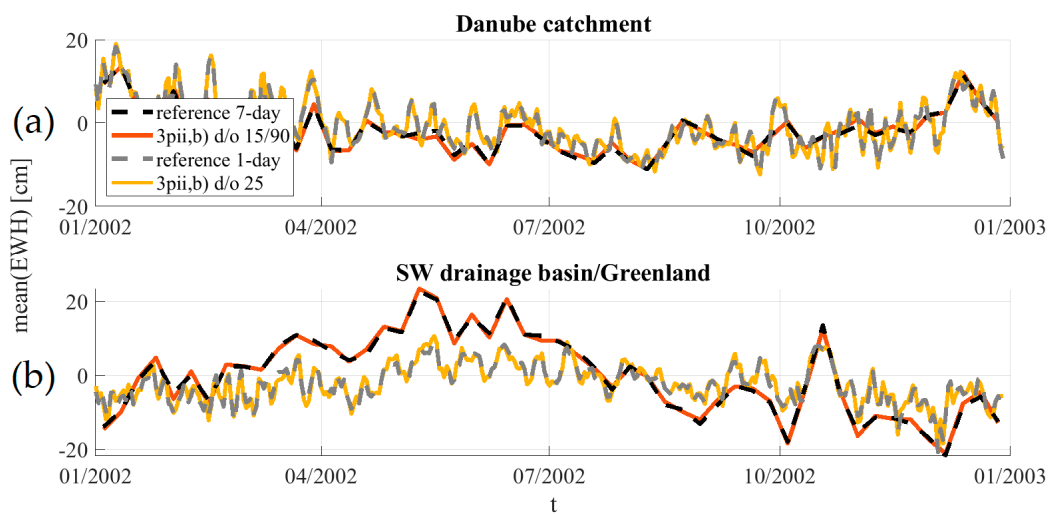


Figure 13. Time series in EWH (cm) for Danube catchment (a) and SW drainage basin in Greenland (b) of Scenario 3pii,b comparing daily solutions (d/o 25) to the signal content of the seven-day solution up to d/o 50 of scenario 3pii,b for one year.

In Figure 14, the magnitude of the daily signal of the SW Greenland example due to the omission error was improved by adding a three-day solution (computed based on the same scenario) starting at the highest d/o of the daily solution (see [28]). This means up to d/o 25 the daily solution was used, artificially enhanced by the three-day solution starting d/o 26 to the maximum degree of 50. As [28] showed, this approach does not significantly distort the daily solution, while at the same time, it adds information with long-wavelength frequency content. Part of the omission error, therefore, can be reduced.

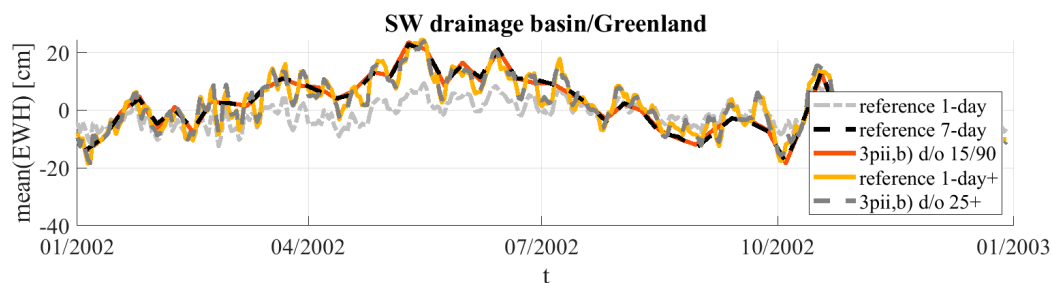


Figure 14. Time series in EWH (cm) for SW Greenland ice drainage basin based on Scenario 3pii,b comparing daily solutions (d/o 25) plus three-day solution (indicated by the “+”) up to 50 to the signal content of the seven-day solution up to d/o 50 of scenario 3pii,b for one year. The reference solution of the former daily solution is visualized in a light grey for comparison.

5. Conclusions

With our closed-loop simulation software, we tested the impact of a third satellite in an inclined or near-polar orbit with GRACE-like or NGGM instrument noise specifications. As the base scenario, we used a Bender-type double-pair constellation. While the second pair, as demonstrated by, e.g., [26], has the added benefit of enhanced de-stripping capabilities and further allows the observation of the full AOHIS, we showed that the impact of an additional third satellite pair is between 5% and 40%. Compared with the expected 22% improvement of the square-root-n rule, this indicates that the additional polar pair does add redundant information, while the third pair in the inclined orbit adds significant observations. Our tests also revealed a dampened striping effect and an improved error RMS variability. The third pair in an inclined orbit is preferable compared to the third pair in a polar orbit. The best third pair option is an inclined pair with improved NGGM instrumentation. Therefore,

we recommend flying an inclined pair, to add not only additional observations, but also a different observation geometry. The error curve of the daily triple pair gravity field meets the signal curve at approximately degree 26. Our tests confirmed that the processing up to d/o 30 is beneficial, while a higher parametrization adds spatial aliasing to the solution. We therefore note that it is crucial to choose the daily maximum degree with care.

To test the best triple-pair scenarios for applications, we extended the time series towards one year. We looked into typical regions regarding hydrology and ice like the Amazon catchment, the Danube basin, or Greenland. Compared to the Bender double pair scenario, the gain of the third pair in a polar orbit is on average 11%, while adding a third pair in an inclined orbit exhibits a gain of approximately 21%, which is achievable for bigger as well as small catchments. Especially the visualized SW Greenland time series demonstrates the importance of a high d/o daily solution, as the omission error in the region can be significant. The tested approach to add higher d/o long-term solutions onto daily solutions as presented in [28] improves the results significantly and can be recommended as methodology for future applications.

As a conclusion, while the benefit of a Bender-type double-pair constellation over a single-pair GRACE like concept is substantial, we can state that a third pair improves the achievable performance of a double pair constellation only moderately. Our results also suggest that an inclined third pair would be the better option to improve the overall performance.

Author Contributions: Conceptualization, A.F.P.; methodology, A.F.P.; software, A.F.P.; validation, A.F.P.; formal analysis, A.F.P.; investigation, A.F.P.; resources, A.F.P.; data curation, A.F.P.; writing—original draft preparation, A.F.P.; writing—review and editing, A.F.P. and R.P.; visualization, A.F.P.; supervision, R.P.; project administration, R.P.; funding acquisition, R.P. All authors have read and agreed to the published version of the manuscript.

Funding: A big part of the investigations presented in this paper was performed in the framework of the study ‘Assessment of satellite constellations for monitoring the variations in Earth gravity field (ADDCON)’, ESA-ESTEC, Contract AO/1-7317/12/NL/AF funded by the European Space Agency.

Acknowledgments: We also acknowledge the provision of supercomputing resources by the Leibniz Supercomputing Centre (LRZ; Address: Boltzmannstraße 1, 85748 Garching bei München, Germany).

Conflicts of Interest: The authors declare no conflict of interest.

References

1. Reigber, C.; Schwintzer, P.; Lühr, H. The CHAMP geopotential mission, *Bollettino di Geofisica Teoretica ed Applicata*, 40/3-4, September-December 1999. In Proceedings of the Second Joint Meeting of the International Gravity and the International Geoid Commission, Trieste, Italy, 7–12 September 1998; Marson, I., Sünkel, H., Eds.; 1999; pp. 285–6729, ISSN 0006-6729.
2. Tapley, B.D.; Bettadpur, S.; Watkins, M.; Reigber, C. The gravity recovery and climate experiment experiment, mission overview and early results. *Geophys. Res. Lett.* **2004**, *31*, L09607. [[CrossRef](#)]
3. Kornfeld, R.P.; Arnold, B.W.; Gross, M.A.; Dahya, N.T.; Klipstein, W.M.; Gath, P.F.; Bettadpur, S. GRACE-FO: The Gravity Recovery and Climate Experiment Follow-On Mission. *J. Spacecr. Rocket.* **2019**, *56*, 931–951. [[CrossRef](#)]
4. Rodell, M.; Famiglietti, J.S.; Wiese, D.N.; Reager, J.T.; Beaudoin, H.K.; Landerer, F.W.; Lo, M.H. Emerging trends in global freshwater availability. *Nature* **2018**, *557*, 651–659. [[CrossRef](#)]
5. Forootan, E.; Didova, O.; Schumacher, M.; Kusche, J.; Elsaka, B. Comparisons of atmospheric mass variations derived from ECMWF reanalysis and operational fields over 2003–2011. *J. Geod.* **2014**, *88*, 503–514. [[CrossRef](#)]
6. Panet, I.; Pajot-Métivier, G.; Greff-Lefftz, M.; Métivier, L.; Diament, M.; Manda, M. Mapping the mass distribution of Earth’s mantle using satellite-derived gravity gradients. *Nat. Geosci.* **2014**, *7*, 131–135. [[CrossRef](#)]
7. Han, S.; Riva, R.; Sauber, J.; Okal, E. Source parameter inversion for recent great earthquakes from a decade-long observation of global gravity fields. *J. Geophys. Res.* **2013**, *118*, 1240–1267. [[CrossRef](#)]
8. Ivins, E.; Watkins, M.; Yuan, D.N.; Dietrich, R.; Casassa, G.; Rülke, A. On land ice loss and glacial isostatic adjustment at the Drake Passage: 2003–2009. *J. Geophys. Res.* **2011**, *116*, B02403. [[CrossRef](#)]

9. Luthcke, S.B.; Sabaka, T.; Loomis, B.; Arendt, A.; McCarthy, J.; Camp, J. Antarctica, Greenland, and Gulf of Alaska land-ice evolution from an iterated GRACE global mascon solution. *J. Geophys.* **2013**, *59*, 613–631. [[CrossRef](#)]
10. Velicogna, I.; Sutterley, T.C.; van den Broeke, M.R. Regional acceleration in ice mass loss from Greenland and Antarctica using GRACE time-variable gravity data. *Geophys. Res. Lett.* **2014**, *41*, 8130–8137. [[CrossRef](#)]
11. Pail, R.; Bingham, R.; Braitenberg, C.; Dobsalw, H.; Eicker, A.; Güntner, A.; Horwarth, M.; Ivins, E.; Longuevergne, L.; Panet, I.; et al. IUGG Expert Panel Science and User Needs for Observing Global Mass Transport to Understand Global Change and to Benefit Society. *Surv. Geophys.* **2015**, *36*. [[CrossRef](#)]
12. Sharifi, M.; Sneeuw, N.; Keller, W. Gravity recovery capability of four generic satellite formations. In Proceedings of the 1st International Symposium of the International Gravity Field Service “Gravity Field of the Earth”. *Gen. Command Mapp.*, Istanbul, Turkey, 28 August–1 September 2007; Kilicoglu, A., Forsberg, R., Eds.; 2007; pp. 211–216, ISSN 1300-5790.
13. Sneeuw, N.; Sharifi, M.; Keller, M. Gravity Recovery from Formation Flight Missions. VI Hotine-Marussi Symposium on Theoretical and Computational Geodesy. *Sensors* **2008**, *132*, 29–34. [[CrossRef](#)]
14. Wiese, D.N.; Folkner, W.M.; Nerem, R.S. Alternative mission architectures for a gravity recovery satellite mission. *J. Geod.* **2008**, *83*, 569–581. [[CrossRef](#)]
15. Elsaka, B.; Kusche, J.; Ilk, K.-H. Recovery of the Earth’s Gravity Field from Formation-Flying Satellites: Temporal Aliasing Issues. *Adv. Space Res.* **2012**, *50*, 1534–1552. [[CrossRef](#)]
16. Iran Pour, S.; Reubelt, T.; Sneeuw, N.; Daras, I.; Murböck, M.; Gruber, T.; Pail, R.; Weigelt, M.; van Dam, T.; Visser, P.; et al. *Assessment of Satellite Constellations for Monitoring the Variations in Earth Gravity field–SC4MGV, ESA–ESTEC Contract No. AO/1-7317/12/NL/AF, Final Report*; ESA-ESTEC: Noordwijk, Netherlands, 2015.
17. Bender, P.L.; Wiese, D.; Nerem, R.S. A Possible Dual-GRACE Mission with 90 Degree and 63 Degree Inclination Orbits. In Proceedings of the 3rd International Symposium on Formation Flying, Missions and Technologies, ESA/ESTEC, Noordwijk, The Netherlands, 23–25 April 2008.
18. Wiese, D.; Nerem, R.; Han, S.-C. Expected Improvements in Determining Continental Hydrology, Ice Mass Variations, Ocean Bottom Pressure Signals, and Earthquakes Using Two Pairs of Dedicated Satellites for Temporal Gravity Recovery. *J. Geophys. Res.* **2011**, *116*, 405. [[CrossRef](#)]
19. Wiese, D.; Nerem, R.; Lemoine, F. Design considerations for a dedicated gravity recovery satellite mission consisting of two pairs of satellites. *J. Geophys.* **2012**, *86*, 81–98. [[CrossRef](#)]
20. Daras, I.; Pail, R. Treatment of temporal aliasing effects in the context of next generation satellite gravimetry missions. *J. Geophys. Res.* **2017**, *22*, 7343–7362. [[CrossRef](#)]
21. Panet, I.; Flury, J.; Biancale, R.; Gruber Th Johannessen, J.; Van den Broeke, M.; Van Dam, T.; Gegout, P.; Hughes Ch Ramillien, G.; Sasgen, I.; Seoane, L.; et al. Earth System Mass Transport Mission (e.motion): A Concept for Future Earth Gravity Field Measurements from Space. *Surv. Geophys.* **2012**. [[CrossRef](#)]
22. Gruber, T.; Murböck, M.; NGGM-D Team. *e2.Motion-Earth System Mass Transport Mission (Square)-Concept for a Next Generation Gravity Field Mission*; DGK, Reihe B, 318; Verlag C.H. Beck: Munich, Germany, 2014.
23. Pail, R.; Bamber, J.; Biancale, R.; Bingham, R.; Braitenberg, C.; Eicker, A.; Flechtner, F.; Gruber, T.; Güntner, A.; Heinzl, G.; et al. Mass variation observing system by high low inter-satellite links (MOBILE)—a new concept for sustained observation of mass transport from space. *J. Geod. Sci.* **2019**, *9*, 48–58. [[CrossRef](#)]
24. Elsaka, B.; Raimondo, J.-C.; Brieden Ph Reubelt, T.; Kusche, J.; Flechtner, F.; Iran Pour, S.; Sneeuw, N.; Müller, J. Comparing Seven Candidate Mission Configurations for Temporal Gravity Retrieval through Full-Scale Numerical Simulation. *J. Geophys.* **2014**, *88*, 31–43. [[CrossRef](#)]
25. Purkhauser, A.F.; Pail, R.; Hauk, M.; Visser, P.; Sneeuw, N.; Saemian, P.; Liu, W.; Engels, J.; Chen, Q.; Siemes, C.; et al. Gravity Field Retrieval of Next Generation Gravity Missions regarding Geophysical Services: Results of the ESA-ADDCON Project. European Geosciences Union General Assembly 2018. Available online: <https://meetingorganizer.copernicus.org/EGU2018/EGU2018-2770.pdf> (accessed on 4 March 2020).
26. Purkhauser, A.; Siemes, C.; Pail, R. Consistent quantification of the impact of key mission design parameters on the performance of next-generation gravity missions. *Geophys. J. Int.* **2020**, *221*, 1190–1210. [[CrossRef](#)]
27. Wiese, D.N.; Visser, P.; Nerem, R.S. Estimating low resolution gravity fields at short time intervals to reduce temporal aliasing errors. *Adv. Space Res.* **2011**, *48*, 1094–1107. [[CrossRef](#)]
28. Purkhauser, A.F.; Pail, R. Next generation gravity missions: Near-real time gravity field retrieval strategy. *Geophys. J. Int.* **2019**. [[CrossRef](#)]

29. Visser, P.M.A.M.; Schrama, E.J.O.; Sneeuw, N.; Weigelt, M. Dependency of Resolvable Gravitational Spatial Resolution on Space-Borne Observation Techniques. *Int. Assoc. Geodesy Symposia* **2011**, *373–379*. [[CrossRef](#)]
30. Weigelt, M.; Sneeuw, N.; Schrama, E.; Visser, P. An improved sampling rule for mapping geopotential functions of a planet from a near polar orbit. *J. Geophys.* **2012**, *87*. [[CrossRef](#)]
31. Sneeuw, N.; Flury, J.; Rummel, R. Science Requirements on Future Missions And Simulated Mission Scenarios. *Future Satell. Gravim. Earth Dyn.* **2005**, *113–142*. [[CrossRef](#)]
32. Swenson, S.; Wahr, J. Post-Processing removal of correlated errors in GRACE data. *Geophys. Res. Lett.* **2006**, *33*, L08402. [[CrossRef](#)]
33. Horvath, A.; Murböck, M.; Pail, R.; Horwath, M. Decorrelation of GRACE time variable gravity field solutions using full covariance information. *Geosciences* **2018**, *8*, 323. [[CrossRef](#)]
34. Kusche, J. Approximate decorrelation and non-isotropic smoothing of time-variable GRACE-type gravity field models. *J. Geophys.* **2007**, *81*, 733–749. [[CrossRef](#)]
35. Daras, I. Gravity Field Processing Towards Future LL-SST Satellite Missions; Deutsche Geodätische Kommission der Bayerischen Akademie der Wissenschaften, Reihe C. Ph.D.Thesis, Technische Universität München, München, Germany, 2016.
36. Daras, I.; Pail, R.; Murböck, M.; Yi, W. Gravity field processing with enhanced numerical precision for LL-SST missions. *J. Geophys.* **2015**, *89*, 99–110. [[CrossRef](#)]
37. Shampine, L.F.; Gordon, M.K. *Computer Solution of Ordinary differential Equations: The Initial Value Problem*; W.H. Freeman: San Francisco, CA, USA, 1975.
38. Montenbruck, O.; Gill, E. Satellite orbits: Models, methods, and applications. *Appl. Mech. Rev.* **2002**, *55*, B27–B28. [[CrossRef](#)]
39. Mayer-Gürr, T.; Pail, R.; Gruber, T.; Fecher, T.; Rexer, M.; Schuh, W.D.; Kusche, J.; Brockmann, J.M.; Rieser, D.; Zehentner, N.; et al. The combined satellite gravity field model GOCO05s. *Geophys. Res. Abstr.* **2015**, *17*. [[CrossRef](#)]
40. Dobslaw, H.; Bergmann-Wolf, I.; Dill, R.; Forootan, E.; Klemann, V.; Kusche, J.; Sasgen, I. The updated ESA Earth System Model for future gravity mission simulation studies. *J. Geophys.* **2015**, *89*, 505–513. [[CrossRef](#)]
41. Ray, R.D. *A Global Ocean tide Model from Topex/Poseidon Altimetry: Got99.2*; Technology report; NASA Technical Memorandum: NASA/TM-1999-209478; Goddard Space Flight Center: Greenbelt, MD, USA, 1999; p. 209478.
42. Savcenko, R.; Bosch, W. *EOT11a—Empirical Ocean Tide Model from Multi-Mission Satellite Altimetry*; DGLF Report: München, Germany, 2012.
43. Hofmann-Wellenhof, B.; Moritz, H. *Physical Geodesy*, 2nd ed.; Springer: Berlin/Heidelberg, Germany, 2012.
44. Pail, R.; Bruinsma, S.; Migliaccio, F.; Förste, C.; Goiginger, H.; Schuh, W.D.; Höck, E.; Reguzzoni, M.; Brockmann, J.M.; Abrikosov, O. First GOCE gravity field models derived by three different approaches. *J. Geophys.* **2011**, *85*, 819–843. [[CrossRef](#)]
45. Cheng, M.K.; Tapley, B.D. Seasonal variations in low degree zonal harmonics of the Earth's gravity field from satellite laser ranging observation. *J. Geophys. Res.* **1999**, *104*, 2667–2681. [[CrossRef](#)]
46. Touboul, P.; Metris, G.; Selig, H.; Le Traon, O.; Bresson, A.; Zahzam, N.; Christophe, B.; Rodrigues, M. Gravitation and Geodesy with Inertial Sensors, from Ground to Space. *Test. Aerosp. Res.* **2016**, *12*. [[CrossRef](#)]
47. Schrama EJO, Wouters B, Lavallée Signal and noise in Gravity Recovery and Climate Experiment (GRACE) observed surface mass variation. *J. Geophys. Res.* **2007**, *116*, B02407. [[CrossRef](#)]
48. Wahr, J.; Molenaar, M.; Bryan, F. Time variability of the Earth's gravity field: Hydrological and oceanic effects and their possible detection using GRACE. *J. Geophys. Res.* **1998**, *201*. [[CrossRef](#)]



A.3. P-III: Next generation gravity missions: near-real time gravity field retrieval strategy

Reference: Purkhauser, A. F. and Pail, R. (2019). Next generation gravity missions: near-real time gravity field retrieval strategy. *Geophysical Journal International*, 217(2):1314–1333. DOI: 10.1093/gji/ggz084

Copyright: This work originally has been published in *Geophysical Journal International*: <https://doi.org/10.1093/gji/ggz084>. The Copyright has been transferred to Oxford University Press.

Abstract

The goal of NGGM is to improve the monitoring of mass transport in the Earth system by an increased space-time sampling capability as well as higher accuracies of a new generation of instrumentation. They should be able to fulfil the scientific and societal needs of providing high-resolution short-time gravity field solutions for geophysical applications like for e.g. service applications such as flood and drought monitoring and forecast or applications in water management. To facilitate this need a NRT processing scheme based on a co-parametrization of low-resolution daily and longer-term gravity field solution, combined with a sliding window averaging, was set up. In contrast to other strategies that are usually based on Kalman filtering, the proposed NRT concept is independent of any prior information about the temporal gravity field, and does not require any regularization. The enhanced spatial-temporal resolution opens the possibility to self-dealias high-frequency atmospheric and oceanic signals, and additionally provides gravity field solutions on short time-scales. In order to quantify the capabilities of the proposed NRT approach, a numerical closed-loop simulation of a LL-SST mission for a two-pair Bender-type constellation with realistic noise assumptions was performed. While for the daily parametrization a spherical harmonics degree and order of 15 turns out to be a favourable choice, by applying the sliding window NRT approach stable daily gravity field estimates up to degree/order 50 with latencies of down to 1 day could be achieved.

Remark: The software version used within this paper has an outdated weighting algorithm, compared to the others. The impact of the HL-SST component was given to much weight. Additionally, the HL-SST component was implemented as a difference of the position.

Appendix A. Publications


Declaration of own contribution


Table A.3.: Contribution to P-III

Involved in	Estimated contribution
Ideas and conceptual design	90%
Computation and results	100%
Analysis and interpretation	90%
Manuscript, figures and tables	90%
Total	92,5%

Confirmation by Co-Authors

I hereby confirm the correctness of the declaration of the contribution of Anna F. Purkhauser for the publication P-III in Table A.3:


.....
Roland Pail
(IAPG, LRG, TUM)


.....
Date

Next generation gravity missions: near-real time gravity field retrieval strategy

Anna F. Purkhauer and Roland Pail

Chair of Astronomical and Physical Geodesy, Arcisstraße 21, 80333 Munich, Germany. E-mail: anna.purkhauer@tum.de

Accepted 2019 February 12. Received 2019 February 4; in original form 2018 August 02

SUMMARY

The goal of next generation gravity missions (NGGM) is to improve the monitoring of mass transport in the Earth system by an increased space–time sampling capability as well as higher accuracies of a new generation of instrumentation. They should be able to fulfil the scientific and societal needs of providing high-resolution short-time gravity field solutions for geophysical applications like for example service applications such as flood and drought monitoring and forecast or applications in water management. To facilitate this need a near-real time (NRT) processing scheme based on a coparametrization of low-resolution daily and longer-term gravity field solution, combined with a sliding window averaging, was set up. In contrast to other strategies that are usually based on Kalman filtering, the proposed NRT concept is independent of any prior information about the temporal gravity field, and does not require any regularization. The enhanced spatial-temporal resolution opens the possibility to self-dealias high-frequency atmospheric and oceanic signals, and additionally provides gravity field solutions on short timescales. In order to quantify the capabilities of the proposed NRT approach, a numerical closed-loop simulation of a low-low satellite-to-satellite tracking (ll-sst) mission for a two-pair Bender-type constellation with realistic noise assumptions was performed. While for the daily parametrization a spherical harmonics degree and order of 15 turns out to be a favourable choice, by applying the sliding window NRT approach stable daily gravity field estimates up to degree/order 50 with latencies of down to 1 d could be achieved.

Key words: Satellite geodesy; Satellite gravity; Time variable gravity.

1 INTRODUCTION

The analysis of the data of dedicated gravimetric satellite missions like the Challenging Minisatellite Payload (CHAMP; Reigber *et al.* 1999), and the Gravity Recovery and Climate Experiment (GRACE; Tapley *et al.* 2004) mission has provided important insight into the observed mass transport processes of the Earth system. The CHAMP mission was the first geopotential satellite mission specifically dedicated to the observation of the Earth's gravity field. Its gravity measurement technique was based on high-low satellite-to-satellite tracking (hl-sst) exploiting the Global Positioning System (GPS; Xu 2003) and a space-borne accelerometer to separate gravitational from non-gravitational accelerations, to deliver precise gravity field models for the long and medium wavelengths. Due to the accuracy of the CHAMP orbit information derived from GPS only a spatial resolution of 500–1000 km for a static gravity field could be achieved (Baur 2013). Applying tailored processing strategies, also time variable gravity field solutions down to spatial scales of approximately 2000 km at the annual frequency and for multiyear trends could be derived (Weigelt *et al.* 2013). Similar accuracies can be achieved when exploiting the perturbed orbit of low-earth orbit (LEO) missions like Swarm (Lück *et al.* 2017). In contrast, the GRACE concept is based on twin satellites flying in a LEO at a nominal distance of 220 km. In addition to the hl-sst observation component of both satellites, the main observation technique is K-band microwave low-low satellite-to-satellite tracking (ll-sst) between the two GRACE satellites combined with a three-axis accelerometer, measuring the non-conservative forces acting on the spacecraft. As a result temporal gravity fields with a spatial resolution of approximately 300 km and better could be obtained. Temporal gravity fields with a resolution of 1 month (Tapley *et al.* 2004), 10 d (Bruinsma *et al.* 2010; Tapley *et al.* 2013) and even daily solutions (Kurtenbach *et al.* 2009; Mayer-Gürr *et al.* 2016), the latter using a Kalman filter, were determined.

GRACE observes the sum of all Earth's mass distribution and mass change effects within the Earth system, that is in the atmosphere, ocean, hydrology, ice and solid earth (AOHIS). GRACE data were subsequently analysed in regard of hydrological processes (Rodell *et al.* 2009; Tiwari *et al.* 2009), ice mass melting (Luthcke *et al.* 2013; Velicogna *et al.* 2014), sea level rise (Willis *et al.* 2010), atmospheric circulation (Forootan *et al.* 2014), changes of the solid Earth like earthquakes (Han *et al.* 2013) and their interaction. For the first time it is now possible to measure phenomena consistently on a large and even global scale, such as the continental water storage (Rodell & Famiglietti

1999). The water storage change over landmasses captured by GRACE is not only a useful indicator of climate variability and human impact on the environment, but also allows for the first time to observe water storage on short timescales (Lettenmaier & Famiglietti 2006). However, the available data has some limitations regarding spatial and temporal resolution, homogeneity as well as the signal strength, meaning if a basin, for example has significant water storage variation it is more likely to be detected even if the spatial extent is rather small. Consequently scientific analysis of the GRACE observations faces several limitations. Adapted processing strategies have allowed to analyse river basins with a minimal spatial extent of about 200 000 km² (Longuevergne *et al.* 2010), that is only 10 per cent of the worldwide river basins can be monitored, or enabled to investigate smaller-scale mass changes with a high amplitude such as in the case of surface water bodies (Awage *et al.* 2013; Tourian *et al.* 2015). Changes in regional groundwater storage in North China were detected (Feng *et al.* 2013), but the current spatial resolution of 300 km for monthly fields does not show the increase of the groundwater storage in the Southeast of the North China Plains (Feng, private communication). Several studies found that earthquakes of a magnitude larger than 8.5, like the 2010 Maule earthquake (Han *et al.* 2010; Heki & Matsuo 2010) or the 2011 Tohoku-Oki (Japan) earthquake (Matsuo & Heki 2011; Wang *et al.* 2012), could be detected by GRACE in post-processing (Pail *et al.* 2015), but also identified its insensitivity regarding the pre-seismic build-up and smaller events.

The successfully launched satellite mission GRACE Follow-On (GRACE FO; Flechtner *et al.* 2017) ensures the continuation of the observation of the Earth mass change. GRACE FO is based on the GRACE mission concept, bridging the gap till a next generation gravity mission (NGGM) is ready to be operated. It features a slightly modified instrumentation and an additional intersatellite laser ranging interferometer as technology demonstrator (Sheard *et al.* 2012), meaning an improved accuracy of a few tens of nanometre compared to the micrometre K-band microwave ranging accuracy can be reached. However, the central issues remain: The typical GRACE-type constellation consists of a twin satellite pair in a coplanar orbit. Due to the observation of the orbit differences between the two satellites in line-of-sight direction, the sensitivity is highest in this direction, introducing an anisotropic error spectrum and strong striping features due to temporal aliasing effects (Seo *et al.* 2007). Since the GRACE FO mission also consists only of one pair of satellites in a near-polar orbit these issues regarding undersampling of the temporal gravity signal remain unchanged.

Besides the already mentioned limitations concerning the currently achievable spatial and temporal resolution, GRACE provides at the moment only 15 yr of data, which is not sufficient regarding climatological assessments. Many applications need a longer time-series for a more reliable separation of anthropogenic and natural contributions to climate change. Apart from the spatial resolution, also the signal strength, called gravimetric resolution as well, determines the limit of feasibility of analysing mass variations (Lorenz *et al.* 2014). And lastly if a service type application should be based on a gravimetric mission the latency of the raw data as well as the processing is of importance. Up till now GRACE products had usually a raw data latency of minimum 2 months. GRACE-FO will be providing so-called 'quicklook' solutions with a latency of 1–3 d (Wen *et al.* 2018). Possible applications like a flood and drought monitoring and forecasting system need, according to Pail *et al.* (2015), a temporal resolution of 1 d or a few days combined with a short overall latency meaning the raw data have to be made available ideally within a few hours, to be processed quickly into reliable temporal gravity solutions.

A future NGGM must be able to fulfil stronger user requirements in terms of spatial resolution, time resolution, latency and continuous data availability. A NGGM concept consisting of two GRACE-type satellites flying in a Bender-type constellation (Bender *et al.* 2008), which is composed of a near-polar orbit pair combined with an inclined pair with an inclination of 60–70°, is expected to improve many of the problems of single pair missions. The needs and requirements of the scientific community as well as society have been collected (Pail *et al.* 2015) to give a comprehensive background for a future satellite mission concept with an enhanced orbit constellation and improved sensor technology.

Analysis of GRACE time-series revealed the possibility to monitor the spatial as well as the temporal evolution of droughts (Seitz *et al.* 2008; Famiglietti & Rodell 2013; Long *et al.* 2014) and floods (Chen *et al.* 2010; Espinoza *et al.* 2013). Therefore, a NGGM concept shall have a service character coupled with a scientific mission statement. The goal is to have a continuous observation of the Earth mass change for possible application at a reasonable cost level. The latest mission proposals like e.motion with a single pair in a pendulum constellation (Panet *et al.* 2013), e².motion (Gruber *et al.* 2014) based on a Bender-type concept, or the innovative high-low tracking formation mission MOBILE (Pail *et al.* 2018) would be steps toward fulfilling these needs. While the e.motion and e².motion mission proposals are based on the observation system of GRACE and GRACE FO, the MOBILE concept proposes a different observation concept as well as new instrumentation. All three proposals emphasize the need for continuous and sustained observations of the Earth's mass transport on a global scale from space (NGGM-D Team 2014).

Although such missions are still fictional at this point in time, numerical simulations of a needed minimum satellite configuration and possible constellations are necessary to analyse if the user requirements can be met. The infrastructure has to meet the following demands: long-term observations meaning a sustained satellite gravity observation system, an increase of spatial resolution to observe small-scale mass transport phenomena, and an increase of the temporal resolution towards 1 or only a few days. Since temporal and spatial resolution are opposing goals a compromise has to be reached among different user needs (Pail *et al.* 2015). In order to address specifically climate-relevant applications, sustained observation of variations in the Earth's gravity field with high spatial resolution is of essence.

Within this paper a Bender-type NGGM concept (e.g. e².motion concept) with a near-polar and an inclined satellite pair with the characteristics of GRACE/GRACE FO are analysed regarding a new near-real time (NRT) approach. The concept is based on the Wiese approach (Wiese *et al.* 2011), which has already been used in numerical simulations for future NGGM concepts (Daras & Pail 2017; Hauk & Pail 2018) for self-dealiasing of temporal gravity field solutions. The Wiese approach introduces short-term long-wavelength gravity field

parameters to represent short-periodic signals, thus avoiding their aliasing into the long term (week to month) solution. Due to this approach it is possible to obtain better gravity field solutions and additionally also avoid the use of de-aliasing products to remove these non-tidal high-frequency atmosphere and ocean mass variation models and the associated model errors that would contaminate the solution.

In the presented NRT approach high-resolution daily normal equations with Wiese coparametrization, which are intermediate products of a standard processing, are combined with a processing method that is based on a sliding window averaging of several days on normal equation level. This leads to solutions with almost daily temporal resolution, but higher spatial resolution than the daily Wiese solutions. In contrast to already existing daily gravity field approaches that are usually based on Kalman filtering, the temporal gravity field estimates are independent of any a priori information. Derived from the user requirements, the main goal is to provide gravity field solutions with rather high spatial resolution, but with very short latencies. The NRT approach attempts to achieve this goal by spectrally enhancing the daily gravity field solution with the high-degree solution of several days. The paper assesses the potential of this approach as well as the quality of the different derived data products within a numerical closed-loop simulated scenario.

The paper is composed of the following parts: Section 2 introduces the first initiatives towards NRT services based on diverse data sets as well as the first results from gravity based concepts. The simulated world, on which the NRT method is based, is described in Section 3. In Section 4, the proposed NRT concept and method are presented. In Section 5, the NRT processed scenarios and their results regarding precision and quality as well as the possible derived data sets are visualized. Finally, Section 6 provides conclusions and an outlook.

2 TOWARDS A GRAVITY-BASED NEAR-REAL TIME SERVICE

After years of successful exploitation of GRACE observations and its continued observations with GRACE FO the incentive to develop services and applications on the basis of global gravimetric observations of the time-variable gravity field has steadily grown. The aim is to shift the justification of NGGM away from a solely scientific community driven satellite mission to an operational observing system enabling us to provide additionally valuable services for managing Earth's resources like water, and to implement an early warning system regarding natural disasters.

Possible applications for a NRT service are within the hydrological extremes like floods and droughts. A flood is the rise and overflow of a large amount of water beyond its normal limits. The European Union (EU) Floods Directive defines a flood as a covering by water of land not normally covered by water. By contrast a drought can have various reasons and results in a prolonged shortage in the water supply. Usually it is caused by below-average precipitation. With gravimetric satellite missions only so called 'gravimetric' droughts are observable, meaning droughts with a deficit in total water storage. Unlike floods, droughts happen over a longer time period and are typically larger in spatial scale. Combined, floods and droughts are responsible for more than half of all natural disasters. Due to missing ground observations and not sufficiently precise weather forecasts (mainly due to lacking monitoring capabilities) they mostly affect densely populated regions in underdeveloped areas. A hydrological monitoring and early-warning/forecasting system fed by space-based gravity observations could fill these gaps by delivering global information and indicators for potential extreme weather phenomena.

Another application for a future NRT observation system is the monitoring of the whole seismic process. GRACE can only detect post-seismic changes of large earthquakes of the magnitude of at least 8.5. The pre-seismic build-up and its physical parameters such as increased seismicity, deformation and ground water variations start, depending on the earthquake, with gradual changes over several months or years prior or only a few months to a few days earlier with rapid change (Wang *et al.* 2018). At this point these precursor phenomena are only observable by ground-based monitoring systems, but not by a gravimetric satellite mission. However due to the noise of ground observation systems overshadowing the slow long-term build-up, a gravimetric observation from space of the pre-seismic phase is desirable.

2.1 Existing monitoring systems

Several regional and global forecasting and early-warning systems already exist. The Global Integrated Drought Monitoring and Prediction System (GIDMaPS) combines multiple drought indices based on precipitation and soil moisture measurements (Hao *et al.* 2014). The European Flood Awareness System (EFAS) is a fully operational system that gets updates in real time and provides early alerts on potential floods. Its predictions are based on topographical, meteorological and hydrological data. These predictions are then assimilated with near real-time river discharge and water level data (Pappenberger *et al.* 2011). In the project FloodMan funded by the European Commission (EC) a NRT flood monitoring system based on space borne SAR (Synthetic Aperture Radar) and optical data combined with *in situ* measurements, hydrological and hydraulic model data was developed (Malnes *et al.* 2005). One of the only data products based on gravimetric satellite data from GRACE available at the moment are weekly groundwater and soil moisture drought indicators computed by National Aeronautics and Space Administration (NASA). The index assimilates GRACE satellite data with other observation sources to a gridded data product of 0.125° resolution (Beaudoing *et al.* 2017).

To establish NRT monitoring applications based on gravimetric observations the EU Horizon2020 program funded the European Gravity Service for Improved Emergency Management (EGSIEM; <http://egsiem.eu/>) project. Its goal is to increase the temporal resolution of the gravity mass transport products from 1 month to 1 d and to reduce the latency for collecting data as well as processing from the current 2 months to 5 d. Due to the sparse coverage of GRACE during 1 d, additional information is introduced and processed within a forward Kalman filter least-squares estimation (LSA) to reach the desired temporal resolution. The dynamics of the underlying processes are derived

Table 1. Orbit parameters for satellite constellations.

Satellite pair	Altitude [km]	Inclination [°]	Revolutions/nodal		Drift rate/nodal days [deg d ⁻¹]
			days in one repeat orbit	Satellite distance [km]	
Near-polar	340	89	110/7	100	1.3/7
Inclined	355	70	109/7	100	1.3/7

from the stochastic properties of geophysical models, trying to avoid biases towards the involved models. Another output of the project is a gravity-based wetness indicator with a 2-d latency (Kvas *et al.* 2017) that supports the satellite-based flood information service GLOFAS (Global Flood Awareness System) as well as the framework of DLR's (Deutsches Zentrum für Luft und Raumfahrt) Center for Satellite Based Crisis Information (ZKI).

2.2 Needs and requirements for gravity-based NRT services

A possible monitoring service for hydrological extremes based on NRT gravity puts requirements onto the NGGM and the derived gravity fields. An ideal scenario would have a daily temporal resolution paired with a spatial resolution of 100 km. The spatio-temporal sampling underlies the Heisenberg rule (Weigelt *et al.* 2012), meaning the better the temporal sampling is, the worse the spatial sampling becomes and vice versa. In the case of the analysed NGGM constellation that means, that only one of the ambivalent goals can be reached. A reasonable and feasible temporal resolution is a daily and short period gravity field solutions (e.g. 3–5 d) with the highest possible spatial resolution achievable with the chosen satellite constellation to enable the detection, monitoring and forecasting of such events. Since it would be an operational service, which has to guarantee continuous measurements as well as a consistent quality, a constant altitude and constant uniform ground track coverage per time period are preferable. Another issue is that the required latencies are 7–10 d or shorter for drought monitoring, or 2–3 d at a maximum for short term event monitoring like floods.

In the following, based on various numerical closed-loop simulations the achievable temporal and spatial resolution of temporal gravity field solutions resulting from the NRT approach with short latencies shall be quantified. The simulation set-up is based on a Bender-type double pair mission, which is, from today's point of view, one of the most technologically feasible concepts.

3 NUMERICAL SIMULATION

3.1 Orbit design

As the first step, optimal orbits for a future constellation of gravimetric satellites need to be identified, such that a NRT application is possible. In the ESA-funded SC4MGV study (Assessment of Satellite Constellations for Monitoring the Variations in Earth Gravity Field, Iran Pour *et al.* 2015), one of the main findings was that there is a certain freedom in the orbit design of Bender-type mission concepts, because there is no perfect constellation and orbit design for the whole variety of potential applications. The study results also showed, that the retrieved time-variable gravity models did not have constant quality over time. This variability was attributed to the relative drift in the orbital nodes of the inclined and the polar pair. Therefore, in the follow-on ESA-study ADDCON (Additional Constellation & Scientific Analysis of the Next Generation Gravity Mission Concept; Purkhauser *et al.* 2018) orbits with the same drift rate within the subcycle for both satellite pairs and a retrieval period equal to the length of the subcycle were designed, so that the gravity field retrieval is always supported by the densest possible ground track pattern.

The chosen constellation is a Bender configuration (Bender *et al.* 2008), since it is a feasible constellation from an engineering point of view with a near-polar pair with an inclination of 89° (same as the GRACE orbit) and an inclined pair with an inclination of 70°. The satellite distance is 100 km and the drift rate as well as the subcycles were chosen according to the findings of the SCV4MGV study. The 7-d near-repeat orbit shifts by 1.3° after 7 d, meaning that the inter-leaving of the polar and inclined pair's ground tracks is the same every 7 d, even though the combined ground track pattern appears to drift eastwards. This allows the orbits to have longer repeat cycles in addition to the above-mentioned short subcycle. This orbit design is chosen to ensure a constantly high performance of the retrieved gravity field throughout the mission lifetime. Therefore, it is implicitly assumed that the satellites are orbiting in a drag-free mode in order to ensure a long-term stable satellite constellation. The orbit parameters of the simulation are listed in Table 1.

This constellation design must correspond with a short delay regarding the raw data availability, which is depending on a ground station in a polar region and a rapid data transfer, as well as the processing latency to enable a NRT service. The optimum case would be less than 1 d for collecting the raw data, which has to be processed within a few hours, plus the time needed for the gravity field processing itself.

3.2 Numerical simulator

For the closed-loop simulations the full-scale gravity field estimation software (Daras *et al.* 2015; Daras 2016) available at the Institute of Astronomical and Physical Geodesy (IAPG) of the Technical University Munich (TUM) was used. The orbit integration, according to the

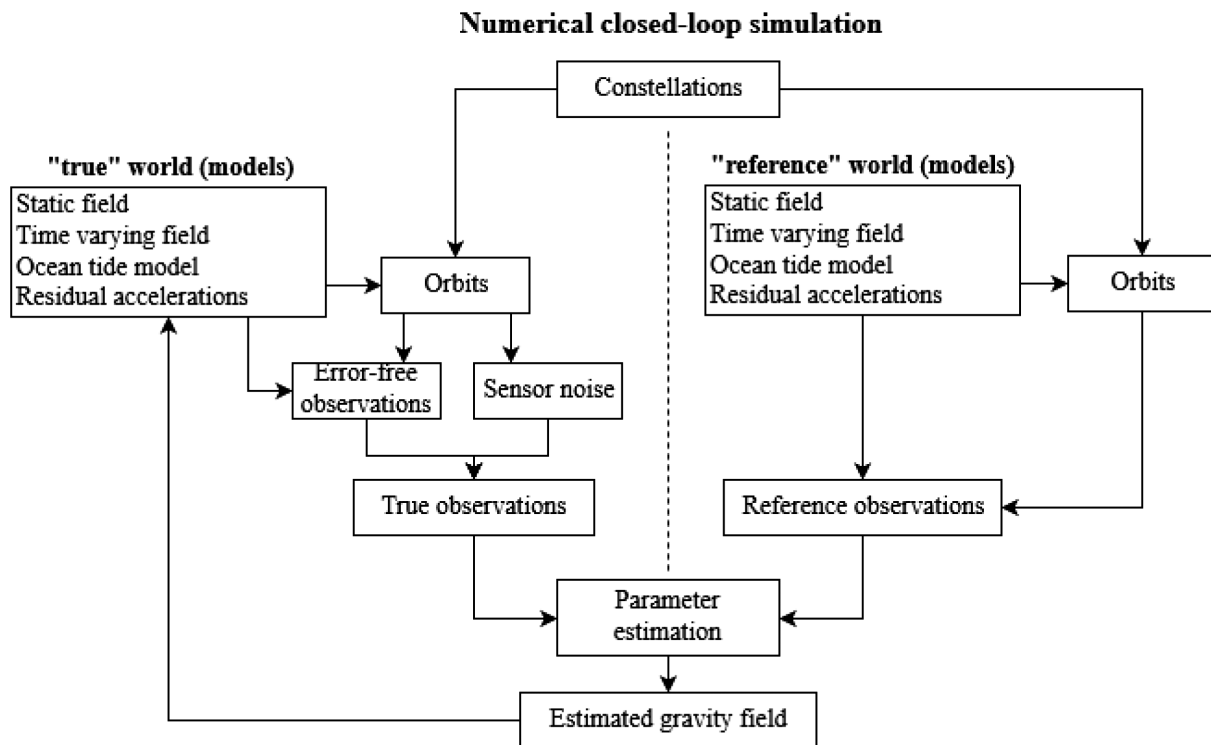


Figure 1. Schematic overview of the closed-loop simulation. Within both, the ‘true’ as well as the ‘reference’ world, observations are computed. While the ‘reference’ world does not include a time varying field, the ‘true’ world includes the time varying gravity field, a different ocean tide model than the ‘reference world’ in order to simulate model inaccuracies, and additionally sensor noise is added.

orbit parameters of Table 1, is based on a multistep method for the numerical integration (Shampine & Gordon 1975) with a modified divided difference form of the Adams Predict-Evaluate-Correct-Evaluate (PECE) formulas and local extrapolation (Montebruck & Gill 2000).

Within the simulator a modification of the integral equation or short-arc approach (Schneider 1969) is used. The approach divides the satellite orbit into equal arcs. In the present case arcs of 30 min length is used, where the coordinates of the nodal points of the arcs are set up as unknown parameters (Yi 2012; Daras 2016). The functional model is based on a hl-sst component, the intersatellite range rates and as the hl-sst component, kinematic orbits are used to determine the position difference of the satellite pairs. These observation types were chosen due to computational efficiency. An improvement of the retrieval and respectively solution could be achieved in the lower degrees, especially degree 2, if the absolute position is used as the hl-sst component. The short arcs are accumulated on a daily basis and results in daily normal equations over a dedicated time span. The system is solved by least-squares adjustment using a standard unbiased Gauss–Markov model, with the expected mean value of the random error being zero.

Additionally the Wiese approach (Wiese *et al.* 2011), already investigated by Daras & Pail (2017) for its potential to retrieve the full AOHIS signal instead of the usage of AO (Atmosphere and Ocean) dealiasing models for NGGM constellations, is used within the simulation. The approach co-estimates low-degree gravity fields at short time periods (e.g. daily) together with higher resolution gravity fields for a longer time interval. Thereby long-wavelength high-frequency signals are estimated by low-degree, daily gravity field parameters, thus avoiding that they alias into the higher-degree estimates. Technically, in order to avoid very large normal equation (NEQ) systems, the parameter groups of low-degree daily gravity parameters are categorized as local parameters and eliminated before the least squares adjustment (Koch 1997), while both full and reduced NEQ systems are stored. After the higher order gravity field coefficients have been estimated, the lower order coefficients can be computed by backward substitution with the help of both sets of NEQs.

On the basis of the defined constellation (see Table 1) a ‘true’ and ‘reference’ world (see Fig. 1) and subsequently ‘true’ and ‘reference’ hl-sst and ll-sst observations are computed on the basis of the models listed in Table 2. As static gravity field the GOCO03s model (Mayer-Gürr *et al.* 2012) up to maximum expansion degree and order (d/o) 120 is included in all generated dynamic orbits. The updated Earth System Model (ESM) of ESA (European Space Agency, Dobslaw *et al.* 2013) is introduced in the true world scenario to simulate the non-tidal time-varying gravity field (AOHIS). The ESA ESM model is available as 6-hourly snapshots that are linearly interpolated and are used as input to generate dynamic orbits. The ‘true’ GOT4.7 (Goddard Ocean Tide) tide model is the latest update of the GOT99 model and is based on altimetric data (Ray 1999), while the ‘reference’ EOT08a (Empirical Ocean Tide) model is based on the FES2004 model (a tidal atlas computed from the tidal hydrodynamic equations) and was updated by the analysis of multimission altimeter data (Savcenko & Bosch 2008).

Table 2. Force and noise models of the ‘true’ and ‘reference’ world used in the full-scale simulations.

Model	‘True’ world	‘Reference’ world
Static gravity field (GF) model	GOCO03s	GOCO03s
Time varying GF model	ESA AOHIS	–
Ocean tide model	GOT4.7	EOT08a
Noise model	Residual drag, eqs (5–7)	Residual drag, eqs (5–7)
Noise model	Laser interferometer noise, eq. (2)	–
Noise model	Accelerometer noise, eqs (3–4)	–
Noise model	Star camera noise, eqs (8 and 9)	–

Additionally the computed observations are superimposed by sensor noise for the laser interferometer, accelerometer, star camera as well as non-compensated non-conservative forces (in the following called residual drag, see Table 2). With this set-up realistic pre-fit residuals can be computed, and the following least squares adjustment can be processed.

The gravity fields are parametrized as spherical harmonics (SH). Therefore, the set-up of the NEQ systems is done with SH base functions of the Earth’s gravitational potential V , which can be expressed by the series expansion (Hofmann-Wellenhof & Moritz 2005):

$$V(r, \theta, \lambda) = \frac{GM}{a} \sum_{n=0}^{\infty} \left(\frac{a}{r}\right)^{n+1} \sum_{m=0}^n \bar{P}_{nm}(\cos\theta) (\bar{C}_{nm} \cos m\lambda + \bar{S}_{nm} \sin m\lambda), \quad (1)$$

where GM represents the product of the gravitational constant and the Earth’s mass, a the semi-major axis of the Earth, \bar{P}_{nm} the fully normalized Legendre polynomial of degree n and order m , \bar{C}_{nm} and \bar{S}_{nm} the fully normalized SH coefficients, and the location is given by the radius r (geocentric distance of the satellite), geocentric colatitude θ and longitude λ .

3.3 Stochastic modelling

The error assumptions of NGGMs used in this paper are identical to the ones used in the frame of the ESA project SC4MGV (Iran Pour *et al.* 2015) and were provided from the consultancy support of Thales Alenia Space Italia (TAS-I). Within the simulations the following four error sources were considered: the laser ranging instrument noise, the accelerometer noise, the star camera noise, that is the pointing noise, and the residual non-conservative accelerations (residual drag), which is caused by imperfect drag compensation. The noise of the error sources are all frequency dependent and are approximated by analytical equations.

The noise time-series of the on-board sensors were scaled by the spectrum of normal distributed random time-series with the individual spectral models. The principal measurement unit of the inter satellite distance, the laser ranging instrument, is characterized by an analytical noise model described by the Amplitude Spectral Density (ASD) and expressed in terms of range rates:

$$d_{range\ rates} = 2 \cdot 10^{-8} \cdot 2\pi f \sqrt{\left(\frac{10^{-2} Hz}{f}\right)^2 + 1} \frac{m}{s\sqrt{Hz}}. \quad (2)$$

The on-board accelerometer senses the linear non-gravitational accelerations and the angular accelerations acting on the satellites with air drag being the main contributor. The assumed accuracy level is similar to the sensors used on the mission GOCE (gravity field and steady-state ocean circulation explorer; Drinkwater *et al.* 2003) and is expressed by:

$$d_{acc. x} = d_{acc. z} = 10^{-11} \sqrt{\left(\frac{10^{-3} Hz}{f}\right)^4 / \left(\left(\frac{10^{-5} Hz}{f}\right)^4 + 1\right) + 1 + \left(\frac{f}{10^{-1} Hz}\right)^4} \frac{m}{s^2\sqrt{Hz}}, \quad (3)$$

$$d_{acc. y} = 10 \cdot d_{acc. z}, \quad (4)$$

with x being the along-track, y across-track and z the quasi-radial component. Since the satellite is assumed to fly in drag-free mode, the biggest part of the non-gravitational forces is compensated by a propulsion system consisting of ion thrusters.

The residual drag accelerations represent errors of the drag compensation and can be observed by the accelerometers. The ASDs of the analytical noise model in all three directions are

$$d_{res.drag.x} = 10^{-9} \sqrt{\left(\frac{2 \cdot 10^{-4} Hz}{f}\right)^4 / \left(\left(\frac{2 \cdot 10^{-5} Hz}{f}\right)^4 + 1\right) + 1 + \left(\frac{f}{10^{-1} Hz}\right)^4} \frac{m}{s^2\sqrt{Hz}}, \quad (5)$$

$$d_{res.drag.y} = 10^{-9} \sqrt{\left(\frac{4 \cdot 10^{-5} Hz}{f}\right)^4 / \left(\left(\frac{2 \cdot 10^{-5} Hz}{f}\right)^4 + 1\right) + 1 + \left(\frac{f}{10^{-1} Hz}\right)^4} \frac{m}{s^2\sqrt{Hz}}, \quad (6)$$

$$d_{res.drag,z} = 2 \cdot 10^{-10} \sqrt{\left(\frac{8 \cdot 10^{-4} Hz}{f}\right)^4 / \left(\left(\frac{10^{-5} Hz}{f}\right)^4 + 1\right) + 1 + \left(\frac{f}{10^{-1} Hz}\right)^4} \frac{m}{s^2 \sqrt{Hz}}. \quad (7)$$

The star camera sensor errors are represented as rotation angles starting from the along-track (*roll*), cross-track (*pitch*) and radial (*yaw*) axes and are used to compute quaternions to simulate the attitude noise. The ASD of the analytical noise model for roll, pitch and yaw can be expressed by

$$d_{roll} = 10^{-5} \sqrt{\left(\frac{10^{-3} Hz}{f}\right)^4 / \left(\left(\frac{10^{-5} Hz}{f}\right)^4 + 1\right) + 1} \frac{rad}{\sqrt{Hz}}, \quad (8)$$

$$d_{pitch} = d_{yaw} = 2 \cdot 10^{-6} \sqrt{\left(\frac{10^{-2} Hz}{f}\right)^2 / \left(\left(\frac{10^{-5} Hz}{f}\right)^2 + 1\right) + 1} \frac{rad}{\sqrt{Hz}}. \quad (9)$$

With the assumption of a stationary sensor noise its weighting can be accomplished by computing the inverse of the covariance matrix (Daras & Pail 2017; Daras 2016) containing the auto-covariance values of the estimated pre-fit residuals. The hl-sst and ll-sst observations are considered as uncorrelated, so that the weighting matrices can be set up separately.

In addition to the sensor noise, the NNGM simulations include temporal aliasing effects due to temporal undersampling of the signal to be recovered, uncertainties in the non-tidal dealiasing models (which are not used within this paper due to the processing strategy to estimate the full time-variable signal by applying Wiese parametrization), and uncertainties in the ocean tide model (represented by differences between two different ocean tide models). If not treated appropriately, the high-frequency signal (all signal components with frequencies above the Nyquist frequency) would alias into the gravity field solution. In order to reduce this effect, as already mentioned in Section 3.2 the Wiese approach is applied. Further information on the simulation environment can be found in Daras (2017) and Hauk & Pail (2018).

4 NRT APPROACH

The following section details the developed NRT approach. First, it introduces the basics of the implemented sliding window technique and the so-called Wiese approach (Wiese *et al.* 2011). Then the differences of the NRT approach in comparison with a nominal processing scheme (see Fig. 2) is shown. The following flow-chart (see Fig. 3) depicts the combined elements of Wiese approach an NRT processing. Lastly, a spectrally enhanced daily solution is presented, with the goal to achieve high temporal as well as spatial resolution.

4.1 Sliding window technique

Up to this point the information going into a gravity field solution (apart from correlations due to the Wiese approach) was completely separate and therefore uncorrelated to information going into the next solution. To decrease the latency of these gravity solutions, the daily NEQ's determined for the previous processing can be used, along with the daily NEQ of the latest day, to quickly create new solutions. The main benefit of this sliding window averaging over several days on the level of NEQ's, is the higher sampling rate and therefore a shorter latency. In terms of filtering the sliding process uses constant weight and can therefore be described as a boxcar window.

In comparison Sakumura *et al.* (2016) uses a CRN filter combined with a regularization and mascons basis functions in a similar approach to obtain high-frequency terrestrial water storage signal from GRACE.

4.2 Wiese approach

The NRT analysis is based on the short-arc approach in combination with the Wiese approach implemented within the IAPG software package (Section 3.2). In this study, daily Wiese parameters are co-estimated, which turned out to be optimum in detailed previous studies (Daras 2016; Daras & Pail 2017). The Wiese approach is used to reduce temporal aliasing effects acting on the gravity field solutions. This 'self-dealiasing' method stands in contrast to the commonly used de-aliasing method, where information about temporal variations in the Earth's gravity field caused by the high-frequency atmosphere and ocean mass variations are reduced a priori from the observations. Additionally it is utilized to estimate gravity field solutions at a convenient short-time interval.

4.3 Normal versus NRT processing

Fig. 2 shows the architecture of the NRT method proposed in this study, exemplarily for a retrieval period of 3 d in comparison with the standard processing for the same retrieval period. In standard processing consecutive time spans of data, in our example 3 d are used to set up daily NEQ's for the low (up to degree N) as well as the high gravity field (GF) coefficients (degrees $N + 1$ to N_{max}) to estimate on the

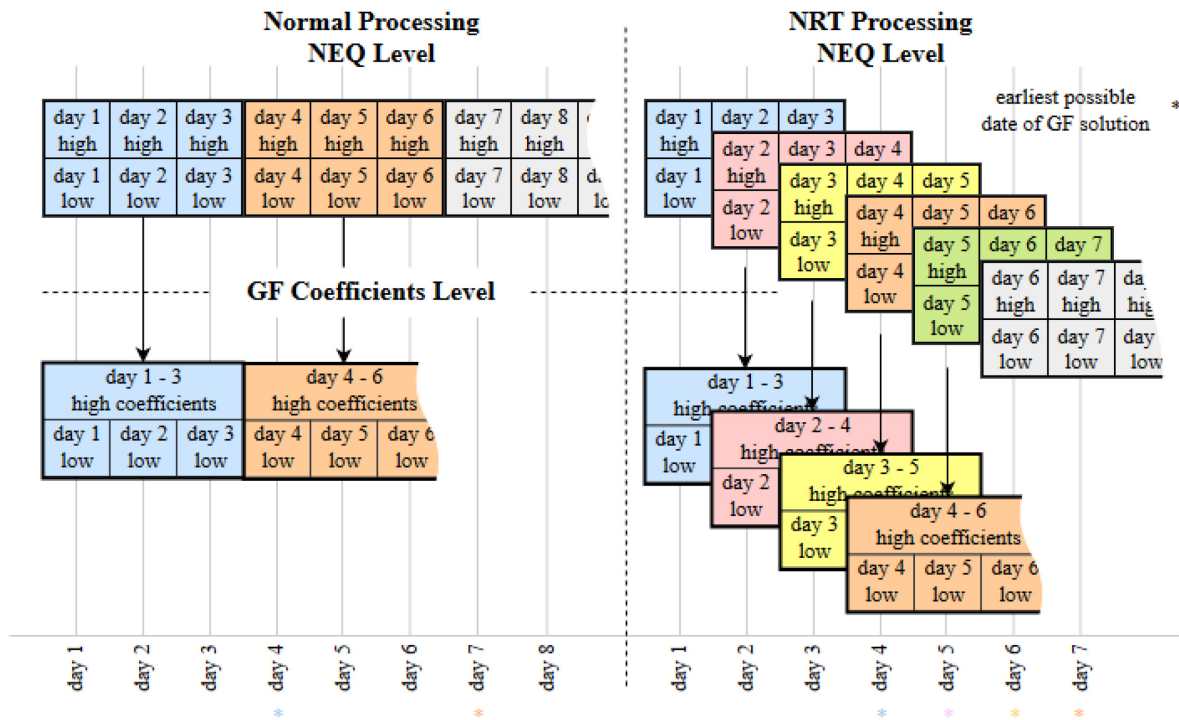


Figure 2. A normal processing as well as the near-real time processing on a NEQ level as well as on the gravity field coefficients level, both with the Wiese parametrization and a retrieval period of 3 d. While the normal processing always picks consecutive, not overlapping time periods according to the retrieval period, the NRT processing is a window averaging on the NEQ level reusing the already computed and stored NEQs of the former GF solutions. Due to the sliding window approach a new set of resulting solutions is determined every day. The earliest possible date (assuming an overall data acquisition and processing time of 1 d) of each processed gravity field is marked with a star (*) in the time axis with the corresponding colour of the data block.

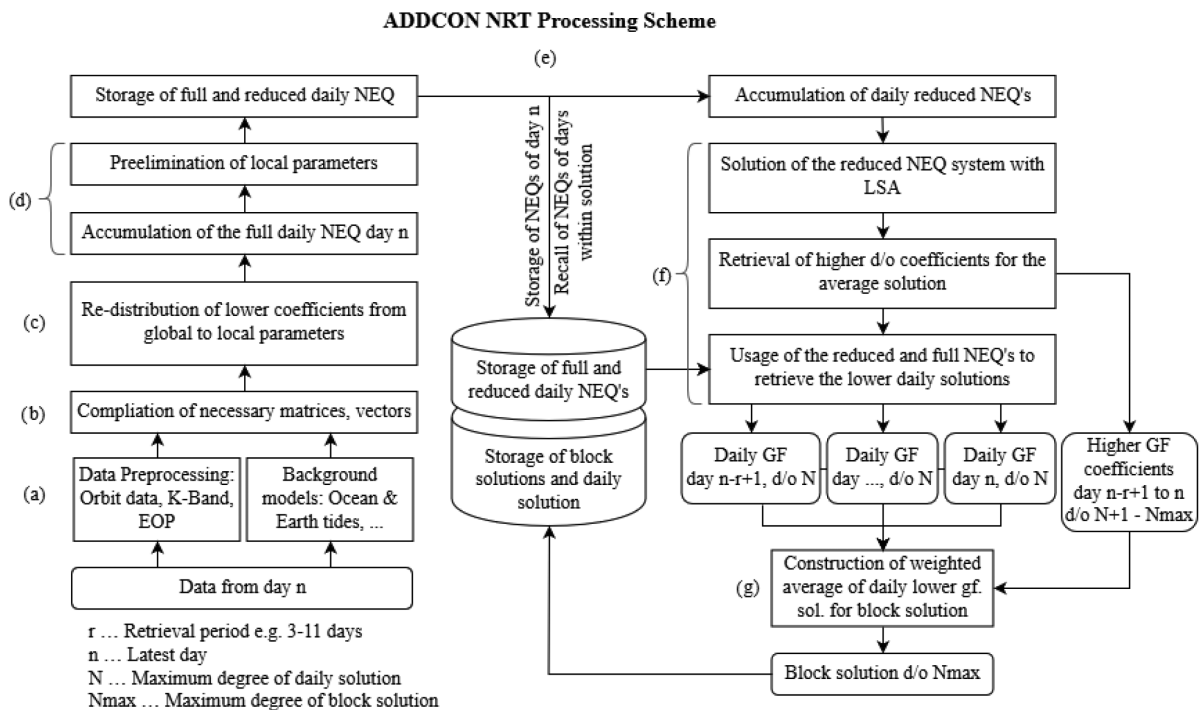


Figure 3. Proposed NRT Processing Scheme. To efficiently determine the NRT GF solutions an adequate storage management is necessary (barrels in the middle).

one hand daily long-wavelength solutions resolved up to a certain degree N (indicated by ‘low’ in Fig. 2), as well as a joint solution from all 3 d for the degrees $N + 1$ to N_{max} (‘high’). In contrast, instead of using consecutive time spans in the NRT method a sliding window is applied. Day by day, only the data of the latest day is added to the time period while the first day of the previous solution is skipped. From a computational point of view, since the short arcs for both ‘low’ as well as the ‘high’ NEQs are accumulated as daily batches, the NEQs can be reused for the following GF solutions. On a GF coefficient level, in contrast to the standard processing, the daily gravity fields of a certain day are computed within different time spans. These daily solutions computed within a certain processing time span are no longer uncorrelated, but rather have a correlation with the other days used in the computation. From the viewpoint of theory, this is one of the major drawbacks of the NRT strategy. However, it will be shown in Section 5.3 that the difference of daily solutions computed within different time spans is marginal.

4.4 NRT processing

Fig. 3 depicts the processing scheme of the NRT approach incorporated into the short-arc approach combined with the Wiese approach, with r representing the retrieval period, n being the latest day in day of year (doy), N being the d/o of the daily Wiese solution, and N_{max} representing the maximum expansion of the whole gravity field solution. Due to the possibility of reusing the determined NEQ’s and reduced observation vectors from former solutions, the first part [steps a) to (e) in Fig. 3] is only necessary for the latest day within the processing (as Fig. 2 shows).

The following steps of the processing chain are necessary to enable a NRT processing:

(i) The processing chain starts with collecting and pre-processing the necessary data of the latest day n such as the kinematic orbit data, the K-band ranging observations as well as the accelerometer and star camera measurements, and the latest EOP (Earth orientation parameter) data sets. Additionally, the necessary background models are computed for the latest time span.

(ii) With those data sets the necessary matrices and vectors can be compiled. This means in case of the short-arc approach the design matrix as well as the boundary condition matrix containing the condition that the initial position of a certain arc must be the same as the position of the end point of the previous arc, the observed and computed vectors for each short arc for the range-rate or KBR measurement and the position difference determined or difference of the kinematic orbit solution.

(iii) To initiate the Wiese approach, the lower GF coefficients are redistributed from global to local parameters (i.e. boundary values and empirical accelerations) to be co-estimated.

(iv) Next, the daily NEQ’s are accumulated, followed by the pre-elimination of the local parameters so that a reduced system of NEQ’s can be formed.

(v) To allow for the future usage of the computed matrices and vectors, they are stored. The former days already stored and necessary for the solution are retrieved from storage to accumulate the reduced NEQ’s over the whole retrieval period r .

(vi) After the accumulation of the daily reduced NEQ’s and of the reduced observation vector the LSA estimates a set of higher coefficient. The reduced and full NEQ’s, previously stored, together with the higher degree GF coefficients are used to retrieve the lower daily GF coefficients by means of a back-substitution.

(vii) To get a GF field solution over the maximum expansion spanning all days included in the solution, the lower daily GF coefficients are combined by a weighted average

$$c_{nm} = \frac{\sum_{days} [s_0^2 c_{nm}^{daily}]}{\sum_{days} s_0^2}, \quad (10)$$

with the a posteriori variance of the unit weight s_0^2 and merged together with the higher coefficients. In the case of homogeneous sampling and the absence of data gaps as in the presented simulation scenario, the difference to an arithmetic mean is vanishingly small.

In our example, for the processing of a new solution the data of the whole latest day is necessary. The GF processing latency depends on the availability of the needed input data. This means that every data set has theoretically a processing latency of maximum 1 d, while the normal processing waits till a whole new set of necessary days of data according to the retrieval period are accumulated before processing a GF solution, meaning a processing latency of 4 d and more for a 3-d retrieval period (see Fig. 2).

In comparison to the sliding-window NRT method proposed here, the two NRT approaches performed within the EGSIM project (Kvas *et al.* 2017) both rely only on the currently available data of the single-pair GRACE data, meaning a very sparse daily data coverage, and therefore they have to use additional information to constrain the daily solutions. In the case of the TUG (Technical University of Graz) strategy the computation is based on the short-arc approach combined with a Kalman filter with a state-transition matrix filled with stochastic properties of the underlying geophysical models (Kvas *et al.* 2017). The GFZ (Geoforschungszentrum Potsdam) in comparison relies on adding covariance information from hydrological, atmospheric and oceanic models as well as GIA (Glacial Isostatic Adjustment) to constrain the NRT products. Both processing strategies rely on the dealiasing product (Gouweleeuw *et al.* 2018). In contrast, no *a priori* information on the signal properties is necessary for the sliding-window NRT approach, which is purely databased. This can be considered as a big advantage. However, the daily higher-degree estimates are no longer uncorrelated, but have a correlation length corresponding to the retrieval period. Additionally, due to the Wiese parametrization being part of the proposed NRT processing scheme, AO dealiasing is not necessary. This advantage, of course, is fostered by the assumption of a Bender-type double-pair mission.

Table 3. Parameters of the processed scenarios.

Scenario	Retrieval period	Daily Wiese solution d/o	Overall d/o	Usable signal till d/o	Determined solutions [d]
1a	7	20	75	60	1–178
1b	7	15	75	60	1–178
2a	3	15	75	50	1–3
2b	3	15	50	50	1–178

Apart from the AO dealiasing product, all NRT processing strategies based on gravimetric satellite observations need the EOP data provided by the IERS (International Earth Rotation and Reference Systems Service) within 1–3 d, rapid GPS orbits and clocks provided by the University of Bern within 17 hr, the GRACE L1B quick look data offered with a latency of approximately 1 d and in the case of the EGSIM approaches the AO dealiasing products provided within a time frame of 1 d. If a reduction of the overall latency is requested, these data sets will have to be provided within a shorter time period.

4.5 Daily solutions with increased spatial resolution

Daras & Pail (2017) found that the optimal sampling period for the Wiese short time solution of Bender pairs is 1 d for reducing the error levels in the overall long time solution. It is the best compromise between capturing the biggest amount of signal and the shortest time in which it changes. The paper also mentions that the largest improvement was detected with a daily coparametrization of d/o 20, with d/o 10, 20 and 30 being tested in the scope of the analysis.

A maximum expansion of, for example d/o $N = 20$ of the daily Wiese gravity field means a spatial resolution of 1000 km in the analysed constellation design. The desired goal (as stated in Section 2.2), however, is to compute a solution with a short temporal resolution combined with a spatial resolution of 100 km. To achieve a spatially improved GF solution, the result can be spectrally enhanced. This is done by extending the daily solution with the corresponding 3-d average solution for the higher coefficients from $N + 1$ to N_{max} with the central day the same as the daily solution. Technically, this means that in Fig. 2 we eliminate the parameters of the daily solution on the outside, leaving the parameters of the middle or reference daily solution as well as the higher coefficients (see Fig. 3). The resulting daily gravity field solution has now the same spatial resolution as the overall block solution of the averaged daily solutions and the higher coefficients and the desired temporal resolution of 1 d. The downside is clearly aliasing from the eliminated daily Wiese solutions into the higher degrees. An evaluation presented in Section 5 shows, that the effects are minor and can therefore be neglected. Simulations run by Gunter *et al.* (2006) demonstrated that in the absence of significant modelling errors the omission error due to the truncation of the measurement partials is not a significant error source.

5 RESULTS

In this study the attempt was made to combine the so-called ‘Wiese approach’ with the processing scheme for NRT GF solutions within a half year time span starting at the beginning of the year 2002. Listed in Table 3 are the possible data products of a NRT GF solution: the daily Wiese solution (hereinafter referred to as *DWSol*, see Fig. 4 and Table 4 as reference), the block solution consisting of the weighted average of the daily Wiese solutions and the higher degree coefficients combined (being referred to as *BSol*) and also the enhanced daily solution described above (single daily solution enhanced by higher-degree coefficients, referred to as *EDSol*). The weighted averaging in the case of *BSol* is done based on the variance-covariance information of the involved daily solutions.

As a first step NRT gravity field solutions according to Scenario 1 with a 7 d repeat period of the orbit and a daily Wiese solution complete to degree and order 20 (Scenario 1a) and 15 (Scenario 1b) were estimated. Since the computation with a 7-d period was successful, it was repeated with an even shorter retrieval period of only 3 d (Scenario 2a). Further the parameter model was cut to a maximum degree of 50, which is the resolution where the signal-to-noise ratio is approximately equal to one (Scenario 2b).

Depending on the observation technique, observation noise, signal attenuation as well as the satellite having an impact on the signal-to-noise ratio (SNR) the maximum resolvable degree varies. Within the analysed scenarios a solution till d/o 60 for a retrieval period of 7 d (see Fig. 5 left), and d/o 50 for a retrieval period of 3 d (see Fig. 5 bottom right) could be achieved.

5.1 Daily Wiese d/o 15 versus 20

Daras & Pail (2017) recommend a short-term Wiese solution with a maximum expansion till d/o 20 and an estimation period of 1 d due to high signal variability of a daily solution up to d/o 20. They also showed that higher daily solutions of, for example d/o 30 lead to artefacts within the solution because of violation of the Nyquist sampling theorem (spatial undersampling; Weigelt *et al.* 2013). Since the short-term GF quality plays a crucial role for the reduction of temporal aliasing effects in the long-term solution, d/o 20 was chosen as a starting point for the analysis (Scenario 1a). In Fig. 5 (top left), all estimated GF over the analysed time range are visualized in terms of degree RMS in

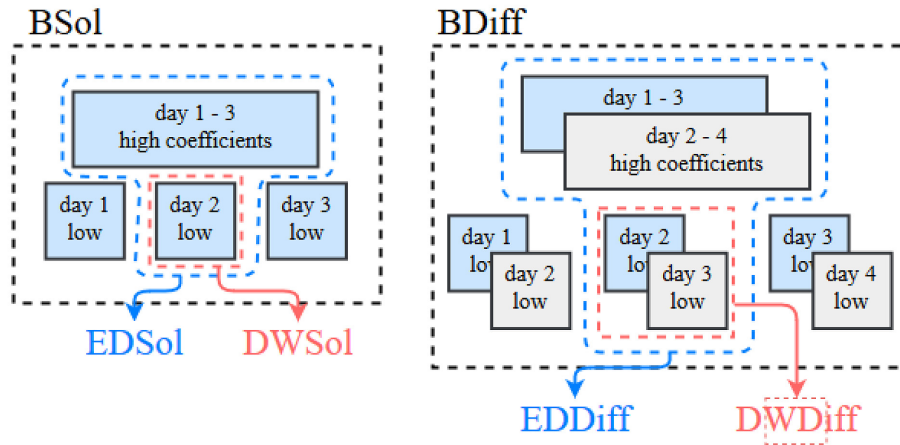


Figure 4. Resulting solutions from the NRT processing: the block solution (BSol, indicated in the dashed black line), the daily Wiese solution (DWSol, the dashed red line) and the enhanced daily solution (EDSol, indicated in the dashed blue line). The differences are correspondingly the block difference (BDiff, indicated in the black dashed line), the daily Wiese difference (DWDiff, marked in the dashed red line) and the spectrally enhanced difference (EDDiff, indicated in the dashed blue line).

Table 4. Possible data products derived from Scenario 2b. (*use with caution).

Product	Time range [d]	Overall [d/o]	Usable signal till [d/o]	Abbreviation
Block Solution	3	50	50	BSol
Block Difference	3	50	20	BDiff
Daily Wiese Solution	1	15	15	DWSol
Daily Wiese Difference	1	15	15	DWDiff
Spectrally Enhanced Daily Solution	1	50	50	EDSol
Spectrally Enhanced Daily Difference	1	50	20*	EDDiff

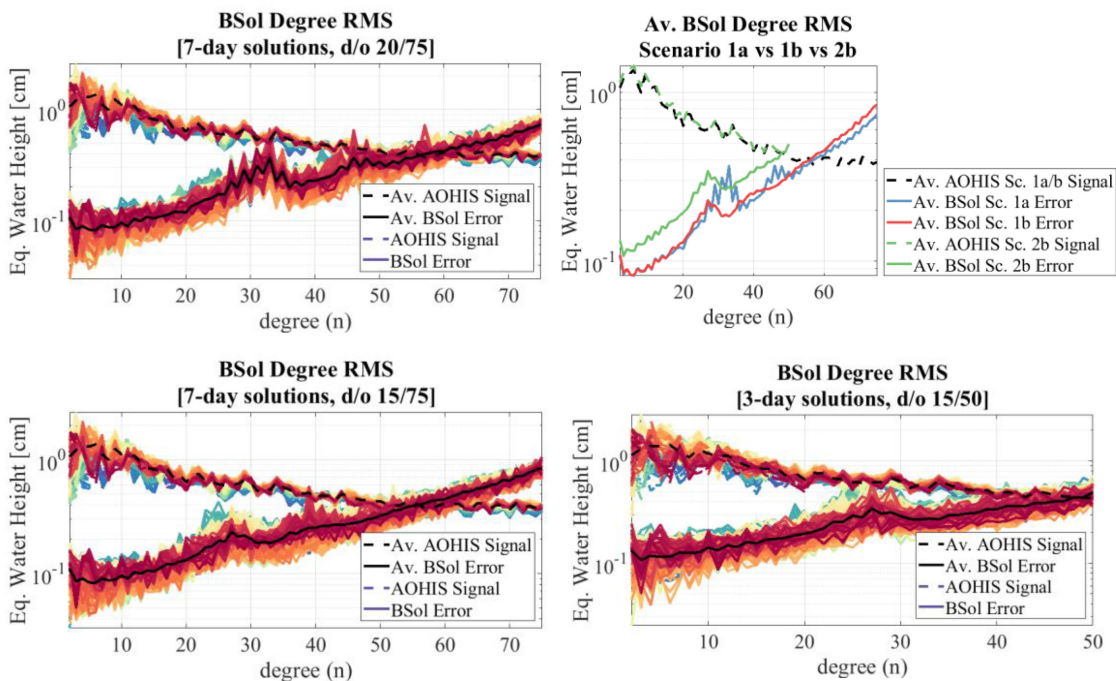


Figure 5. Degree RMS of block solution (BSol). All blocks within the half year time span in are visualized in different colour ranging from the first block solution in blue, over yellow, orange to the last block solution in a dark red, while an average signal and error curve depicted in black. Top left: Scenario 1a with a retrieval period of 7 d and a daily Wiese solution complete to d/o 20. Top right: Comparison of the average signal and error curves of the three scenarios displayed the other graphs of the figure. Bottom left: Scenario 1b with a retrieval period of 7 d and a daily Wiese solution complete to d/o 20. Bottom right: Scenario 2b with a retrieval period 3 d and a daily Wiese solution complete to d/o 15.

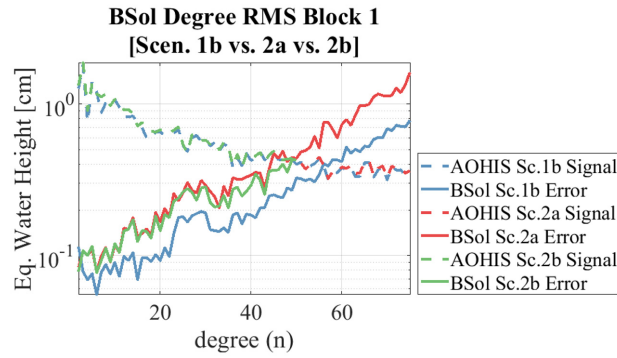


Figure 6. Degree variances of Scenario 1b, 2a and 2b. A reduction of the maximum degree of the expansion leads to an improved accuracy within the maximum resolvable degrees.

equivalent water heights (EWH)

$$\sigma_n(EWH) = \frac{a\rho_e}{3\rho_w} \frac{2n+1}{1+k_n} \sqrt{\sum_{m=0}^n c_{nm}^2 + s_{nm}^2}, \quad (11)$$

where ρ_w and ρ_e represent the average density of water and Earth, a the semi-major axis of the Earth, k_n the love numbers and c_{nm} and s_{nm} represent the SH coefficients. In black the average signal and error curves are displayed (Wahr *et al.* 1998; Schrama *et al.* 2007). They cross each other around d/o 55 corresponding to a spatial resolution of 360 km. Apart from small parts (e.g. between d/o 20 and 25 the degree variances within the blue colour range are visible above the other lines) the different error curves show very similar behaviour within a certain bandwidth. Small deviations from a smooth error curve are visible between d/o 25 and 35 and again in a lower intensity between 45 and 50. This behaviour is very similar to the already detected issues by Daras & Pail (2017) due to a non-ideal temporal parametrization of the co-estimation of the non-tidal high-frequency atmospheric and mass variations.

To improve the error behaviour Scenario 1b was created with a reduced daily maximum expansion of d/o 15. Fig. 5 bottom left shows the degree variances per block displayed on top of each other, with the reduced maximum degree of the *DWSol*. In comparison to Fig. 5 (top left) the high peaks are removed almost completely, instead a small bump between d/o 20 and 30 that was previously concealed by the larger artefacts is visible.

Fig. 5 on the top right depicts a direct comparison of the average degree variances over the whole study period of all three long-term scenarios (1a and b, 2b) that were estimated. If only Scenario 1a and b are compared (decrease the maximum d/o of the daily SH coefficients from 20 to 15 degree), the average error signal between d/o 0 and 15 is not affected, while a marginal deterioration over the whole error range is visible apart from the artefact areas, where a clear improvement can be observed. As a conclusion the reduction of the daily Wiese solution to degree 15 is recommended. It is the best compromise between short term solution with the highest possible spherical harmonics expansion and good quality of the long term gravity fields determined in parallel.

5.2 7-d solution versus 3-d solution

Since the NRT solutions with a retrieval period of 7 d were successful, a shorter retrieval time period, namely a 3-d retrieval period, was chosen. The latter corresponds to the set-up that is exemplarily shown in Fig. 2. A first test (Scenario 2a) with coefficients estimated till d/o 75 showed that the SNR turned 1 at around d/o 50, meaning a spatial resolution of 400 km (compared to 360 km of the 7-d retrieval period). When comparing the degree variances to the 7-d solutions the same behaviour of the average degree variances curve as Scenario 1b is visible. This means that the chosen retrieval period does not have an effect on the characteristics of the error curve.

Due to the SNR turning 1 shortly before d/o 50, a reduction of the estimated coefficients to 50 (named Scenario 2b) was performed. A comparison of Scenario 2a and 2b (see Fig. 6) shows, that due to the earlier cut-off period the overall solution accuracy improved by approximately 1 mm in equivalent water height (EWH) cumulative error up to d/o 50 for the first analysed block. Therefore, in this case a gravity field retrieval up to d/o 50 was chosen. An overall recommendation however of a determination of gravity field solutions only slightly above the cross-over point of the signal and noise curves cannot be stated, since the degree RMS representation is a global average, and therefore underestimates short spatial-scale high-amplitude phenomena, which might be missed by cutting the series expansion too early.

If all degree variances of the computed *BSol* within the analysed time span are visualized (see Fig. 5 bottom right) the same error characteristics as Scenario 1b can be detected. This also is depicted in Fig. 5 top right, where the average error and signal curves are shown.

5.3 Daily solutions of the same day calculated within different time spans

Due to the sliding window characteristics of the NRT processing scheme, where always the first day of the previous solution is excluded and the data of the latest day is added, data of the same day is used for various gravity field solutions. Regarding the daily Wiese solutions

DWSol, the number of multiple solutions for a specific day equals to the number of days of the retrieval period. These daily solutions are based upon the same daily accumulated NEQs, but due to their multiple usage in the sliding window NRT approach, different correlations with the respective higher-degree coefficients (degrees $N + 1$ to N_{max}) show up (see Fig. 2 as reference). However, a detailed analysis of these various daily solutions of the same day show negligible differences among each other, indicating that the process is stable. Even though the estimated low spatial resolution daily fields *DWSol* are almost identical, we find that in 44 per cent of the cases the central solution (i.e. the second day in a 3-d solution) is the best solution, and in only 15 per cent of the cases it is the worst. Due to this reason as well as being in the centre of the solution the middle day of any *BSol* is generally picked as the daily baseline solution of the NRT processing scheme and furthermore called reference day. This also means a larger latency for the ‘middle day’. Therefore, for time-critical applications the first day should be used. Within the spectrally enhanced solution *EDSol*, the reference day is used within this analysis as the basis for the computation.

5.4 Possible resulting solutions and their characteristics

The following discussed solutions of the NRT processing are based on Scenario 2b with a retrieval period of 3 d, a *DWSol* of 15 d/o, and an overall maximum expansion up to d/o 50 (see as reference Table 4). The base product is the *BSol* determined from the weighted average of the *DWSol* and the corresponding estimated higher GF coefficients. The *BSol* has a 3-d temporal resolution and the SNR on average becomes one right before d/o 50 meaning a spatial resolution of 400 km. If visualized as differences to the true reference solution (AOHIS from ESA ESM model) some striping can be seen in the solution (Fig. 7), and its cumulative error is 16.4 mm in EWH.

The Wiese approach delivers a solution with the desired short temporal resolution of 1 d with the drawback of having only a maximum spherical harmonics expansion of d/o 15 corresponding to 1350 km spatial wavelength. For the complete spectrum of the *DWSol* of the reference day, the error curve lies beneath the signal curve (see Fig. 9). Fig. 7 top row depicts the three daily Wiese solutions of block 1 with a cumulative error ranging between 6 and 7 mm in EWH. To improve the spatial resolution of the *DWSol*, the *EDSol* was created. The *EDSol* features a daily temporal resolution combined with the spatial resolution of the block solution. Due to the influences of the border days (in case of block 1, consisting of day 1, 2 and 3 this means that in the higher degrees the signal of day 1 and 3 influences the solution) the SNR is not as good as in the block solution, however the error curve is below the signal, meaning that the gravity field is resolvable up to the same d/o same as the block solution (see Fig. 9 bottom left). The cumulative error of the *EDSol* is with 19.1 mm in EWH higher, than the cumulative error of the *BSol* of 16.4 mm EWH (both values of the first block (block 1) in the time span).

A detailed analysis shows that the arising leakage in a spatial representation in EWH is dominant in the higher altitudes (see as example block 1 in Fig. 8 left) throughout the analysed time period. The cumulative error of the error signal is 7.7 mm. If the true daily AOHIS signal is compared with the signal truly present in the simulated signal, the true daily AOHIS signal appears to be damped. The complete *EDSol* error is computed by the difference of the *EDSol* and the true daily AOHIS signal, consisting therefore of the error itself and a bias due to the signal of the two additional days in the higher SH coefficients. Excluding these 2 d in the reference AOHIS signal results in the orange dashed line in Fig. 8 (right). Starting at degree 16 a drop due to the removal of the bias (meaning the additional days needed to solve the LSA) can be seen, that approaches the complete error more and more. The Δ Degree RMS is decreasing from 0.04 to below 0.01 EWH cm in the signal as well as in the error curve.

This reduction of accuracy can be accepted, since the biased error lies within the variability of the signal for the whole processing period of half a year. Also the gained spatial resolution has to be taken in account.

All estimated gravity fields (in case of the *DWSol* always the reference solution was picked) for the analysed time period are visualized in terms of degree variances in Fig. 9. The error and signal curves of the average block solution *BSol*, the daily Wiese solution *DWSol* and the enhanced daily solution *EDSol* are additionally visualized in the top right figure for an easier comparison. The error curve of the *BSol* is the difference of the estimated block solution and the reference AOHIS signal of the same time and up to the same maximum SH degree of expansion. In the same way the difference of the *DWSol* is computed by subtracting the estimated daily Wiese solution and the reference daily AOHIS signal.

It is clearly visible that the enhanced daily solution (*EDSol*) stems from the *DWSol* as well as the *BSol*. Although the *EDSol* uses the higher block solution coefficients, these coefficients represent now only the daily solution. Accordingly the reference AOHIS signal is only the daily signal with the same maximum degree of expansion. The curve is almost identical with the *DWSol* up to degree N and approaches the block solution error curves in the higher degrees. The larger error beyond the maximum degree N of *DWSol* compared to the *BSol* stems from the signal content of the bordering days within the *BSol*, which is used in these degrees. Therefore the *EDSol* error curve deviates from *BSol* error curve due to the ‘erroneous’ signal above the maximum degree N of *DWSol* before the curve approaches the error curve of the *BSol*.

5.5 Signal change

Since many applications are primarily interested in the short-period signal change instead of the signal itself, one needs to investigate this signal change in more detail. The various possible difference products derived from the data outputs are described and depicted within the next section (see Table 4 as reference). Derived from the block solution a block difference (*BDiff*) of two consecutive blocks can be determined. A block difference is the difference between, for example block 1 consisting of day 1, 2 and 3, thus covering January 1st–3rd of the year 2002

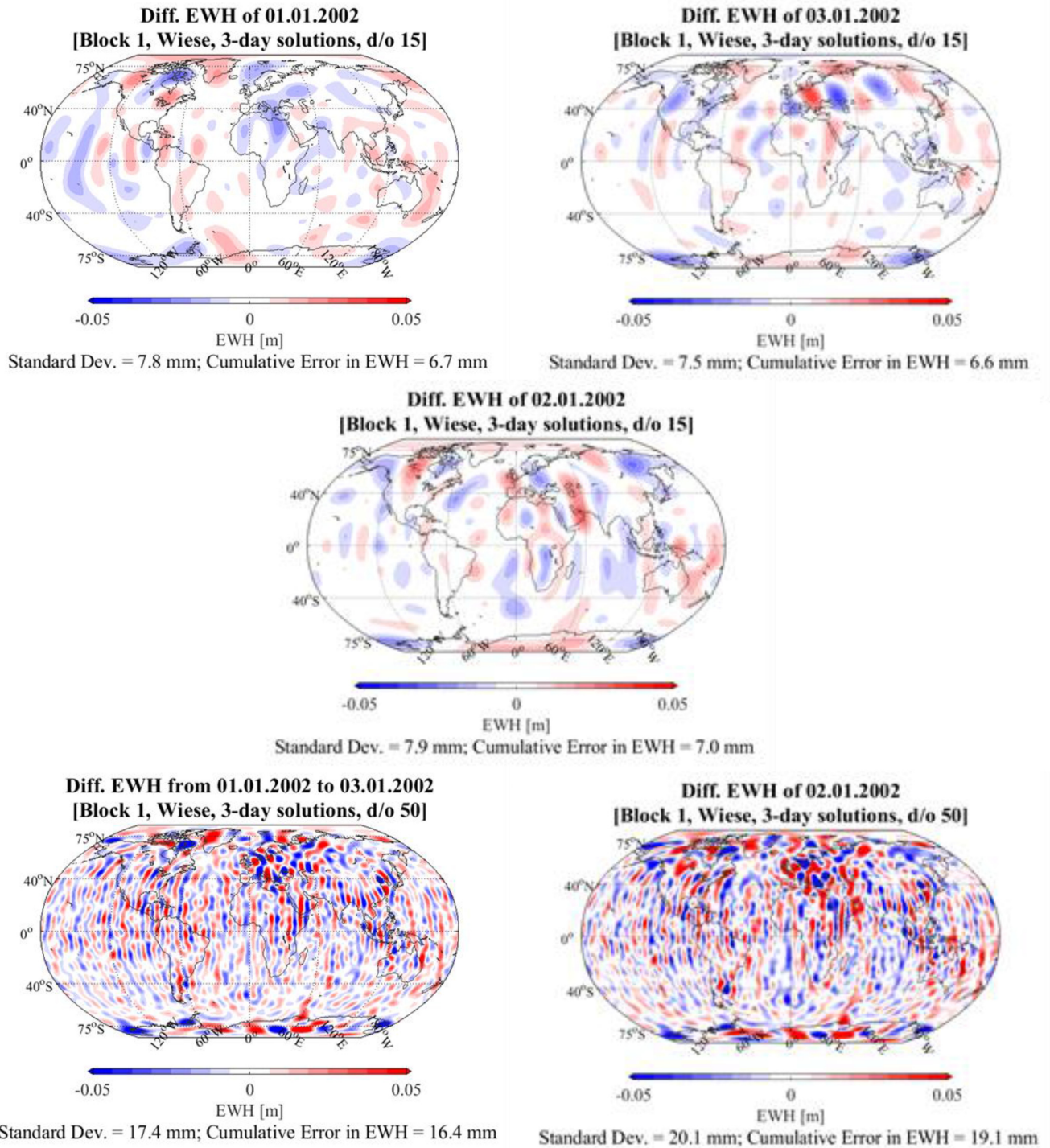


Figure 7. Estimated AOHIS solution of block 1 consisting of day 1 to 3 of the year 2002 minus the respective reference AOHIS signal. Top row: DWSol of day 1 (6.7 mm cumulative error in EWH) and day 3 (6.6 mm cumulative error in EWH). Middle row: DWSol of day 2 or reference day (7.0 mm cumulative error in EWH). Bottom row: BSol (16.4 mm cumulative error in EWH) and EDSol (19.1 mm cumulative error in EWH). For this example the performance of the middle day within this 3 d is worst, compared to the same day computed within the next 3-d solution, this daily solution is however better.

and block 2 consisting of block 2, 3 and 4, thus covering January 2nd to 4th of the year 2002, cancels out day 2 and 3, and leaves the difference of day 1 and 4. Due to the differencing the SNR is 1 roughly at d/o 20. The reference signal curve is determined accordingly. A simple Gauss filter of 350 km helps to suppress still existing noise in the solution, which was amplified by the differencing, but also dampens the signal within the solution and does not increase the SNR beyond d/o 20, as Fig. 10 depicts. The application of the VADER filter already described and analysed by Horvath *et al.* (2018) shows improved results, since the signal is almost fully preserved leading to a clearer distinguishability of signal and error curve in the *BSol* and also an improved SNR in the *BDiff* from 20° to 23°.

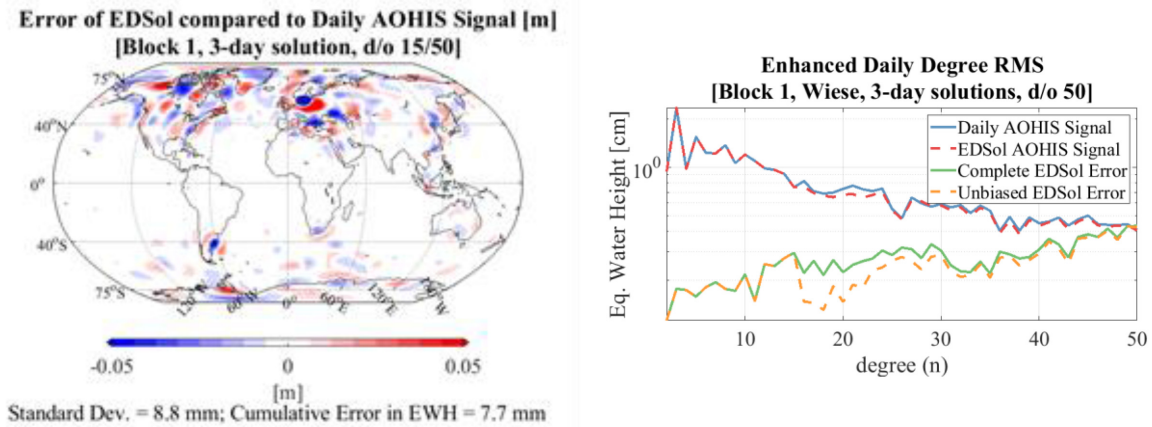


Figure 8. Analysis of error in EDSol. Left: Example from block 1 of the arising error due to leakage in a spatial visualization in EWH. The biggest error is visible in the higher altitudes. Right: Average of the actual daily AOHIS signal in blue, the AOHIS signal estimated by the EDSol (namely with the 2 d included in the higher degrees) in red, the error of the estimated EDSol in green, and the unbiased error meaning the EDSol AOHIS Signal was used for the computation in orange.

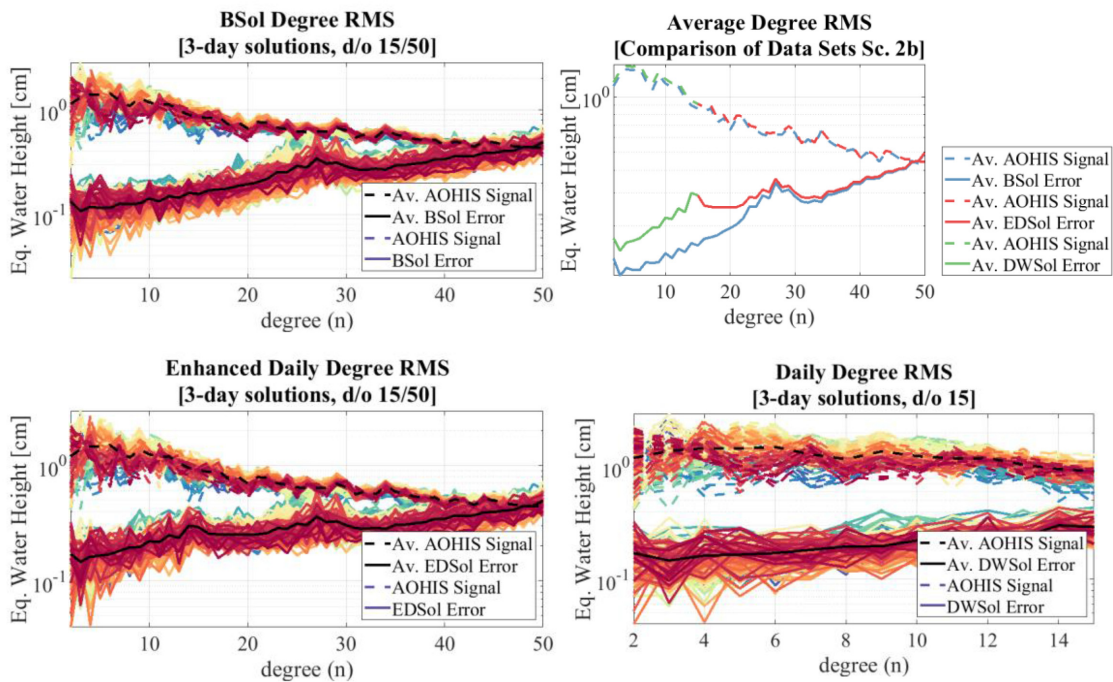


Figure 9. Degree RMS of Scenario 2b. The degree RMS of the different solutions range in colour from blue, over yellow, orange to dark red and the average error as well as signal curve are visualized in black. Top left: The block solution (BSol). Bottom right: The daily Wiese solution (DWSol). Bottom right: The spectrally enhanced daily solution (EDSol). All three data products are usable up to their maximum degree of expansion. The comparison depicts the higher error level of the daily (DWSol) as well as the spectrally enhanced (EDSol) product. Top right: Comparison of the three data products stemming from Scenario 2 b.

The daily Wiese differences (*DWDiff*) are the difference between two consecutive days. For the whole analysis the reference day in the middle of each respective block was chosen. On average the whole data set is usable till the estimated maximum expansion of d/o 15. Depending on the signal for analysis the difference of two consecutive days (*DWDiff*) with its expansion of d/o 15 or the *BDiff* of the 2 d with a shift of 3 d and a better spatial resolution of d/o 20 can be used.

The difference between two consecutive *EDSol* solutions are called enhanced daily difference (*EDDiff*). Fig. 11 shows the resulting *EDDiff* curves. Evidently, the error and signal curves tangent each other around d/o 15. This means that the gravity field coefficients higher than the daily maximum expansion of d/o 16 have to be used with caution. This error behaviour is due to the processing method of combining the reference *DWSol* and the *BSol* to an enhanced daily solution, and therefore combining the *DWDiff* and *BDiff*, leading to error and signal

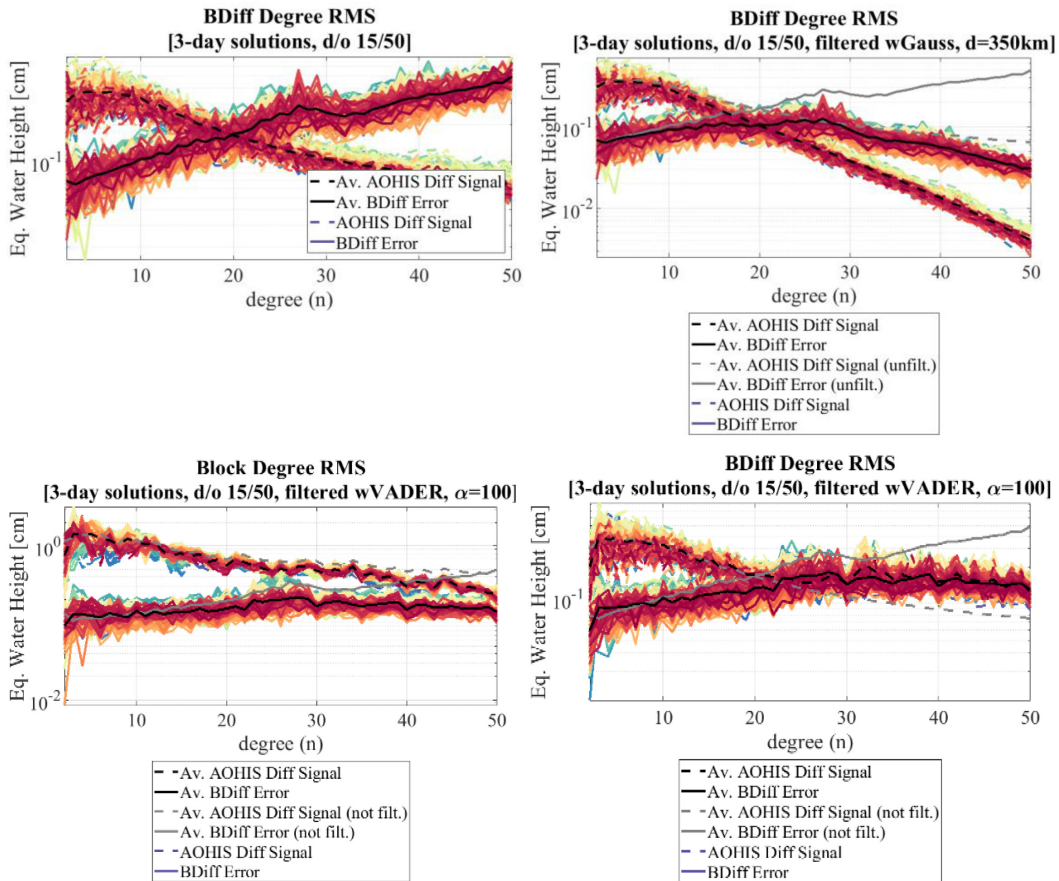


Figure 10. Top left: The degree RMS of the block differences (BDiff) displayed one over each other in different colour shadings as well as the average signal and the related error curve in black. Top right: By filtering the result with a Gauss filter of 350 km the usability of the data cannot be extended due to the ancilliary signal damping of the actual signal within the filter process. In gray he original, unfiltered curves are displayed for comparison. Bottom: Block and BDiff filtered with VADER filter ($\alpha = 100$). The result could be improved significantly, with the signal of the BDiff being usable on average till d/o 23 and the rest of the signal and error being on the same level. For comparison the original curves are again displayed in gray.

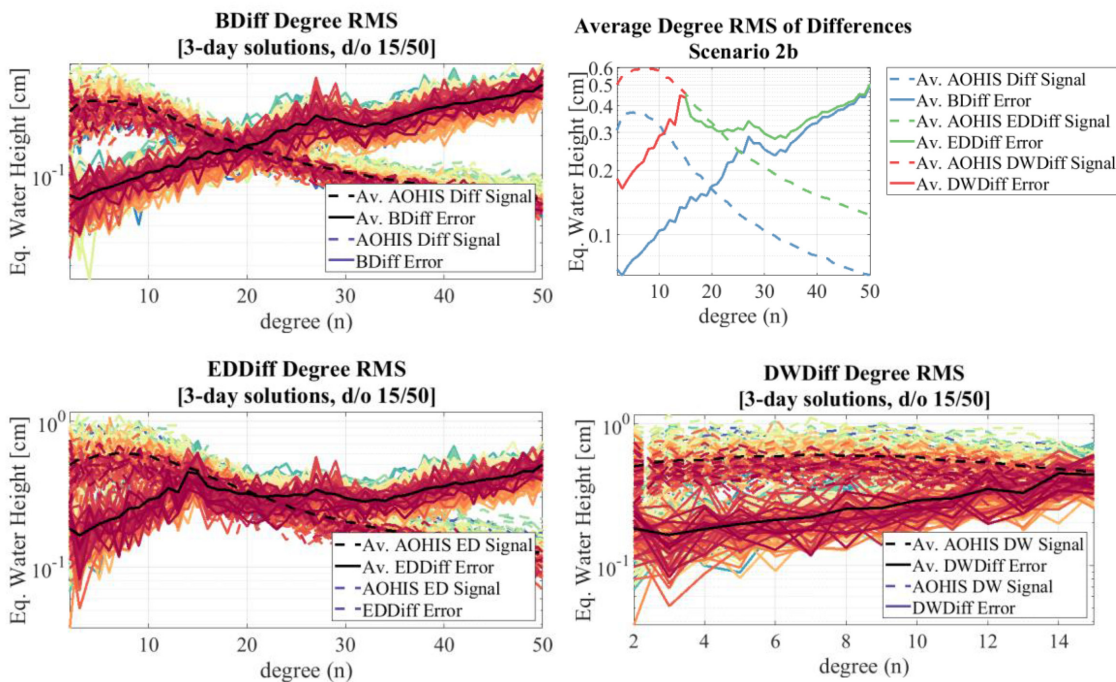


Figure 11. Degree RMS of the difference of consecutive solutions. Top left: Block solutions difference (BDiff). Bottom right: Daily solutions difference (DWDiff). Bottom left: Spectrally enhanced solutions difference (EDDiff). These solutions can be used up to d/o 20 respectively 15, but the comparison (top right) shows, that the average block difference has the best SNR and should be the preferred data product.

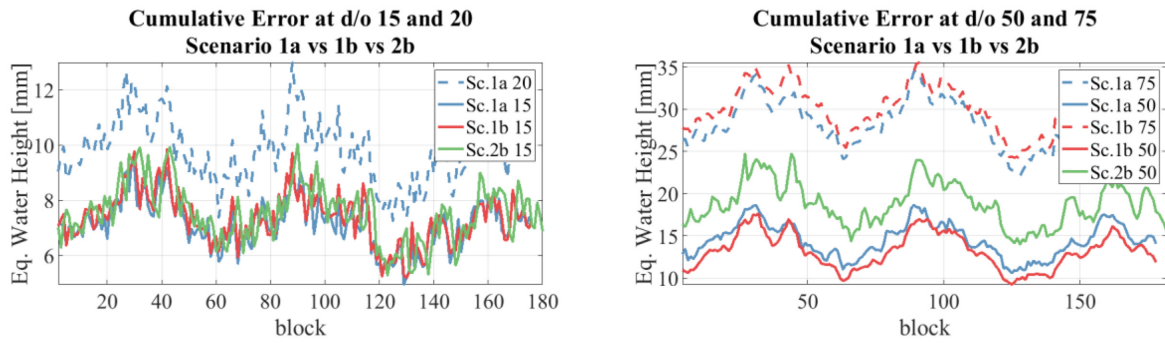


Figure 12. Cumulative error of the daily Wiese solution (left) and the block solution (right) of Scenario 1a, 1b and 2b depicted over the analysed time span. For Scenario 1a and b the cumulative error of d/o 50 was determined and depicted in the Figure as well to give a comparison at the same degree.

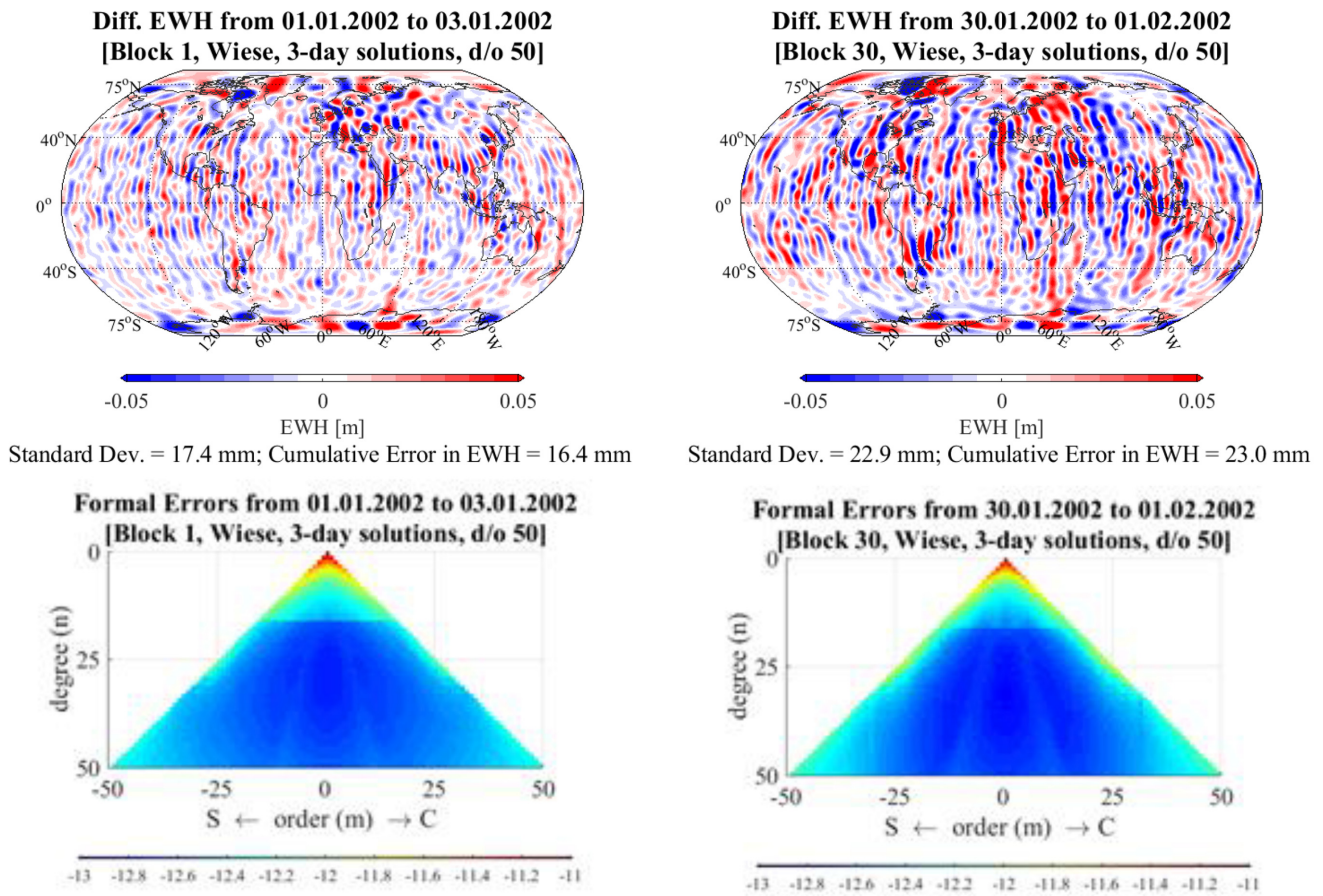


Figure 13. Difference of estimated signal and AOHIS reference signal in EWH. Top left: Block 1 has a cumulative error of 16.4 mm in EWH. Top right: Block 30 (right) has a cumulative error of 23.0 mm in EWH. Formal error derived from the GF covariance matrix of Scenario 2b. Bottom left: Block 1 (better quality). Bottom right: Block 30 (lesser quality). The degradation is especially visible between d/o 15 and 30 in the sectorial spherical harmonics.

curves being very close beyond degree 15 as the average *EDDiff* depicted in Fig. 11 shows, where the signal encompasses the 2 adjoining days.

5.6 Long-term quality stability

One of the necessary features of a service based on a NGGM is constant quality of the gravity field solutions. Fig. 9, depicting the degree variances of all blocks, shows a small deviation of some blocks. Due to the colour selection the block displayed in a blueish hue (around block 30) are visible above the other block's degree variances. To further investigate the overall quality, the cumulative errors of the three scenarios, calculated for the half year time span, were determined. Fig. 12 depicts the cumulative error of the daily Wiese solution *DWSol* (left) and the

block solution *BSol* (right) of Scenario 1a, 1b and 2b. Since Scenario 1a and b have a maximum d/o of 75, the cumulative errors for d/o 50 and also d/o 75 have been determined. For Scenario 1a additionally the daily cumulative error at d/o 15 was determined and plotted. All scenarios are based on the same orbit design with a 7-d subcycle and repeat period. The only difference is the retrieval period of 3, respectively, 7 d. Regardless of the retrieval period the quality of the GF solutions are consistently oscillating. The peaks appear approximately at the end of January, end of March and of May. This means a repeat pattern of approximately 60 d.

A computational reason like, for example numerical instabilities for the oscillating behaviour can therefore be excluded. Also the reference AOHIS signal does not show the same behaviour when analysed within the same time span. The hydrological extremes found in the time period are all geographically and spatially limited and also do not have any periodic repeat behaviour.

The difference of the error of a good quality (block 1 from 1.1.2002 to 2.1.2002) and a low quality (block 30 from 30.1.2002 to 1.2.2002) time period is visible in the top of Fig. 13 (top), while the bottom figures depicts the corresponding formal errors of the coefficients (bottom). It also reveals that these deviations are especially visible between the d/o from the higher 20 s to the higher 30 s in the sectorial harmonics (see the formal errors from the GF covariance matrix in Fig. 13 bottom). The quality of the estimated sectorial harmonics is strongly influenced by the inclined pair due to the observation method of along-track ranging. A deeper analysis of the orbits showed, that a possible adjustment for the future is the different drift rates of the orbital planes due to the difference in the inclination, leading to a slightly different interleaving pattern during the analysed time period. Another potential explanation for the behaviour that could be excluded are the ocean tides models used in the simulations. A comparison of affected and unaffected time spans in the spatial as well as the frequency domain have shown no indication of peaks in the impaired degrees. Further investigation into this issue is necessary to precisely pinpoint the issue.

6 CONCLUSION AND OUTLOOK

This paper describes the processing scheme for a NRT approach based on the ‘self-dealiasing’ or Wiese gravity field approach in case of a ll-sst NGGM with a Bender-type constellation and the method of computing spectrally enhanced daily solutions, with the goal to achieve daily gravity field estimates with increased spatial resolution. Based on an orbit design with a 7-d repeat pattern, the NRT approach was analysed for two different retrieval periods of 7 d (consistent with the orbit repeat period) and a shorter retrieval period of 3 d. When co-estimating daily gravity field estimates with lower spatial resolution (Wiese parametrization), it turns out that a maximum expansion of d/o 15 is optimal to both, obtain high-quality daily estimates, and de-alias the higher-degree gravity field solutions. The reduction from 7- to 3-d gravity field retrieval within the NRT was successful and leads to an achievable spatial resolution of approximately 400 km. The derived data products, namely the block solution (*BSol*), the daily Wiese solution (*DWSol*) and their differences as well as the derived spectrally enhanced daily solution (*EDSol*) created by eliminating the parameters of the border days in the solution, vary in spatial as well as temporal resolution. It could be shown that stable daily estimates up to a harmonic degree of 15 can be achieved with product latencies of 1 d in a combination with 3-d solutions, a favoured temporal resolution of the hydrology community. The created enhanced daily solutions produce an additional error, but achieve an enhanced daily solution up to d/o 50 with a reasonable error level.

Although previous studies found, that the importance of subcycles is small (Iran Pour *et al.* 2015), the NRT GF analysis shows, that the orbit configuration, especially the inclined orbit, has an effect on the long-term stability of the GF solution quality. A long-term analysis of different subcycles and repeat patterns within the proposed satellite constellation is necessary to give a decisive answer if the necessary long-term stability can be achieved by a modified orbit configuration. Also introducing an additional satellite pair to the analysed Bender-type constellation may help stabilizing the quality. Furthermore different constellations like, for example Bender multipair, a pendulum constellation with at least two pairs or a completely different approach like the MOBILE concept presented by Pail *et al.* (2018) might be the answer to guarantee long-term stability for possible NRT applications.

Not only the long term quality is an issue, but also errors still left in the solution, which exhibit the typical GRACE-type striping. A simple Gauss filter of 350 km did not improve the solution, while a different filter approach like the Vader filter achieved better data usability, especially regarding the block difference, where a simple Gauss filter removes too much signal to actually improve the solution apart from removing striping.

Another issue of the short-term GF solutions is, that also long-term solutions are of interest for various applications. A multitime resolution gravity field processing of sequential coparametrization as already described by Daras & Pail (2017) would be of interest to achieve more data products with several different time and spatial resolutions simultaneously. Based on the presented 3-d solution a pyramid-shaped processing scheme, allowing for 9-d and possibly a near-monthly 27-d solution, could be crafted.

In contrast to other strategies to achieve daily gravity field estimates, which are usually based on Kalman filtering, the NRT concept proposed here is independent of any prior information, and does not require any regularization. In addition, coupled with the Wiese parametrization, the use of external atmosphere and ocean models for the purpose of dealiasing can be avoided. These aspects could be important advantages in view of using gravity field information for service applications such as flood and drought monitoring and forecast or applications in water management, which usually require high spatial resolution and short product latencies.

ACKNOWLEDGEMENTS

A big part of the investigations presented in this paper was performed in the framework of the study ‘Assessment of satellite constellations for monitoring the variations in Earth gravity field (ADDCON)’, ESA-ESTEC, Contract AO/1–7317/12/NL/AF funded by the European Space Agency. We also acknowledge the provision of supercomputing resources by the Leibniz Supercomputing Centre (LRZ; Address: Boltzmannstraße 1, 85748 Garching bei München, Germany).

REFERENCES

- Awage, J.L., Forootan, E., Kusche, J., Kiema, J.B.K., Omondi, P.A., Heck, B. & Goncalves, R.M., 2013. Understanding the decline of water storage across the Ramser-Lake Naivasha using satellite-based methods, *Adv. Water Res.*, **60**, 7–23.
- Baur, O., 2013. Greenland mass variation from time-variable gravity in the absence of GRACE, *Geophys. Res. Lett.*, **40**(16), 4289–4293.
- Beaudoin, H., Rodell, M., Getirana, A. & Li, B., NASA/GSFC/HSL, 2017. *Groundwater and Soil Moisture Conditions from GRACE Data Assimilation L4 7-days 0.125 x 0.125 degree V2.0*, Greenbelt, MD, USA, Goddard Earth Sciences Data and Information Services Center (GES DISC), <http://dx.doi.org/10.5067/ASNKR4DD9AMW>.
- Bender, P.L., Wiese, D.N. & Nerem, R.S., 2008. A possible dual-GRACE mission with 90 degree and 63 degree inclination orbits, in *Proceedings of the Third International Symposium on Formation Flying, Missions and Technologies*, pp. 1–6, ESA/ESTEC, Noordwijk (ESA SP-654, June 2008), ISBN 978-92-9221-218-6.
- Bruinsma, S., Lemoine, J., Biancale, R. & Valès, N., 2010. CNES/GRGS 10-day gravity field models (release 2) and their evaluation, *Adv. Space Res.*, **45**(4), 587–601.
- Chen, J.L., Wilson, C.R. & Tapley, B.D., 2010. The 2009 exceptional Amazon flood and interannual terrestrial water storage change observed by GRACE, *Water Resour. Res.*, **46**(12), doi:10.1029/2010wr009383.
- Daras, I., Pail, R., Murböck, M. & Yi, W., 2015. Gravity field processing with enhanced numerical precision for LL-SST missions, *J. Geod.*, **89**(2), 99–110.
- Daras, I., 2016. Gravity field processing towards future LL-SST satellite missions, in Deutsche Geodätische Kommission der Bayerischen Akademie der Wissenschaften, Reihe C, Dissertationen, Heft 770, Verlag der Bayerischen Akademie der Wissenschaften, pp. 23–39. ISBN(Print) 978-3-7696-5182-9, ISSN 0065–5325, 2016.
- Daras, I. & Pail, R., 2017. Treatment of temporal aliasing effects in the context of next generation satellite gravimetry missions, *J. geophys. Res.*, doi:10.1002/2017JB014250.
- Dobslaw, H., Flechtner, F., Bergmann-Wolf, I., Dahle, C., Dill, R., Esselborn, S., Sasgen, I. & Thomas, M., 2013. Simulating high-frequency atmosphere-ocean variability for dealiasing of satellite gravity observations: AOD1b RL05: Atmosphere-Ocean mass variability: AOD1b, *J. geophys. Res.: Oceans*, **118**(7), 3704–3711.
- Drinkwater, M.R., Floberghagen, R., Haagmans, R., Muzi, D. & Popescu, A., 2003. GOCE: ESA’s first Earth Explorer Core mission, in *Earth Gravity Field from Space—from Sensors to Earth Science, Space Sciences Series of ISSI, Vol 18*, pp 419–432, eds Beutler, G. et al., Kluwer Academic Publishers, ISBN 1-4020-1408-2.
- Espinoza, J.C., Ronchail, J., Frappart, F., Lavado, W., Santini, W. & Guyot, J.-L., 2013. The major floods in the Amazonas River and tributaries (Western Amazon basin) during the 1970–2012 period: a focus on the 2012 flood, *J. Hydrometeorol.*, **14**, 1000–1008.
- Famiglietti, J.D. & Rodell, M., 2013. Water in balance, *Science*, **340**(6138), 1300–1301.
- Feng, W., Zhong, M., Lemoine, J.-M., Biancale, R., Hsu, H.-T. & Xia, J., 2013. Evaluation of groundwater depletion in North China using the Gravity Recovery and Climate Experiment (GRACE) data and ground-based measurements, *Water Resour. Res.*, **49**, 2110–2118.
- Flechtner, F., Webb, F. & Watkins, M., 2017. Current status of the GRACE follow-on mission, *Geophys. Res. Abstracts*, **19**, EGU2017–4566, EGU General Assembly 2017. Deutsche Geodätische Kommission der Bayerischen Akademie der Wissenschaften, Reihe B, Angewandte Geodäsie, 318.
- Forootan, E., Didova, O., Schumacher, M., Kusche, J. & Elsaka, B., 2014. Comparisons of atmospheric mass variations derived from ECMWF re-analysis and operational fields over 2003–2011, *J. Geod.*, **88**, 503–514.
- Gouweleew, B., Kvas, A., Gruber, C., Gain, A.K., Mayer-Gürr, T., Flechtner, F. & Güntner, A., 2018. Daily GRACE gravity field solutions track major flood events in the Ganges–Brahmaputra Delta, *Hydrol. Earth Syst. Sci.*, **22**, 2867–2880.
- Gruber, T. & Murböck, M., & NGGM-D Team, 2014. e2.motion—Earth system mass transport mission (Square)—concept for a next generation gravity field mission, Verlag C.H. Beck 12/2014, Nr. 318, <http://dgk.badw.de/fileadmin/docs/b-318.pdf>.
- Gunter, B., Ries, J., Bettadpur, S. & Tapley, B., 2006. A simulation study of the errors of omission and commission for GRACE RL01 gravity fields, *J. Geod.*, **80**(7), 341–351.
- Han, S.C., Sauber, J. & Luthcke, S., 2010. Regional gravity decrease after the 2010 Maule (Chile) earthquake indicates large-scale mass distribution, *Geophys. Res. Lett.*, **37**(23), doi:10.1029/2010GL045449.
- Han, S., Riva, R., Sauber, J. & Okal, E., 2013. Source parameter inversion for recent great earthquakes from a decade-long observation of global gravity fields, *J. geophys. Res.: Solid Earth*, **118**, 1240–1267.
- Hao, Z., AghaKouchak, A., Nakhjiri, N. & Farahmand, A., 2014. Global integrated drought monitoring and prediction system, *Scientific Data*, doi:10.1038/sdata.2014.1.
- Hauk, M. & Pail, R., 2018. Treatment of ocean tide aliasing in the context of a next generation gravity field mission, *Geophys. J. Int.*, **214**, 345–365.
- Heki, K. & Matsua, K., 2010. Coseismic gravity changes of the 2010 earthquake in central Chile from satellite gravimetry, *Geophys. Res. Lett.*, **37**(24306), doi:10.1029/2010GL045335.
- Hofmann-Wellenhof, B. & Moritz, H., 2005. *Physical Geodesy*, 2nd edn, Springer.
- Horvath, A., Murböck, M., Pail, R. & Horwath, M., 2018. Decorrelation of GRACE time variable gravity field solutions using full covariance information, *Geosciences*, **8**(9), ISSN 2076–3263, doi:10.3390/geosciences8090323.
- Iran Pour, S. et al., 2015. Assessment of satellite constellations for monitoring the variations in earth gravity field – SC4MGV, ESA – ESTEC Contract No. AO/1-7317/12/NL/AF, Final Report.
- Koch, K.R., 1997. *Parameterschätzung und Hypothesentests in Linearen Modellen*. Dümmler-Verlag.
- Kurtenbach, E., Mayer-Gürr, T. & Eicker, A., 2009. Deriving daily snapshots of the Earth’s gravity field from GRACE L1B data using Kalman filtering, *Geophys. Res. Lett.*, **36**(17), L17102, doi:10.1029/2009GL039564.
- Kvas, A., Christian, G., Gouweleew, B., Chen, Q., Poropat, L., Flechtner, F., Mayer-Gürr, T. & Güntner, A., 2017. First results of the EGSIEM Near Real-Time service, *Geophys. Res. Abstracts*, **19**, EGU2017–15174.
- Lettenmaier, D.P. & Famiglietti, J.S., 2006. Hydrology: water from on high, *Nature*, **444**, 562–563.
- Long, D., Shen, Y., Sun, A., Hong, Y., Longuevergne, L., Yang, Y. & Chen, L., 2014. Drought and flood monitoring for a large karst plateau in Southwest China using extended GRACE data, *Rem. Sens. Environ.*, **155**, 145–160.
- Longuevergne, L., Scalon, B.R. & Wilson, C.R., 2010. GRACE Hydrological estimates for small basins: evaluating processing approaches on the High Plains Aquifer, USA, *Water Resour. Res.*, **46**(11), doi:10.1029/2009wr008564.
- Lorenz, C., Kunstmann, H., Devaraju, B., Tourian, M.J., Sneeuw, N. & Rieger, J., 2014. Large-scale runoff from landmasses: a global assessment of the closure of the hydrological and atmospheric water balances, *J. Hydrometeorol.*, **15**(6), 2111–2139.

- Lück, C., Kusche, J., Rietbroek, R. & Löcher, A., 2017. Time-variable gravity fields and ocean mass change from 37 months of kinematic Swarm orbits, *Solid Earth Discuss.*, 1–25, doi:10.5194/se-2017-127.
- Luthcke, S.B., Sabaka, T., Loomis, B., Arendt, A., McCarthy, J. & Camp, J., 2013. Antarctica, Greenland, and Gulf of Alaska land-ice evolution from an iterated GRACE global mascon solution, *J. Glaciol.*, **59**(216), 613–631.
- Malnes, E., Solbø, S., Lauknes, I., Evertsen, G., Tøllefsen, T.A., Solheim, I. & Indegard, M., 2005. FLOODMAN – global near-real time flood monitoring for hydrological users, in *Proceedings of the ACTIF Workshop*, At Tromsø, Norway.
- Matsuo, K. & Heki, K., 2011. Coseismic changes of the 2011 Tohoku-Oki earthquake from satellite gravimetry, *Geophys. Res. Lett.*, **38**(7), doi:10.1029/2011GL049018.
- Mayer-Gürr, T. *et al.*, 2012. The new combined satellite only model GOCO03s, in *Presentation at IAG Symposium Gravity, Geoid and Height Systems*, Venice, Italy.
- Mayer-Gürr, T. *et al.*, 2016. European gravity service for improved emergency management – status and project highlights, *Geophys. Res. Abstracts*, **18**, EGU2016–14970, EGU General Assembly 2016.
- Montenbruck, O. & Gill, E., 2000. Satellite Orbits, doi:10.1007/978-3-642-58351-3.
- NGGM-D Team, 2014. e2.motion (Earth System Mass Transport Mission (Square)) – Concept for a Next Generation Gravity Field Mission – Final Report of Project “Satellite Gravimetry of the Next Generation (NGGM-D)”, Deutsche Geodätische Kommission der Bayerischen Akademie der Wissenschaften, Reihe B, Angewandte Geodäsie, Heft Nr. 318, ISBN 978-3-7696-8597-8.
- Pail, R. *et al.*, 2015. Science and user needs for observing global mass transport to understand global change and to benefit society, *Surv. Geophys.*, **36**(6), 743–772.
- Pail, R., the European gravity science team, 2018. Mass variation observing system by high-low inter-satellite links (MOBILE) – a mission proposal for ESA Earth Explorer 10, *Geophys. Res. Abstracts*, **20**, EGU2018–EGU1972, 2018, EGU General Assembly 2018.
- Panet, I. *et al.*, 2013. Earth system mass transport mission (e.motion): A concept of future earth gravity field measurements from space, *Surv. Geophys.*, **34**(141), doi:10.1007/s10712-012-9209-8.
- Pappenberger, F., Thielen Del Pozo, J. & Del Medico, M., 2011. The impact of weather forecast improvements on large scale hydrology: analysing a decade of forecasts of the European Flood Alert System, *Hydrol. Process.*, **25**(7), 1091–1113.
- Purkhauser, A.F. *et al.*, 2018. *Gravity Field Retrieval of Next Generation Gravity Missions regarding Geophysical Services: Results of the ESA-ADDCON Project*, European Geosciences Union General Assembly 2018, <https://meetingorganizer.copernicus.org/EGU2018/EGU2018-2770.pdf>.
- Ray, R.D., 1999. A global ocean tide model from topex/Poseidon altimetry: Got99.2, Tech. rep., NASA Technical Memorandum 209478.
- Reigber, C., Schwintzer, P. & Lühr, H., 1999. The CHAMP geopotential mission, *Bollettino di Geofisica Teoretica ed Applicata*, 40/3-4, September–December 1999, in *Proceedings of the Second Joint Meeting of the International Gravity and the International Geoid Commission*, pp. 285–289, eds Marson, I. & Sünkel, H., Trieste 1998 September 7–12, ISSN 0006–6729.
- Rodell, M. & Famiglietti, J., 1999. Detectability of variations in continental water storage from satellite observation of time dependent gravity field, *Water Resour. Res.*, **35**, 2705–2723.
- Rodell, M., Velicogna, I. & Famiglietti, J., 2009. Satellite-based estimates of groundwater depletion in India, *Nature*, **460**, 999–1002.
- Sakumura, C., Bettapur, S., Save, H. & McCullough, C., 2016. High-frequency terrestrial water storage signal capture via a regularized sliding window mascon product from GRACE, *J. geophys. Res.: Solid Earth*, **121**, 4014–4030.
- Savcenko, R. & Bosch, W., 2008. *EOT08a – Empirical Ocean Tide Model from Multi-Mission Satellite Altimetry*, Vol. **81**, DGFI Report, München, Germany.
- Schneider, M., 1969. Outline of a general orbit determination method, in *Space Research IX, Proceedings of Open Meetings of Working Groups (OMWG) on Physical Sciences of the 11th Plenary Meeting of the Committee on Space Research (COSPAR)*, Tokyo, ed., KSW Champion, PA.
- Schrama, E.J.O., Wouters, B. & Lavallée, D.A., 2007. Signal and noise in Gravity Recovery and Climate Experiment (GRACE) observed surface mass variation, *J. geophys. Res.*, **116**(B2), B02407, doi:10.1029/2006JB004882.
- Seitz, F., Schmidt, M. & Shum, C.K., 2008. Signs of extreme weather conditions in Central Europe in GRACE 4-D hydrological mass variations, *Earth planet. Sci. Lett.*, **268**(1), 165–170.
- Seo, K.-W., Wilson, C.R., Chen, J. & Waliser, D., 2007. GRACE’s spatial aliasing error, *Geophys. J.*, doi:10.1111/j.1365-246X.2007.03611.x.
- Shampine, L.F. & Gordon, M.K., 1975. *Computer Solution of Ordinary Differential Equations: the Initial Value Problem*, W.H. Freeman.
- Sheard, B.S., Heinzl, G., Danzmann, K., Shaddock, D., Kilpstein, W. & Folkner, W., 2012. Intersatellite laser ranging instrument for the GRACE Follow-On mission, *J. Geod.*, **86**(12), 1083–1095.
- Tapley, B.D., Bettadpur, S., Watkins, M. & Reigber, C., 2004. The gravity recovery and climate experiment mission overview and early results, *Geophys. Res. Lett.*, **31**, L09607, doi:10.1029/2004GL019920.
- Tapley, B.D., Flechtner, F., Bettadpur, S. & Watkins, M., 2013. *The Status and Future Prospect for GRACE After the First Decade*, American Geophysical Union, Fall Meeting 2013, abstract #G32A-01.2013AGUFM.G32A.01T.
- Tiwari, V.M., Wahr, J. & Swenson, S., 2009. Dwindling groundwater resources in northern India, from satellite gravity observations, *Geophys. Res. Lett.*, **36**, L18401, doi:10.1029/2009GL039401.
- Tourian, M.J., Elmi, O., Chen, Q., Devaraju, B., Roohi, S. & Sneeuw, N., 2015. A spaceborne multisensory approach to monitor the desiccation of Lake Urmia in Iran, *Rem. Sens. Environ.*, **156**, 349–360.
- Velicogna, I., Sutterley, T.C. & van den Broeke, M.R., 2014. Regional acceleration in ice mass loss from Greenland and Antarctica using GRACE time-variable gravity data, *Geophys. Res. Lett.*, **41**(22), 8130–8137.
- Wahr, J., Molenaar, M. & Bryan, F., 1998. Time variability of the Earth’s gravity field: hydrological and oceanic effects and their possible detection using GRACE, *J. geophys. Res.*, **201**, B12, doi:10.1029/98JB02844.
- Wang, H., Zhang, Y., Liu, J., Shen, X., Yu, H., Jiang, Z. & Zhang, G., 2018. Pre-earthquake observations and their application in earthquake prediction in China: a review of historical and recent progress, in *Pre-Earthquake Processes: A Multidisciplinary Approach to Earthquake Prediction Studies*, Chapter 3, ISBN: 978-1-119-15693-2.
- Wang, L., Shum, C.K., Simons, F.J., Tapley, B. & Dai, C., 2012. Coseismic and postseismic deformation of the 2011 Tohoku-Oki earthquake constrained by GRACE gravimetry, *Geophys. Res. Lett.*, **39**(7301), doi:10.1029/2012GL051104.
- Weigelt, M., Sneeuw, N., Schrama, E.J.O. & Visser, P.N.A.M., 2012. An improved sampling rule for mapping geopotential functions of a planet from a near polar orbit, *J. Geod.*, **87**, 127, doi:10.1007/s00190-012-0585-0.
- Weigelt, M., van Dam, T., Jäggje, A., Prange, L., Tourian, M.J., Keller, W. & Sneeuw, N., 2013. Time-variable gravity signal in Greenland revealed by high-low satellite-to-satellite tracking, *J. geophys. Res.: Solid Earth*, **118**, 3848–3859.
- Wen, H.Y., Krusinga, G., Meegyeong, P., Landerer, F., Bertinger, W. & Sakumura, C., 2018. *Gravity Recovery and Climate Experiment (GRACE) Follow-On (GRACE-FO) Level-1 Data Product User Handbook*, JPL D-56935, NASA Jet Propulsion Laboratory, California Institute of Technology, <ftp://podaac-ftp.jpl.nasa.gov/allData/gracefo/docs/Level1DataProductUserHandbook.pdf>.
- Wiese, D.N., Visser, P. & Nerem, R.S., 2011. Estimating low resolution gravity fields at short time intervals to reduce temporal aliasing errors, *Adv. Space Res.*, **48**(6), 1094–1107.
- Willis, J.K., Chambers, D.P. & Kuo, C.Y., 2010. Global sea level rise: recent progress and challenges for the decade to come, *Oceanography*, **23**, 26–35.
- Yi, W., 2012. The Earth’s Gravitational Field from GOCE. *Dissertation*, CGE Report No. 2, Centre of Geodetic Earth System Research, ISBN (Print) 978-3-934205-34-5. ISSN 2195–7126, 2012.
- Xu, G., 2003. *GPS: Theory, Algorithms and Applications*, Springer, ISBN 3-540-67812-3.

A.4. P-IV: Applicability of NGGM near-real time simulations in flood detection

Reference: Purkhauser, A. F., Koch, J. A., and Pail, R. (2019). Applicability of NGGM near-real time simulations in flood detection. *Journal of Geodetic Science*, 9(1):111–126. DOI: 10.1515/jogs-2019-0011

Copyright: This work originally has been published in Journal of Geodetic Science: <https://doi.org/10.1515/jogs-2019-0011>. This work is licensed under the Creative Commons Attribution 4.0 Public License.

Abstract

The GRACE mission has demonstrated a tremendous potential for observing mass changes in the Earth system from space for climate research and the observation of climate change. Future mission should on the one hand extend the already existing time series and also provide higher spatial and temporal resolution that is required to fulfil all needs placed on a future mission. To analyse the applicability of such a NGGM concept regarding hydrological applications, two GRACE-FO-type pairs in Bender formation are analysed. The numerical closed loop simulations with a realistic noise assumption are based on the short arc approach and make use of the Wiese approach, enabling a self-de-aliasing of high-frequency atmospheric and oceanic signals, and a NRT approach for a short latency.

Numerical simulations for future gravity mission concepts are based on geophysical models, representing the time-variable gravity field. First tests regarding the usability of the hydrology component contained in the ESM by the ESA for the analysis regarding a possible flood monitoring and detection showed a clear signal in a third of the analysed flood cases. Our analysis of selected cases found that detection of floods was clearly possible with the reconstructed AOHIS/HIS signal in 20% of the tested examples, while in 40% of the cases a peak was visible but not clearly recognisable.

Declaration of own contribution

Table A.4.: Contribution to P-IV

Involved in	Estimated contribution
Ideas and conceptual design	100%
Computation and results	70%
Analysis and interpretation	80%
Manuscript, figures and tables	90%
Total	85%

Appendix A. Publications

Confirmation by Co-Authors

I hereby confirm the correctness of the declaration of the contribution of Anna F. Purkhauser for the publication P-IV in Table A.4:

Julia Aumi Koch *28.01.2020*
Julia A. Koch Date

Roland Pail *30.01.2020*
Roland Pail Date
(IAPG, LRG, TUM)



Research Article

Open Access

A. F. Purkhauser*, J. A. Koch, and R. Pail

Applicability of NGGM near-real time simulations in flood detection

DOI: <https://doi.org/10.1515/jogs-2019-0011>

Received October 26, 2018; accepted June 28, 2019

Abstract: The GRACE mission has demonstrated a tremendous potential for observing mass changes in the Earth system from space for climate research and the observation of climate change. Future mission should on the one hand extend the already existing time series and also provide higher spatial and temporal resolution that is required to fulfil all needs placed on a future mission. To analyse the applicability of such a Next Generation Gravity Mission (NGGM) concept regarding hydrological applications, two GRACE-FO-type pairs in Bender formation are analysed. The numerical closed loop simulations with a realistic noise assumption are based on the short arc approach and make use of the Wiese approach, enabling a self-de-aliasing of high-frequency atmospheric and oceanic signals, and a NRT approach for a short latency.

Numerical simulations for future gravity mission concepts are based on geophysical models, representing the time-variable gravity field. First tests regarding the usability of the hydrology component contained in the Earth System Model (ESM) by the European Space Agency (ESA) for the analysis regarding a possible flood monitoring and detection showed a clear signal in a third of the analysed flood cases. Our analysis of selected cases found that detection of floods was clearly possible with the reconstructed AOHIS/HIS signal in 20% of the tested examples, while in 40% of the cases a peak was visible but not clearly recognisable.

Keywords: Flood detection, Future gravity mission, Near-real time, Time variable gravity

Introduction

Since the year 2000, the mass transport processes of the Earth system are observed by dedicated gravity missions such as CHAMP (CHALLENGING Minisatellite Payload) (Reig-

ber et al. 1999) and GRACE/GRACE-FO (Gravity Recovery And Climate Experiment (Follow-On)) (Tapley et al. 2004; Flechtner et al. 2017). The CHAMP satellite mission's main observing technique is a high-low satellite-to-satellite tracking (hl-sst) leading to a spatial resolution of 500 to 1000 km (Baur 2013). The GRACE concept is based on twin satellites flying in a LEO (low Earth orbit) with the main observation being the K-band microwave low-low satellite-to-satellite tracking (ll-sst) between the two satellites. GRACE-FO features an additional inter-satellite laser ranging interferometer as technology demonstrator (Sheard et al. 2012), establishing that a further improvement of the ranging accuracy down to a few nanometres is possible.

Based on this observation techniques the computation of temporal gravity fields with a resolution of 1 month (Tapley et al. 2004), 10 days (Bruinsma et al. 2010; Tapley et al. 2013) and even 1 day solutions (Kurtenbach et al. 2009; Mayer-Gürr et al. 2016), the latter using a Kalman filter, are possible, supporting the global and continuous analysis of atmosphere, ocean, hydrology, ice and solid Earth (AOHIS) for hydrological processes (Rodell et al. 2009; Tiwari et al. 2009), ice mass melting (Luthcke et al. 2013; Velicogna et al. 2014), sea level risk (Willis et al. 2010), atmospheric circulation (Forootan et al. 2014), changes of the solid Earth like earthquakes (Han et al. 2013), and their interaction.

Possible NGGMs will have to address the issue of an anisotropic error spectrum and resulting strong striping features due to observation geometry in combination with temporal aliasing effects (Seo et al. 2007), hampering more challenging user requirements in terms of spatial resolution, time resolution and latency. A NGGM constellation usually consists of two GRACE-like pairs in a polar and an inclined orbit, also called Bender-pair, to address these issues. In addition to the improved scientific analysis that would be possible with such a satellite constellation, time-variable gravity field products shall contribute to operational services and applications such as water management, coastal vulnerability monitoring and forecasting of floods and droughts (Pail et al. 2015).

To analyse the applicability of a NGGM constellation regarding the detection and possible future prediction of

*Corresponding Author: A. F. Purkhauser: Technische Universität München München, Germany, E-mail: anna.purkhauser@tum.de
J. A. Koch, R. Pail: Technische Universität München München, Germany

droughts and floods, 6 months of data based on a Bender-type NGGM constellation was simulated. Chapter 1 introduces shortly the simulation environment, the orbit parameters of the satellite constellation, the noise characteristics used and the post-processing. Chapter 2 describes the used data sources and details the processing of the gravity fields towards a time series for floods and droughts detection. Among the results, a comprehensive analysis of the simulation itself, the analysis of the content of the hydrological layer, the comparison of the H component to HIS and AOHIS are presented, the applicability of the reconstructed gravity fields for the proposed application is studied and open questions within the analysis are discussed (see Chapter 3), followed by a short conclusion and outlook in Chapter 4.

Within the paper the following definitions are used: A flood is the rise and overflow of a large amount of water beyond its normal limits and can happen depending on the overall situation within hours, while a drought is the prolonged shortage in the water supply and can only be detected in long-term monitoring. Their possible detection is limited by the fact that with gravity data only so-called gravimetric floods and droughts are visible, meaning events that are associated with a change of mass and a corresponding change in the temporal gravity field. In this paper we focus on flood events.

1 Simulation

1.1 Orbit design

While various studies have analysed the potential of a second pair (Bender et al. 2008; Wiese et al. 2011; Wiese et al. 2012), the study by Elsaka et al. (2014) has concluded that a Bender configuration consisting of a polar and an inclined pair gives the best gain in accuracy on a global average. The orbit design itself is in accordance with the findings of the ESA-funded study SC4MGV (Assessment of Satellite Constellations for Monitoring the Variations in Earth Gravity Field) (Iran Pour et al. 2015). The main finding being that there is a certain freedom to tailor the orbits to potential applications, because a multitude of different scenarios delivered very comparable results regarding achievable gravity field performance. The study also showed that the retrieved gravity models did not have constant quality over time. Therefore, in order to improve the situation the orbits selected in this study have the same drift rate to ensure optimal interleaving at all times. The analysed constellation consists of a near-polar pair similar to GRACE

Table 1. Orbit parameters for satellite constellations.

Satellite pair	Altitude [km]	Inclination [degree]	Inter-satellite distance [km]
Near-polar	340	89	100
Inclined	355	70	100

and an inclined pair with an inclination of 70° , see also Table 1. The state vectors used for the orbit integration are from the ESA-funded ADDCON study (Additional Constellation & Scientific Analysis of the Next Generation Gravity Mission Concept) (Purkhauser et al. 2018).

1.2 Numerical simulator

The simulation was processed by a numerical closed-loop simulator available at the Institute of Astronomical and Physical Geodesy (IAPG) (Daras et al. 2015; Daras 2016) using the short-arc approach (Schneider 1969) with a low-low satellite-to-satellite tracking (ll-sst) and high-low satellite-to-satellite tracking (hl-sst) component sampled at 5 seconds. Additionally, the NRT processing consisting of a combination of the Wiese approach (Wiese et al. 2011) and a sliding window averaging at normal equation level (Purkhauser and Pail 2019), is used. The Wiese approach co-estimates a low spatial resolution gravity field at a short time interval together with higher resolution gravity fields sampled at longer time intervals, allowing for a self-dealiasing and the stable processing of solutions of a few days combined with a daily gravity field solution. The sliding window averaging allows for an optimal latency of one day, due to the fact that the data of each day is processed as soon as all necessary data products like EOP (Earth orientation product), rapid GNSS orbits and clocks are available, while the data of the first day in the previous solution is excluded. Consequently, the data analysis is performed with redundancies on the daily solution level and features overlapping gravity solutions. Based on this processing scheme, a variety of different data sets are available. More details on the approach can be found in Purkhauser and Pail (2019).

Since a short time sampling was desired, gravity fields with a temporal resolution of three days and a spatial sampling of d/o 30 corresponding to a spatial resolution of approx. 670 km or 160.000 km², accompanied by daily solutions with a spatial resolution of d/o 15 corresponding to a spatial resolution of approx. 1300 km or 1.700.000 km² were determined. The gravity fields were processed from 1st of January till 30th of June of the year 2002.

1.3 Data

The simulation is based on the static gravity field GOCO05s model (Mayer-Gürr and the GOCO Team 2015) and ESA's ESM (Dobslaw et al. 2015), a synthetic model of the time variable gravity field of the Earth available in spherical harmonics up to degree and order (d/o) 180 from the years 1996 to 2005 at 6-hourly snapshots. The time variable gravity field consists of AOHIS which are computed as coupled geophysical models as well as gravity field changes due to solid Earth processes like continuous glacial isostatic adjustment (GIA) or a sudden earthquake with co-seismic and post-seismic signals. It is used as model for the time variable gravity field information in order to perform the simulation study and also to validate the simulated gravity fields.

The H component of the AOHIS includes a global model of all terrestrially stored water. The model is validated with satellite altimetry over surface water bodies and also GRACE.

A realistic de-aliasing model for high-frequency mass variability in atmosphere and ocean is also provided by the ESM in two separate components (Dobslaw et al. 2016). The AO error (AOerr) model represents both large-scale and small-scale errors with zero mean and a stationary variance.

As ocean models either the GOT4.7 (Goddard Ocean Tide) tide model (Ray 1999) or the EOT08a (Empirical Ocean Tide) model (Savcenko and Bosch 2008) are used. Starting from the same state vectors but different force models the orbits and observations representing the “true” world as closely as possible and a reference world are propagated. The observations of the “true” world are additionally superimposed by noise time series according to the potential measuring system (see Table 2).

1.4 Stochastic modelling

In the context of the simulations the following two error sources were considered: the laser ranging instrument noise (see Eq. (1)) and the accelerometer noise (see Eq. (2) and (3)). The noise characteristics of the error sources are all frequency dependent (f) and are approximated by analytical equations in terms of range rates

$$d_{range\ rates} = 2 \cdot 10^{-8} \cdot 2\pi f \sqrt{\left(\frac{10^{-2} Hz}{f}\right)^2 + 1} \frac{m}{s\sqrt{Hz}} \quad (1)$$

$$d_{acc. x} = d_{acc. z} = 10^{-11} \sqrt{\left(\frac{10^{-3} Hz}{f}\right)^4 / \left(\left(\frac{10^{-5} Hz}{f}\right)^4 + 1\right) + 1 + \left(\frac{f}{10^{-1} Hz}\right)^4} \frac{m}{s^2\sqrt{Hz}}, \quad (2)$$

$$d_{acc. y} = 10 \cdot d_{acc. z} \quad (3)$$

with x being the along-track, y across-track and z the quasi-radial component. Since the satellite is assumed to fly in drag-free mode, the biggest part of the non-gravitational forces is compensated by a propulsion system consisting of ion thrusters.

The error assumptions of NGGMs were provided from the consultancy support of Thales Alenia Space Italia (TAS-I). In addition to the sensor noise, the NGGM simulations includes uncertainties in the ocean tide model (represented by the differences between two different ocean tide models), see Table 2. The impact of orbit errors is taken into account by propagating 1 cm of white noise onto the orbit positions.

1.5 Post Processing

To enhance the signal-to-noise ratio (SNR) of the NRT results in post-processing, a time variable decorrelation (VADER) filter was applied (Horvath et al. 2018). The main relation between filtered (\hat{x}_α^{VADER} , see Eq. (4)) and unfiltered (\hat{x}) spherical harmonics coefficients, is given by

$$\hat{x}_\alpha^{VADER} = (N + \alpha M)^{-1} N \hat{x} = W_\alpha \hat{x} \quad (4)$$

with the corresponding normal equation matrix N , the inverse signal variance matrix M and the scaling factor α , for an adjustment of the filter strength. These three components form the filter matrix W_α . In the case of the simulation the signal variance matrix can easily be computed from the known true signal, namely the ESA ESM AOHIS. This is a kind of best-case scenario, but in (Horvath et al. 2018) it was shown that the influence of the chosen signal variance model on the filter result is rather small.

2 Data Analysis

The following chapter describes the process of creating time series of flooded areas. For the information on floods the collection of the Dartmouth Flood Observatory (DFO) is used (Brakenridge et al. 2002). The collected data of

Table 2. Force and noise models of the “true” and reference world used in the full-scale simulations.

model	“true” world	reference world
Static gravity field (GF) model	GOCO05s	GOCO05s
Time varying GF model	ESA AOHIS	-
Ocean tide model	EOT08a	GOT4.7
Noise model	Laser interferometer noise	-
Noise model	Accelerometer noise	-

large floods spans from 1985 to the present and is derived from the news, governmental, instrumental and remote sensing sources. It is available as Excel and shapefile with each flood having the outline of the affected area in longitude and latitude, time span, affected countries and area in square kilometres.

2.1 Input data

The flood time series is determined for the following data products:

- The ESM’s H component to check the signal content of the hydrology component and investigate which flood events are visible.
- The whole ESM signal, namely AOHIS, which contains the full time variable gravity information, down-sampled.
- The ESM’s HIS signal consisting of the hydrological signal as well as the ice and solid Earth information, also down-sampled.
- The AOHIS reconstructed by the numerical closed-loop simulation as described in Chapter 1 as NRT solutions with a temporal resolution of 3 days. Additionally, the reconstructed AOHIS is VADER filtered ($\alpha=1000$).
- The HIS signal, reconstructed by subtracting the AO dealiasing product from the full reconstructed AOHIS.

To make the different data sets comparable, a down-sampling of the ESM by computing a weighted mean of the 6h snapshots to the temporal and spatial resolution of reconstructed signals (3 days, d/o 30-50) was necessary.

Additionally, an average year time series to enable the analysis of the deviation from the normal year is computed for each input signal. The computation is done from the ESA ESM model solely, which is available for 12 years (for further discussion see Section 3.4).

2.2 Time series of specific areas

The following process was applied for all data specified in Section 2.1:

- For a spatial representation in equivalent water heights (EWH, see Eq. (5)) (Wahr 1998) the spherical harmonics are evaluated on a grid with a spacing of 0.25° :

$$EWH(\lambda, \theta) = \frac{a\rho_e}{3\rho_w} \sum_{n=0}^{\infty} \frac{2n+1}{1+k_n} \sum_{m=0}^n \bar{P}_{nm}(\cos\theta) (\bar{C}_{nm} \cos m\lambda + \bar{S}_{nm} \sin m\lambda), \quad (5)$$

where ρ_w and ρ_e represent the average density of water and Earth, a the semi-major axis of the Earth, k_n the love numbers and c_{nm} and s_{nm} represent the spherical harmonic (SH) coefficients

- Next, a definition of areas of interest is needed. This analysis is based on the flood data from the DFO. The flood data set includes the affected area itself in latitude and longitude coordinates. Additionally, circles situated at the centroid of the affected area with different radius are chosen. Also, river basins¹ and sub-basins² have been identified as potential areas of interest.
- These polygons were used to be intersected with the EWH information on the grid, keeping only the data points of the area of interest.
- A weighted average EWH (\bar{x} , see Equ. 6) of the selected grid points is determined per epoch to form a time series for a specific area

$$\bar{x} = \frac{\sum wx}{\sum w} \quad (6)$$

$$w = \cos(\varphi)$$

with w the weight, depending on the latitude φ , and x the EWH per grid point of the area of interest.

¹ https://www.bafg.de/GRDC/EN/02_srvcs/22_gslrs/221_MRB/riverbasins_node.html

² <ftp://rockyftp.cr.usgs.gov/vdelivery/Datasets/Staged/Hydrography/WBD/National/GDB/>

- This leads then to three identically processed time series of a specific area: One for the average year, the second containing the noise-free reference time-variable gravity field (thereafter called AOHIS, HIS or H); and third the reconstructed AOHIS or HIS as output of the numerical simulation.

3 Results

The following chapter will first validate the simulation results of the gravity field retrieval spatially as well as in the frequency domain. Further, the recoverability of the signal is also checked within the time series. Then the possibility to detect floods in comparison with an average year, computed from the same data basis (ESA ESM) is validated and open questions regarding the computation of the average year, definition of the area of interest and spatial leakage of flood events are discussed.

3.1 Validation of the Simulation

Within the simulation time period 179 3-day solutions were computed. As Fig. 1 shows the solutions are stable and on average the reconstruction error surpasses the signal strength around degree 30. To improve the performance of the gravity field solution, different settings for a VADER filter were tested and finally set to $\alpha = 1000$. This allows for an improvement of the resolvability of on average up to d/o 50. For the following analysis the spherical harmonics of the filtered gravity fields are truncated to d/o 40. The cumulative error in EWH for the non-filtered data till d/o 40 is 4.8 cm, while the filtered cumulative error is reduced to 1.8 cm EWH.

3.2 Signal Content of the ESA-ESM H component

The signal content of the hydrology component of the ESA-ESM model was checked against the recorded floods by the DFO. For each of the 113 floods in the first half of the year 2002, a flood time series for the affected area was determined for both the H component directly as well as the average year computed from the same component with a temporal resolution of a day and spatial resolution of d/o 100. After the exclusion of very small and therefore local floods (34% of the data set) and the visual analysis of the remaining events of 74 floods a set of 15 flood cases (see Ta-

ble 3) with clear visual indications, meaning an ascending trend and/or a peak in the flood time series at the indicated time period, was selected for further testing, marked with black circles in Fig. 2.

Next, the detected floods were examined regarding their signal amplitude in different SH resolutions. Figure 3 visualizes the flood time series for three examples for the hydrological component: On the top a smaller flood in Australia (a) with an affected area of approx. 60.000 km² and short duration is depicted. In magenta the EWH minus the average EWH, computed from the 12 years of available ESM data, in the same area taking spherical harmonics till d/o 100 into account is depicted. In blue and green the time series with a lower SH resolution, namely d/o 50 and 30 is displayed. The comparably large signal bias is due to its small spatial expansion, but strong amplitude and was also observed in other small scale examples. The other examples are in the US (b) with a large area of approx. 280.000 km² and a long duration, and a middle scale flood in China (c) with an expansion of approx. 130.000 km² and an intermediate duration. Both time series show only a small deviation when using a lower SH resolution. In all analysed cases the flood is visible in all SH resolutions, which is important for the following analysis. Also, the size of the analysed area of interest as well as the magnitude of the signal plays a role in the detectability of floods.

Below each time series figure the general area of the flood is visualized spatially at the beginning and in the middle of the indicated flood. The SH resolution from left to right is: d/o 100, 50 and 30. The reduction of SH resolution and therefore the signal content can be observed in the spatial pattern and magnitude. The flood in Illinois (US) is large enough to be easily recognizable in the spatial plot as well, however, the indicated spatial expansion indicates a larger affected area. Overall, the spatial plot is not as easily interpretable as the computed time series.

3.3 Signal Content of the ESA-ESM H vs HIS vs AOHIS component

The NGGM gravity field retrieval can be done for the whole AOHIS signal. This is one of the main advantages of a NGGM concept over a single-pair. For floods, and in the future also droughts, the hydrology component is of interest. The main contributing components over continents hampering the detection of floods is the atmosphere. The HIS components can be retrieved from AOHIS by removing atmosphere and ocean (AO) via AO dealising products, also available from the ESA ESM model.

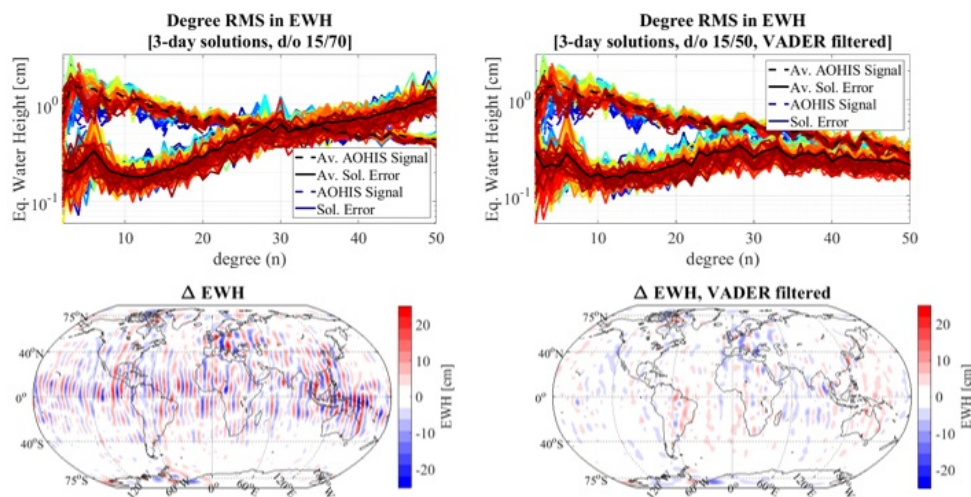


Fig. 1. Top: Degree RMS of the simulated EWH derived from the NGGM Bender pair without (left) and with (right) the VADER filter applied. All AOHIS signal as well as every error of the computed solutions is displayed in colours ranging from blue to red, with the average signal and error visualized in black. Bottom: Reconstructed AOHIS solution (first 3-day solution, d/o 50) minus the respective reference AOHIS signal without (left) and with (right) the VADER filter applied. The setting of the VADER filter is $\alpha=1000$.

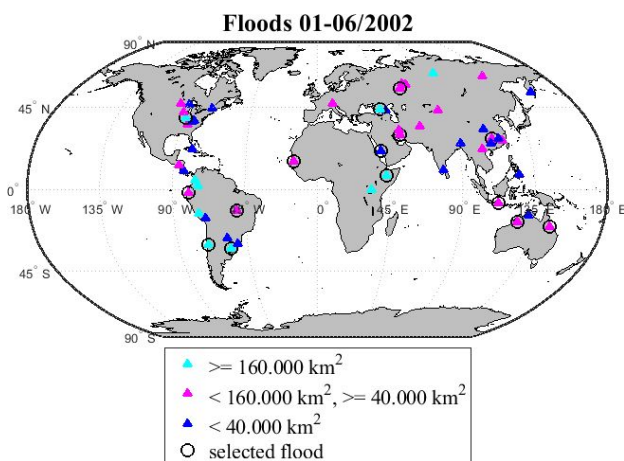


Fig. 2. Geographical locations of the floods in the time span of January to June 2002. According to the affected area, the floods are marked in cyan for floods equal or larger than 160.000 km², magenta for floods equal or larger than 40.000 km² and smaller than 160.000 km². Small flood (smaller than 40.000 km²) are marked in blue. Floods smaller than 3.000 km² are excluded from the graph. Floods selected for further analysis, due to a visibility of the indicated flood in the hydrological layer of the ESA ESM model are circled in black.

Figure 4 shows the EWH for the same three selected flood areas with the H, HIS and AOHIS component till d/o 30 in comparison. In grey the duration of the flood is marked. Clearly the most variations are visible in the full AOHIS signal visualized in red. These variations are due to the atmospheric component in the full signal. In comparison the HIS signal (displayed in cyan), without

the atmosphere and ocean (not applicable in this case, due to analysing only areas on the continents) has clearly less fluctuation in the signal. However, this signal is only available after using AO-dealiasing products, which entail their own errors as well. And lastly in green the hydrology, which is the signal of interest.

Fig. 4 shows clearly the impact of the atmospheric signal in the AOHIS, as well as the potential of the HIS signal for the detection of floods. Note that both ice and solid Earth have smaller and also more long term characteristics compared to hydrology. The question is now how well the signal can be recovered in the closed-loop gravity field retrieval experiment to enable the monitoring and detection of floods.

3.4 Flood detection from reconstructed signal

The simulated scenario of a NGGM double pair mission allows for a full reconstruction of the AOHIS, due to the possibility of self-dealiasing with the Wiese approach. A first analysis of data is therefore the correlation of the reconstructed AOHIS to the ESA ESM AOHIS for the flooded zones. Table 4 shows the correlation of the reconstructed AOHIS and the original ESA ESM AOHIS in terms of percent and RMS error. Using the reconstructed signal directly till the SNR is met, leads on average to a correlation of 87.5%, if the affected area is used as area of interest directly. The best cases indicate correlations of up to 99%, while the

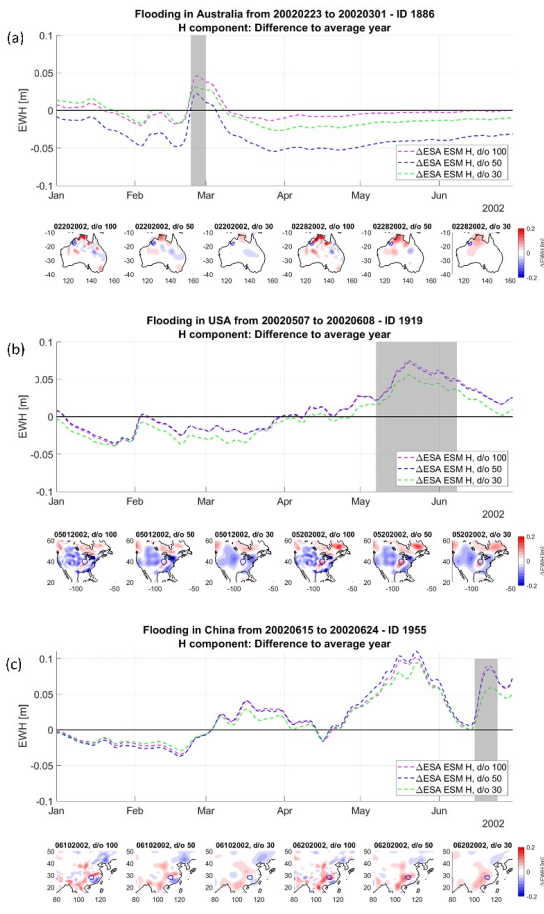


Fig. 3. The hydrology component of the ESA ESM displayed till d/o 100 (magenta), 50 (blue) and 30 (green) for the flood in Australia (a, ID 1886 according to the DFO), the US (b, ID 1919) and China (c, ID 1955). The duration of each flood is indicated with the grey shading. Below a spatial plot of the general affected area before and in the middle of the flood with d/o 100, 50 and 30 is visualized. As area of interest the affected area according to the DFO is used, also called floodzone.

worst are about 78%. These differences, however, cannot be directly linked to features like area, shape or location. The RMS values show value wise the same behaviour as the correlation in percent. The analysed case of Indonesia (ID 1870) is an outlier due to its shape and structure as an insular state with the biggest problem being the signal separation between land and ocean in coastal regions. Also, in case of floods close to the coast the generalized circular shape has to be considered with care or results dismissed, due to the possible inclusion of oceanic data in the averaged result.

Table 5 lists the correlation using the VADER filtered reconstructed signal. While the performance of the signal is expanded by 10 degrees, the correlation is on average decreased by 10%. This reduction is caused due to the fil-

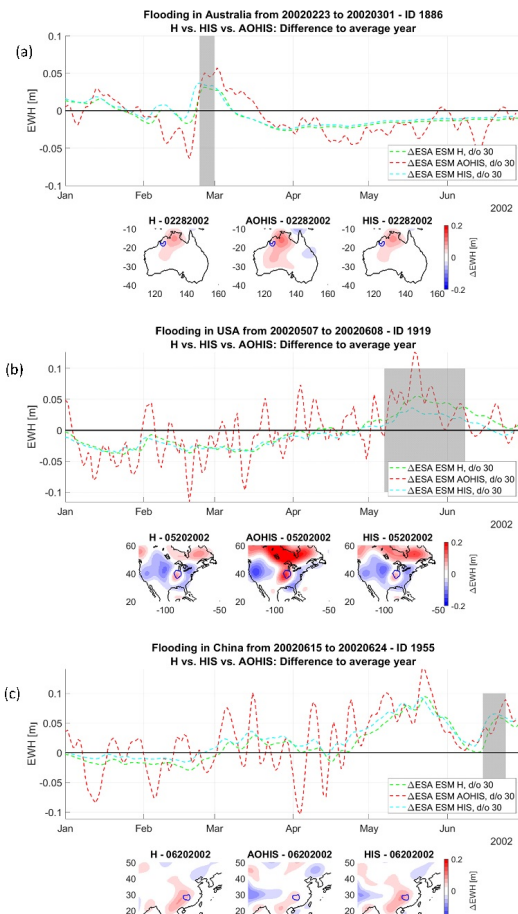


Fig. 4. Comparison of the H (green), HIS (cyan) and AOHIS (red) component of the ESA ESM for the chosen areas of interest. The variability of the whole AOHIS signal due to the atmosphere is clearly visible. The HIS signal is enhanced in the example of Australia (a), while in the example of the US (b) and China (c) it is dampened. The duration of the flood is indicated in grey. Below each time series graph, a spatial plot of the area for the H, AOHIS and HIS component is shown at a time within the flooding.

tering and inherent damping of the signal as well as spatial leakage due to the filtering process. Figure 5 shows the reconstructed AOHIS in the unfiltered version till d/o 30 and the VADER filtered reconstructed AOHIS signal till d/o 40. While the filter helps a lot with the typical GRACE striping, that in a NGGM concept is reduced but still visible, the computed time series displays the effects of the filtering as amplified peaks. Therefore, filtering for such an application has to be evaluated carefully, and based on the results of this analysis, it seems recommendable to filter the data on the flood time series level.

If a more generalized approach for the area of interest is chosen, in this case circles drawn around the centroids with different radius (for further discussion see Sec-

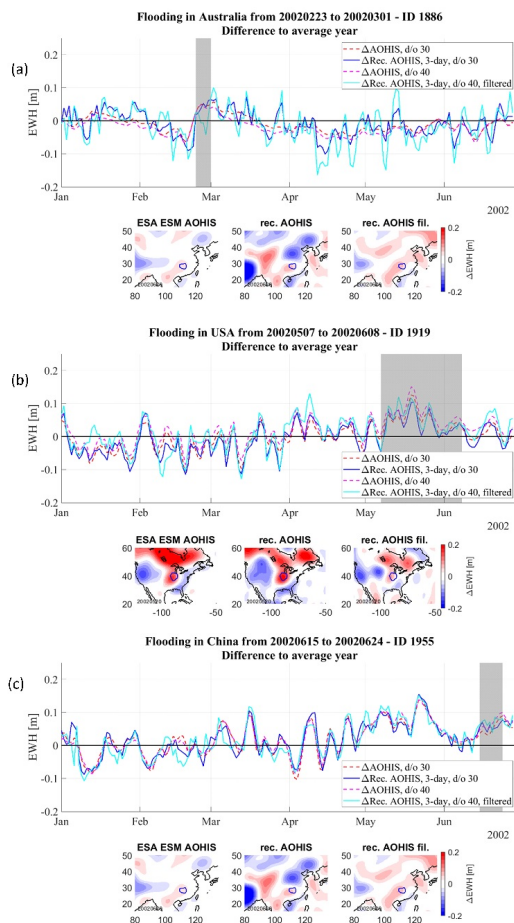


Fig. 5. Comparison between the ESA ESM AOHIS signal and the reconstructed AOHIS signal. The AOHIS signal is displayed for d/o 30 in red, and for d/o 40 in magenta, while the reconstructed AOHIS signal with d/o 30 is visualized in blue and the VADER filtered rec. AOHIS signal with d/o 40 is cyan. Below a spatial plot of the AOHIS reference signal, and the reconstructed AOHIS signal (filtered and not filtered) for d/o is displayed.

tion 3.4), similar results can be achieved. A radius of 2° means that the analysed area corresponds to the spatial resolution of a gravity retrieved with d/o 50, where on average 86.3% of the signal can be restored, while a larger area means a better recoverability by 89.3%, which is even better than for the flooded area itself (see Table 4). A very similar result is also observable for the VADER filtered cases (see Table 5), with an improvement of the circle with a radius of 4° due to the larger area used in the analysis.

Figure 6 displays the reconstructed AOHIS for the floodzone as well as the circular shape with a radius of 3 arc degree. The difference between the results is, as in the case of the correlation and RMS values, negligible.

Next, the atmosphere and ocean (AO) dealiasing component is subtracted from the full AOHIS signal to finally assess the reconstructed signal in comparison to the hy-

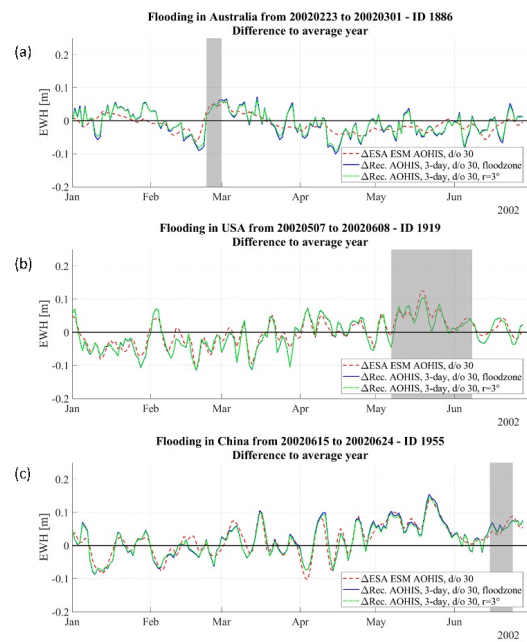


Fig. 6. The reconstructed AOHIS from the floodzone (blue) as well as the reconstructed AOHIS from a circular area of interest (green) with a radius of 3 arc degrees vs. the ESA ESM AOHIS (red). The choice of area of interest does not influence the resulting time series strongly. The time series of the flood in Australia in a coastal region shows more variation. However, since this flood is also the smallest one, it can be concluded, that there are no negative influences by the circular shape and the possible inclusion of oceanic signal.

drological input signal. Table 6 lists the correlation and RMS of the reconstructed HIS signal. While the correlation to the original time series is 20% less than when the full AOHIS is compared, the RMS stays in the same range. However, the change in correlation is not at the same level overall. Small floods in coastal areas experience the biggest degradation when using AO-dealiasing products to compute the reconstructed HIS signal. Also the second flood in Russia (ID 1962), with a large spatial expansion, but small amplitude, has a distinct decreased correlation factor.

Figure 7 visualizes the reconstructed HIS signal compared to the ESA ESM H component. It is clearly visible that the errors of the reconstructed gravity fields can be as large as the signal of interest. The reconstruction error compared to the signal amplitude depends on the size of the flooded area. While in the small example in Australia (Fig. 7a) the reconstruction error is dominating, the error becomes less important if larger areas are affected. Also the quality of the AO-dealiasing product plays a role.

To smoothen the time series a moving average with different window lengths is applied. Visually the moving average with the shortest window of 7 days performs best,

while the moving average with the longest window of 31 days removes too much information from the data. The correlations in Table 7 comparing the reconstructed HIS to the desired H component of the ESA ESM reflects the results of Table 6, because the components ice and solid Earth do not produce a lot of valuable signal in the analysed regions. Also the results of the smoothed time series shows, that none of the applied moving averages performs optimal for the intended application.

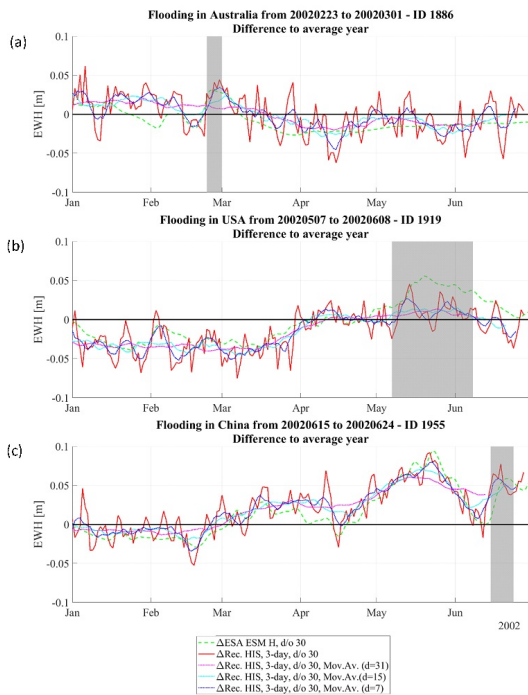


Fig. 7. The reconstructed HIS signal (by subtracting the AO Dealiasing products) for the 4 arc degree radius areas directly (red), with a moving average with $d=31$ (magenta), $d=15$ (cyan) and $d=7$ (blue) compared to the hydrological component of the ESA ESM (green).

From the 15 analysed flood events 20% are visually clearly identifiable as peaks in the reconstructed HIS signal, while 40% are visible, but are surrounded by other peaks and not as single flood event distinguishable. This result suggests, that the methodology is applicable for the suggested monitoring and detection of floods but needs improvement. The analysis showed clearly that a direct use of the reconstructed NGGM gravity fields without any post-processing is possible. The retrieval error, which depends on the size of the studied area, is still a big factor hampering the application based solely on gravity data. Also issues like average year (for more information see Section 3.4) and signal dealiasing with AO-dealiasing prod-

ucts have to be addressed, before an actual implementation with unambiguous results can be undertaken.

3.5 Open Questions

Average Year

The computation of the reference year is done from the ESA ESM model solely, which is only available for 12 years. This means that the climatology expressed by the average for the reference year by itself is influenced by floods and droughts. A climatologically relevant time scale is at least 30 years and more, so that extreme years in terms of weather are balanced out by the other years of data. It can be expected that an average year of the recommended 30 or more years will be smoother and less likely to be influenced by onetime events such as floods and droughts themselves. A detailed comparison to the current averaged reference year (in spherical harmonics on a global level and as flood time series in EWH on a local level) has shown that for each analysed area, a different year (or even years) would have to be excluded to improve the average year significantly.

Since there are no plans for an extension of the ESA-ESM, a possibility to extend the time series would be to use GRACE data. However, different data sources would be mixed in that case. In a possible future automated process and alerting scheme the used average year is of great importance to give correct and precise information about the potential of a drought or flood.

Analysed Area

The analysed gravity time series initially was derived for the exact area of the flooding indicated by the DFO. While at this point the general detection of floods is analysed, in a future application the monitoring and detection beforehand is of interest. Therefore the next question is, which kind of definition of the area of interest would be best suitable for a more general approach.

In Fig. 8 different definitions of area of interest are visualized. The actually affected area (Fig. 8, top left) is only known after a flooding event took place. However, to analyse the potential of a monitoring system, and possibly detection system the affected area is an important factor. For an automated scheme circles on a grid could be an option to objectively judge each area - in Fig. 8 circles with the radius of 2° , 3° and 4° are visualized. Overall these generally defined areas have given good results and are useful for such an analysis. Only the island state of Indonesia was not well covered by the analysis. Another possi-

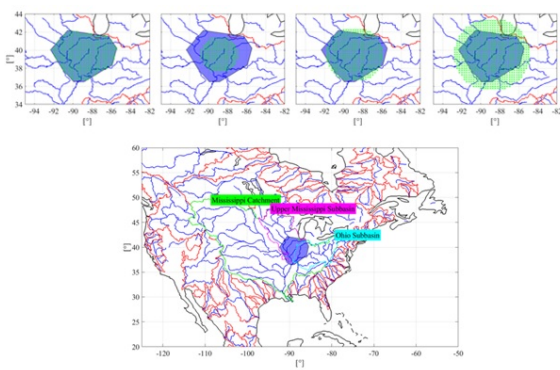


Fig. 8. Possible definitions of area of interest. Top: Affected area (historical data only), circles with $R = 2, 3$ and 4 arc degrees. Bottom: Catchment and Subbasins in the case of the US flooding (ID 1919).

bility are naturally defined areas or regions such as catchment borders and river basins. The selected example of the *Mississippi catchment* depicted in the bottom left of Fig. 8 demonstrates, that in a few cases the catchment is a too general selection since the area is too large. In this specific case a smaller-scale definition like the subbasin *Upper Mississippi River* as depicted is more suitable, since not the whole river system was affected by the flood. However the overall analysis of the 15 cases showed, that only in a few cases, the catchments or the subbasin would have been a useful spatial definition.

Signal Aliasing

Another challenging aspect of the analysis is the occurrence of several flood events in a similar, neighbouring or overlapping region. Figure 9 depicts the time series of the Yangtze River catchment. The catchment is, as the Mississippi River catchment, rather large and consists of various rivers. Within the small time span of mid-May to the end of June, seven floodings occurred in the region as the top right corner Fig. 9 depicts. The individual peaks are not distinguishable due to spatial leakage, with some peaks being visible in other time series as well, while others are not visible among the outliers. For such overlapping events additional data with a higher spatial resolution for a data assimilation is necessary to distinguish the events from each other.

Post-Processing

Both implemented post-processing strategies, namely the VADER filter as well as the moving average, did not achieve the hoped for results. Compared to other commonly used

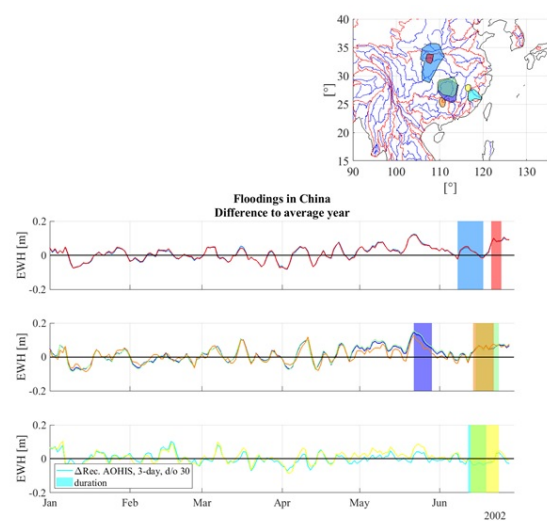


Fig. 9. Floods in China between January and June 2002 in a spatial plot (top, right) and the respective reconstructed HIS flood time series incl. ESA ESM HIS reference signal and the durations in the same colour.

filters, the VADER filter is specifically tailored to its data and signal. However, even with its fine-tuned filter matrix based on the solutions own NEQ, the filter still creates signal leakage on a spatial level. In comparison, the moving average window, indiscriminately smoothes the time series according to its input parameter and does not take into account the behaviour of the underlying time series. From this results it must be concluded further investigation is needed to give a conclusive answer on what post-processing methodology achieves the best result for the application.

4 Conclusion and Outlook

The analysis within the paper is based on a closed loop simulation for a NGGM Bender pair using the Wiese approach for selfdealising and additionally a NRT retrieval approach to achieve a very short gravity field retrieval latency for the application of flood detection. For the analysed time span of the first half of the year 2002 15 floods, detectable in the hydrology component of ESA's ESM, are analysed based on the reconstructed HIS signal.

In 20% of the analysed floods a clear detection was possible with the simulated NGGM gravity fields only, while 40% were visible but not clearly distinguishable as flood due to other similar peaks in the time series. How well the flood is detectable is dependent on the flood characteristics itself like spatial expansion and signal magni-

tude. When reconstructing HIS with the help of AO dealiasing products, the retrieval error of especially coastal and small floods suffer. However, a conclusive answer of the impact of different factors in the detectability could not be given within the scope of the paper. This would be a valid starting point for a more in-depth analysis.

When using different definitions of areas of interest similar result could be obtained, leading to the conclusion that a generalized approach would be a great option for a future service. The implementation of a post-processing scheme has shown, that although it is possible with NGGM to retrieve the complete AOHIS, a tailored post-processing is of essence to fully exploit the potential of NGGM constellations and their advantages. The implemented VADER filter as well as the moving average on time series level, are both not the optimal fit for the presented application.

Going forward several research topics have emerged from the presented analysis. On the one hand there are improvements to the data and analysis possible: First of all the average year has to be improved by adding additional years of data or removing outliers from the data set. One possibility would be to use real GRACE data to prolong the time series as long as no extension of the ESA-ESM is planned. Another, to calculate overall the average year not on a global, but on a local level, so that a potential outlier detection is meaningful.

Of interest in the future is also an analysis regarding droughts, which usually build up over years, or at least several months, so that at least a year-long simulation is necessary to quantify the possibilities in this area adequately.

Additionally, there are some general questions that still miss a conclusive answer: The influence of spatial leakage on neighbouring areas in regards of overlapping events. Also what kind of droughts and floods are detectable and in the end predictable via gravimetric satellite data (only).

References

- Baur O (2013) Greenland mass variation from time-variable gravity in the absence of GRACE. *Geophys. Res. Lett.*, Volume 40(16), 4289–4293. <http://dx.doi.org/10.1002/grl.50881>.
- Bender PL, Wiese D and Nerem RS (2008) A Possible Dual-GRACE Mission with 90 Degree and 63 Degree Inclination Orbits. *Proceedings of the 3rd International Symposium on Formation Flying, Missions and Technologies, ESA/ESTEC, Noordwijk, 23-25 April 2008*, 1-6.
- Brakenridge GR, Anderson E, and Caquard S (2002) *Global Annual Maps of Affected Areas*, Dartmouth Flood Observatory, Hanover, USA, digital media, <http://www.dartmouth.edu/%7Efloods/Archives/index.html>.
- Bruinsma S, Lemoine J, Biancale R, and Valès N (2010) CNES/GRGS 10-day gravity field models (release 2) and their evaluation. *Adv. Space Res.* 45 (4), 587-601. <http://dx.doi.org/10.1016/j.asr.2009.10.012>.
- Daras I (2016) *Gravity Field Processing Towards Future LL-SST Satellite Missions*; Deutsche Geodätische Kommission der Bayerischen Akademie der Wissenschaften, Reihe C, Dissertationen, Heft 770, Verlag der Bayerischen Akademie der Wissenschaften, pp. 23-39. ISBN (Print) 978-3-7696-5182-9, ISSN 0065-5325, 2016.
- Daras I, Pail R, Murböck M, and Yi W (2015) Gravity field processing with enhanced numerical precision for LL-SST missions. *J. Geodesy* 89 (2), 99-110. <http://dx.doi.org/10.1007/s00190-014-0764-2>.
- Dobslaw H, Bergmann-Wolf I, Dill R, Forootan E, Klemann V, Kusche J, and Sasgen I (2015) The updated ESA Earth System Model for future gravity mission simulation studies. *Journal of Geodesy*, Vol. 89, p. 505-513, <https://doi.org/10.1007/s00190-014-0787-8>
- Dobslaw H, Bergmann-Wolf I, Forootan E, Dahle C, Mayer-Gürr T, Kusche J, and Flechtner F (2016) Modeling of present-day atmosphere and ocean non-tidal de-aliasing errors for future gravity mission simulations. *Journal of Geodesy*, 90, 5, pp. 423-436, <https://doi.org/10.1007/s00190-015-0884-3>
- Elsaka B, Raimondo J-C, Brieden Ph, Reubelt T, Kusche J, Flechtner F, Iran Pour S, Sneeuw N, and Müller J (2014) Comparing Seven Candidate Mission Configurations for Temporal Gravity Retrieval through Full-Scale Numerical Simulation. *Journal of Geodesy*, 88, 31-43. <http://dx.doi.org/10.1007/s00190-013-0665-9>.
- Flechtner F, Webb F, and Watkins M (2017) Current Status of the GRACE Follow-On Mission. *Geophysical Research Abstracts*, vol. 19, EGU2017-4566, EGU General Assembly 2017. Deutsche Geodätische Kommission der Bayerischen Akademie der Wissenschaften, Reihe B, *Angewandte Geodäsie*, 318.
- Forootan E, Didova O, Schumacher M, Kusche J, and Elsaka B (2014) Comparisons of atmospheric mass variations derived from ECMWF reanalysis and operational fields over 2003-2011. *Journal of Geodesy*, 88, 503-514. <http://doi.org/10.1007/s00190-014-0696-x>
- Han S, Riva R, Sauber J, and Okal E (2013) Source parameter inversion for recent great earthquakes from a decade-long observation of global gravity fields. *J. Geophys. Res. Solid Earth*, 118, 1240-1267, <http://dx.doi.org/10.1002/jgrb.50116>.
- Horvath A, Murböck M, Pail R, and Horvath M (2018) Decorrelation of GRACE time variable gravity field solutions using full covariance information. *Geosciences* Vol. 8(9), ISSN 2076-3263. <https://doi.org/10.3390/geosciences8090323>
- Iran Pour S, Reubelt T, Sneeuw N, Daras I, Murböck M, and Gruber T (2015) Assessment of satellite constellations for monitoring the variations in earth gravity field – SC4MGV, ESA – ESTEC Contract No. AO/1-7317/12/NL/AF, Final Report.
- Kurtenbach E, Mayer-Gürr T, and Eicker A (2009) Deriving daily snapshots of the Earth's gravity field from GRACE L1B data using Kalman filtering. *Geophys. Res. Lett.* 36 (17), L17102. <http://dx.doi.org/10.1029/2009GL039564>.
- Luthcke SB, Sabaka T, Loomis B, Arendt A, McCarthy J, and Camp J (2013) Antarctica, Greenland, and Gulf of Alaska land-ice evolu-

- tion from an iterated GRACE global mascon solution, *J. Glaciol.*, 59(216), 613-631. <https://doi.org/doi:10.3189/2013jog12j147>
- Mayer-Gürr T and the GOCO Team (2015): The combined satellite gravity field model GOCO05s. Presentation at EGU 2015, Vienna, April 2015.
- Mayer-Gürr T, Jäggi A, Meyer U, Yoomin J, Susnik A, Weigelt M, van Dam T, Flechtner F, Gruber C, Günter A, Gouweleeuw B, Kvas A, Klinger B, Flury J, Bruinsma J, Lemoine JM, Zwenzner H, Bourgogne S, and Bandikova T (2016) European Gravity Service for Improved Emergency Management – Status and Project Highlights. *Geophysical Research Abstracts*, vol. 18, EGU2016-14970, EGU General Assembly 2016.
- Pail R, Bingham R, Braitenberg C, Dobsalw H, Eicker A, and Güntner A (2015) Science and User Needs for Observing Global Mass Transport to Understand Global Change and to Benefit Society. *Surveys in Geophysics* 36 (743). <https://doi.org/10.1007/s10712-015-9348-9>.
- Purkhauser AF and Pail R (2019) Near-real time gravity field retrieval on short time scales in the context of next generation gravity missions: *Geophysical Journal International*, ggz084, <https://doi.org/10.1093/gji/ggz084>
- Purkhauser AF, Pail R, Hauk M, Visser P, Sneeuw N, and Saemian P (2018) Gravity Field Retrieval of Next Generation Gravity Missions regarding Geophysical Services: Results of the ESA-ADDCON Project. *European Geosciences Union General Assembly 2018*. <https://meetingorganizer.copernicus.org/EGU2018/EGU2018-2770.pdf>.
- Ray RD (1999) A global ocean tide model from topex/Poseidon altimetry: Got99.2, Tech. rep., NASA Technical Memorandum 209478.
- Reigber C, Schwintzer P, and Lühr H (1999) The CHAMP geopotential mission, in *Bollettino di Geofisica Teoretica ed Applicata*, 40/3-4, September-December 1999, Proceedings of the Second Joint Meeting of the International Gravity and the International Geoid Commission, Trieste 1998 September 7-12, ISSN 0006-6729, pp. 285-289, eds Marson I, & Sünkel H.
- Rodell M, Velicogna I, and Famiglietti J (2009) Satellite-based estimates of groundwater depletion in India, *Nature*, 460, 999-1002. <https://doi.org/10.1038/nature08238>
- Savcenko R and Bosch W (2008) EOT08a – Empirical Ocean Tide Model from Multi-Mission Satellite Altimetry. DGF Report, München, Germany, 81.
- Schneider M (1969) Outline of a general orbit determination method, in *Space Research IX, Proceedings of Open Meetings of Working Groups (OMWG) on Physical Sciences of the 11th Plenary Meeting of the Committee on Space Research (COSPAR)*, Tokyo, edited by K.S.W. Champion, P.A. Smith, and R.L. Smith-Rose, pp. 37-40, North Holland Publ. Company, Mitteilungen aus dem Institut für Astronomische und Physikalische Geodäsie, Nr. 51., Tokyo, Japan.
- Seo K-W, Wilson CR, Chen J, and Waliser D (2007) GRACE's spatial aliasing error. *Geophysical Journal*. <https://doi.org/10.1111/j.1365-246X.2007.03611.x>.
- Sheard BS, Heinzl G, Danzmann K, Shaddock D, Kilpstein W, Folkner W (2012) Intersatellite laser ranging instrument for the GRACE Follow-On mission. *J. Geodesy* 86 (12), 1083-1095. <http://dx.doi.org/10.1007/s00190-012-0566-3>.
- Tapley BD, Bettadpur S, Watkins M, and Reigber C (2004) The gravity recovery and climate experiment experiment, mission overview and early results, *Geophys. Res. Lett.*, 31, L09607, <http://dx.doi.org/10.1029/2004GL019920>.
- Tapley BD, Flechtner F, Bettadpur S, and Watkins M (2013) The Status and Future Prospect for GRACE After the First Decade. *American Geophysical Union, Fall Meeting 2013*, abstract #G32A-01.2013AGUFM.G32A.01T.
- Tiwari VM, Wahr J, and Swenson S (2009) Dwindling groundwater resources in northern India, from satellite gravity observations. *Geophys. Res. Lett.* 36, L18401. <http://dx.doi.org/10.1029/2009GL039401>.
- Velicogna I, Sutterley TC, and van den Broeke MR (2014) Regional acceleration in ice mass loss from Greenland and Antarctica using GRACE time-variable gravity data. *Geophys. Res. Lett.* 41 (22), 8130-8137. <http://dx.doi.org/10.1002/2014/GL061052>.
- Wahr J, Molenaar M, and Bryan F (1998), Time variability of the earth's gravity field: Hydrological and oceanic effects and their possible detection using grace, *Journal of Geophysical Research: Solid Earth*, 103 (B12), 30,205.
- Wiese D, Nerem R, and Han S-C (2011) Expected Improvements in Determining Continental Hydrology, Ice Mass Variations, Ocean Bottom Pressure Signals, and Earthquakes Using Two Pairs of Dedicated Satellites for Temporal Gravity Recovery. *Journal of Geophysical Research*, 116, 405. <http://dx.doi.org/10.1029/2011JB008375>.
- Wiese D, Nerem R, and Lemoine F (2012) Design considerations for a dedicated gravity recovery satellite mission consisting of two pairs of satellites. *Journal of Geodesy* 86:81–98. <http://dx.doi.org/10.1007/s00190-011-0493-8>.
- Wiese DN, Visser P, and Nerem RS (2011) Estimating low resolution gravity fields at short time intervals to reduce temporal aliasing errors. *Adv. Space Res.* 48 (6), 1094-1107. <http://dx.doi.org/10.1016/j.asr.2011.05.027>
- Willis JK, Chambers DP, and Kuo CY (2010) Global sea level rise: recent progress and challenges for the decade to come. *Oceanography* 23, 26-35. <http://dx.doi.org/10.5670/oceanog.2010.03>.

Tables

Table 3. Analysed floods selected from the DFO archive. The ID (*) is taken from the archive.

ID*	Country [main]	Area [km ²]	Coast/Inland	Shape	Beginning [dd.mm.yyyy]	Duration [days]
1863	Iran	59660	Coast/Inland	L-shaped	11.01.2002	3
1866	Senegal	62710	Coast/Inland	Rectangular	09.01.2002	4
1870	Indonesia	41000	Various ilands	Circles	27.01.2002	17
1881	Australia	47740	Coast/Inland	S-shaped	15.02.2002	4
1885	Brazil	139100	Inland	Elongated	15.01.2002	78
1886	Australia	57870	Coast/Inland	L-shaped	23.02.2002	7
1890	Ecuador	52930	Coast	Rectangular	06.03.2002	55
1902	Saudi Arabia	22810	Coast	Rectangular	08.04.2002	6
1907	Ethiopia	282500	Inland	Square	16.04.2002	6
1919	USA	286800	Inland	Round	07.05.2002	33
1932	Chile	166900	Coast	Elongated	24.05.2002	13
1939	Uruguay	205300	Coast/Inland	Square	23.04.2002	17
1946	Russia	66440	Inland	Round	09.06.2002	7
1955	China	130300	Inland	Round	15.06.2002	10
1962	Russia	224600	Inland	Rectangular	19.06.2002	13

Table 4. Correlation [%] and RMS [cm] of reconstructed AOHis signal to the original ESA ESM AOHis for the 15 selected study cases (d/o 30).

ID	Reconstructed AOHis, d/o 30 [%]							
	Floodzone		Circle, R=2°		Circle, R=3°		Circle, R=4°	
	Corr [%]	RMS [cm]	Corr [%]	RMS [cm]	Corr [%]	RMS [cm]	Corr [%]	RMS [cm]
1863	83.5	1.8	81.3	2.0	84.1	1.8	87.4	1.6
1866	85.2	1.8	85.6	1.8	87.4	1.6	89.6	1.3
1870	79.3	1.2	66.5	2.3	69.1	2.0	73.2	1.7
1881	82.0	2.1	81.2	2.1	83.5	1.9	86.5	1.7
1885	95.7	2.3	96.0	2.3	96.3	2.1	96.8	1.8
1886	83.5	2.9	83.7	2.8	85.3	2.6	87.5	2.2
1890	90.8	2.3	91.5	2.2	92.3	1.9	93.5	1.6
1902	80.4	1.9	82.3	1.8	85.0	1.6	88.2	1.3
1907	78.1	1.8	75.3	2.2	77.8	1.9	81.2	1.6
1919	90.1	1.9	89.2	2.1	89.9	1.9	90.5	1.8
1932	78.9	1.7	79.2	1.8	79.1	1.6	79.1	1.5
1939	98.1	1.9	98.1	2.0	98.1	1.9	98.2	1.7
1946	99.3	0.7	99.3	0.7	99.3	0.6	99.4	0.6
1955	93.6	1.9	93.4	1.9	93.6	1.8	94.0	1.6
1962	94.7	1.0	92.6	1.3	93.1	1.2	93.9	1.1
	87.5	1.8	86.3	2.0	87.6	1.8	89.3	1.5

Table 5. Correlation [%] and RMS [cm] of reconstructed and VADER filtered AOHIS signal to the original ESA ESM AOHIS for the 15 selected study cases (d/o 40).

ID	Reconstructed AOHIS, VADER, d/o 40 [%]							
	Floodzone		Circle, R=2°		Circle, R=3°		Circle, R=4°	
	Corr [%]	RMS [cm]	Corr [%]	RMS [cm]	Corr [%]	RMS [cm]	Corr [%]	RMS [cm]
1863	75.8	2.3	70.8	2.5	75.7	2.2	82.0	1.8
1866	68.4	2.4	70.5	2.3	76.8	2.0	83.9	1.5
1870	70.4	1.7	52.0	4.2	56.7	3.4	64.4	2.4
1881	73.5	2.8	72.2	2.9	77.1	2.4	83.1	1.9
1885	93.7	3.2	94.2	3.0	95.2	2.6	96.3	2.0
1886	66.8	4.7	67.7	4.6	73.0	3.8	79.8	3.0
1890	88.9	3.1	90.1	2.9	91.5	2.4	93.3	1.8
1902	50.9	2.6	56.1	2.4	65.6	2.0	77.5	1.6
1907	70.3	2.3	65.9	3.0	71.2	2.5	78.0	1.9
1919	74.2	3.2	68.9	3.7	73.0	3.3	78.2	2.7
1932	68.3	2.4	73.4	2.5	74.2	2.1	75.5	1.8
1939	96.7	2.6	96.4	2.8	96.8	2.5	97.3	2.1
1946	98.0	1.1	98.1	1.1	98.3	1.0	98.6	0.9
1955	93.7	2.5	93.3	2.6	93.7	2.2	94.3	1.8
1962	92.9	1.3	86.0	1.9	87.8	1.7	90.1	1.4
	78.8	2.5	77.0	2.8	80.4	2.4	84.8	1.9

Table 6. Correlation [%] and RMS [cm] of reconstructed HIS signal to the original ESA ESM HIS for the 15 selected study cases (d/o 30).

ID	Reconstructed HIS (AO + Error)							
	Floodzone		Circle, R=2°		Circle, R=3°		Circle, R=4°	
	Corr [%]	RMS [cm]	Corr [%]	RMS [cm]	Corr [%]	RMS [cm]	Corr [%]	RMS [cm]
1863	31.6	2.0	30.2	2.1	29.6	2.0	28.6	1.8
1866	63.1	1.9	63.9	1.9	67.4	1.7	71.7	1.4
1870	46.9	1.3	20.9	2.4	24.7	2.1	31.4	1.8
1881	63.9	2.2	62.6	2.2	64.4	2.0	67.1	1.7
1885	96.0	2.4	96.3	2.3	96.6	2.1	97.0	1.8
1886	63.3	2.9	63.0	2.8	65.6	2.6	69.1	2.3
1890	90.7	2.4	91.3	2.2	92.1	2.0	93.2	1.7
1902	26.9	1.9	25.1	1.8	22.0	1.6	18.3	1.4
1907	75.8	1.9	74.2	2.2	76.1	2.0	78.9	1.6
1919	84.0	1.9	83.4	2.1	83.4	2.0	83.6	1.8
1932	69.0	1.8	69.9	1.9	68.2	1.7	65.3	1.6
1939	96.3	2.1	96.2	2.1	96.3	2.0	96.5	1.8
1946	94.9	0.6	94.9	0.6	95.1	0.6	95.3	0.6
1955	97.7	1.9	97.6	2	97.7	1.8	97.9	1.6
1962	30.8	1.1	23.8	1.3	28.5	1.3	35.1	1.2
	68.7	1.9	66.2	2.0	67.2	1.8	68.6	1.6

Table 7. Correlation [%] and RMS [cm] of reconstructed HIS signal to the original ESA ESM HIS for the 15 selected study cases with a moving average applied (d/o 30, circles R=4°).

ID	Reconstructed HIS (AO + Error) vs. H							
	Circle, R=4°		MovAv., d=31		MovAv., d=15		MovAv., d=7	
	Corr [%]	RMS [cm]	Corr [%]	RMS [cm]	Corr [%]	RMS [cm]	Corr [%]	RMS [cm]
1863	47.5	1.6	46.8	1.0	46.2	0.8	46.1	0.8
1866	42.7	1.3	43.4	0.7	42.7	0.5	36.8	0.5
1870	16.8	1.7	19.8	0.9	18.0	0.6	16.9	0.4
1881	38.2	1.8	39.9	1.0	40.4	0.8	40.3	0.9
1885	90.0	2.2	90.0	1.5	90.1	1.5	90.5	2.0
1886	49.0	2.3	49.2	1.5	49.6	1.3	51.1	1.3
1890	62.1	1.8	61.8	1.2	61.0	1.1	60.7	1.2
1902	12.4	1.5	12.3	1.2	13.7	1.1	13.1	1.0
1907	49.5	1.7	50.2	1.0	50.4	0.8	50.6	0.7
1919	71.0	2.4	71.1	1.9	71.8	1.8	71.6	1.8
1932	53.4	1.6	54.2	1.1	53.9	0.9	52.6	0.8
1939	93.5	2.3	93.4	1.8	93.2	1.8	93.6	1.8
1946	79.9	3.4	80.6	3.4	80.6	3.4	81.2	3.4
1955	84.7	1.8	84.5	1.3	84.6	1.3	85.3	1.6
1962	44.3	1.1	43.1	0.8	42.6	0.5	42.6	0.4
	55.7	1.9	56.0	1.4	55.9	1.2	55.5	1.2

Declaration of Authorship

I hereby declare that the thesis submitted is my own unaided work. All direct or indirect sources used are acknowledged as references.

Anna Purkhauer 29/01/2020
.....
Anna F. Purkhauer Date
(IAPG, LRG, TUM)